Molecular Modeling and Thermodynamic Studies on the Selective Extraction of Poly Aromatic Hydrocarbons from Fuel oil using Deep Eutectic Solvents

A thesis submitted in partial fulfillment of the requirements for the degree of

DOCTOR OF PHILOSOPHY

By

PAPU KUMAR NAIK

Centre for the Environment

Indian Institute of Technology Guwahati

Guwahati – 781039, India

July 2019

INDIAN INSTITUTE OF TECHNOLOGY GUWAHATI

भारतीय प्रौद्योगिकी संस्थान गुवाहाटी

Center for the environment, Guwahati 781039, Assam, India

पर्यावरण केंद्र, गुवाहाटी 781039, असम, भारत

CERTIFICATE

This is to certify that the work contained in the thesis entitled "***Molecular Modeling and Thermodynamic Studies on the Selective Extraction of Poly Aromatic Hydrocarbons from Fuel oil using Deep Eutectic Solvents"*** is the result of investigations carried out by **Mr. Papu Kumar Naik** under our supervision and is an authentic record of the results obtained from the research work carried out at the Center for the Environment, Indian Institute of Technology Guwahati, Assam, India for the award of degree of Doctor of Philosophy. This work has not been submitted elsewhere for a degree.

Thesis Supervisor

Dr. Tamal Banerjee

Professor

Department of Chemical Engineering

IIT Guwahati

Thesis Co-supervisor

Dr. Sandip Paul

Professor

Department of Chemistry

IIT Guwahati

Guwahati

July 2019

INDIAN INSTITUTE OF TECHNOLOGY GUWAHATI
भारतीय प्रौद्योगिकी संस्थान गुवाहाटी
Center for the environment, Guwahati 781039, Assam, India
पर्यावरण केंद्र, गुवाहाटी 781039, असम, भारत

DECLARATION

It is to declare that the content embodied in this thesis entitled "***Molecular Modeling and Thermodynamic Studies on the Selective Extraction of Poly Aromatic Hydrocarbons from Fuel oil using Deep Eutectic Solvents"*** is the result of investigations carried out by me at the Centre for the Environment, Indian Institute of Technology Guwahati, Assam, India under the supervision of **Prof. Tamal Banerjee**, Department of Chemical Engineering and **Prof. Sandip Paul**, Department of Chemistry for the award of degree of Doctor of Philosophy. This work has not been submitted elsewhere for any degree or diploma of any institute or university to the best of my knowledge and belief.

In keeping with the general practice of reporting scientific observations, due acknowledgments have been made wherever the work described is based on the findings of other investigators.

Guwahati
July 2019

PAPU KUMAR NAIK
Roll No: 146152006

Dedicated

To

My Mother

Acknowledgments

I would like to thank all the people who contributed in some way to the work described in this thesis and supported me to complete my Ph.D. Working for this Ph.D. has been an unforgettable experience for me and it would not be possible without these people.

I express my deepest gratitude and sincere thanks to my supervisors **Prof. Tamal Banerjee** and **Prof. Sandip Paul** for their invaluable guidance and constant encouragement. I am much inspired by not only their rich experience and knowledge but also the way of approaching a problem, immense patience and extreme care. I am highly obligated to them for their persistent devotion and willingness. During my research, they provided me with the most precious ideas and resources that played a vital role in completing the thesis successfully. I enjoyed every moment working under their supervision and learned many things from them, which will be an asset for my future research. It was really honored to work under them.

I would like to thank my Doctoral Committee members, **Dr. Amit Kumar**, **Dr. Anki Katha Reddy**, Department of Chemical Engineering and **Dr. Manabendra Sarma**, Department of Chemistry. Their valuable inputs and evaluation during my research progress kept the flow of research work in the right direction.

I would like to express my sincere thanks to **Prof. Vaibhav V. Goud**, **Dr. Ashok Kumar Dasmahapatra, Dr. Mahuya De**, and **Dr. Ashish Kumar Gupta** for their research-oriented teaching, which helped me during my Ph.D. I take this opportunity to thank all the faculty members for their valuable suggestions and cooperation during my course work.

I want to thank the Department of Science and Technology (DST), Government of India, for providing INSPIRE Fellowship (Grant no. DST/INSPIRE Fellowship/2015/IF150175) and the international travel grant through Science and Engineering Research Board (SERB) for presenting the research output in the international conference, International Symposium on Solubility Phenomena and Related Equilibrium Processes (ISSP 2018) held at Tour, France (Grant No: ITS/2018/001920).

I would take this opportunity to thank the Director, IITG for providing necessary facilities and a conducive academic environment. I am grateful to Centre for the Environment, IITG for financial support in the form of national travel grants, consumables and equipment, also providing laboratory and software facilities. I owe my gratitude to the Central Instruments Facility, IITG and Central Library, IITG for providing me the necessary facilities. I would like to acknowledge the PARAM Ishan Super-computer facility of IIT Guwahati for its computational times for performing MD simulation. I express my sincere gratitude and acknowledgment to IIT Guwahati for all the facilities that were made available to me.

I am thankful to the Head of Centre for the Environment, **Prof. Mihir Kumar Purkait**, and technical staff of Centre for the Environment, **Dr. Deepmoni Deka**, **Mr. Partha Protim Bakal, Mr. Rajiv Gogoi**, **Mr. Kaustubh Rakshit** and **Mr. Mridul Das** of IIT Guwahati for their kind co-operation, which helps me in several ways.

I would like to express my sincere thanks to **Prof. Punyaban Patel, Prof. Bhisma Kumar Patel**, **Prof. Gopal Das,** and **Prof. Kaustubha Mohanty** for their valuable suggestion and inspiration, which made my thesis successful.

My sincere thanks to **Dr. Mood Mohan** and **Dr. Debashis Kundu,** who helped me a lot during the research work. I also deeply acknowledge my research group members Dr. Anand Bharti, Dr. Sanjukta Bhoi, Dr. Basudhrity Banerjee, Dr. Rima Biswas, Dr. Rupesh Verma, Mr. Pyarimohan Dehury, Mr. Dhirendra Mishra and other lab mates.

I express my gratitude towards my labmates in Centre for the Environment, Mr. Smruti Ranjan Dash, Ms. Paulomi Bose, Mr. Rahul Verma, Dr. Gopi Kiran, Dr. Nanendra Naik, Dr. Lalit Goswami, Mr. Arnab Ghosh, Mr. Jaya Krishna, Mr. Smonath Chanda, Mr. Arun Kumar and all members for providing me technical and moral support.

I am thankful to my friends Mr. Satrudhan Palsaniya, Mr. Krishan Kumar, Mr. Bhidhu Bhushan Mukut, Mr. Dilip Sahu and Mr. Bhibhuti Naik for all the laughs, joyful moments, for their support and suggestions.

Finally, I would like to express my sincere gratitude to my family, (Late) father **Vesaj Chandra Naik**, mother **Jugeswari Naik**, and sister **Ms. Santosini Naik**. Whose blessings and never-ending support is the real stimulus that constantly inspires me to do my best. Last but not least, my deepest gratitude goes to my wife, **Mrs. Omi Patel** for her constant encouragement, unlimited sacrifices and patience, sincere prayers, continuous support and motivation for the completion of this thesis work.

Above all, I would like to thank the "**Almighty GOD**" for blessing me and providing me the unseen moral support that directed me through my good as well as hard times.

Papu Kumar Naik

SYNOPSIS

Poly Aromatic Hydrocarbon (PAH) along with nitrogen and sulfur hetero-atoms are the main impurities in the fuel oil. These are required to remove from oil in the refinery tough various process. These PAHs are the main cause of air pollution due to the release of SO_x and NO_x during combustion of fuel oil. The high utilization of fuel oil, which has increased the production of air pollutant and had a direct impact on the economic, environmental, political, and life quality of population The nitrogen containing PAH are more difficult to remove than sulfur containing PAH. There refinery uses the conventional method like hydrodenitrification (HDN) method to remove these PAH. However, the process has certain limitation and it cannot remove the lower concentration completely. Solvent-based extraction processes are useful in such cases for selective removal of aromatics. Therefore, the current thesis work aims to extract the nitrogen base PAH from fuel oil with the application of liquid liquid extraction as efficient method. For this, the new generation green solvent called Deep Eutectic Solvent (DES) has been used as extractive solvent. DESs are very good alternative for the conventional organic solvent as an extracting agent. DESs are also replacements for the more expensive ionic liquids with better capacity. DES is the result of strong interaction between hydrogen bond acceptor (HBA) and hydrogen bond donor (HBD) when mixed in a specific molar ratio. DESs are also characterized by a very large depression of freezing point, which makes them liquid at room temperature.

In order to evaluate the potential of DESs, the properties of four set DESs based on quaternary ammonium and phosphonium salt were studied. The choice of DESs were based on literature review and current studies, due to its numerous application on the separation of aliphatic and aromatic hydrocarbon with higher extraction efficiency than others. The

DESs were synthesized by mixing HBD (ethylene glycol and glycerol) with HBA (methyltriphenylphosphonium bromide (MTPB) and tetrabutylammonium bromide (TBAB) in a molar ratio of 1:4. Fourier Transform Infrared (FTIR) and Thermo Gravimetric Analysis (TGA) analysis were then carried out to understand the functional groups along with their thermal stability. NMR analysis was also ascertained to validate the molar ratio of 1:4 in solution. The eutectic behavior of the studied DESs were analyzed and compared with existing data. It is found that variation in HBD leads to eutectic mixtures having difference in eutectic composition as well as temperature. This effect can be primarily attributed to the hydrogen bond appearing between active sites of donor and acceptor.

Thereafter the four DESs were simulated with Molecular Dynamics (MD) simulations to evaluate and measure the pure component properties of these solvents at room temperature. Thermodynamics insights such as non-bonded interaction energies, hydrogen bonds, coordination number and radial distribution functions (RDF) were also discussed to understand their atomistic interactions involved in the eutectic mixture. The MD simulated density results were validated by comparing the measured experimental densities, which gave an excellent agreement within a range of ±5%. The results from MD simulations revealed that the hydrogen bonded interactions between the anions of HBA and HBD is the main contribution for the formation of eutectic mixture. The RDF disclosed the fact that the bromide ion interacts more strongly with the hydroxyl group of the ethylene glycol or glycerol molecule. It is to be noted that the phosphonium based DESs shows less interaction between the cation and the anion as compared to HBD. This further supports by hydrogen bonding analysis. In summary, the bromide ion interacts more strongly with

the hydroxyl group of the ethylene glycol molecule and it can be concluded that the phosphonium based DES can be good candidates for extraction especially for aromatic moiety.

The phosphonium based DES comprising of methyltriphenylphosphonium bromide (MTBP) along with hydrogen bond donor namely ethylene glycol (DES1) and glycerol (DES2) were taken for further extraction studies. In order to study their effectiveness, Liquid-liquid Equilibrium (LLE) experiments were performed for the removal of toluene and quinoline respectively. LLE data corresponding to the ternary systems: [DES1(1)+Toluene(2)+Heptane(3)], [DES2(1)+Toluene(2)+Heptane(3)], [DES1(1)+Quinoline(2)+Heptane(3)] and [DES2(1)+Quinoline(2)+Heptane(3)] were generated at 308.15 K and atmospheric pressure. ^{1}H NMR analysis were then used for the quantification of both extract and raffinate phases. Distribution coefficient (β) and selectivity (S) were subsequently obtained and it was found that toluene had a poor selectivity than quinoline. Both the values were found to be higher at low concentration of aromatic feed. The cross contamination of DES and heptane across either phases were found to be nearly zero, thereby enabling the ease of solvent recycling. Further, the Non-random two liquid (NRTL) and UNiversal QUAsi Chemical (UNIQUAC) thermodynamic model were used to compare the experimental tie line data. This gave an excellent fit with a root mean square deviation (RMSD) values for both models ranging from (0.28- 0.31%) and (0.22- 0.73%) respectively. In summary, between the two deep eutectic solvents, DES2 shows a less value of solute distribution ratio. Hence, DES1 namely methyltriphenylphosphonium bromide + ethylene glycol (1:4) was thus recommended as a potential solvent for the separation of aromatic and PAH component.

The simultaneous extraction of multi PAH component within the hydrocarbon stream was again studied. Quinoline and indoline as model PAH were extracted from the toluene-heptane mixture at 308.15 K. The DES1 consisting of methyltriphenylphosphonium bromide (MTPB)+ethylene glycol (1:4) was taken, which was found to be effective solvent for quinoline extraction. The LLE data for the ternary system namely: DES (1) + indoline (2) + heptane (3) and quaternary systems; namely DES (1) + quinoline (2) + indoline (3) + heptane (4), DES (1) + quinoline (2) + toluene (3) + heptane (4) and DES (1) + indoline (2) + toluene (3) + heptane (4) were measured. The PAH concentrations in the system were varied from 5 to 70 wt% to understand the extraction efficiency of DES. The composition of the respective components in both extract and raffinate phases were measured by ^{1}H NMR technique. It was observed that all the systems followed a type-II phase behavior where a positive slope was seen towards the PAH peak. The distribution coefficient and selectively values for PAH in extract phase were two times higher than toluene. It was also noticed that the pseudo component (PAH + toluene) has higher selectivity when compared to individual solute. Similarly, the selectivity of the pure PAH (quinoline or indoline) was higher than that of a mixture of toluene and PAH. Thus, the mixture of PAHs are efficiently and selectively extracted when compared to heptane or toluene. The indoline ternary system also suggests that indoline was effectively extracted from heptane rich phase in a similar manner as quinoline.

The reliability of the measured tie line data was then correlated with the local thermodynamic models, namely NRTL and UNIQUAC models, which gave RMSD value of less than 1%. This indicates that the thermodynamic models gave an excellent agreement between them. Further, Quantum chemical based COnductor like Screening MOdel for

Real Solvents (COSMO-RS) model was also employed to predict the phase behavior of investigated systems. In summary, The DES was extensively able to extract PAH from both single and multi component system. The presence of toluene in the quaternary system reduced the efficiency of DES. It was also observed that the concentration of DES in raffinate phase was zero. This will imply lesser number of processing units or unit operations for solvent recovery. The study reveals that the DES1 can be used as a potential solvent for the selective removal of PAH from fuel oil.

Precise experimental data and reliable theoretical models are basic requirements for the better understanding of the extraction process. Thus, the classical Molecular Dynamic (MD) simulation technique was employed to investigate and compare the experimental LLE data of the DES1 [MTPB+EG(1:4)]-quinoline-heptane ternary system, which was previously reported in our chapter 3. This explains the behaviour of different molecules and the mechanism involved. For performing the MD simulations, two experimental feed points are considered which gave high selectivity and distribution coefficient values. The results suggest that the deviation between experimental and simulated data was very less and gave good agreement between them. The higher values of selectivity (*S)* indicates the better ability of DES for the extraction of quinoline from heptane. The interaction energies of different species and the structural properties such as radial distribution functions (RDFs), average number of hydrogen bonds and spatial distribution functions (SDFs) are then computed.

The result shows that the van der Waals interactions are found to be higher than the electrostatic interactions, which is the primary controlling parameter for DES-quinoline-heptane interactions. It is found that the cation within the hydrogen bond acceptor HBA

namely MTP possess favorable interactions with quinoline when compared to HBD or anion (Br). MTP cation here acts as a hydrogen bond acceptor and contributes to the hydrogen bonding with quinolone, which results in higher experimental selectivity values. The calculations of SDFs further reveals the fact that the DES molecules are evenly distributed around the active sites of quinoline molecule, whereas heptane molecules are found to distributed around the non-active sites of the aromatic ring. From MSD, it is found that closer the values of the self-diffusion coefficient within the species, higher the miscibility and more interaction between the molecules. This makes quinoline to be more susceptible towards the DES molecule. In summary, the cation (MTP) of hydrogen bond acceptor plays a predominating role in the quinoline extraction process. Therefore, this study provides new insights for the computational analysis of LLE equilibria in the absence of experimental data.

Finally, reactive force field (ReaxFF) simulations is adopted to study its degradation and pyrolytic behaviour of quinoline. This study was carried out to understand the non-catalytic hydrogenation and degradation mechanism of quinoline where it forms several small fragments or useful chemicals. It helps us in elucidating the mechanism and the primary reaction pathways for the initiation reaction leading to the hydrogenation of quinoline and for describing the formation of intermediates (IMs) and products. To confirm the intermediate and final products, a range of ReaxFF MD simulations at different temperatures with NVT ensembles for a total duration of 700 ps were implemented. Five different temperatures ranging from 2500 K–4500 K are chosen so as to allow the chemical reactions to be observed at a computationally affordable time scale. Other than 2500 K, all the temperatures provided a pyrolysis scan on the entire quinolone molecule.

The intermediate mechanism, the overall product/ intermediate distributions, and the corresponding reaction behavior for the quinoline hydrogenation are investigated. The main decomposition pathways and the composition of the main decomposition products of quinoline at different temperatures are revealed. The results indicate that the active site of hydrogenation initiation reaction is the aromatic ortho-position of the quinolone. We have found a qualitative agreement between the previously reported experimental results and our simulation results with respect to initiation step of the quinoline hydrogenation and formation of major intermediate products such as Tetrahydroquinoline (THQ), Propylaniline (PA) and decahydroquinoline (DHQ). The hydrogenation of quinoline is mainly through the C−C bond fission pathways for denitrification. However, on further degradation of quinoline with time it gives smaller stable products along with many intermediates. Most of the intermediate reactions are found to be intramolecular while intermolecular reactions dominate at higher temperatures. The main products include ammonia, ethylene, methane, ethane and acetylene. For the stable product, the number of the species would reach its maximum after the complete decomposition of quinoline molecule. Acetylene is the major compound formed. The decomposition rate of quinoline and the rate of the products are found to increase with temperature. In conclusion, the ReaxFF MD simulation method provides an effective approach towards the study of hydrogenation/degradation reactions of quinoline at molecular level.

Overall, the results of the present study suggest the use of DES in PAH extraction is a comparatively new technique and must be explored further for commercial application. Moreover, it appears to be environmentally benign and offers several advantages over conventional catalytic extraction process in terms of efficiency and contamination.

Table of Contents

List of Figures

List of Tables

List of Abbreviations and Symbols

Abbreviations	
AMBER	Assisted Model Building with Energy Refinement
B3LYP	Becke three-parameter, Lee-Yang-Parr
CN	Coordination Number
COSMO-RS	COnductor like Screening MOdel for Real Solvents
COSMO-SAC	COnductor like Screening MOdel Segment Activity Coefficient
DES	Deep Eutectic Solvent
DFT	Density Functional Theory
DGA1	Density Gradient Approximation
DMSO	Dimethyl sulfoxide
EG	Ethylene Glycol
FTIR	Fourier transform spectroscopy
GA	Genetic Algorithm
GAFF	Generalized AMBER Force Field
GEPOL	GEometry of POLyhedron
HF	Hartree–Fock
IL	Ionic Liquid
IE	Interaction Energy
LLE	Liquid Liquid Equilibrium
MD	Molecular Dynamics
MTPB	Methyltriphenyl phosphonium bromide

NAMD	Nanoscale Molecular Dynamics
NMR	Nuclear Magnetic Resonance
NRTL	Non-Random Two-Liquid model
PCM	Polarizable Continuum Model
RDF	Radial Distribution Functions
ReaxFF	Reactive Force Field
RESP	Restrained Electrostatic Potential
RMSD	Root Mean Square Deviation
SDF	Spatial Distribution Function
SCRF	Self-Consistent Reaction Field
TBAB	Tetrabutyl ammonium bromide
TGA	Thermo-Gravimetric Analysis
TZVP	Triple Zeta Valence Potential
UNIQUAC	UNIversal QUAsi-Chemical
VMD	Visual Molecular Dynamics

Symbols	
a_{eff}	Effective contact surface area of a segment in Å^2
A_{ij}	UNIQUAC interaction parameter between component i and j
c	Number of components in the LLE system
F	Objective function
H_i	Peak area under NMR spectra of species i
l	Staverman-Guggenheim combinatorial term parameter
m	Number of tie lines
E_{vdW}	Van der Waals (vdW) interaction energy
$p_s(\sigma)$	Probabilistic surface charge distribution for mixture
$p^X{}_i(\sigma)$	Sigma profile of the pure component i
r_n	Radius of the nth segment
r_{eff}	Radius of the standard surface segment (a_{eff}) in Å
r	Pure component volume
q	Pure component area
r_{avg}	Average radius in Å
R	Universal gas constant in (kcal mol^{-1} K^{-1})
T	Temperature
SG	Staverman-Guggenheim term
Q	Normalized area parameter
A^{PCM}	Molecular surface area in Polarizable Continuum Model, in^2
V^{PCM}	Molecular surface volume in Polarizable Continuum Model, in^3

g_{ij}	Energy parameter characterizing the interaction of species i and j (NRTL binary interaction parameter)
u_{ij}	Energy parameter characterizing the interaction of species i and j (UNIQUAC binary interaction parameter)
$\Gamma_s(\sigma)$	Segment activity coefficient for mixture
$\Gamma_i(\sigma)$	Segment activity coefficient for pure component (i)
$\gamma_{i/s}$	Component activity coefficient in the mixture
Φ_i	Fugacity coefficient of the component in mixture
α	Non-randomness parameter
σ, σ'	Screening charge density in e $Å^{-2}$
$\mu_s(\sigma)$	Sigma potential in kJ mol^{-1} $Å^{-2}$ for a surface segment in solution
β	Distribution coefficient
S	Selectivity
τ_{vdW}	Dispersion coefficient in kJ mol^{-1} $Å^{-2}$
x_i^I	Mole fraction of component *i* of phase I in the LLE system
τ_{ij}	NRTL interaction parameter between component *i* and *j*
θ	Area fraction in UNIQUAC equation

CHAPTER 1

Introduction and Review of Literature

1.1 Introduction

Nowadays, it is necessary to produce ultra-low sulphur and nitrogen containing fuel oil. The sulphur content as per current convention limited to maximum of 15 ppm and the nitrogen content to less than 0.1 ppm [1]. The Poly Aromatic Hydrocarbons (PAH) of both nitrogen and sulphur points out to a hazardous threat due to its emission into the atmosphere. The toxic effects are mainly due to the carcinogenic products released in the environment as a result of combustion [2]. Thus, desulphurization and denitrification are an essential part of a refinery set up. It is hence invariably necessary to remove the sulphur and nitrogen containing PAH species from fuel oil. Fuel oil consists of 25% aromatics, 15% paraffin, 45% naphthalene and 15% non-hydrocarbon compounds. The aliphatic sulphur and nitrogen compounds are highly reactive in conventional hydroprocessing and they can be completely removed from the fuels without much difficulty. The poly-aromatic sulfur and nitrogen compounds including alkyl indoles and alkyl carbazoles are generally more difficult to convert over hydroprocessing catalysts. Therefore, the poly-aromatic compounds present the most difficult challenges to the hydrodesulphurization (HDS) and hydro-denitrification (HDN) processes. Some typical polyaromatic structures of sulphur and nitrogen compounds present in fuel oil are given below in Figure 1.1.

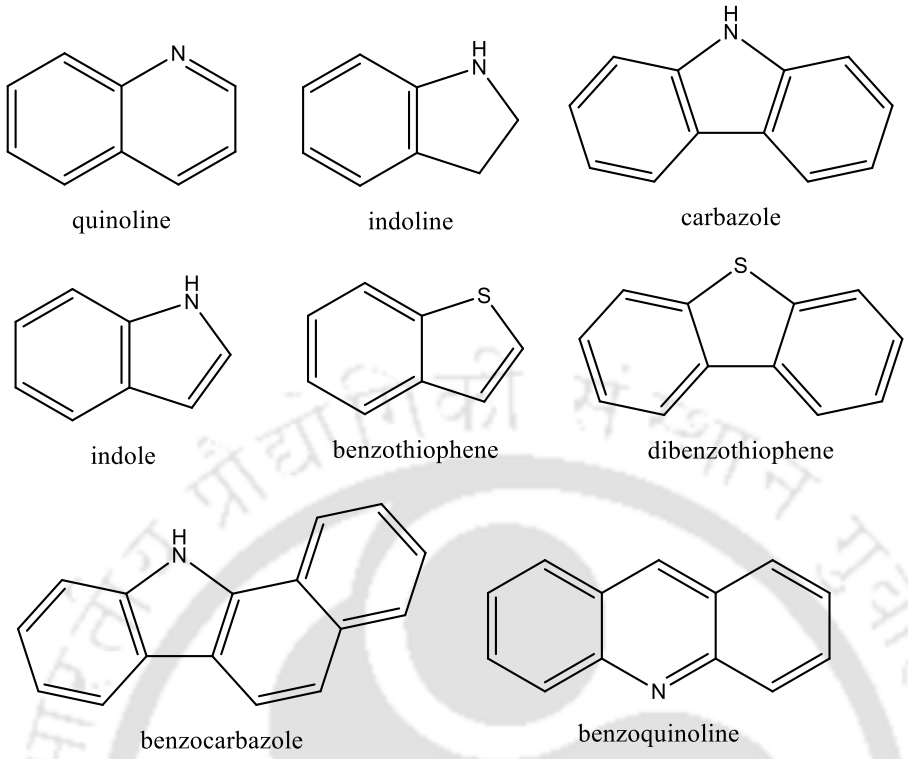

Figure 1.1: Nitrogen and sulphur containing polyaromatic compounds

Usually, the fuel oil contains small amount of nitrogen-based compounds (0.1% - 2%). The nitrogen content increases with increasing boiling point of the fuel [3]. The poly aromatics nitrogen-based compounds are the main cause of air pollution [4]. and are also considered as strong inhibitors for the hydrodesulphurization process (HDS) of diesel oil because of its role in catalytic deactivation [5]. The aromatic nitrogen compounds exist in two different types namely non-basic and basic nitrogen compounds. The former includes compounds such as pyrrole, indole, indoline, carbazole and benzocarbazole. The basic nitrogen compounds known are pyridine, quinoline and benzoquinoline. Nitrogen compounds having non-heteroaromatic or heteroaromatic structure with multiple rings adversely affect the stability of diesel oil during its storage [1]. This reduces the efficiency

of hydrodenitrification (HDN) process due to the poisoning of the catalyst. Hence, it is important to reduce the nitrogen level of the diesel oil due to both its potential pollution threat and its storage requirements. Hydrodenitrification (HDN) of diesel oil is the prime attention of refineries worldwide due to strict environmental regulations globally. It is essential to reduce the nitrogen and sulfur level of the diesel oil with the ultimate goal of zero emissions. The nitrogen-based compounds are known to have low reactivity and high refractoriness as compared to the conventional sulfur compounds in diesel oil.

There are various methods adopted for the removal of these aromatics from fuel oil. PAH are usually removed in a hydrotreater. In such as process the hydrogen concentration in terms of partial pressure is increased to an extent in the reactor, such that the PAH are converted to straight chain compounds. However, due to the rate limiting thermodynamic step, the PAH are not readily converted even at high operating conditions. In summary, the increase in temperature or H_2 partial pressure is not able to reduce the PAH content significantly [6]. Recently catalytic processes were devised for the extraction of these PAH. However, these catalysts used were found to be highly selective with lower efficiency for a single PAH [7]. Further, the catalysts are expensive and hence not used commercially. Other separation process includes ion exchange, alkylation, metal complexation, extractive distillation and azeotropic distillation. For these processes, the aromatic extraction usually ranges from medium to high content (70-20) %. But below 20% there is no suitable industrial process available [8]. As a rule of thumb for the lower range of 20% wt. and below, liquid-liquid extraction methodology is recommended. Thus solvent extraction process becomes an eminent operation for removing PAHs both at the ambient condition as well as moderate condition.

Therefore, the extractive solvents should be sufficiently selective for the extraction of PAH species at high capacity. In addition, the solvent must be readily regenerated after the extraction step. The separation efficiency in liquid–liquid extraction depends on the availability of a suitable solvent. Most of the commercial solvents commonly used in the extraction process are acetonitrile, n-methyl pyrrolidone (NMP), sulfolane and ethylene glycol. These organic solvents are toxic and volatile in nature and are thus environmentally non-benign. Further solvent recovery is cumbersome and contributes roughly 90% of the extraction cost [9]. Keeping in mind the limitations of these conventional solvents, the new generation green solvents are being explored so as to replace these conventional solvents. Along these lines, the two new variants developed recently are Ionic Liquid (IL) and Ionic Liquid analogues namely Deep Eutectic Solvents (DES).

Most of the research work carried out till date uses IL as a solvent for aromatic extraction. However high purity IL are difficult to synthesize and some of them degrade at temperature well below 100°C inhibiting its use in extraction even though it is highly selective towards PAH. Green solvents such as DES which is analogous to IL attracted recent attention in several separation processes, often as a replacement for the conventional organic solvents as well as costly ionic liquids. These DES are now used as an alternative to traditional solvent for the extraction of aromatic from naphthalene [10]. They have similar physical properties with IL and are formed with combination of salt and a hydrogen bond donor (HBD). It has a low melting point than their respective individual component [11]. DESs are easy to synthesize possessing high purity and most importantly economically applicable. Recent studies have proved them to be biodegradable, environmental friendly and hydrophobic in nature [12].

1.2 Deep Eutectic Solvent (DES) and its Properties

Most of the scientific publication with respect to DES emerged from 2012. There is rapid growth of research activities due to its versatile usability. DES are sustainable and cheap alternative to far more cumbersome solvents used today. A DES is generally a mixture of two cheap and solid/liquid components which are capable of associating with each other, through hydrogen bond interactions, to form a eutectic mixture with a melting point significantly lower than the melting points of the constituting compounds. The formation of liquid molten salts at room temperature is due to the establishment of hydrogen bonds between the hydrogen bond donor (HBD) and hydrogen bond acceptor (HBA), usually a halide anion present in the salt. DESs are characterized by a very large depression of freezing point and are liquid at room temperatures. Some researchers also named them as low-transition-temperature mixtures (LTTMs). The freezing point depression of the mixture results from the formation of halide ion−hydrogen bond donor supramolecular complexes that alter the free energy of the solid phase compared to that of the liquid [13]. In most cases, a DES is obtained by mixing a hydrogen bond donor (HBD) that has the ability to form a complex with the halide anion of the quaternary ammonium or phosphonium salt [14]. Figure 1.2 summarizes the different quaternary salts that are widely used in combination with various HBDs in the formation of DESs. The earliest definition of DES was given by Abbott et al. [15]. In their work DES was synthesized by the mixture of substituted quaternary ammonium salts such as hydroxyethyltrimethylammonium (choline) chloride with urea. The final product was found to be a liquid at ambient temperature.

DESs are currently attracting widespread scientific and technological interest as low-cost alternatives to conventional and unconventional solvents, such as ionic liquids (ILs). DESs are now widely acknowledged as a new class of ionic liquid (IL) analogues because they share many characteristics and properties with ILs. DESs are systems formed from a eutectic mixture of Lewis or bronsted acids and bases which can contain a variety of anionic and/or cationic species, whereas ILs are formed from systems composed primarily of one type of discrete anion and cation.

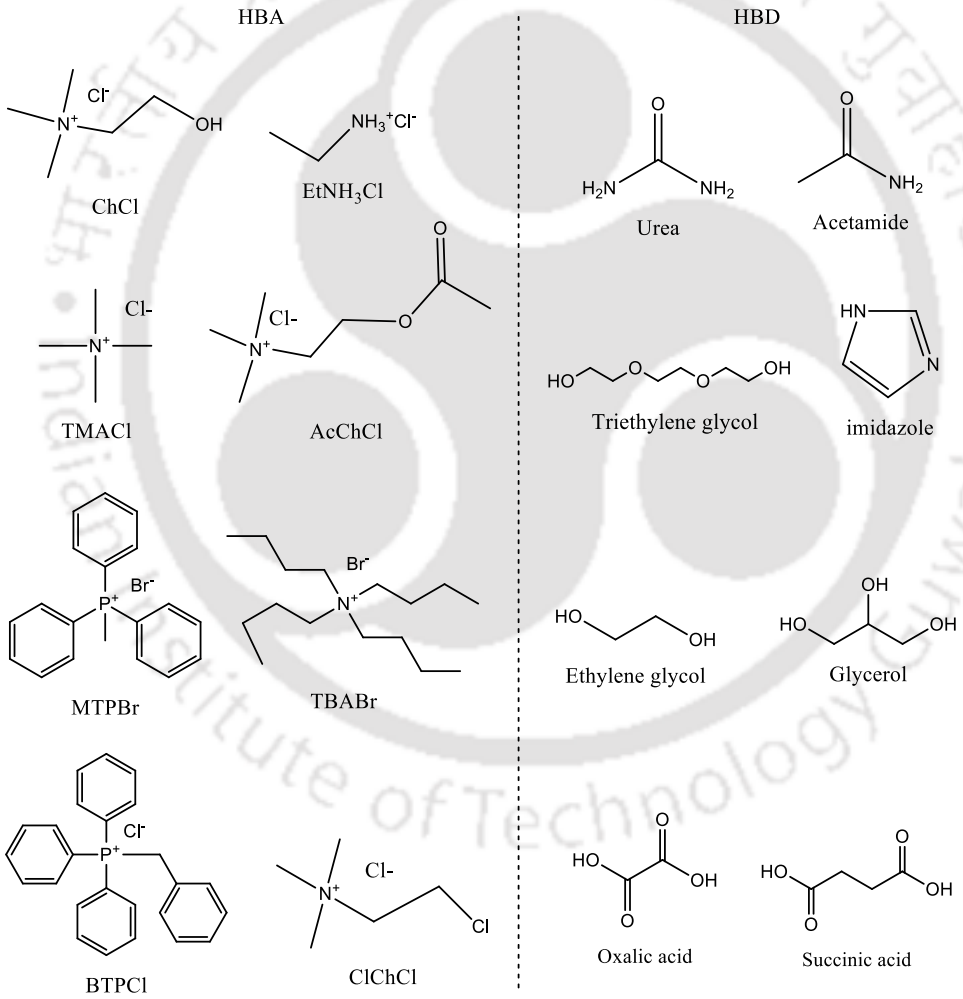

Figure 1.2: Typical structures of the halide salts and hydrogen bond donors used for DES syntheses

The preparation of DESs can be regarded as a strategy to overcome some of the disadvantages of ILs, such as high melting temperature, high price, and toxicity, because they share many of the ILs appealing solvent properties such as low volatility, high thermal stability and conductivity, wide liquid range, and high solvation capacity. Besides these properties, DESs possess other interesting advantages over ILs. They are easier to synthesize and just require the stirring of the two components upon gentle heating because the components are easily mixed without any further purification. They have low production cost due to the low price of starting materials. They are chemically inert and most of the synthesized DESs are biodegradable, biocompatible, and nontoxic. Figure 1.3 shows different types of application of DES.

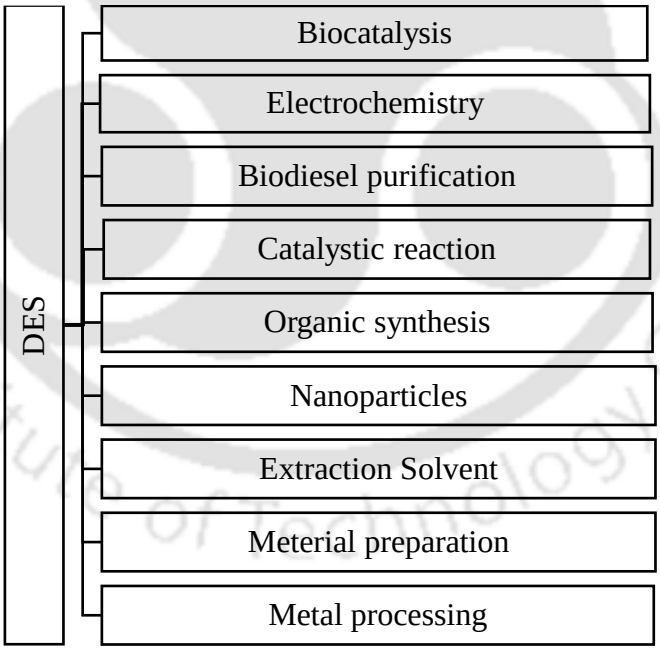

Figure 1.3: Different application of DES

1.3 Environmental Aspect of DES

Clerk et al. [16] studied the criteria for green solvent in terms of life cycle assessment, on the basis of their solvency, ease of use, reusability, health and safety, environmental impact, and economic cost which is best suited for a DES. Due to the interesting properties of DES, primarily their low ecological footprint and their attractive price, research on these solvents have been exponentially growing in the last years. As a result, their emergence in new laboratory and industrial applications (not existing at the moment) will be enhanced in the near future. Figure 1.4 shows the various properties of DES. The deep aspect of DES and green properties along with the toxicity of the starting material of the DES are discussed in Appendix-A (Section A.1).

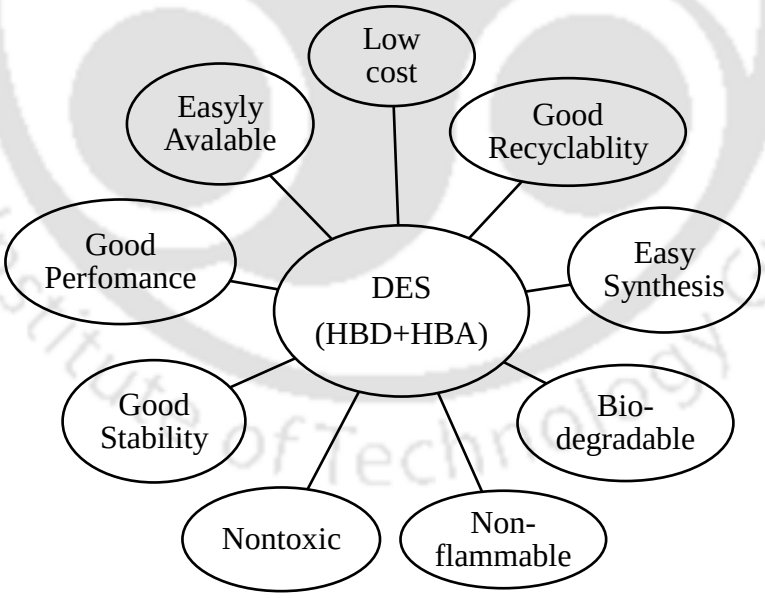

Figure 1.4: Different properties of DES as green solvent

Advantage of DES:

1) *Availability*: The raw material of most of the DES are mostly available easily on a large-scale such as urea and common halide salt.
2) *Price*: Most constituents of the DES are cheap and economically viable and cost will not volatile during time for sustainability of the chemical process. Some of them are obtained naturally.
3) *Recyclability:* The solvent DES is fully recyclable in extraction process without contamination or loss [17].
4) *Synthesis*: Preparation of the DES is an easy and energy-saving process with the synthetic reaction being highly atom-efficient.
5) *Toxicity*: In order to reduce the risk for humans or nature, most of the DES exhibit negligible toxicity.
6) *Biodegradability*: DES being a green solvent, it does not produce any toxic metabolites and biodegradable [18].
7) *Performance*: Compared to currently employed solvents, most of the DES show similar and even superior performances in terms of their application like extraction capacity.
8) Stability: During a chemical process, most DES are thermally and chemically stable up to high temperature [19].
9) *Flammability*: These green solvents being non-flammable and have safe manipulation.
10) *Storage*: The storage of DESs are easy and safe because it is stable and self-stainable in nature.

Once the properties of green solvent such as DESs are discussed, we shall now move on towards its use as an extractive solvent. Prior to that, we shall discuss briefly about LLE or Liquid Liquid Equilibrium process in general for extraction of aromatics.

1.4 Liquid Liquid Equilibrium Extraction (LLE) of Aromatics

1.4.1 Ionic Liquids as Solvents

LLE involving aromatic extraction with IL have been extensively reported in the literature [20-23]. Banerjee et al. [24] studied different IL with respect to denitrification of diesel oil namely 1-ethyl 3-methylimidazolium methylsulfonate [EMIM][$MeSO_3$], 1-ethyl 3-methylimidazolium ethylsulfate [EMIM][$EthSO_4$] and 1-ethyl-3-methylimidazolium acetate [EMIM][Ac]. Marcos et al. [25] studied the use of ionic liquids (ILs) as replacements of sulfolane has been extensively studied. They studied the use of 1-ethyl-4-methylpyridinium bis(trifluoromethylsulfonyl)imide ([4empy][Tf2N]) and 1-ethyl-3-methylimidazolium dicyanamide ([emim][DCA]) binary IL mixtures as toluene extraction solvent from its mixtures with n-heptane, 2,3-dimethylpentane, and cyclohexane

Meindersma et al. [26] studied LLE for the systems toluene + n-heptane + a solvent. Ternary data were collected for the solvents sulfolane and the ionic liquids [mebupy]BF_4, [emim]$C_2H_5SO_4$, [mmim]$CH_3SO_4$and[bmim]CH_3SO_4. Deenadayalu et al. [20] investigated the liquid liquid equilibria data for the ionic liquids 1-ethyl-3-methylimidazolium octyl sulfate and 1-methyl-3-octylimidazolium diethylenglycol monomethyl ether sulfate at T=298.2 K and atmospheric pressure to determine their potential as solvents for extraction of aromatic compound from alkanes. Cassol et al. [27] studied liquid-liquid equilibrium for the ternary system formed by n-octane and aromatic

(alkylbenzenes) and heteroaromatic compounds (nitrogen and sulfur containing heterocycles) and 1-alkyl-3-methylimidazolium ionic liquids (ILs) associated with various anions. They found that the selectivity on the extraction of a specific aromatic compound is influenced by anion volume, hydrogen bond strength between the anion and the imidazolium cation and the length of the 1-methyl-3-alkylimidazolium alkyl side chain. Ananth and Banerjee [28] used Ionic Liquids as green alternative for the removal of aromatic sulphur compounds from diesel oil by Liquid–Liquid Extraction (LLE). Continuum solvation models based on the COnductor like Screening MOdel (COSMO) along with its extension to Real Solvents (RS) have been used to directly predict the LLE data [28].

In another study Alonso et al. [29] investigated (Liquid + liquid) equilibrium (LLE) data for {1-methyl-3-octylimidazolium bis[trifluoromethy- lsulfonyl] imide + thiophene + *n*-dodecane} and {1-methyl-3-octylimidazolium bis [trifluoromethylsulfonyl] imide + thiophene + cyclohexane} at 298.15 K. Xie et al. [30] studied the extraction of neutral nitrogen-containing compounds (N-compounds) with chloride based ionic liquids (ILs) with varying cation classes (imidazolium, pyridinium). 1-butyl-3-methylimidazolinium chloride (BMIMCl) and 1-octylpyridinium chloride (OcPyCl) were evaluated using a synthetic solution with dibenzothiophene and carbazole as model compounds, where a high selectivity for N-compounds was found. Zhang et al. [31] demonstrated two types of ionic liquids, 1-alkyl-3-methylimidazolium [AMIM] tetrafluoroborate and hexafluo-rophosphate and trimethylamine hydrochloride (AlCl3-TMAC), to be potentially applicable for sulfur removal from transportation fuels. Also [EMIM][BF_4](E=ethyl), [BMIM][PF_6](B=butyl), [BMIM][BF_4], and heavier

[AMIM][PF_6] showed high selectivity, particularly toward aromatic sulfur and nitrogen compounds. Domańska et al. [32] studied pyrrolidinium-based ionic liquids such as 1-butyl-1-methylpyrrolidinium tris(pentafluoroethyl)trifluorophosphate, ([BMPYR][FAP]), 1-butyl-1-methylpyrrolidinium tetracyanoborate, [BMPYR][TCB] and 1-butyl-1-methylpyrrolidinium tricyanomethanide, [BMPYR][TCM] for removing sulfur compounds from gasoline and diesel oils. Ternary (liquid + liquid) equilibrium data are presented for mixtures of {ionic liquid (1) + thiophene (2) + heptane (3)} at T = 298.15 K and ambient pressure to analyze the performance of the ionic liquid in the extraction of thiophene from the alkanes.

1.4.2 DES as Solvents

For the studies involving DES, LLE data are scarce. Tang et al. [33] studied deep eutectic solvents (DESs), which were prepared by using $AlCl_3$, chlorinated paraffins-52 ($C_{15}H_{26}Cl_6$), and various aromatics like benzene, toluene gave excellent desulfurization performance for various thiophenic sulfur compounds. In DESs, aromatic compounds strongly influence the desulfurization performance, and the order found is toluene > xylene > ethylbenzene > benzene > chlorobenzene. Kareem et al. [34] studied the extraction of toluene from hydrocarbon mixtures using ethyltriphenylphosphonium iodide as a salt with either ethylene glycol or sulfolane as hydrogen-bond donors (HBDs). Zahra et al. [35] studied a novel sample preparation method based on the complete dissolution of marine biological samples in choline chloride-oxalic acid (ChCl-Ox) deep eutectic solvent for fast and efficient extraction of eight polycyclic aromatic hydrocarbons (PAHs) using minimum volumes of cyclohexane. Tongnian et al. [36] developed DES extractants for the

enrichment of phenols from model oil. The DES was found to effectively extract the polar analytes not only from hexane but also from other non-polar or weak polar solvents such as toluene and chloroform. The activity of the regenerated DES was also examined. Perkins et al. [37] simulated three choline chloride-based DESs using molecular dynamics to study the hydrogen bonding interactions of the system. Molecular simulations performed on several DES showed very good agreement with experimental densities and thermodynamic properties.

Oliveira et al. [38] studied three different DES, all based on choline chloride, for the liquid–liquid separation of an azeotropic mixture of heptane + ethanol at 25 °C. The data obtained helped DES to surpass the performance of existing extraction solvents, leading to an increase in efficiency and a reduction in energy consumption of the overall process. Kareem et al. [39] examined phosphonium based deep eutectic solvent (DES) in the extraction of aromatic hydrocarbons from aromatic/aliphatic mixtures. Experimental data for liquid liquid equilibria (LLE) were obtained for various mixtures of (benzene + hexane + DES) at 27, 35 and 45 °C.

Mulyono et al. [40] investigated the possibility of using a selected deep eutectic solvent (DES) for the liquid liquid extraction of benzene, toluene, ethylbenzene and m-xylene (BTEX) aromatics. The DES used in their work was synthesized by combining tetrabutylammonium salt and sulfolane. Equilibrium data for the ternary system consisting of BTEX aromatics, n-octane and DES were measured at 25 °C. The Non-Random Two Liquid (NRTL) model was successfully used to correlate the experimental tie-lines and to calculate the phase compositions of the ternary systems. In addition, the performance of COSMO-RS to predict the ternary tie-lines for the studied systems was evaluated and the

σ-profiles were used to explain the interaction between the DES and the aromatic compounds. Hou Yucui, et al. [41] found that DES formed by levulinic acid as hydrogen bond donor and tetrabutylphosphonium bromide (TBPB) as hydrogen bond acceptor could efficiently separate aromatic hydrocarbons from aromatic/aliphatic mixtures. Rodriguez et al. [42] used tetrahexylammonium bromide:ethylene glycol with molar ratio = 1:2 (DES 1) and (ii) tetrahexylammonium bromide:glycerol with molar ratio = 1:2 (DES 2) for aromatic extraction. The selected DESs were characterized by measurement of density and viscosity at atmospheric pressure and temperatures T = 293.2–343.2 K. The liquid–liquid equilibria (LLE) of the ternary systems {hexane + benzene + DES 1} and {hexane + benzene + DES 2} were determined at T (K) = 298.2 and T (K) = 308.15 and atmospheric pressure.

Sarwono et al. [43] investigated the possibility of using selected Deep Eutectic Solvents from ammonium salt with ethylene glycol, lactic acid and sulfolane as Hydrogen Bond Donor (HBD). Equilibrium data for the ternary system consisting of ethylbenzene and n-octane with all DESs were measured at 25°C and atmospheric pressure. The results showed comparable distribution ratio and selectivity with commercial solvents. Sander et al. [44] studied Liquid-liquid equilibria for six ternary systems with choline chloride/urea or choline chloride glycerol (molar ratio, 1:2) as selective solvent at atmospheric pressure and 25°C. The suitability of deep eutectic solvents for the separation of pyridine and toluene from n-hexane and n-butanol from toluene was evaluated in terms of properties of solvents, solute distribution ratio, and extraction efficiency. Choline chloride glycerol has a better potential for separation of pyridine from its mixture with n-hexane. The equilibrium data were well described with the NRTL model.

Nerea et al. [45] investigated four different glycerol-based deep eutectic solvents (DESs) as extracting agents for the separation of the azeotropic mixture {methyl ethyl ketone + ethanol} via liquid–liquid extraction. The selected DESs for this work were: glycerol/choline chloride with molar ratios (4:1) and (2:1), and glycerol/tetramethylammonium chloride with molar ratios (4:1) and (2:1). Mohammad et al. [46] reported a novel denitrogenation method of fuels using DES as extractants and demonstrated the essential role of rational control of the physicochemical character of DESs in achieving superior denitrogenation performance. Among the investigated DESs, the 1 : 2 molar mixture of choline chloride and phenylacetic acid presented the best denitrogenation performance, showing simultaneous efficient removal of both basic and non-basic N-compounds.

1.5 Objectives of the Thesis

From the detailed literature study, the following objectives for the thesis have been defined:

1. *Identification* of suitable ammonium and phosphonium based Deep Eutectic Solvents (DES) for extraction of Poly Aromatic Hydrocarbon (PAH) from fuel oil.
2. *Measure* the thermophysical properties of ammonium and phosphonium based DES with both experiments and molecular dynamics (MD) simulations.
3. *Obtain* ternary Liquid Liquid Equilibria (LLE) for the ternary system of selected DES with nitrogen based poly aromatic hydrocarbon (quinoline) and model diesel compound (n-heptane).
4. *Investigate* the quaternary LLE phase behaviour of DES and PAH for the simultaneous extraction of quinoline and indoline from hydrocarbon stream or n-heptane

5. *Modeling* of experimental LLE data with Non-random two liquid (NRTL), UNiversal QUAsi-Chemical (UNIQUAC) and Quantum chemical based COnductor like Screening MOdel for Real Solvents (COSMO-RS) model.
6. *Initiate* molecular dynamics prediction of LLE with the DES and PAH system and compare it with measured experimental data.
7. *Conduct* thermal degradation of quinoline with Reactive Force Field (ReaxFF) simulation.

1.6 Thesis Organization

This thesis is organized into following chapters. Schematic outlines of the current thesis are presented in Figure 1.5.

Chapter 1 represents an introductory discussion on nitrogen based polyaromatic compound such as quinolone and benzoquinoline. These impurities are present in the fuel oil and a key discussion on the environment and society is communicated. It emphasizes on the various available techniques for the extraction of such species. This also highlights the important expect of liquid liquid extraction using potential DES as solvent. Therefore, the requirement of the alternative green solvent such as ionic liquid and DES have been focused based on the detailed review of the literatures. It additionally discuss the various advantage and usability of DES. It also discuss the importance of LLE and DES as green solvents in the extraction of poly aromatics from fuel oil.

Chapter 2 describes the synthesis and properties of ammonium and phosphonium based DES. These DES are selected based on literature review and the current studies on aromatic extraction. Here studies concerning four set of DES namely; methyltriphenylphosphonium bromide (MTPB) + ethylene glycol (DES1),

methyltriphenylphosphonium bromide (MTPB) + glycerol (DES2), tetrabutylammonium bromide (TBAB) + ethylene glycol (DES3), and tetrabutylammonium bromide (TBAB) + glycerol (DES4) in a molar ratio of 1:4 are reported. Thermophysical Properties such as density, viscosity, refractive index, NMR, FTIR and TGA are measured. Molecular Dynamics (MD) simulations are then employed to evaluate and measure the pure component properties of these solvents at room temperature. Thermodynamics insights such as Non-bonded interaction energies, hydrogen bonds, coordination number and radial distribution functions (RDF) were also discussed to understand their atomistic interactions involved in the eutectic mixture.

Chapter 3 presents the experimental Liquid Liquid Equilibrium (LLE) data for the ternary systems containing different phosphonium based DES with heptane and quinoline/toluene. Here methyltriphenylphosphonium bromide (MTPB) + ethylene glycol (DES1) methyltriphenylphosphonium bromide (MTPB) + glycerol (DES2) are selected. In order to study their effectiveness, LLE experiments were performed for the removal of toluene and quinoline respectively. Ternary systems namely [DES1(1)+Toluene(2)+Heptane(3)], [DES2(1)+Toluene(2)+Heptane(3)], [DES1(1)+Quinoline(2)+ Heptane(3)] and [DES2(1)+Quinoline(2) +Heptane(3)] were discussed. The selectivity and distribution coefficient were also discussed for the extraction Of aromatics from heptane. Further, the Non- random two liquid (NRTL) and UNiversal QUAsi Chemical (UNIQUAC) thermodynamic model were used to correlate the experimental data.

Chapter 4 presents the experimental Liquid Liquid Equilibrium data for the quaternary systems, namely DES (1) + quinoline (2) + indoline (3) + heptane (4), DES (1)

+ quinoline (2) + toluene (3) + heptane (4) and DES (1) + indoline (2) + toluene (3) + heptane (4) and ternary system DES (1) + indoline (2) + heptane (3). The equilibrium composition is calculated using ^{1}H NMR spectroscopy. The distribution coefficient and selectively values were investigated for the simultaneous extraction of polyaromatic from heptane. The experimental data were correlated with the NRTL and UNIQUAC model. The COSMO-RS model was also employed for predicting phase behaviour of the systems.

Chapter 5 deals with classical Molecular Dynamic (MD) simulation technique which has been employed to investigate and compare the experimental phase behaviour of DES-quinoline-heptane ternary LLE system. Here two experimental feed points are considered which gave high selectivity and distribution coefficient values. The interaction energies of different species and the structural properties such as radial distribution functions (RDFs), average number of hydrogen bonds and spatial distribution functions (SDFs) are then computed. This reveals the intermolecular mechanism how DES molecules distributed around the active sites of quinoline molecule in order to extract it from heptane rich phase.

Chapter 6 describes the Reactive Molecular Dynamics (ReaxFF MD) where the hydrogenation and degradation mechanism of quinolone is predicted and compared. The simulation was carried out at temperatures ranging from 2500 K–4500 K. Detailed reaction mechanism and product distribution for the pyrolysis of quinoline is compared with the previously reported experimental results. The initiation step of the quinoline hydrogenation and formation of major intermediate products were discussed. **Chapter 7** summarizes the important findings obtained from the present work. The later part of this chapter also focuses on the scope for future work that can be carried out.

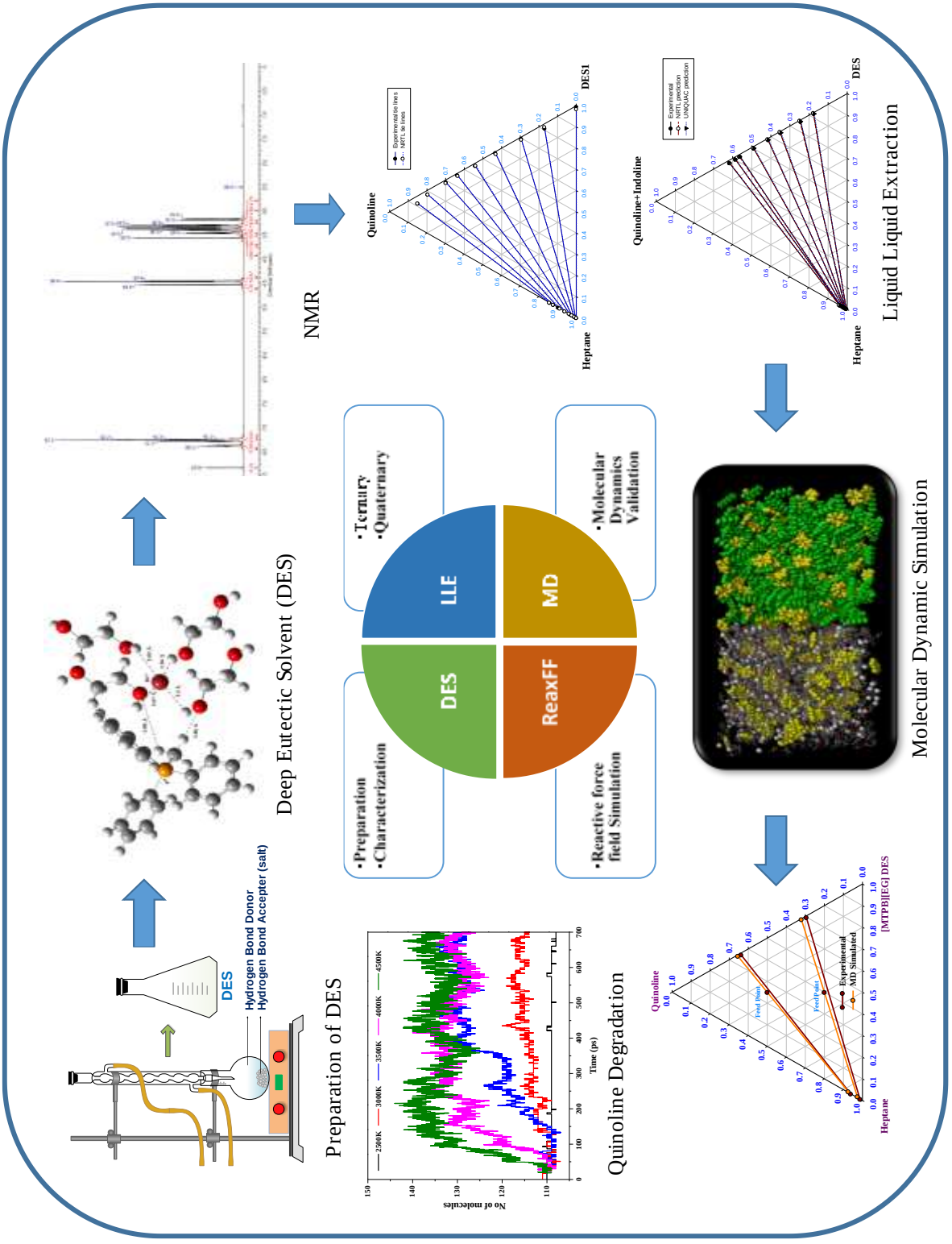

Figure 1.5: Schematic outline of the current thesis

References

[1] M. Macaud, M. Sévignon, A. Favre-Réguillon, M. Lemaire, E. Schulz, M. Vrinat, Novel methodology toward deep desulfurization of diesel feed based on the selective elimination of nitrogen compounds, Ind. Eng. Chem. Res. 43 (2004) 7843-7849.

[2] Y. Yongtan, Determination of nitrogen compounds in catalytic diesel oil using gas chromatography, Chin. J. Chromatogr. 26 (2008) 478-483.

[3] P. Wiwel, K. Knudsen, P. Zeuthen, D. Whitehurst, Assessing compositional changes of nitrogen compounds during hydrotreating of typical diesel range gas oils using a novel preconcentration technique coupled with gas chromatography and atomic emission detection, Ind. Eng. Chem. Res. 39 (2000) 533-540.

[4] A. Jayaraman, F.H. Yang, R.T. Yang, Effects of nitrogen compounds and polyaromatic hydrocarbons on desulfurization of liquid fuels by adsorption via π-complexation with Cu (I) Y zeolite, Energy & Fuels 20 (2006) 909-914.

[5] H. Yang, J. Chen, Y. Briker, R. Szynkarczuk, Z. Ring, Effect of nitrogen removal from light cycle oil on the hydrodesulphurization of dibenzothiophene, 4-methyldibenzothiophene and 4, 6-dimethyldibenzothiophene, Catal. Today 109 (2005) 16-23.

[6] J. Chen, M. Te, H. Yang, Z. Ring, Hydrodesulfurization of dibenzothiophenic compounds in a light cycle oil, Petroleum science and technology 21 (2003) 911-935.

[7] C. Song, An overview of new approaches to deep desulfurization for ultra-clean gasoline, diesel fuel and jet fuel, Catalysis today 86 (2003) 211-263.

[8] K. Weissermel, Industrial organic chemistry, John Wiley & Sons, New York, 2008.

[9] S.H. Ali, H.M. Lababidi, S.Q. Merchant, M.A. Fahim, Extraction of aromatics from naphtha reformate using propylene carbonate, Fluid Phase Equilib. 214 (2003) 25-38.

[10] Y. Hou, Y. Gu, S. Zhang, F. Yang, H. Ding, Y. Shan, Novel binary eutectic mixtures based on imidazole, J. Mol. Liq. 143 (2008) 154-159.

[11] K. Shahbaz, S. Baroutian, F.S. Mjalli, M.A. Hashim, I.M. AlNashef, Densities of ammonium and phosphonium based deep eutectic solvents: Prediction using artificial intelligence and group contribution techniques, Thermochim. Acta 527 (2012) 59-66.

[12] K. Shahbaz, F. Mjalli, M. Hashim, I. AlNashef, Prediction of the surface tension of deep eutectic solvents, Fluid Phase Equilib. 319 (2012) 48-54.

[13] A.P. Abbott, G. Capper, D.L. Davies, H.L. Munro, R.K. Rasheed, V. Tambyrajah, Preparation of novel, moisture-stable, Lewis-acidic ionic liquids containing quaternary ammonium salts with functional side chainsElectronic supplementary information (ESI) available: plot of conductivity vs. temperature for the ionic liquid formed from zinc chloride and choline chloride (2∶ 1), Chem. Comm. DOI (2001) 2010-2011.

[14] Q. Zhang, K. De Oliveira Vigier, S. Royer, F. Jerome, Deep eutectic solvents: syntheses, properties and applications, Chem Soc Rev 41 (2012) 7108-7146.

[15] A.P. Abbott, G. Capper, D.L. Davies, R.K. Rasheed, V. Tambyrajah, Novel solvent properties of choline chloride/urea mixturesElectronic supplementary information (ESI) available: spectroscopic data., Chem. Comm. DOI 10.1039/b210714g(2003) 70-71.

[16] J.H. Clark, S.J. Tavener, Alternative solvents: shades of green, Organic process research & development 11 (2007) 149-155.

[17] K.M. Jeong, M.S. Lee, M.W. Nam, J. Zhao, Y. Jin, D.-K. Lee, S.W. Kwon, J.H. Jeong, J. Lee, Tailoring and recycling of deep eutectic solvents as sustainable and efficient extraction media, Journal of Chromatography A 1424 (2015) 10-17.

[18] I. Juneidi, M. Hayyan, M.A. Hashim, Evaluation of toxicity and biodegradability for cholinium-based deep eutectic solvents, RSC Adv. 5 (2015) 83636-83647.

[19] N. Delgado-Mellado, M. Larriba, P. Navarro, V. Rigual, M. Ayuso, J. García, F. Rodríguez, Thermal stability of choline chloride deep eutectic solvents by TGA/FTIR-ATR analysis, J. Mol. Liq. 260 (2018) 37-43.

[20] N. Deenadayalu, K.C. Ngcongo, T.M. Letcher, D. Ramjugernath, Liquid− liquid equilibria for ternary mixtures (an ionic liquid+ benzene+ heptane or hexadecane) at T= 298.2 K and atmospheric pressure, J. Chem. Eng. Data 51 (2006) 988-991.

[21] M.A. Hughes, Y. Haoran, Liquid-liquid equilibria for separation of toluene from heptane by benzyl alcohol tri (ethylene glycol) mixtures, Journal of chemical and engineering data 35 (1990) 467-471.

[22] S.K. Cheruku, T. Banerjee, Liquid–liquid equilibrium data for 1-ethyl-3-methylimidazolium acetate–thiophene–diesel compound: experiments and correlations, Journal of solution chemistry 41 (2012) 898-913.

[23] S.R. Pilli, T. Banerjee, K. Mohanty, Ionic liquids as green solvents for the extraction of endosulfan from aqueous solution: a quantum chemical approach, Chemical Product and Process Modeling 8 (2013) 1-14.

[24] U.K. Ravilla, T. Banerjee, Liquid liquid equilibria of imidazolium based ionic liquid+ pyridine+ hydrocarbon at 298.15 K: Experiments and correlations, Fluid Phase Equilib. 324 (2012) 17-27.

[25] S. García, M. Larriba, J. García, J.S. Torrecilla, F. Rodríguez, Separation of toluene from n-heptane by liquid–liquid extraction using binary mixtures of [bpy][BF4] and [4bmpy][Tf2N] ionic liquids as solvent, J. Chem. Thermodyn. 53 (2012) 119-124.

[26] A.R. Hansmeier, M. Jongmans, G.W. Meindersma, A.B. de Haan, LLE data for the ionic liquid 3-methyl-N-butyl pyridinium dicyanamide with several aromatic and aliphatic hydrocarbons, J. Chem. Thermodyn. 42 (2010) 484-490.

[27] C.C. Cassol, A.P. Umpierre, G. Ebeling, B. Ferrera, S.S. Chiaro, J. Dupont, On the extraction of aromatic compounds from hydrocarbons by imidazolium ionic liquids, Int. J. Mol. Sci. 8 (2007) 593-605.

[28] A.A.P. Kumar, T. Banerjee, Thiophene separation with ionic liquids for desulphurization: A quantum chemical approach, Fluid Phase Equilib. 278 (2009) 1-8.

[29] L. Alonso, A. Arce, M. Francisco, A. Soto, (Liquid+ liquid) equilibria of [C 8 mim][NTf 2] ionic liquid with a sulfur-component and hydrocarbons, J. Chem. Thermodyn. 40 (2008) 265-270.

[30] L.-L. Xie, A. Favre-Reguillon, S. Pellet-Rostaing, X.-X. Wang, X. Fu, J. Estager, M. Vrinat, M. Lemaire, Selective extraction and identification of neutral nitrogen compounds contained in straight-run diesel feed using chloride based ionic liquid, Ind. Eng. Chem. Res. 47 (2008) 8801-8807.

[31] S. Zhang, Q. Zhang, Z.C. Zhang, Extractive desulfurization and denitrogenation of fuels using ionic liquids, Ind. Eng. Chem. Res. 43 (2004) 614-622.

[32] U. Domanska, K. Walczak, Ternary Liquid-Liquid Equilibria for Mixtures of {Ionic Liquid + Thiophene or Benzothiophene + Heptane} at = 308.15 K, J Solution Chem 44 (2015) 382-394.

[33] X.-d. Tang, Y.-f. Zhang, J.-j. Li, Y.-q. Zhu, D.-y. Qing, Y.-x. Deng, Deep extractive desulfurization with arenium ion deep eutectic solvents, Ind. Eng. Chem. Res. 54 (2015) 4625-4632.

[34] M.A. Kareem, F.S. Mjalli, M.A. Hashim, M.K. Hadj-Kali, F.S.G. Bagh, I.M. Alnashef, Phase equilibria of toluene/heptane with deep eutectic solvents based on ethyltriphenylphosphonium iodide for the potential use in the separation of aromatics from naphtha, J. Chem. Thermodyn. 65 (2013) 138-149.

[35] Z. Helalat-Nezhad, K. Ghanemi, M. Fallah-Mehrjardi, Dissolution of biological samples in deep eutectic solvents: an approach for extraction of polycyclic aromatic hydrocarbons followed by liquid chromatography-fluorescence detection, J Chromatogr A 1394 (2015) 46-53.

[36] T. Gu, M. Zhang, T. Tan, J. Chen, Z. Li, Q. Zhang, H. Qiu, Deep eutectic solvents as novel extraction media for phenolic compounds from model oil, Chem. Comm. 50 (2014) 11749-11752.

[37] S.L. Perkins, P. Painter, C.M. Colina, Experimental and Computational Studies of Choline Chloride-Based Deep Eutectic Solvents, J. Chem. Eng. Data 59 (2014) 3652-3662.

[38] F.S. Oliveira, A.B. Pereiro, L.P. Rebelo, I.M. Marrucho, Deep eutectic solvents as extraction media for azeotropic mixtures, Green Chem. 15 (2013) 1326-1330.

[39] M.A. Kareem, F.S. Mjalli, M.A. Hashim, I.M. AlNashef, Liquid–liquid equilibria for the ternary system (phosphonium based deep eutectic solvent–benzene–hexane) at different temperatures: A new solvent introduced, Fluid Phase Equilib. 314 (2012) 52-59.

[40] S. Mulyono, H.F. Hizaddin, I.M. Alnashef, M.A. Hashim, A.H. Fakeeha, M.K. Hadj-Kali, Separation of BTEX aromatics from n-octane using a

(tetrabutylammonium bromide+ sulfolane) deep eutectic solvent–experiments and COSMO-RS prediction, RSC Adv. 4 (2014) 17597-17606.

[41] Y. Hou, Z. Li, S. Ren, W. Wu, Separation of toluene from toluene/alkane mixtures with phosphonium salt based deep eutectic solvents, Fuel Process. Technol. 135 (2015) 99-104.

[42] N.R. Rodriguez, P.F. Requejo, M.C. Kroon, Aliphatic–Aromatic Separation Using Deep Eutectic Solvents as Extracting Agents, Ind. Eng. Chem. Res. 54 (2015) 11404-11412.

[43] M. Sarwono, M. Hadj-Kali, I. Alnashef, Application of deep eutectic solvents for the separation of aliphatics and aromatics, Technology, Informatics, Management, Engineering, and Environment (TIME-E), 2013 International Conference on, IEEE, 2013, pp. 48-53.

[44] A. Sander, M. Rogošić, A. Slivar, B. Žuteg, Separation of Hydrocarbons by Means of Liquid-Liquid Extraction with Deep Eutectic Solvents, Solvent Extr. Ion Exch. 34 (2016) 86-98.

[45] N.R. Rodriguez, J. Ferre Guell, M.C. Kroon, Glycerol-based deep eutectic solvents as extractants for the separation of MEK and ethanol via liquid–liquid extraction, Journal of Chemical & Engineering Data 61 (2016) 865-872.

[46] M.C. Ali, Q. Yang, A.A. Fine, W. Jin, Z. Zhang, H. Xing, Q. Ren, Efficient removal of both basic and non-basic nitrogen compounds from fuels by deep eutectic solvents, Green Chem. 18 (2016) 157-164.

CHAPTER 2

Preparation and Prediction of Thermophysical Properties of DES

2.1 Introduction

Deep eutectic solvents (DESs) are solvents that have attracted academic community in recent years. These substances are created by the right blending of two or more compounds, which leads to a eutectic blend with low dissolving temperature [1]. The blending of a high-melting-point salt such as a hydrogen bond acceptor (HBA) (halogenated quaternary salt), and a hydrogen bond donor (HBD) such as ethylene glycol creates DES [2,3]. The number of possible HBA/HBD combinations resulting in DESs with melting points near to ambient temperature is exceptionally high according to literature [4,5]. Thus, DES can be used as multi task-specific fluids. The effective application of DESs includes technologies such as metal processing, solvent extraction, CO_2 capture and biomass dissolution [6,7]. DESs have numerous technological advantages which lie in their amalgamation within an economic and lucid manner. It is also known that some DES possess low toxicity, biodegradability, good recyclability which eventually invokes interest in the industry as well as scientific community [3,8,9]. DES have been considered as better substitutes to ionic liquids (ILs), due to its advantage concerning cost and certain toxicological issues when compared with Ionic Liquids [10].

For a better understanding of these DES mixtures require an exact information about their physicochemical properties and intermolecular interaction. Experimental studies concerning the measurement of their thermodynamics properties have been recently reported in literature [11-13]. However, considering the huge number of conceivable HBA/HBD combinations and to get a reasonable structure-property relation, insights with respect to the properties of DESs at the nanoscopic level study is required. For this reason, computational chemistry tools such as Density Functional Theory and classical molecular

dynamics (MD) simulations have been effectively applied in order to obtain a profound knowledge about the properties of DESs [14-17]. It is exactly this part that the current work has considered both structural properties and dynamics of the DES components together as a single moiety in liquid phases. This study will hence help us to explore its physiochemical and thermophysical properties at molecular level for its effective applicability. Considering this fact, we report a comprehensive study concerning both experimental analysis and classical MD simulations to explain their liquid behavior.

In recent years, DESs are used for liquid liquid extraction (LLE) of various organic compounds [7,18-20]. The application of ammonium and phosphonium based DES have been studied recently with respect to their physiochemical properties along with their aromatic extraction [21-23]. It was reported that the halide based quaternary ammonium and phosphonium salt easily mixes with HBD to form DESs which were found to be highly selective for aromatic compounds. Their usefulness is further enhanced in advantages such as low viscosity and density. For e.g., it has been used for the purification of fuel through LLE process where Hizaddin et al. [21] have adopted the quaternary ammonium and phosphonium based DESs for denitrification. Due to the favorable aspects of quaternary phosphonium and ammonium salts, the current work has adopted HBA comprising of a phosphonium and ammonium based DES.

The HBA namely methyltriphenylphosphonium bromide (MTPB) and tetrabutylammonium bromide (TBAB) have been used in this work along with HBD such as ethylene glycol and glycerol. This has paved us for the creation of four new DES comprising the combination of the HBA (phosphonium or ammonium salt) and HBD (ethylene glycol and glycerol). These HBA and HBD are combined in different

combination to produce four sets of DES in the molar ratio of 1:4. Thereafter MD simulations were carried out to study the non bonded interaction between the HBD and HBA which are the key factors for the formation of DES. We shall initially discuss the experimental details and then demonstrate MD simulations.

2.2 Experimental Section

2.2.1 Chemicals Used

Methyltriphenyl phosphonium bromide (MTPB) and tetrabutyl ammonium bromide (TBAB) were purchased from SRL India. Ethylene glycol and glycerol ware obtained from Merck, India. The chemicals, the source and their purity are presented in Table 2.1. The chemicals were of analytical grade and used without further purification.

Table 2.1: Chemicals and their sources with purity

Chemical name	**CAS number**	**Source**	**Purity**	**Water content (ppm)**
Methyltriphenyl phosphonium Bromide	1779-49-3	SRL, India	>99%	--
Tetrabutyl ammonium Bromide	1643-19-2	SRL, India	>99%	--
Ethylene Glycol	107-21-1	Merck, India	>98%	102
Glycerol	56-81-5	Merck, India	>98%	86

2.2.2 Analysis of Water Content in Chemicals

A Karl Fischer titrator (Metrohm, 787 KF Titrino, Switzerland) was used to determine the water content of ethylene glycol, glycerol and the prepared DES. The salt MTPB and TBAB is hygroscopic when in contact with air. Hence, we have dried the salts in the oven for 12 hours to remove the moisture content before preparing the DESs. Thereafter the prepared DESs were kept in a vacuum oven drier at 40 °C and 380 mm Hg for 24 h in order

to remove the moisture content [24]. Further, ^{1}H NMR spectrum of the DES was also performed. It is evident that an absence of peak at 3.5 ppm corresponds to negligible moisture content.

2.2.3 Preparation of DES

Appropriate weights of the chemicals were measured using a Denver instrument (SI-234) balance with a precision of 0.01 mg. Proper amounts (molar ratio of 1:4) of the HBA (MTPB or TBAB) and the HBD (ethylene glycol or glycerol) (Table 2.2) were mixed and then heated at 60°C under continuous stirring until a clear homogeneous liquid was observed (Figure 2.1). The molar ratio 1:4 was chosen because the salt is a solid and it has to completely mix to form a clear liquid [25]. The temperature was controlled using a hot magnetic plate with continuous temperature monitoring system. Overall, the water content of the DESs were found to be lower than 0.01 wt% (Table 2.3).

Figure 2.1: Formation of DESs with HBA and HBD ratio of 1:4

2.2.4 Analysis Methods

Initially thermo physical properties such as density were measured using Anton Paar DMA 4500M (Table 2.3). The density meter uses the oscillating U-tube sensor principle and has a reported accuracy of 0.0005 $g \cdot cm^{-3}$ in density and ±0.05 K in temperature. Refractive indices were also measured relative to the sodium D-line ($\pm 1 \times 10^{5}$) using an automated

Leica AR600 refractometer (Table 2.3). A standard supplied by the manufacturer was used for refractometer calibration. The viscosities of the DESs were measured using an interfacial Rheometer (MCR 301, Anton Paar, Austria) with an accuracy of 0.001 mPa·s in viscosity and ±0.05 K in temperature. All the measurement were performed at room temperature (25°C) (Table 2.3).

Table 2.2: DESs synthesized in the current study

Name	HBA[a]	HBA:HBD ratio	HBD[b]
DES1	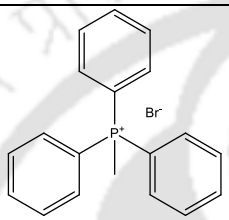 Methyltriphenyl phosphonium Bromide	1:4	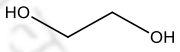 Ethylene Glycol
DES2	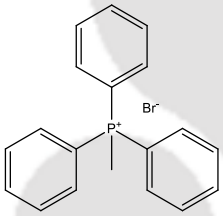 Methyltriphenyl phosphonium Bromide	1:4	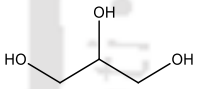 Glycerol
DES3	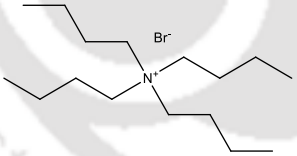 Tetrabutyl ammonium Bromide	1:4	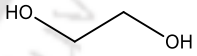 Ethylene Glycol
DES4	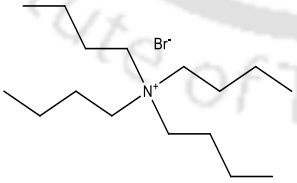 Tetrabutyl ammonium Bromide	1:4	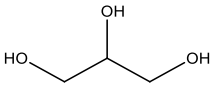 Glycerol

[a] MTP (Methyltriphenyl Phosphonium cation), TBA (Tetrabutyl Ammonium cation), Br (Bromide anion), [b] ETH (Ethylene glycol), GLC (Glycerol)

Table 2.3: Experimental and predicted density and properties of DESs at 298.15K

DES	Experimental Density (ρ/g·cm^{-3})	Simulated Density (ρ/g·cm^{-3})	Refractive Index (n_D)	Viscosity (η/mPa·s)	Water content (ppm)
DES1	1.232	1.268	1.556	64.482	98
DES2	1.292	1.303	1.550	351.691	79
DES3	1.079	1.087	1.465	41.514	97
DES4	1.154	1.156	1.485	333.907	82

Standard uncertainty u are u (T) = 0.05 K, u (p) = 1 kPa, u (ρ) = 0.0005, u (n_D) = 0.005 and u (η) = 0.001 mPa·s

Further ^{1}H NMR spectra in $CDCl_3$ solvent were obtained on the DES samples using 600 MHz NMR spectrometer (Bruker). The formation of DES was also examined and confirmed using a Fourier transform infrared (FTIR) spectrometer (Spectrum 400, PerkinElmer, USA). The thermo gravimetric analysis (TGA) of DESs ware performed on a Mettler Toledo thermo gravimetric analyzer (TGA/SDTA 851® model). Samples were heated from 30 to 700 °C in a 60 ml/min flow of N_2 at a heating rate of 1 °C per min. For the FTIR measurements, the DES liquid was placed on a polished KBr window in order to record the IR spectra using a Perkin Elmer 6700 FTIR spectrometer. The spectra were obtained at a resolution of 400 cm^{-1} using 16 interferometer scans. After the experimental preparation procedure, we now move on to discuss its implementation in Molecular Dynamics simulations.

2.3 Computational Details for Molecular Dynamics Simulation

Initial geometries of HBA and HBD were constructed using Gauss View 05 [26] (Fig. 1). These optimized geometries were obtained at the B3LYP/6-31G* level of theory [14],

while the partial charges were obtained using the restrained electrostatic potential (RESP) [27] charge derivation method using the Gaussian 09 software package [28]. The lowest energy structure of the compounds were taken for further calculations. The generalized amber force field (GAFF) functional form and its force field parameters were used in MD calculations [29]. A short description of the AMBER force field is given in Appendix-A. HBA, HBD or DES were described using the ANTECHAMBER [30] mode of AMBER 12 [31]. The initial configuration of solvent molecules in each system was generated using Packmol [32]. Cubical box lengths for the systems containing the entire molecule were of side 40Å each. Three-dimensional periodic boundary conditions were employed in order to mimic a bulk system. MD simulations were carried out for simulation boxes containing 100 HBA ion pairs and 400 HBD molecules for 1:4 DESs. All molecular dynamics simulations were run using NAMD 2.9 [33]. The system was energy minimized prior to a MD run under constant NVT conditions for a time period of 0.5 ns.

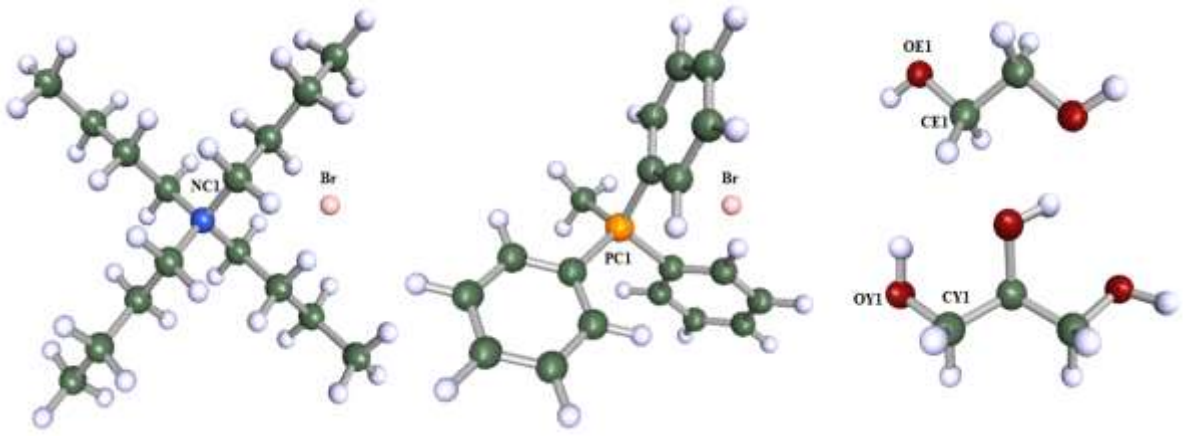

Figure 2.2: Structure and atomic labels for the tetrabutylammonium bromide (TBAB) (left), methyltriphenylphosphonium bromide (MTPB) (middle), ethylene glycol (ETH) (top right), and glycerol molecule (bottom right)

After minimization, the system was gradually heated to bring it to the desired room temperature. Subsequently, the systems were studied under constant NPT conditions for 8 ns of equilibration in order to bring the system under stable condition. The Langevin dynamics thermostat was used with a collision frequency of 5 ps^{-1} in order to ensure accurate temperature control [34]. The SHAKE algorithm was applied to constrain the bonds attached to hydrogen atoms in the system [35]. The PME procedure was implemented to calculate long-range electrostatic interactions. A constant NVT production run of 25 ns after equilibration was used for predicting the average thermodynamic property and structural analysis. The final configuration constituted an analysis from VMD software [36]. Simulations in the NVT and NPT ensembles were carried out with pressure and temperature controlled via the Nose-Hoover thermostat [37,38]. The Ewald method was applied for Columbic interactions. The equations of motion were solved using the velocity verlet step algorithm. Equations of motion were integrated with 0.5 fs time step. All the analyses were carried out in the last 10 ns of the NAMD trajectory.

2.4 Results and Discussion

2.4.1 Eutectic Behaviour

Deep Eutectic Mixtures or solvent refers to the mixing of a hydrogen bond donor (HBD) and hydrogen bond acceptor (HBA) so as to form a liquid phase. This is primarily attributed to the hydrogen bond appearing between active sites of donor and acceptor. The variation in molar ratio of HBD and HBA can significantly affect their physical properties such as eutectic temperature, density and viscosity [16,39-46]. A comparison with other DES having similar HBA or HBD can be found in Table 2.4.

Table 2.4: Comparison of eutectic point and physiochemical properties of DES having similar HBA or HBD

Sl.No.	HBA	HBD	Molar ratio	$T_{eutectic}$/°C	Density (ρ/g·cm^{-3})	Viscosity (η/mPa·s)	Refractive Index(n_D)	Reference
1	Tetrabutylammonium bromide	Levulinic acid	1:4	<-60	1.1061	252	1.4696	[39]
2	Methyltriphenylphosphonium bromide	Triethylene glycol	1:4	-18	1.186	645	1.5178	[40]
3	Choline chloride	Ethylene glycol	1:2	-66	1.1171	44.4	1.4691	[41,42]
4	Tetrapropylammonium bromide	Ethylene glycol	1:4	-23	1.1339	70.3	1.4677	[43]
5	Tetrabutylammonium chloride	Ethylene glycol	1:3	-31	1.0263	85.6	1.4635	[44]
6	N,N-diethylethanolammonium chloride	Ethylene glycol	1:2	-31	1.0987	50.6	1.465	[40,45]
7	Tetrabutylammonium chloride	Glycerol	1:4	-43	1.1714	816	1.4768	[44]
8	Tetrapropylammonium bromide	Glycerol	1:3	-16	1.1924	739	1.4872	[43]
9	Propylammoniun bromide	Glycerol	1:2	-4	1.328	398	1.495	[46]
10	Ethylammonium bromide	Glycerol	1:2	-6	1.358	307	1.497	[46]
11	Butylammonium bromide	Glycerol	1:2	-10	1.293	421	1.492	[46]
12	N,N-diethylethanolammonium chloride	Glycerol	1:2	-1	1.1131	513	1.4853	[40,45]
13	Methyltriphenylphosphonium bromide	Ethylene glycol	1:4	-50*	1.232	64.5	1.556	This work
14	Methyltriphenylphosphonium bromide	Glycerol	1:4	15*	1.292	351.7	1.550	This work
15	Tetrabutylammonium bromide	Ethylene glycol	1:4	-30*	1.079	41.5	1.465	This work
16	Tetrabutylammonium bromide	Glycerol	1:4	10*	1.154	334	1.485	This work

An interesting point here lies in the fact that a eutectic mixture of 1:1.175 for MTPB:Glycerol has been reported earlier [47]. A similar observation is also obtained in literature where a similar HBA namely MTPB has given different eutectic points with the same HBA (glycerol) namely 1:2, 1:3 and 1:4 [48]. In the same work cited with Ethylene Glycol as HBD also points out to different eutectic ratios namely 1:3, 1:4 and 1:5. This implies that variation in HBD leads to eutectic mixtures having difference in eutectic composition as well as temperature. This inherently implies that the tradeoff between enthalpic (temperature) and entropic forces (physical state) is indeed a critical property which needs to be addressed in greater detail in our work for DES2 (Table 2.2). This effect can be primarily attributed to the hydrogen bond appearing between active sites of donor and acceptor. This implies in order to sample the entire phase, the –OH group of glycol or ethylene glycol scans the anionic part of HBA i.e. Br ion for potential hydrogen bonding. It results in the requirement of increased entropy which can only exist in liquid phase and or conformers with different molar ratio. This is the reason that a particular ratio and temperature balances the increased entropy required for liquid phase formation.

In order to confirm this phenomenon, we have predicted the Solid Liquid Equilibria (SLE) phase diagram using the well-known and documented COSMO-SAC (Conductor like Screening Model Segment Activity Coefficient) model. The details of the COSMO-SAC can found in literature [49,50]. A brief description of the COSMO-SAC model along with the solubility thermodynamics involved in prediction of the solid liquid equilibria (SLE) is discussed in Appendix-A (Section A.2). In addition, the sigma profiles and sigma potential of each starting material of the DES are also provided in Appendix-A (Section A.3, Figs. A.2-A.3).

A close inspection on the sigma profile (Fig. 2.3) and sigma potential (Fig. 2.4) reveals the hydrogen bonding nature between the donors and acceptors. This can be ascertained due to the part of profile lying to the far side of the cut off region for hydrogen bonding (dashed line,±0.0084 e/Å2) indicates a negative value of chemical potential (Fig. 2.4). The negative value arises from the sum of two contributions namely restoring free energy (+ve in nature) and the hydrogen bond energy (-ve in nature).

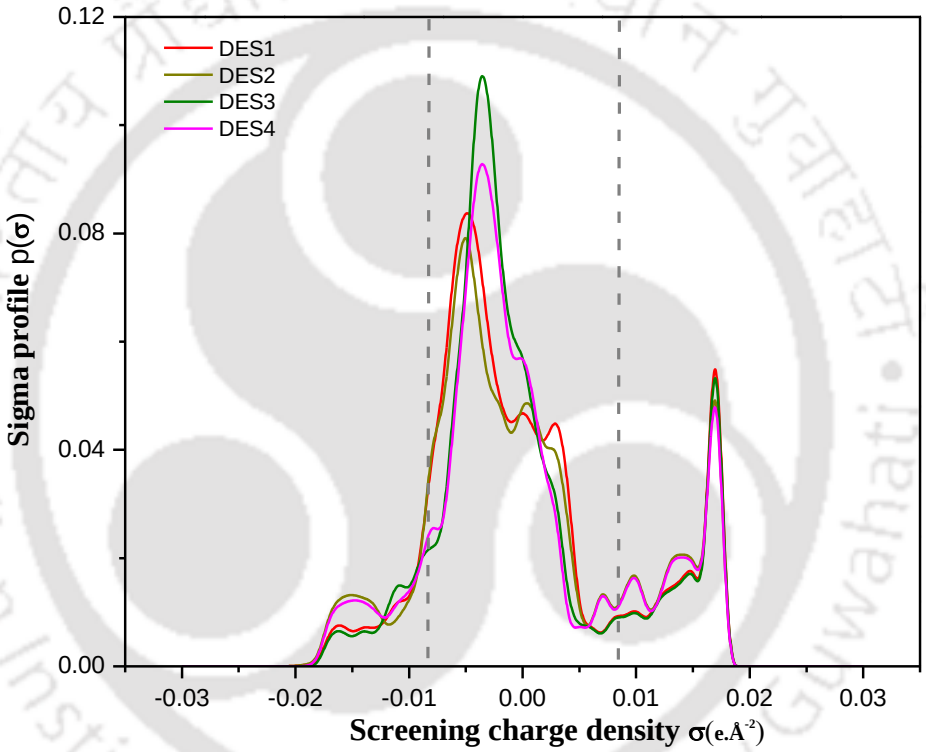

Figure 2.3: σ-Profiles of the DESs used in this work. The dashed vertical lines represent the threshold value for the hydrogen bond interaction, σ_{hb} = ± 0.0084 e.Å^{-2}

The SLE phase diagram (Fig. 2.5) for the DESs are predicted to conform its eutectic point (composition and temperature). The predictions agree with the literature [48] referring to the phosphonium (DES 1 and DES 2) reported in this work (Figs. 2.5a-2.5b). For the other set of DES i.e. tetrabutylammonium (DES 3 and DES 4) (Figs. 2.5c-2.5d), a

comparison could not be done as the experimental data were not available. It is clear that the obtained ratio of HBA to HBD is 1:4 as observed from COSMO-SAC predictions.

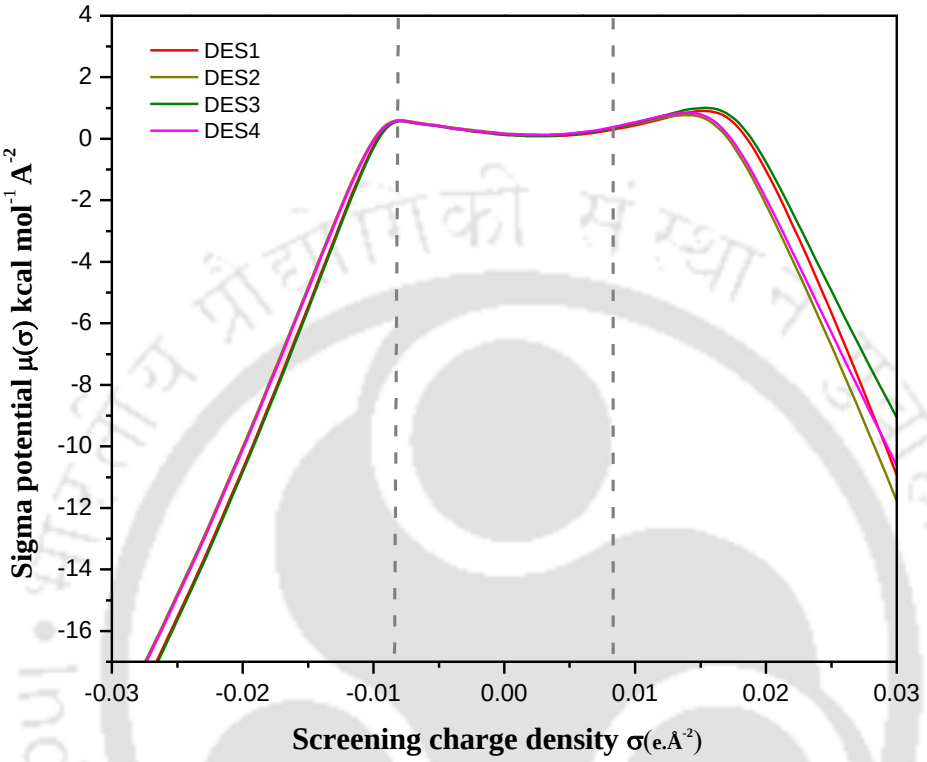

Figure 2.4: σ-Potential of the DESs used in this work. The dashed vertical lines represent the threshold value for the hydrogen bond interaction, σ_{hb} = ± 0.0084 e.Å^{-2}

2.4.2 Physical Properties

2.4.2.1 FTIR Analysis

The structure of DESs were investigated with FTIR (Fig. 2.6) to explore the type of interactions along with the atoms involved in the interactions of the two components. The FTIR spectra of the four DES were recorded at room temperature. The infrared spectroscopic results for the 1:4 molar mixture gave no detectable free (non-hydrogen bonded) groups. IR spectroscopy is very sensitive to hydrogen bonding interactions and the useful regions are the OH stretching modes observed between 3600 and 3000 cm-1

[51]. Typically, OH—OH hydrogen-bonded groups in alcohols appear near 3350 cm−1, and here the lower frequency of the OH stretching mode suggests that it is engaged in much stronger hydrogen bonds. The –OH stretching vibration of DES shifts to lower wavenumber, indicating that –OH of ethylene glycol or glycerol takes part in the formation of the hydrogen bond with the anion of HBA [11,52].

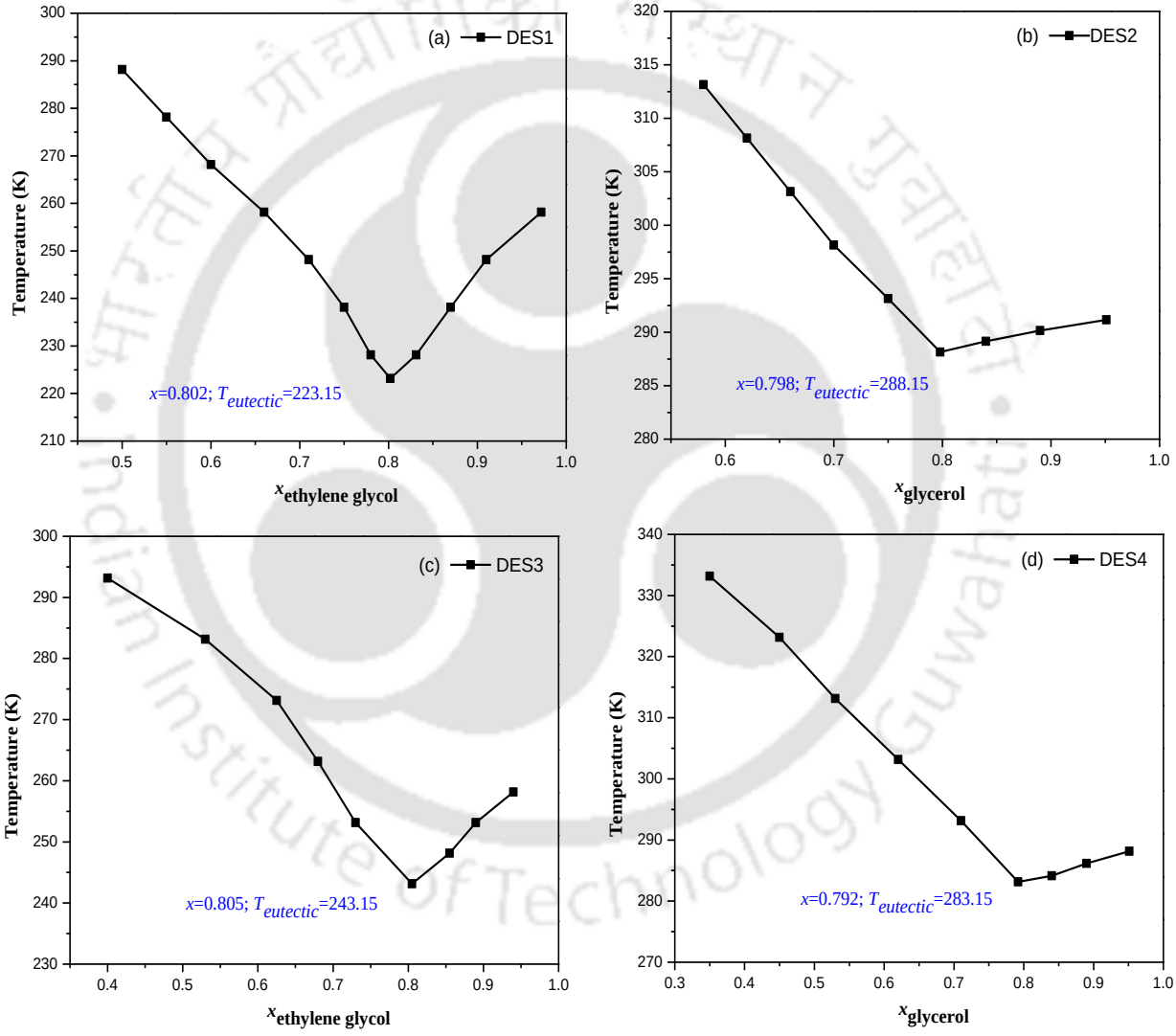

Figure 2.5: COSMO-SAC predicted solid liquid phase diagram with eutectic composition and temperature for (a) DES1(x=0.8; $T_{eutectic}$=223.8 K [48]), (b) DES2 (x=0.8; $T_{eutectic}$=288.9 K [48]), (c) DES3 and (d) DES4 (DES as per Table 2.2)

These regions of the spectrum are shown in Fig. 2.6 where the spectrum of the DES mixtures are compared. It can be seen that there are no significant changes in the regions of the spectrum upon formation of the DES. All the four DESs possess similar pattern with respect to the relative transmittance.

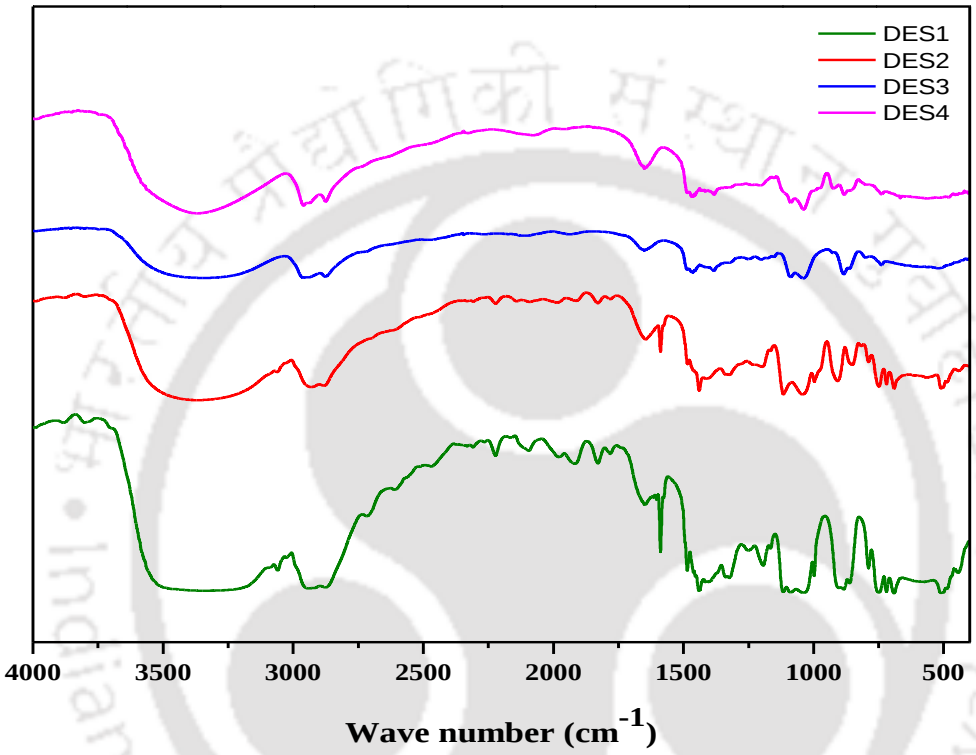

Figure 2.6: FTIR spectra of studied DESs

2.4.2.2 TGA Analysis

TGA is the most commonly used technique to investigate the thermal stability. Figure 2.7 represents the TGA profiles of the DESs. The deep eutectic solvents have shown a wide variation in their thermal degradation phenomena, which is clearly visible in Fig. 2.7 for both the systems. For the DES1 and DES2 system, the first weight loss occurs near 200°C and the second major weight loss takes place at 300 °C. For the second major loss, there is a gradual loss when the sample is heated from 300 °C to 700 °C, thereby leaving a

residual mass. For DES3 and DES4 the degradation of DESs takes place in a narrow temperature range starting at 150 °C with gradual loss up to 300°C (Fig. 2.7b). However, there are no significant visible second loss here. In TGA analysis, the MTPB based DES (Fig. 2.7a) has a pronounced two stage mass loss as compared to the TBAB based DES [53].

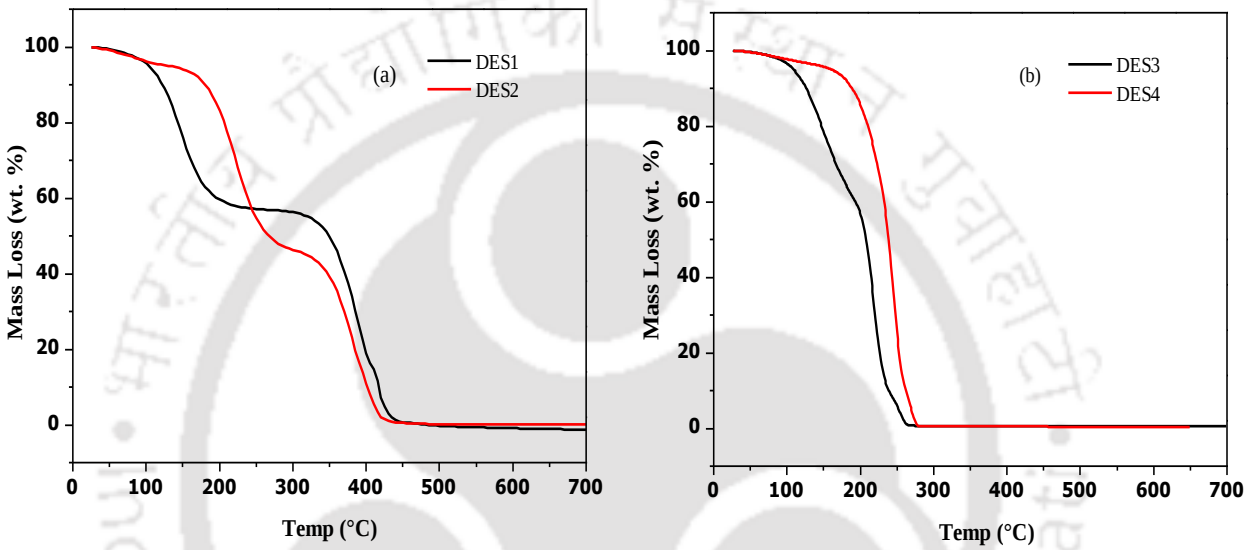

Figure 2.7: Thermo gravimetric (TGA) curve of DESs at heating rate of 1°C/min under nitrogen atmosphere

The gradual and slow mass loss along with the rise of temperature suggests that phosphonium based DES forms a more stable solvent as compared to ammonium base DES. The comparison study of thermal stability with some other ionic liquid and DES with current one suggest that these DES are having a better result (Table 2.5).

2.4.2.3 ^{1}H NMR Analysis

For DES, we have adopted an approach, which relates the number of hydrogens with their areas to the functional groups of HBA and HBD in their respective DES. This method can be successfully applied for the determination of experimental tie lines in liquid–liquid

equilibria studies [20,54]. Here the area of a certain peak was counted as unity and taken as the reference. The area of other peaks were then integrated with reference to unity or with the reference peak.

Table 2.5: Comparison of thermal stability of studies DES with other literature

Sl.No.	DES/ IL	Decomposition Temperature	Reference
1	Allyltriphenylphosphonium bromide + Diethylene glycol(1:4)	178	[55]
2	Allyltriphenylphosphonium bromide + Triethylene glycol(1:4)	204	[55]
3	Choline chloride + Urea(1:2)	172	[56]
4	Choline chloride + Ethelene glycol(1:2)	90	[56]
5	Choline chloride + glycerol(1:2)	175	[56]
6	1-ethyl-3-methyl-imidazolium tetra-fluoroborate	413	[57]
7	1-butyl-3-methyl-imidazolium tetra-fluoroborate	399	[57]
8	1-ethyl-3-methyl-imidazolium acetate	221	[57]
9	1-butyl-3-methyl-imidazolium acetate	216	[57]
10	1-butyl-3-methyl-imidazolium bromide	272	[57]
11	1-octyl-3-methyl-imidazolium chloride	276	[57]
12	N-butyl-pyridinium bis(tri-fluoromethylsulfonyl)imide	390	[57]
13	N-butyl-pyridinium nitrate	263	[57]
14	Tetra-butylphosphonium bromide	356	[57]
15	DES1	390	This work
16	DES2	384	This work
17	DES3	220	This work
18	DES4	244	This work

This method is particularly useful to locate peaks of compounds in mixtures. The ^{1}H NMR spectra for the four DES are shown in Figs. 2.8-2.11. In this work (Fig. 2.8) the chemical shift between 6.0 and 7.7 ppm was assigned to the three benzyl ring $–C_6H_5$ (15 hydrogen atoms) which has an area of 37.88, implying a contribution of 2.52 (i.e 37.88/15) for each hydrogen atom for MTPB. The summation of two $–CH_2$ groups within ethylene glycol (i.e four hydrogen atoms) at 3.5 ppm gave us a peak area of 38.21. This when divided by 16 (i.e the number of atoms in four HBD molecule) gives us 2.38 which is ~2.52 as obtained for MTPB. This confirms a molar ratio of 1:4 i.e. mixture of one molecule of HBA and four molecules of HBD. The above chemical shifts also verify the range as reported in the literature [58]. On similar lines, the molar ration of other DES is also obtained. This confirms the fact that there is no chemical reaction between them to produce new compounds as evident in the absence of an extra peak in the spectra. The ^{1}H NMR spectra of all starting material and 2D-NOSEY spectra of DES are provided in Appendix-A (Section A.4). NOESY analysis reveals H−H interactions between HBA and HBD indicated by the contours above and below the diagonal (Figures A.8 - A.11).

2.4.3 Non-Bonded Interaction Energies

Once the physiochemical properties were evaluated, the intermolecular insights were then obtained through MD simulations. To quantify the interactions between different system species, we have decomposed the total non-bonded interaction energies into electrostatic and van der Waals (vdW) components as shown in Table 2.6. The different components of total nonbonded interaction energies were calculated from the MD simulation. It can be observed that the nonbonded interaction of HBD and bromide anion is higher or in other words, HBD-Br interaction is higher than MTP-Br or MTP-HBD interaction.

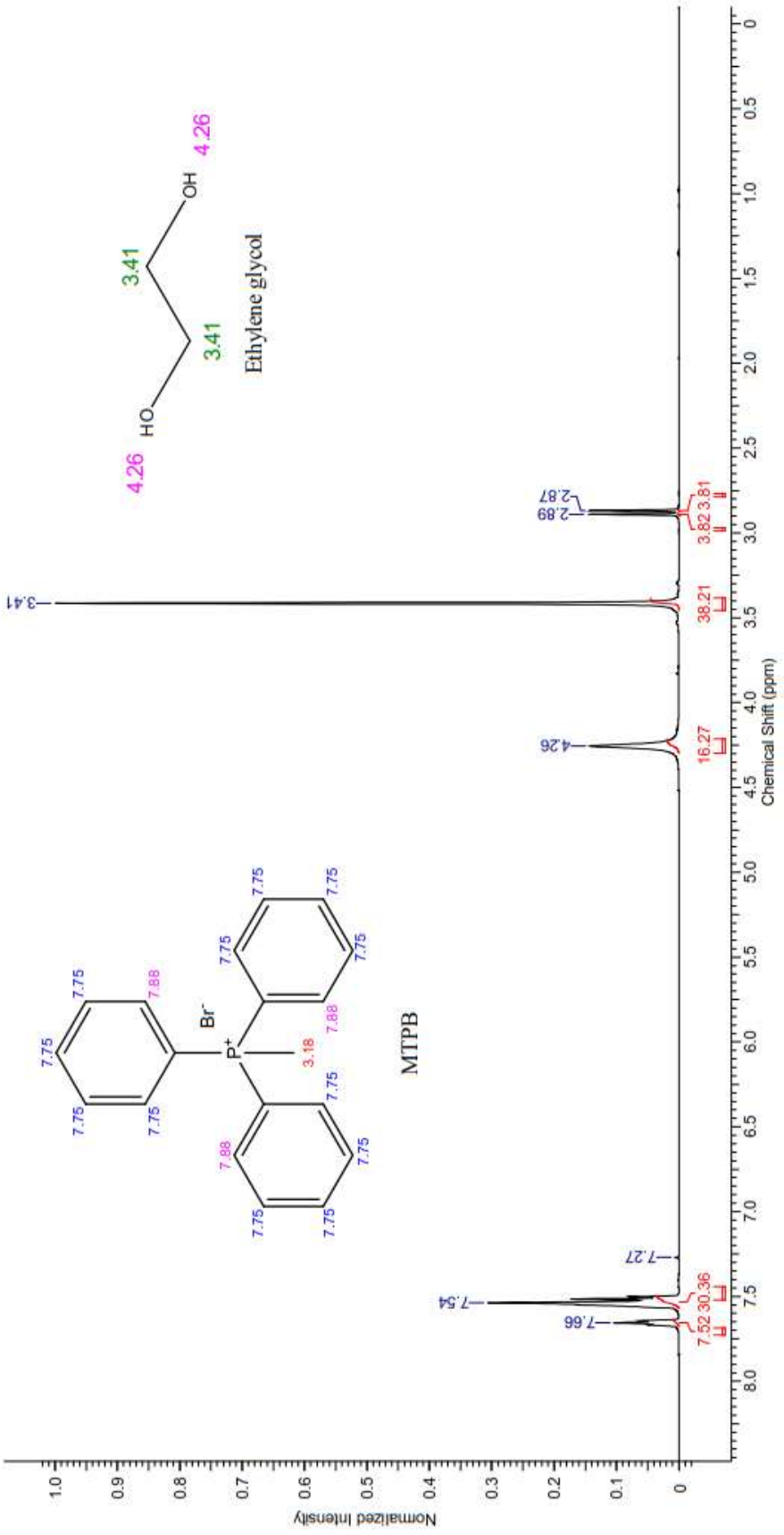

Figure 2.8: ^{1}H NMR spectra of DES1

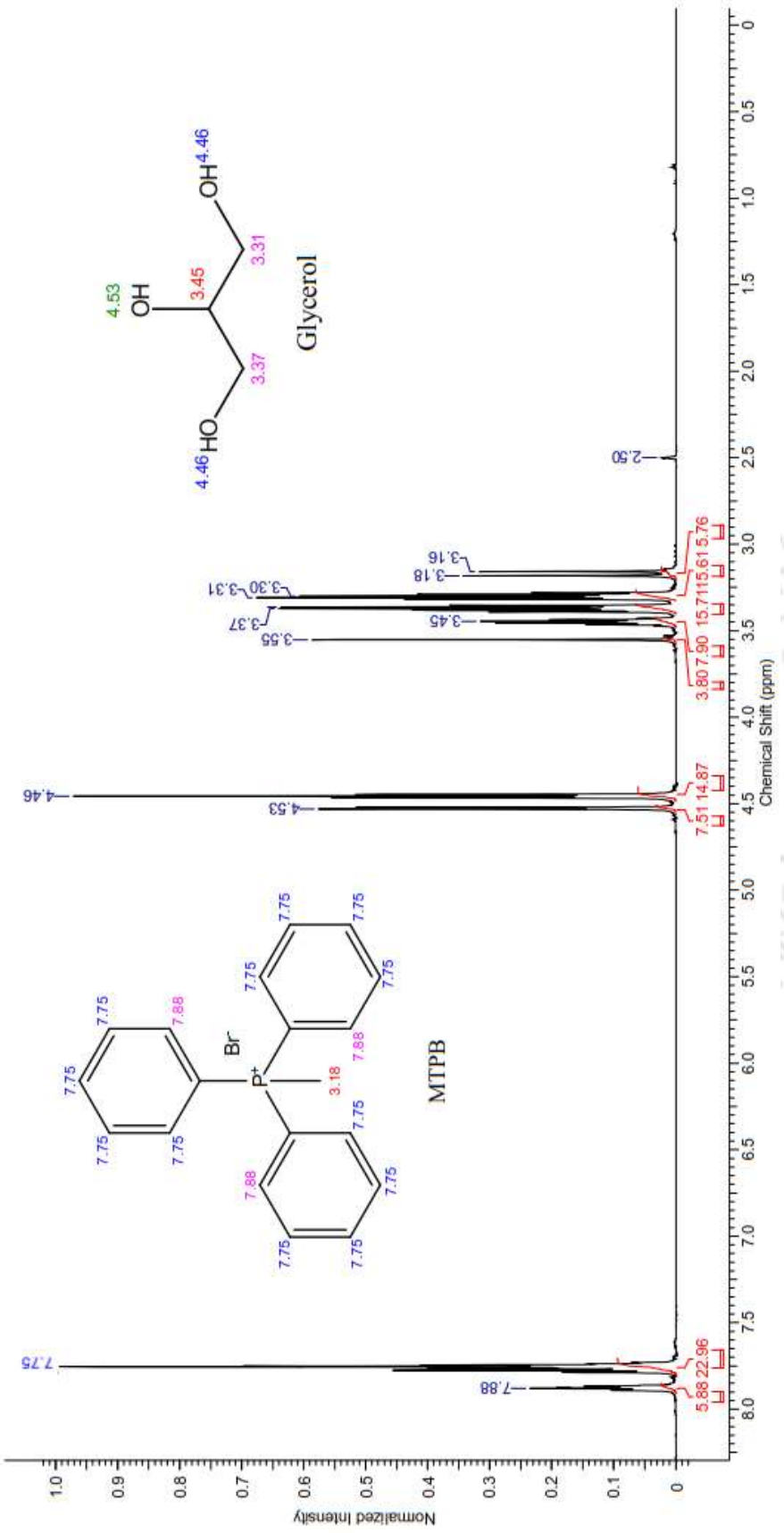

Figure 2.9: ^{1}H NMR spectra of DES2

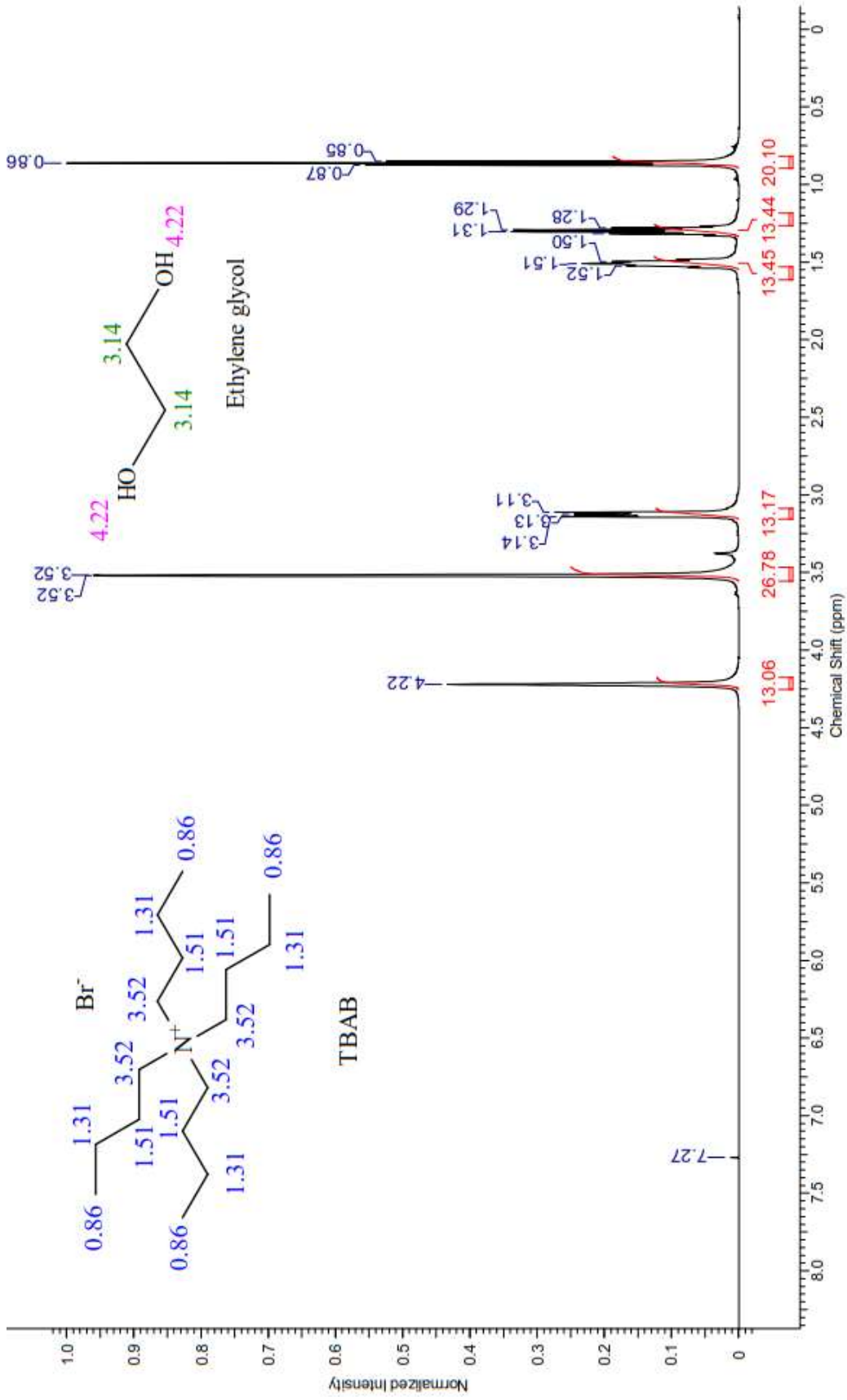

Figure 2.10: ^{1}H NMR spectra of DES3

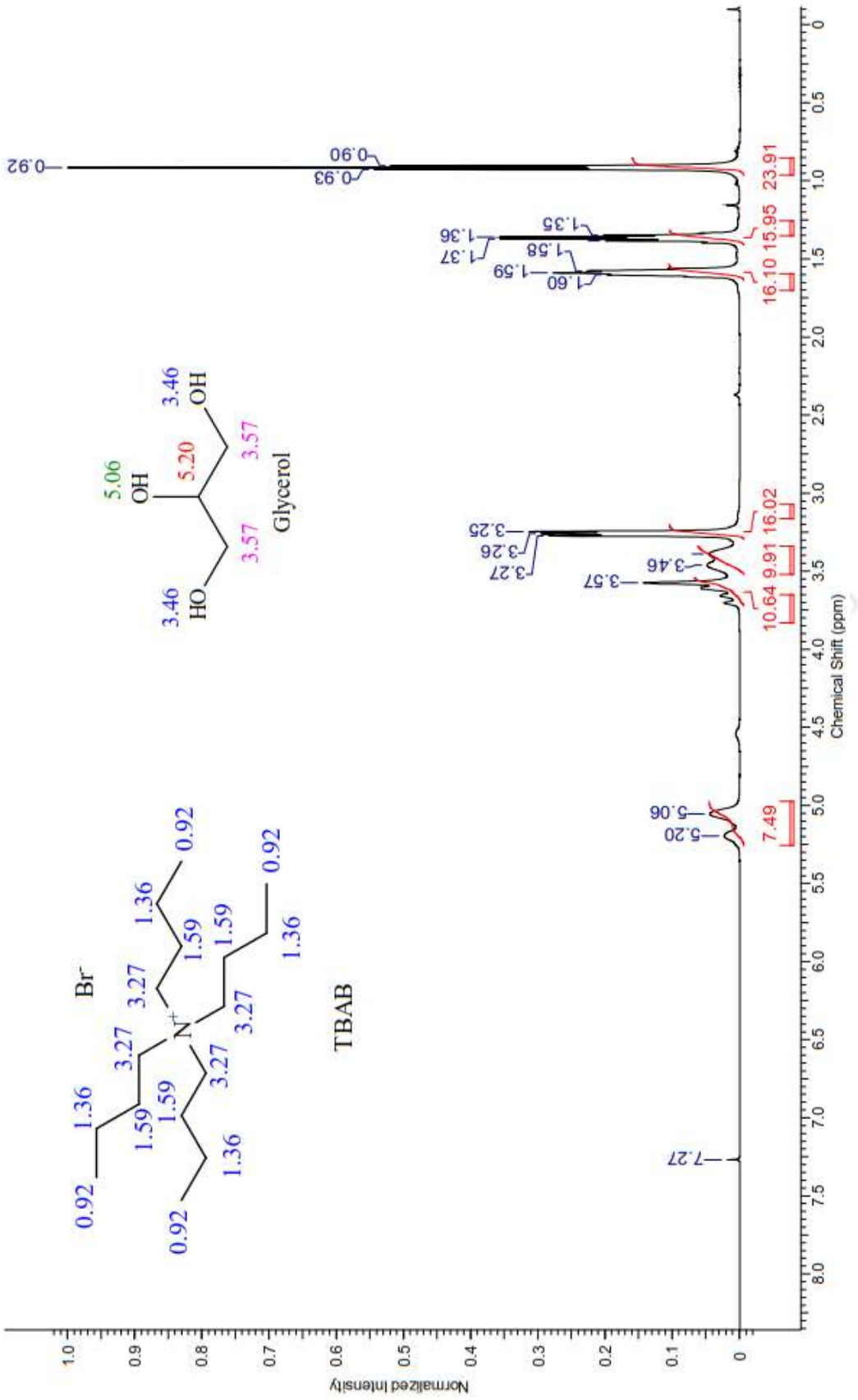

Figure 2.11: ^{1}H NMR spectra of DES4

From Table 2.6, the van der Waals interaction energy between the HBA cation (MTP) and the HBD (ETH or GLC) was prominent in comparison with the electrostatic energy component. However, in all the cases the Br anion of the HBA (MTP) has a twenty fold higher electrostatic interaction energy with the HBD group (ETH or GLC) when compared to its vdW interaction.

Table 2.6: Non-bonded interaction energy within DES[a]

DES	Interacting species	Electrostatic interactions ($kJ \cdot mol^{-1}$)	vdW interactions ($kJ \cdot mol^{-1}$)	Non-bonded interactions ($kJ \cdot mol^{-1}$)
DES1	MTP-ETH	-48.98	-98.22	-147.20
	MTP-Br	-78.66	-9.57	-88.23
	ETH-Br	-362.80	28.61	-334.19
DES2	MTP-GLC	-45.20	-120.44	-165.64
	MTP-Br	-52.15	-9.65	-61.80
	GLC-Br	-241.83	8.93	-232.90
DES3	TBA-ETH	-23.43	-105.92	-129.35
	TBA-Br	-62.14	-13.48	-75.61
	ETH-Br	-221.56	13.75	-207.81
DES4	TBA-GLC	-25.45	-124.82	-150.27
	TBA-Br	-63.61	-12.34	-75.96
	GLC-Br	-238.12	11.26	-226.86

[a] Nomenclature as per Table 2.2 and Fig. 2.2

Further, the least favorable interaction among these species is the HBA-Br interaction or the cationic and halide interaction. This implies that the ionic interaction between the MTP and Br reduces drastically when in combination with HBD. This explains the eutectic nature of the mixture. Overall, the degree of interaction energy is found to be in the following order: HBD-Br anion > HBA cation-HBD > HBA cation-Br anion. Within the

four DES, DES1 and DES2 having slightly higher total non-bonded energy when compared to DES3 and DES4. The HBD-Br interaction can be seen as the dominating one owing to their higher electrostatic energies, which is short range in nature. This eventually to the formation of hydrogen bonds between the HBA and HBD moieties, which is similar in line with the ionic liquid formation [59]. Hence, the choice of the anionic part of HBA is crucial in realizing certain applications such as separation or extraction. This is also confirmed from the RDF plots, which are discussed later.

2.4.4 Radial Distribution Function

The RDF were plotted both within the (HBA and HBD) and interspecies i.e. HBD-HBD or HBA-HBA. In order to obtain additional insight into the interactions involved in the formation of 1:4 molar ratio in DES, average radial distribution functions (RDF) curves of the HBA cation and HBD molecule relative to the anion(Br) were computed at 25°C (Figs. 2.12-2.13).

Figure 2.2 indicates the structure and atomic labels used for computation of RDF. This RDF gives information about positions of atom-atom pairs as a function of their outspread separation. The first peaks of the function relate to the first solvation shell (Table 2.7). Figure 2.12 shows the interspecies RDF for the different DES. The central phosphonium atom for the methyltriphenyl phosphonium (MTP) cation and the oxygen atom for the ethylene glycol (ETH) or glycerol (GLC) molecules were selected for calculating RDF (Figs. 2.12a-2.12b).

One prominent peak near 3 Å with a very subtle shoulder can be seen in all cases for the HBD and the Br atom. On the other hand, there are no significant peak observed for the RDFs of MTP-ETH and MTP-Br indicating that each of the hydrogen atoms in the

groups are equally favorable for interaction. Similarly, the central nitrogen atom for the tetrabutyl ammonium (TBA) cation and the oxygen atom of HBD was considered for RDF (Figs. 2.12c-2.12d).

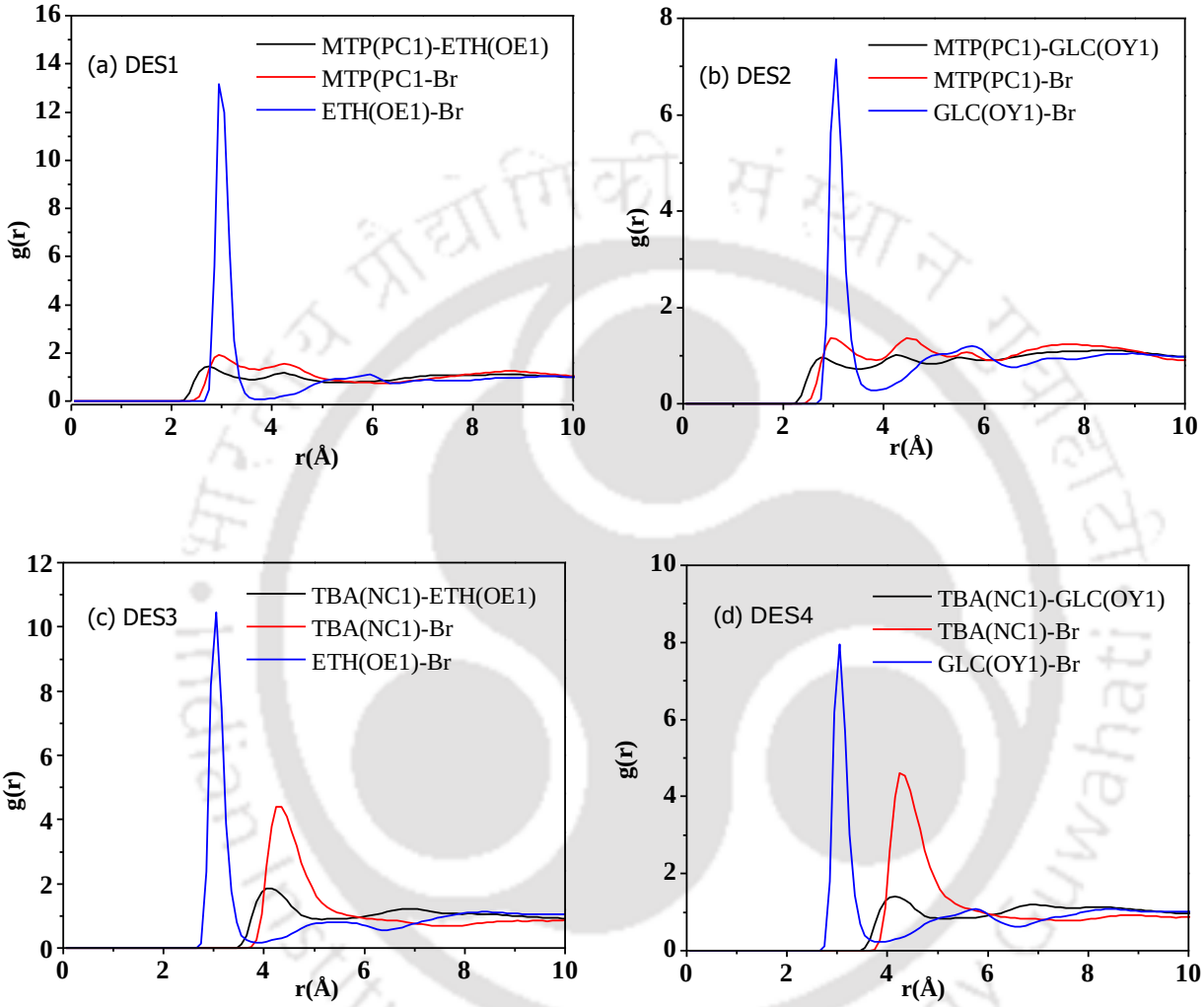

Figure 2.12: RDF plots within functional entities/groups of DES (Nomenclature as per Table 2.2 and Fig. 2.1)

The HBD group and the bromide anion of the DESs possess strong interaction when compared to other ion pairs. This is also evident from the magnitude of the electrostatic interactions as discussed in the previous section. However, it is to be noted that the

phosphonium based DESs shows less interaction between the cation and the anion as compared to HBD. So in terms of extraction capability, phosphonium based DES can be recommended owing to its higher interaction with the HBD through the halide ion.

The cation-cation radial distance in all cases was roughly 6-10 Å for all DES. This is three times more than inter species distances (MTP-HBD or HBD-Br). The main reason behind this phenomenon is the ability for the formation of hydrogen bond between HBD and HBD (HBD-HBD or O-O). Overall HBD thus possess hydrogen bonds with itself as well as with the Br ion. Thus it can be said that the sphere of influence of the HBD and halide (Br) ion is complimentary and results in inter as well as intramolecular hydrogen bonding.

Table 2.7: Coordination number (CN), peak distance, and hydrogen bonding between different components of DES[a]

DES	Interacting species	CN	r (Å)	Number of H-bonds
DES1	MTP-ETH	0.227	2.75	3.915
	MTP-Br	0.075	2.95	0.166
	ETH-Br	1.038	2.95	5.413
DES2	MTP-GLC	0.090	2.75	4.851
	MTP-Br	0.075	2.95	0.236
	GLC-Br	0.176	3.05	3.777
DES3	TBA-ETH	0.900	4.15	3.635
	TBA-Br	0.298	4.25	0.760
	ETH-Br	1.057	2.95	3.887
DES4	TBA-GLC	0.761	3.95	4.010
	TBA-Br	0.275	4.25	0.706
	GLC-Br	0.181	3.05	3.898

[a] Nomenclature as per Table 2.2 and Fig. 2.2

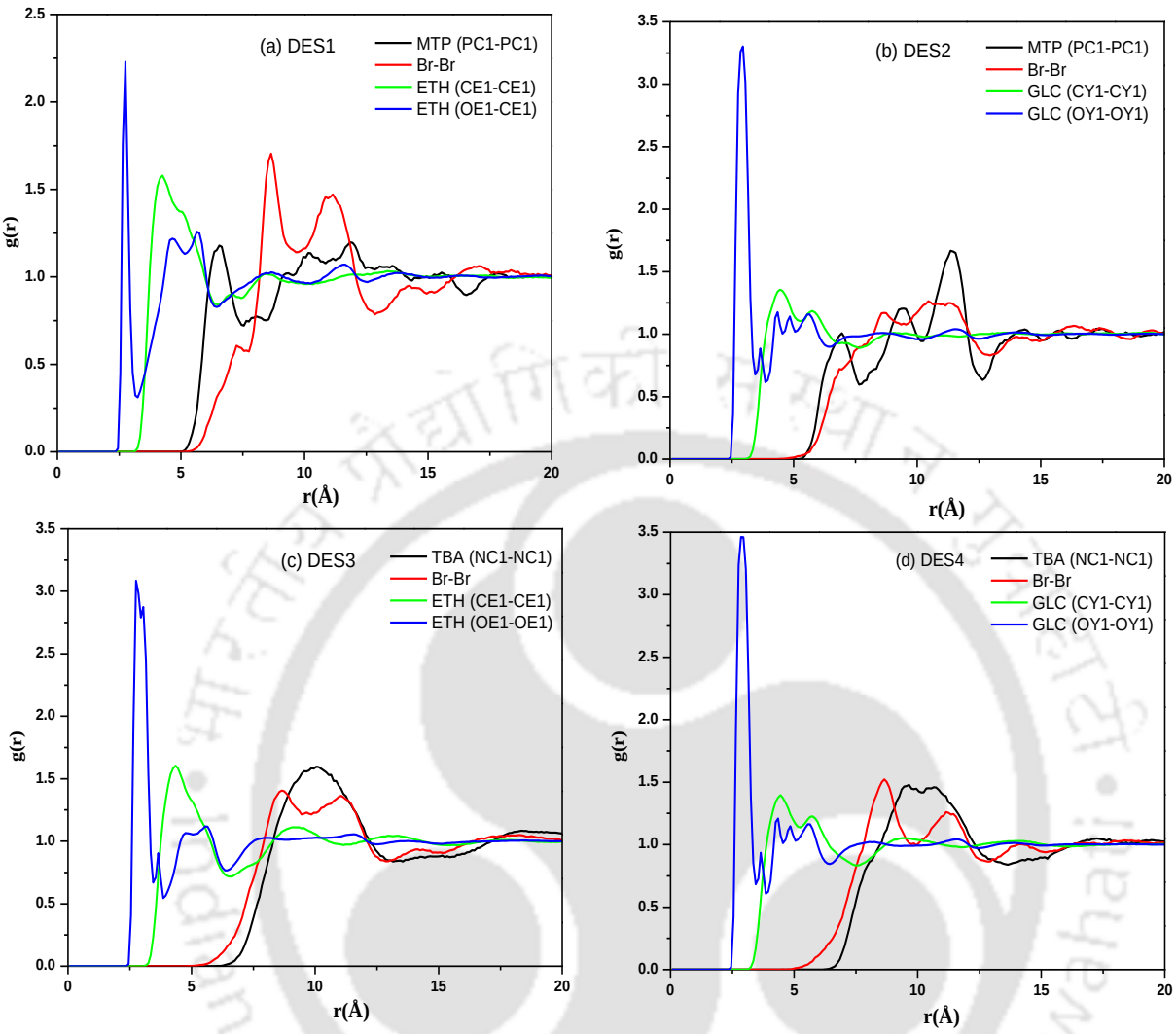

Figure 2.13: Partial RDF plots within intra groups of DES (Nomenclature as per Table 2.2 and Fig. 2.2)

This implies that the DES will also be thermally and chemically stable in different environment. We have also computed the site-site RDF within the same DES in order to analyze the individual interactions (Fig. 2.13). The peak distance of all pairwise RDF are comparatively larger as compared to the inter species or intermolecular RDF except for the case of –OH groups within the HBD species (Table 2.8). The spatial distribution function (SDF) to visualize the interaction between HBD and HBA are shown in the Appendix-A (Section A.5, Fig. A.12).

Table 2.8: Coordination number (CN) and peak distance between in the components of DES[a]

DES	Intra species interaction	CN	r (Å)
DES1	PC1-PC1	0.517	6.55
	Br-Br	1.063	8.25
	CE1-CE1	0.991	4.25
	OE1-OE1	0.204	2.75
DES2	PC1-PC1	0.448	6.85
	Br-Br	1.677	8.65
	CY1-CY1	0.952	4.45
	OY1-OY1	1.496	2.95
DES3	NC1-NC1	3.742	10.05
	Br-Br	1.615	8.65
	CE1-CE1	1.040	4.35
	OE1-OE1	0.455	2.75
DES4	NC1-NC1	2.270	9.55
	Br-Br	1.603	8.65
	CY1-CY1	0.893	4.45
	OY1-OY1	1.049	2.85

[a] Nomenclature as per Table 2.2 and Fig. 2.2

This work can also be compared with the RDF reported for some other choline chloride based DES [60,61]. The intra species RDF between choline-chloride and choline–choline was reported to have the first solvation peak at 6.4 Å and 4.6 Å respectively. This compares to values obtained as 6-10 Å in the current work indicating very low long range correlation. The HBD –chloride RDF was reported to be at 3.9 Å [60], where as in our case, HBD-bromide peak distance is approximately 3 Å. This indicates that the strength of hydrogen bond is higher in our work as compared to Choline-Chloride based DES. This indicates that formation of DES is strongly influenced with the formation of hydrogen bond between HBD and the halide anion. This phenomena (or HBD-Br) is absent in case of

imidazolium chloride based ionic liquids where the first RDF peak (cation-cation) is seen at 7 Å [62]. Overall, in case of DES, the higher peak at lower radial distance was assigned to strong hydrogen-bonding interaction between HBD species and halide anion association. It can also be attributed to the longer distance of the halide ions with the bulky cation so as to prevent its association with the cationic part of HBA region. These differences in RDF peak indicate the formation of eutectic mixture, which is the cause of reduction of melting temperature significantly in case of DES. This phenomenon has been further elucidated in the next section with the measurement of coordination number and hydrogen bonds.

2.4.5 Coordination Number and Hydrogen Bonding

The coordination number (CN) is the quantification of the first solvation shell in the RDF peak and an estimation of the average number of molecules surrounding the reference molecule [63]. Integration of g(r) in spherical coordinates to the first minimum of the RDF will give us the coordination number of a molecule (Eq. 2.1)[64]

$$CN = 4\pi\rho_N \int_{r_0}^{r_1} g(r) r^2 dr \qquad (2.1)$$

Here, r_0 is the rightmost position starting from r = 0, where g(r) is approximately zero and r_1 is the first minimum of g(r). ρ_N is the number density. Coordination numbers are listed in Tables 2.7-2.8, between the different groups of the four DESs. The first solvation shell of the RDF was considered and integrated for the calculation of the coordination number. Here we have chosen the central cation atom (phosphorous or nitrogen atom) of HBA as it is approximately symmetrical (Fig. 2.2). Further, for HBD we have chosen the terminal oxygen atom which is most susceptible to H-bonding so as to aid in the calculation of RDF and coordination number (Fig. 2.2).

In DES1, the cation salt MTP is considered as the reference molecule. The ETH molecule is surrounded, albeit to a lower extent at a distance of 2.75 Å to the MTP cation. The bromide anion of HBA is surrounded within the ETH molecule at a distance of 2.95 Å (Fig. 2.12a). Similarly, in all cases we have calculated the CN at the first peak of the corresponding RDF (Table 2.7). For all the cases we found low value of CN for cation and anion of the same HBA salt as compared to the HBD-HBD molecule species. In addition, for the ammonium based DES the first solvation shell is extended up to 4.25 Å, which portray weak interaction. This types of pattern of CN was seen in literature for ammonium based DES [59,65]. The simulations reported here indicate that a large number of HBD molecules interact with the anion as compared to the cation of the HBA. As evident, DES1 and DES3 possessing ethylene glycol as HBD corresponds to a higher coordination number in comparison to other DES. So overall a phosphonium based DES with ethylene glycol, as HBD is a favorable DES for extraction studies.

To further complement this phenomena, a hydrogen bonding analysis was performed for the last 10 ns of the trajectory using VMD software [36]. The angles (∠DHA is the angle D-H-A: where D is hydrogen donor and A is hydrogen acceptor) and distances between both groups were computed. A cutoff distance and angle (∠DHA) of 3.5 Å and 135º were used as strict hydrogen bond criteria in order to calculate the fraction of hydrogen bonds of each type in this system. These typical hydrogen bond criteria was used by several other studies, including ionic liquid simulations [11,66].

Table 2.7 shows the fraction of hydrogen bonds formed between different groups in the four DESs. Very few hydrogen bonds were observed between HBA cation and anion. On the other hand, the contribution to hydrogen bond was mainly due to the HBD groups

such as ethylene glycol and glycerol. The number of hydrogen bonds that can form between the "donor" and "acceptor" groups present in the mixture depends on both the HBA and HBD type.

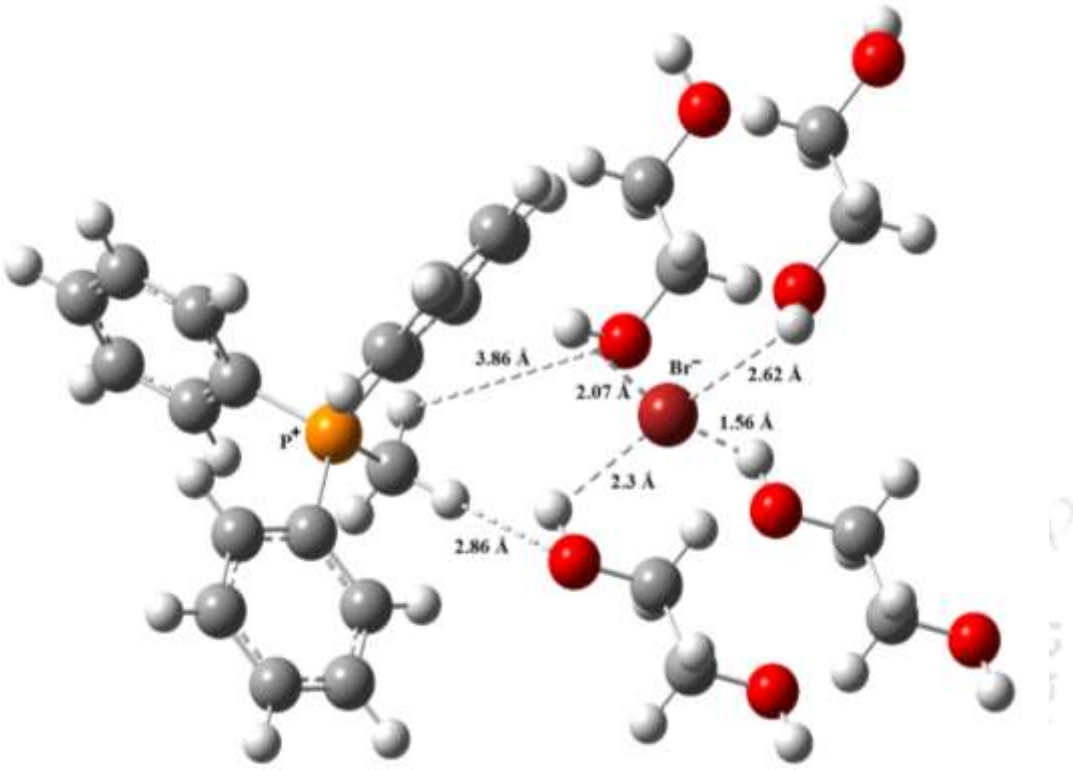

Figure 2.14: Depiction of molecular interaction between salt cation, anion and HBD component for the DES1 (MTPB/ETH (1:4)). The dashed line represents hydrogen bonding

It is noticed that the H-bonds are primarily dominated within the pair Cationic-HBD and Br-HBD which posses a higher fraction of hydrogen bonds. However, it is interesting to note that the hydrogen bond strength between Cation-Br is higher in ammonium based DES (DES3 and 4) as compared to phosphonium based DES (DES 1 and 2) (Fig. 2.14). This implies that the cationic part is strongly bound to the halide atom in case of ammonium DES. This hinders or lowers the attractive nature for other incoming solutes. It also

complements the results of section 2.4.4 where the RDF has concluded that the phosphonium based DES can be good candidates for extraction. Looking at these promising results, we shall now proceed for the extraction studies of Poly Aromatic Hydrocarbon namely (PAH) i.e. quinoline/indoline. Here DES1 (Methyltriphenyl phosphonium bromide (MTPB) and ethylene glycol) and DES2(Methyltriphenyl phosphonium bromide (MTPB) and Glycerol) shall be mixed in the ratio of 1:4 so as to measure the liquid liquid equilibrium of systems containing quinoline/indoline and heptane.

2.5 Conclusion

The current work reports the synthesis of four DES consisting of methyltriphenylphosphonium bromide (MTPB) and tetrabutylammonium bromide (TBAB) with ethylene glycol or glycerol as HBD. Fourier Transform Infrared (FTIR) and Thermo Gravimetric Analysis (TGA) analysis were carried out to understand the nature of DESs along with their thermal stability. ^{1}H NMR analysis confirmed that there was no reaction between the HBA and HBD. Furthermore, classical Molecular Dynamic (MD) simulations were carried in NAMD to elucidate the structural properties. This was examined in terms of non-bonded interaction energies, hydrogen bonds, coordination number and radial distribution functions of pure DES. The MD simulated density results were then validated by comparing the measured experimental densities, which gave an excellent agreement within a range of ±5%. The results from MD simulations revealed that the hydrogen bonded interactions between the anions of HBA and HBD is the main contribution for the formation of the eutectic mixture. The MD insights reveal the weakening of interaction between HBD molecules and between the ions within HBA in

the DESs. On the contrary, strong interactions were observed between HBD and Br ions. A high number of hydrogen bonds between the bromide ion and HBD was observed through MD simulations. The RDF disclosed the fact that the bromide ion interacts more strongly with the hydroxyl group of the ethylene glycol or glycerol molecule. Overall it can be said that the phosphonium based DES can be good candidates for extraction, especially for aromatic moiety.

References

[1] A.P. Abbott, G. Capper, D.L. Davies, R.K. Rasheed, V. Tambyrajah, Novel solvent properties of choline chloride/urea mixtures, Chem. Comm. DOI (2003) 70-71.

[2] Q. Zhang, K.D.O. Vigier, S. Royer, F. Jérôme, Deep eutectic solvents: syntheses, properties and applications, Chem. Soc. Rev. 41 (2012) 7108-7146.

[3] E.L. Smith, A.P. Abbott, K.S. Ryder, Deep eutectic solvents (DESs) and their applications, Chem. Rev. 114 (2014) 11060-11082.

[4] A.P. Abbott, D. Boothby, G. Capper, D.L. Davies, R.K. Rasheed, Deep eutectic solvents formed between choline chloride and carboxylic acids: versatile alternatives to ionic liquids, J. Am. Chem. Soc. 126 (2004) 9142-9147.

[5] F.S. Oliveira, A.B. Pereiro, L.P. Rebelo, I.M. Marrucho, Deep eutectic solvents as extraction media for azeotropic mixtures, Green Chem. 15 (2013) 1326-1330.

[6] T. Gu, M. Zhang, T. Tan, J. Chen, Z. Li, Q. Zhang, H. Qiu, Deep eutectic solvents as novel extraction media for phenolic compounds from model oil, Chem. Comm. 50 (2014) 11749-11752.

[7] M.A. Kareem, F.S. Mjalli, M.A. Hashim, M.K. Hadj-Kali, F.S.G. Bagh, I.M. Alnashef, Phase equilibria of toluene/heptane with deep eutectic solvents based on ethyltriphenylphosphonium iodide for the potential use in the separation of aromatics from naphtha, J. Chem. Thermodyn. 65 (2013) 138-149.

[8] T. Zhekenov, N. Toksanbayev, Z. Kazakbayeva, D. Shah, F.S. Mjalli, Formation of type III Deep Eutectic Solvents and effect of water on their intermolecular interactions, Fluid Phase Equilib. 441 (2017) 43-48.

[9] Y. Dai, J. van Spronsen, G.-J. Witkamp, R. Verpoorte, Y.H. Choi, Natural deep eutectic solvents as new potential media for green technology, Analytica chimica acta 766 (2013) 61-68.

[10] M. Mohan, P.K. Naik, T. Banerjee, V.V. Goud, S. Paul, Solubility of glucose in tetrabutylammonium bromide based deep eutectic solvents: Experimental and molecular dynamic simulations, Fluid Phase Equilib. 448 (2017) 168-177.

[11] S.L. Perkins, P. Painter, C.M. Colina, Molecular dynamic simulations and vibrational analysis of an ionic liquid analogue, J. Phys. Chem. B 117 (2013) 10250-10260.

[12] M.A. Kareem, F.S. Mjalli, M.A. Hashim, I.M. AlNashef, Phosphonium-based ionic liquids analogues and their physical properties, J. Chem. Eng. Data 55 (2010) 4632-4637.

[13] B. Tang, K.H. Row, Recent developments in deep eutectic solvents in chemical sciences, Monatshefte für Chemie - Chemical Monthly 144 (2013) 1427-1454.

[14] W. Kohn, A.D. Becke, R.G. Parr, Density functional theory of electronic structure, J. Phys. Chem. 100 (1996) 12974-12980.

[15] M.P. Allen, D.J. Tildesley, Computer simulation of liquids, Oxford university press1989.

[16] G. García, M. Atilhan, S. Aparicio, An approach for the rationalization of melting temperature for deep eutectic solvents from DFT, Chemical Physics Letters 634 (2015) 151-155.

[17] S. Kaur, A. Gupta, H.K. Kashyap, Nanoscale spatial heterogeneity in deep eutectic solvents, J. Phys. Chem. B 120 (2016) 6712-6720.

[18] M.A. Kareem, F.S. Mjalli, M.A. Hashim, I.M. AlNashef, Liquid–liquid equilibria for the ternary system (phosphonium based deep eutectic solvent–benzene–hexane) at different temperatures: A new solvent introduced, Fluid Phase Equilib. 314 (2012) 52-59.

[19] S. Mulyono, H.F. Hizaddin, I.M. Alnashef, M.A. Hashim, A.H. Fakeeha, M.K. Hadj-Kali, Separation of BTEX aromatics from n-octane using a (tetrabutylammonium bromide+ sulfolane) deep eutectic solvent–experiments and COSMO-RS prediction, RSC Adv. 4 (2014) 17597-17606.

[20] M.K. Hadj-Kali, S. Mulyono, H.F. Hizaddin, I. Wazeer, L. El-Blidi, E. Ali, M.A. Hashim, I.M. AlNashef, Removal of Thiophene from Mixtures with n-Heptane by Selective Extraction Using Deep Eutectic Solvents, Ind. Eng. Chem. Res. 55 (2016) 8415-8423.

[21] H.F. Hizaddin, M.K. Hadj-Kali, A. Ramalingam, M. Ali Hashim, Extractive denitrogenation of diesel fuel using ammonium- and phosphonium-based deep eutectic solvents, J. Chem. Thermodyn. 95 (2016) 164-173.

[22] H.F. Hizaddin, A. Ramalingam, M.A. Hashim, M.K.O. Hadj-Kali, Evaluating the Performance of Deep Eutectic Solvents for Use in Extractive Denitrification of Liquid Fuels by the Conductor-like Screening Model for Real Solvents, J. Chem. Eng. Data 59 (2014) 3470-3487.

[23] K.J. Fraser, D.R. MacFarlane, Phosphonium-based ionic liquids: an overview, Australian journal of chemistry 62 (2009) 309-321.

[24] X. Meng, K. Ballerat-Busserolles, P. Husson, J.-M. Andanson, Impact of water on the melting temperature of urea+ choline chloride deep eutectic solvent, New Journal of Chemistry 40 (2016) 4492-4499.

[25] K. Shahbaz, S. Baroutian, F. Mjalli, M. Hashim, I. AlNashef, Densities of ammonium and phosphonium based deep eutectic solvents: Prediction using artificial intelligence and group contribution techniques, Thermochim. Acta 527 (2012) 59-66.

[26] T. Keith, J. Millam, K. Eppinnett, W. Hovell, R. Semichem, Gauss View 05, Dennington II, Inc., Shawnee Mission, KS DOI (2005).

[27] C.I. Bayly, P. Cieplak, W. Cornell, P.A. Kollman, A well-behaved electrostatic potential based method using charge restraints for deriving atomic charges: the RESP model, J. Phys. Chem. 97 (1993) 10269-10280.

[28] M. Frisch, G.W. Trucks, H.B. Schlegel, G.E. Scuseria, M.A. Robb, J.R. Cheeseman, G. Scalmani, V. Barone, B. Mennucci, G.A. Petersson, H. Nakatsuji, M. Caricato, Li X, H.P. Hratchian, A.F. Izmaylov, J. Bloino, G. Zheng, J.L. Sonnenberg, M. Hada, M. Ehara, K. Toyota, R. Fukuda, Hasegawa, J, , M. Ishida, T. Nakajima, Y. Honda, O. Kitao, H. Nakai, Vreven, , M. T, Jr J A,, J.E. Peralta, F. Ogliaro, M. Bearpark, J.J. Heyd, E. Brothers, K.N. Kudin, V.N. Staroverov, T.

Keith, R. Kobayashi, J. Normand, K. Raghavachari, A. Rendell, J.C. Burant, S.S. Iyengar, J. Tomasi, M. Cossi, N. Rega, J.M. Millam, M. Klene, J.E. Knox, J.B. Cross, V. Bakken, C. Adamo, J. Jaramillo, R. Gomperts, R.E. Stratmann, O. Yazyev, A.J. Austin, R. Cammi, C. Pomelli, J.W. Ochterski, R.L. Martin, K. Morokuma, V.G. Zakrzewski, G.A. Voth, P. Salvador, J.J. Dannenberg, S. Dapprich, A.D. Daniels, O. Farkas, J.B. Foresman, J.V. Ortiz, J. Cioslowski, D.J. Fox, Gaussian 09 Revision B. 01, Gaussian, Inc, Wallingford, CT, DOI (2010).

[29] J. Wang, R.M. Wolf, J.W. Caldwell, P.A. Kollman, D.A. Case, Development and testing of a general amber force field, J. Comput. Chem. 25 (2004) 1157-1174.

[30] J. Wang, W. Wang, P.A. Kollman, D.A. Case, Antechamber: an accessory software package for molecular mechanical calculations, J. Am. Chem. Soc 222 (2001) U403.

[31] D. Case, T. Darden, T. Cheatham, C. Simmerling, J. Wang, R. Duke, R. Luo, R. Walker, W. Zhang, K. Merz, Amber 12 reference manual, University of California, San Francisco DOI (2012).

[32] L. Martínez, R. Andrade, E.G. Birgin, J.M. Martínez, PACKMOL: a package for building initial configurations for molecular dynamics simulations, J. Comput. Chem. 30 (2009) 2157-2164.

[33] J.C. Phillips, R. Braun, W. Wang, J. Gumbart, E. Tajkhorshid, E. Villa, C. Chipot, R.D. Skeel, L. Kale, K. Schulten, Scalable molecular dynamics with NAMD, J. Comput. Chem. 26 (2005) 1781-1802.

[34] P.H. Hünenberger, Thermostat algorithms for molecular dynamics simulations, Adv. Comput. Simul. DOI (2005) 130-130.

[35] H.C. Andersen, Rattle: A "velocity" version of the shake algorithm for molecular dynamics calculations, J. Comput. Phys. 52 (1983) 24-34.

[36] W. Humphrey, A. Dalke, K. Schulten, VMD: visual molecular dynamics, J. Mol. Graph. 14 (1996) 33-38.

[37] S. Nosé, A unified formulation of the constant temperature molecular dynamics methods, J. Chem. Phys. 81 (1984) 511-519.

[38] W.G. Hoover, Canonical dynamics: equilibrium phase-space distributions, Phys. Rev. A. 31 (1985) 1695.

[39] Y. Wang, Y. Hou, W. Wu, D. Liu, Y. Ji, S. Ren, Roles of a hydrogen bond donor and a hydrogen bond acceptor in the extraction of toluene from n-heptane using deep eutectic solvents, Green Chem. 18 (2016) 3089-3097.

[40] K. Shahbaz, F.G. Bagh, F. Mjalli, I. AlNashef, M. Hashim, Prediction of refractive index and density of deep eutectic solvents using atomic contributions, Fluid Phase Equilib. 354 (2013) 304-311.

[41] C. Ma, Y. Guo, D. Li, J. Zong, X. Ji, C. Liu, Molar enthalpy of mixing and refractive indices of choline chloride-based deep eutectic solvents with water, J. Chem. Thermodyn. 105 (2017) 30-36.

[42] A.R. Harifi-Mood, R. Buchner, Density, viscosity, and conductivity of choline chloride+ ethylene glycol as a deep eutectic solvent and its binary mixtures with dimethyl sulfoxide, J. Mol. Liq. 225 (2017) 689-695.

[43] B. Jibril, F. Mjalli, J. Naser, Z. Gano, New tetrapropylammonium bromide-based deep eutectic solvents: synthesis and characterizations, J. Mol. Liq. 199 (2014) 462-469.

[44] F.S. Mjalli, J. Naser, B. Jibril, V. Alizadeh, Z. Gano, Tetrabutylammonium chloride based ionic liquid analogues and their physical properties, J. Chem. Eng. Data 59 (2014) 2242-2251.

[45] K.R. Siongco, R.B. Leron, M.-H. Li, Densities, refractive indices, and viscosities of N, N-diethylethanol ammonium chloride–glycerol or–ethylene glycol deep eutectic solvents and their aqueous solutions, J. Chem. Thermodyn. 65 (2013) 65-72.

[46] Z. Chen, M. Ludwig, G.G. Warr, R. Atkin, Effect of cation alkyl chain length on surface forces and physical properties in deep eutectic solvents, Journal of colloid and interface science 494 (2017) 373-379.

[47] Z. Chen, T.L. Greaves, G.G. Warr, R. Atkin, Mixing cations with different alkyl chain lengths markedly depresses the melting point in deep eutectic solvents formed from alkylammonium bromide salts and urea, Chem. Comm. 53 (2017) 2375-2377.

[48] K. Shahbaz, F. Mjalli, M. Hashim, I. AlNashef, Using deep eutectic solvents based on methyl triphenyl phosphunium bromide for the removal of glycerol from palm-oil-based biodiesel, Energy & Fuels 25 (2011) 2671-2678.

[49] A. Klamt, Conductor-like screening model for real solvents: a new approach to the quantitative calculation of solvation phenomena, Journal of Physical chemistry 99 (1995) 2224-2235.

[50] D. Kundu, T. Banerjee, Multicomponent vapor–liquid–liquid equilibrium prediction using an a priori segment based model, Ind. Eng. Chem. Res. 50 (2011) 14090-14096.

[51] J. Xu, C.L. Toh, X. Liu, S. Wang, C. He, X. Lu, Synthesis and Self-Assembly of Donor− Spacer− Acceptor Molecules. Liquid Crystals Formed by Single-Component "Complexes" via Intermolecular Hydrogen-Bonding Interaction, Macromolecules 38 (2005) 1684-1690.

[52] M. Francisco, A. van den Bruinhorst, M.C. Kroon, Low-transition-temperature mixtures (LTTMs): A new generation of designer solvents, Angew. Chem. Int. Ed 52 (2013) 3074-3085.

[53] K. Tsunashima, M. Sugiya, Physical and electrochemical properties of room temperature ionic liquids based on quaternary phosphonium cations, Electrochemistry 75 (2007) 734-736.

[54] R. Anantharaj, T. Banerjee, Liquid–liquid equilibria for quaternary systems of imidazolium based ionic liquid+ thiophene+ pyridine+ iso-octane at 298.15 K: experiments and quantum chemical predictions, Fluid Phase Equilib. 312 (2011) 20-30.

[55] H. Ghaedi, M. Ayoub, S. Sufian, S.M. Hailegiorgis, G. Murshid, S.N. Khan, Thermal stability analysis, experimental conductivity and pH of phosphonium-based deep eutectic solvents and their prediction by a new empirical equation, J. Chem. Thermodyn. 116 (2018) 50-60.

[56] C. Wenjun, X. Zhimin, W. Jinfang, J. Jingyun, Z. Xinhui, M. Tiancheng, Investigation on the Thermal Stability of Deep Eutectic Solvents, Acta Physico-Chimica Sinca 34 (2017) 904-911.

[57] Y. Cao, T. Mu, Comprehensive investigation on the thermal stability of 66 ionic liquids by thermogravimetric analysis, Ind. Eng. Chem. Res. 53 (2014) 8651-8664.

[58] C. Manohar, D. Rabari, A.A.P. Kumar, T. Banerjee, K. Mohanty, Liquid–liquid equilibria studies on ammonium and phosphonium based ionic liquid–aromatic–

aliphatic component at T= 298.15 K and p= 1bar: correlations and a-priori predictions, Fluid Phase Equilib. 360 (2013) 392-400.

[59] R. Hayes, G.G. Warr, R. Atkin, Structure and nanostructure in ionic liquids, Chem. Rev. 115 (2015) 6357-6426.

[60] M. Gilmore, L.M. Moura, A.H. Turner, M. Swadźba-Kwaśny, S.K. Callear, J.A. McCune, O.A. Scherman, J.D. Holbrey, A comparison of choline: urea and choline: oxalic acid deep eutectic solvents at 338 k, J. Chem. Phys. 148 (2018) 193823.

[61] C. Araujo, J. Coutinho, M. Nolasco, S. Parker, P. Ribeiro-Claro, S. Rudić, B. Soares, P. Vaz, Inelastic neutron scattering study of reline: shedding light on the hydrogen bonding network of deep eutectic solvents, Physical Chemistry Chemical Physics 19 (2017) 17998-18009.

[62] C. Hardacre, J.D. Holbrey, M. Nieuwenhuyzen, T.G. Youngs, Structure and solvation in ionic liquids, Accounts of chemical research 40 (2007) 1146-1155.

[63] M.L. Batista, H. Passos, B.J. Henriques, E.J. Maginn, S.P. Pinho, M.G. Freire, J.R. Gomes, J.A. Coutinho, Why are some cyano-based ionic liquids better glucose solvents than water?, Physical Chemistry Chemical Physics 18 (2016) 18958-18970.

[64] C.D. Wick, S.S. Xantheas, Computational investigation of the first solvation shell structure of interfacial and bulk aqueous chloride and iodide ions, J. Phys. Chem. B 113 (2008) 4141-4146.

[65] S. McDonald, T. Murphy, S. Imberti, G.G. Warr, R. Atkin, Amphiphilically Nanostructured Deep Eutectic Solvents, The journal of physical chemistry letters 9 (2018) 3922-3927.

[66] T. Méndez-Morales, J. Carrete, O. Cabeza, L.J. Gallego, L.M. Varela, Molecular dynamics simulation of the structure and dynamics of water–1-Alkyl-3-methylimidazolium ionic liquid mixtures, J. Phys. Chem. B 115 (2011) 6995-7008.

CHAPTER 3

DES as Extraction Media in Liquid Liquid Equilibria (LLE): Ternary System

3.1 Introduction

Desulphurization and denitrification are an essential part of a refinery set up. Nowadays, the maximum nitrogen content is also limited to < 0.1 ppm. The nitrogen based PAH compounds are more reactive to form pollutant in combustion process. The nitrogen molecules are also known to influence the formation of coke at specified and/or moderate operating conditions [1]. They sometimes inhibit the sulphur removal process. Thus, these PAH molecules point out to a hazardous threat due to its emission into the atmosphere. The toxic effects are mainly due to the carcinogenic products released in the environment as a result of combustion [2]. This makes the removal of aromatic and PAHs from the fuel oil an essential step before utilization. Thus, the primary focus is the extraction of the nitrogen containing PAH such as quinoline from fuel oil.

The efficiency of liquid liquid extraction process depends on its solvent. Thus, the new generation green solvents are been explored so as to replace the conventional solvents. These are extensively reported in the literature [3-8]. However high purity ionic liquids are difficult to synthesize and some of them degrade at temperature well below 100°C inhibiting its use in extraction even though it is highly selective towards PAH. DESs which are analogous to ILs, now used as an alternative to traditional solvent for extraction of aromatic from naphthalene [9]. They formed with combination of a salt and a hydrogen bond donor (HBD)[10,11]. DESs are easy to synthesize, possess a high purity and most importantly economically applicable [12]. Studies involving DESs for LLE of aromatics and hydrocarbons mixtures are scarce [13-15]. The phosphonium based salt being a constituent of DES, is more stable than the ammonium counterpart as they form strong interaction with HBD such as ethylene glycol and glycerol [16,17]. The same was also

verified in our previous chapter 2. In this respect, we have adopted the two DES using the phosphonium based salt as HBA providing DES, namely DES1 and DES2 as discussed in chapter 2 and given in Table 2.2. Both the physiochemical and transport properties have already been discussed in chapter 2 with respect to MD simulations and experimental measurements. Further, it has been confirmed that the extraction increase with a decrease in the alkyl chain length [18,19]. This has also prompted us in synthesizing the above DES with a phosphonium salt possessing methyl chain along with the two HBD's namely ethylene glycol and glycerol. These DES has been used for the extraction of an aromatic (toluene) and PAH (quinoline) from a hydrocarbon (heptane) at ambient condition. Along with the LLE experimental data, the distribution coefficient (β) and selectivity (S) were also computed for both the systems. Finally, the NRTL and UNIQUAC model were used for correlating the experimental data.

3.2 Experimental Details

3.2.1 Chemicals

Heptane, toluene and ethylene glycol were purchased from Merck India. Quinoline and glycerol were procured from SRL India Pvt. Ltd. The DES component namely, Methyltriphenyl phosphonium bromide was supplied by Sigma–Aldrich, Germany. Dimethyl sulfoxide-d6 (DMSO-d6, 99.8%) and $CDCl_3$ of purity > 99.8% were supplied by Merck, Germany. All chemicals were of analytical grade and were used without further purification. Purities of heptane, toluene, glycerol and ethylene glycol were confirmed by ^1H NMR spectroscopy and analysis of peaks indicated negligible impurities. The chemical details used in this work are listed in Table 3.1.

Table 3.1: Chemical structure, Source, purities and method of purification of the chemicals used in the work

S.l. no.	Compound name	Structure	CAS no.	Sources	Mole fraction Purity	Purification method	Analysis method
1	Heptane		142-82-5	Merck, India	>0.99	none	^{1}H NMR
2	Toluene	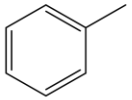	108-88-3	Merck, India	>0.99	none	^{1}H NMR
3	Quinoline	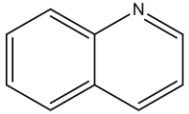	91-22-5	SRL Pvt. Ltd, India	>0.98	none	^{1}H NMR
4	Ethylene glycol	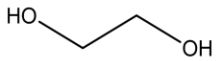	107-21-1	Merck, India	>0.99	none	^{1}H NMR
5	Glycerol	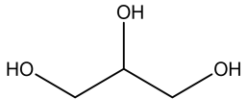	56-81-5	SRL Pvt. Ltd, India	>0.99	none	^{1}H NMR
6	Methyltriphenyl phosphonium bromide	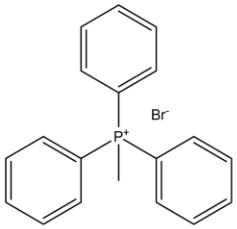	1779-49-3	Sigma–Aldrich, Germany	>0.98	none	^{1}H NMR

3.2.2 DES Preparation

Methyltriphenyl phosphonium bromide (MTPB) and ethylene glycol were mixed in a molar ratio of 1:4 to produce DES1. In a similar fashion, methyltriphenyl phosphonium bromide and glycerol (1:4) were used for synthesizing DES2. The details are provided in chapter 2 and also described in detail by Kareem *et al.* [20]. Here MTPB is taken as a salt i.e. hydrogen bond acceptor (HBA) and ethylene glycol or glycerol as hydrogen bond donor (HBD). The respective proportion of chemicals were weighted by digital weight balance (Denver Instrument, Model SI-234) and mixed inside a flat bottom flask which was fitted with a reflux condenser. The total mixture was mixed by magnetic stirring at a temperature of 60 °C with a rotational speed of 800 rpm. This was further mixed for 24 hours after which a clear liquid of DES was observed after overnight settling. The densities of the synthesized DES were then measured at atmospheric pressure with a digital densitometer (Anton Paar DMA 4500) having an uncertainty of ±0.001g/cm^3.

3.2.3 Experimental Procedure

In the LLE experiment, desired amount of the three components were mixed in a 15 ml stoppered bottle such that they form a heterogeneous mixture. For generating the tie lines, the feed composition was varied with respect to the quantity of the solute which ranged from 0.1 to 0.8 mole fraction. A total of eight compositions (corresponding to eight tie lines) were carried out such that they cover the entire area of the ternary diagram. The corresponding feed volumes were computed according to the densities, molecular weight and proportion of the individual compounds. The total volume of the DES was kept at 10 ml. Thereafter the desired volume of components was transferred into a 15ml culture bottle

for mixing. All the bottles were properly covered with parafilm tape to prevent loss of compound to the atmosphere due to evaporation. The bottles were then kept inside an incubator shaker (Daihan Lab Tech, China) which was capable of controlling both shaking speed and temperature. The shaker was set to 308.15 K (35°C) at 200 rpm for a time of 6 hours. The uncertainty in temperature was within ±0.01K. The mixture was then kept overnight (12 hours) for settling at the same temperature so as to ensure a clear and stable separation of layers.

3.2.4 Composition Analysis

LLE data for the ternary system were analyzed by ^{1}H NMR spectra analysis. In recent times ^{1}H NMR spectra are used for the determination of composition of phases at equilibrium [21-25] successfully. .Both the phases namely extract and raffinate were analyzed using 600 MHz NMR spectrometer (Bruker). The proton peak areas of each component were located in order to obtain the molar phase concentration of each compound. A small amount (0.1 ml) of each phase was dissolved in 0.5 ml deuterated solvent in two different NMR (thrift Grade) tubes after which they were sealed properly. The deuterated solvent used was $CDCl_3$ and DMSO for DES1 and DES2 respectively. This was required as DES2 was not found to be miscible in $CDCl_3$. The caps of the NMR tubes were then closed with parafilm tape to prevent losses. The tubes are then placed in a NMR spectrometer for proton analysis. The reference peak for $CDCl_3$ and DMSO were found to lie at 7.27 and 2.5 respectively. Peak with respect to individual components were identified and then integrated from the NMR spectra. From the integral area, the compositional mole fraction is calculated as:

$$x_i = \frac{H_i}{\sum_{i=1}^{3} H_i} \qquad (3.1)$$

Here H_i and x_i represent the peak area and mole fraction for single hydrogen of i^{th} component in the mixture. ^{1}H NMR spectra of DES1 and DES2 are shown in Figure 2.8 and Figure 2.9 respectively in chapter-2. In case of DES1, MTPB has a triphenyl (—$(C_6H_5)_3$—) group peak at ~(7.66-7.54) ppm, which is the region for the aromatic ring. The methyl group (–CH_3) shows a peak at ~2.89 ppm. Similarly, the –OH and –CH_2– group of ethylene glycol depicts a peak at ~4.26 ppm and ~3.41 ppm respectively. For DES2 the triphenyl (—$(C_6H_5)_3$—) and methyl group (–CH_3) were obtained at ~(7.88-7.75) and ~3.18 ppm respectively. Glycerol having three hydroxyls (–OH) group is evident at ~(4.53-4.46) ppm, while the –CH_2– presence is confirmed at ~(3.45-3.31) ppm. The ^{1}H NMR spectra of extract and raffinate phases of system 1 are in Figure 3.1 and Figure 3.2. For system 2 (DES2+ Toluene+ Heptane) the NMR spectra of both phases are shown in Figure 3.3 and Figure 3.4. In both the extract and raffinate phases, the peak due to the phenyl group of MTPB (~7.7) has been used for the quantification of DES1 and DES2. In other words, the $(–C_6H_5–)_3$ peak at ~7.7 ppm consisting of 15 hydrogen atoms was taken for the calculation. Similarly, the aromatic peak of ~7.2 was used for the quantification of toluene in extract phases of both systems. Continuing with the same trend the methyl peak (–CH_3–) consisting of 3H atoms at ~2.47 ppm in system-1 and ~2.41 ppm in system-2 were considered for toluene in raffinate phases. Heptane shows peaks at different domains namely ~0.9 ppm for $(–CH_3–)_2$ and ~1.2 ppm for $(–CH_2–)_5$ group. In this case, we consider $(–CH_3–)_2$ consisting of 6 hydrogen atoms for the quantification of heptane in both phases of DES1.

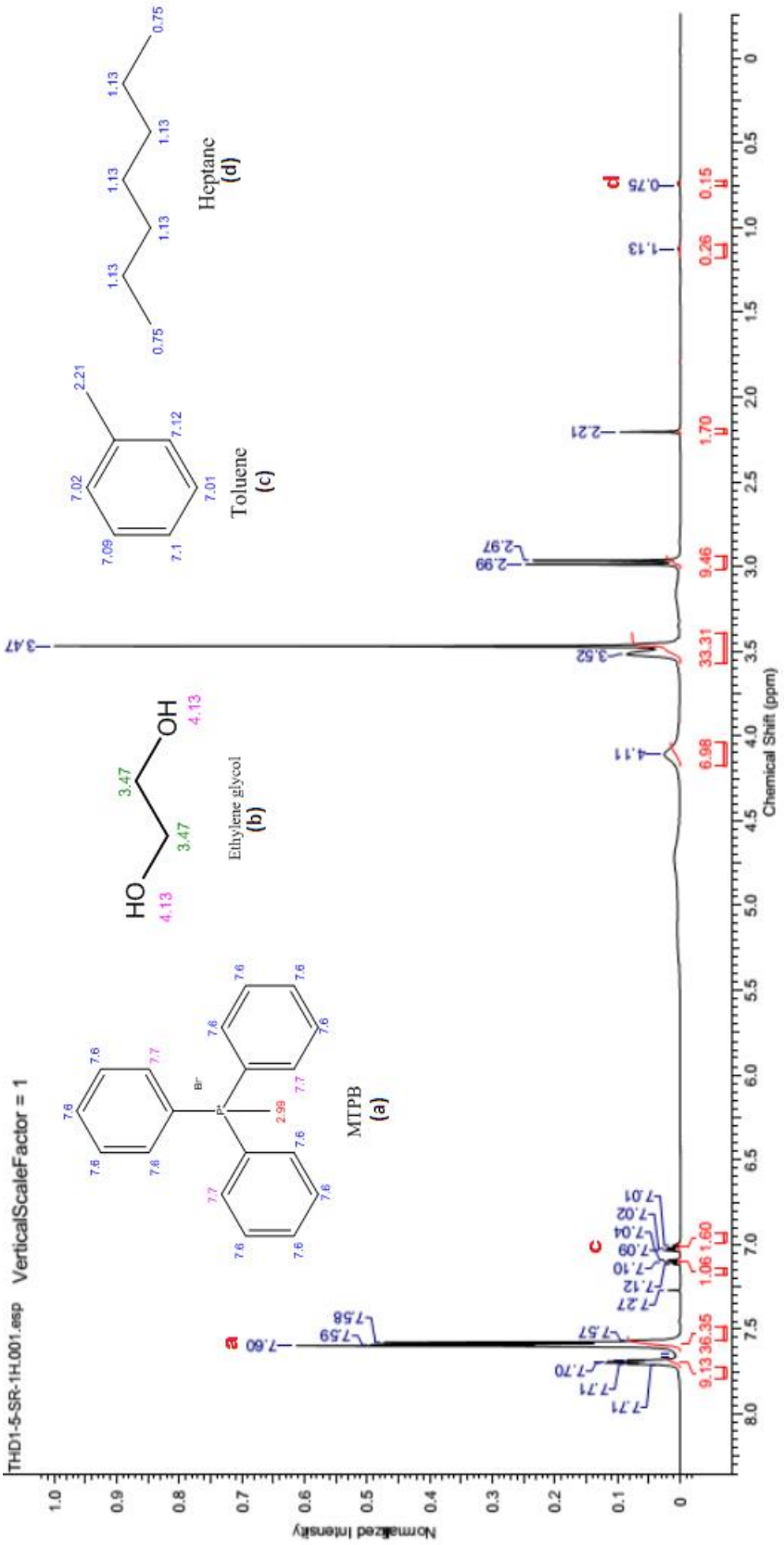

Figure 3.1: NMR spectra for the extract phase of system-1[DES1+ Toluene+ Heptane] at T=308.15 K

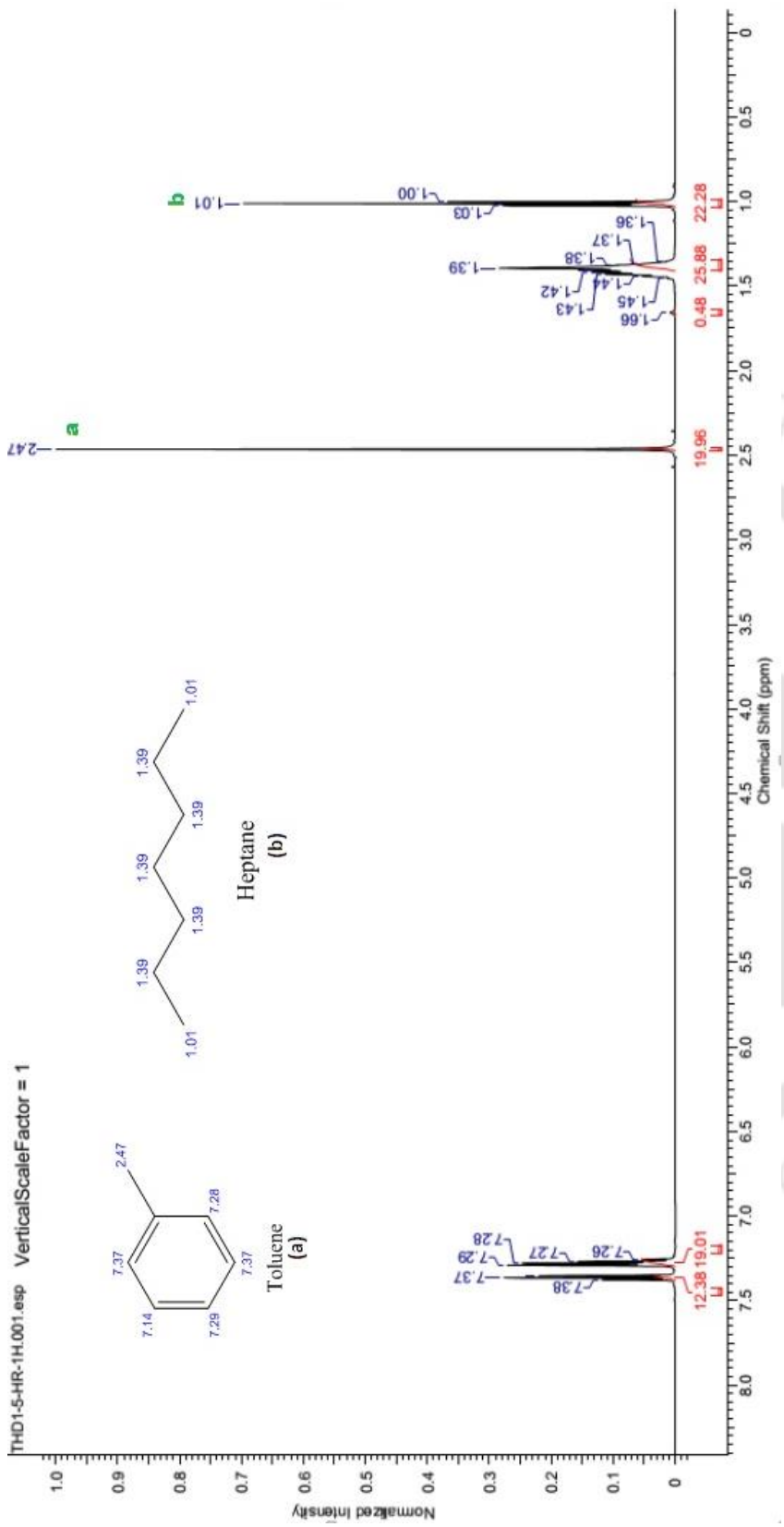

Figure 3.2: NMR spectra for the raffinate phase of system-1[DES1+Toluene+ Heptane] at *T*=308.15

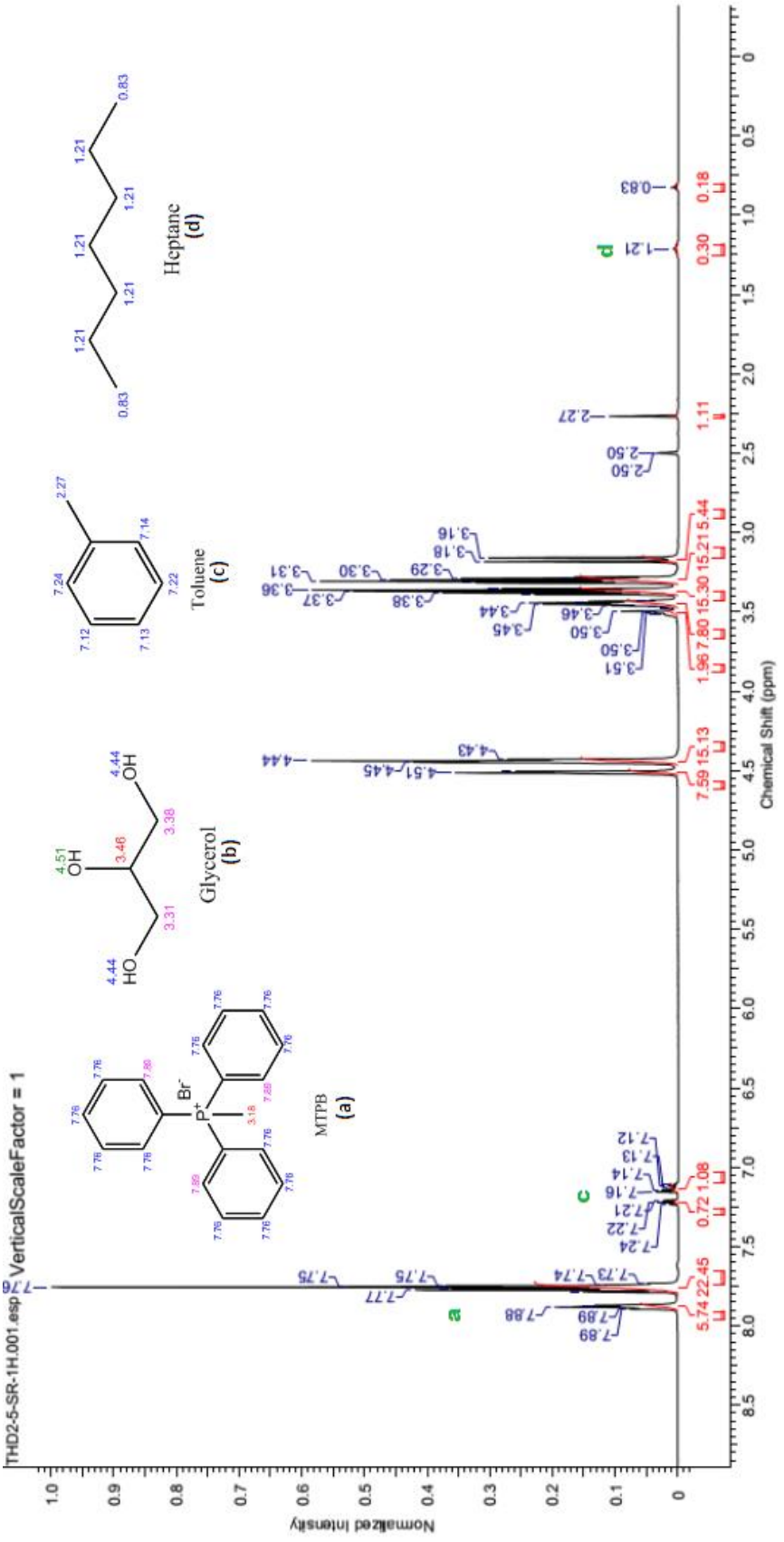

Figure 3.3: NMR spectra for the extract phase of system-2[DES2+ Toluene+ Heptane] at T=308.15 K

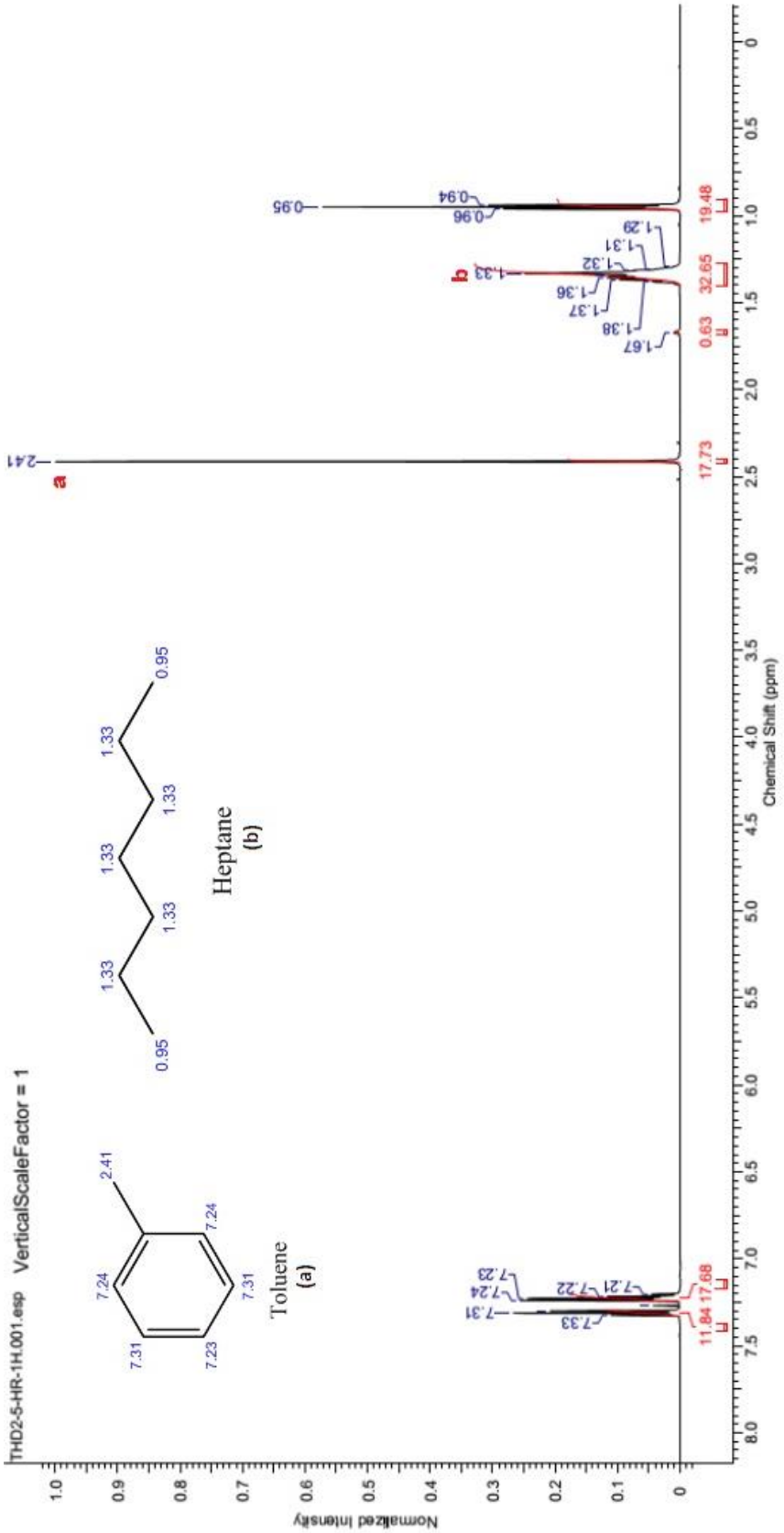

Figure 3.4: NMR spectra for the raffinate phase of system-2 [DES2+ Toluene+ Heptane] at T=308.15

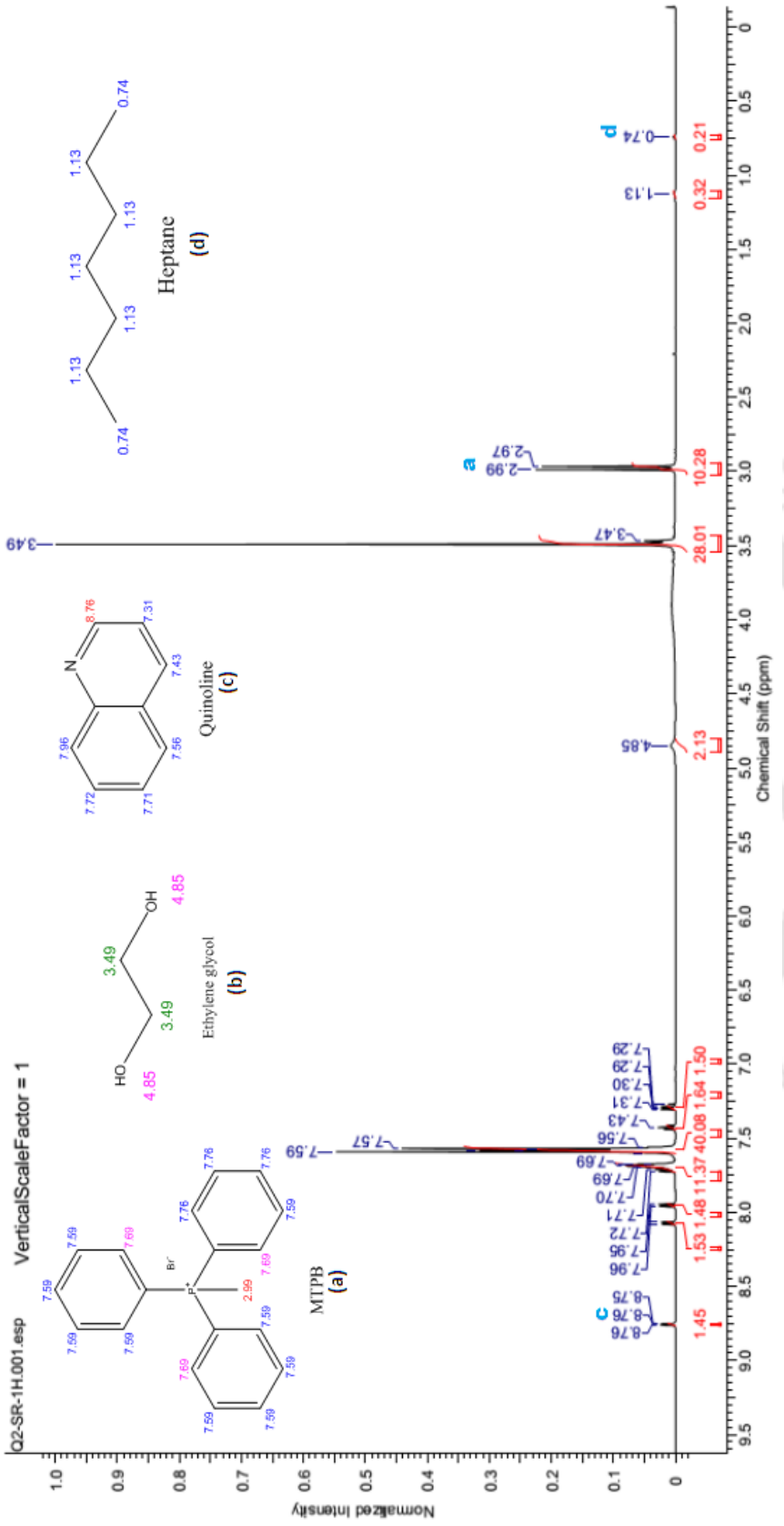

Figure 3.5: NMR spectra for the extract phase of system-3[DES1+ Quinoline+ Heptane] at T=308.15

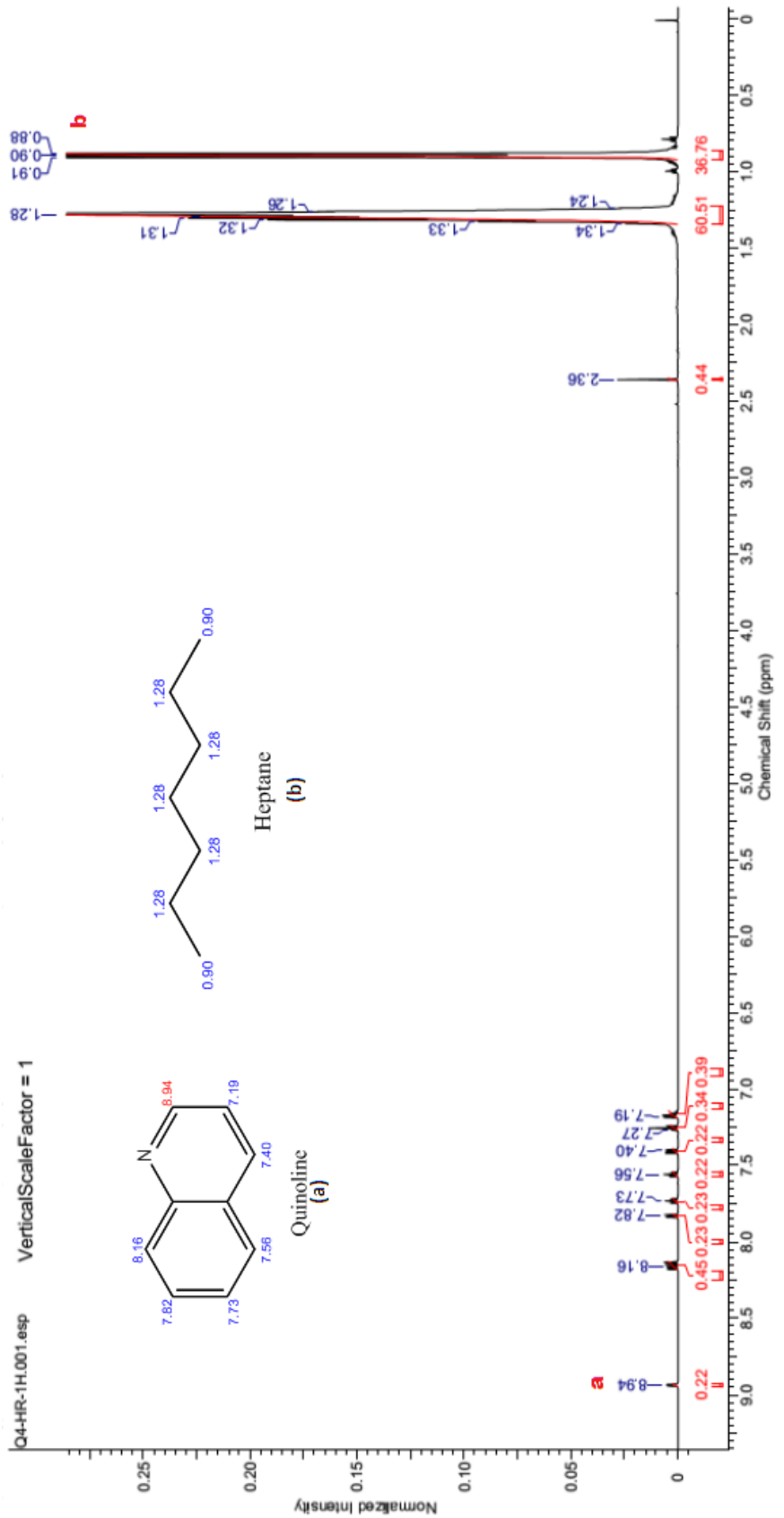

Figure 3.6: NMR spectra for the raffinate phase of system-3[DES1+ Quinoline + Heptane] at T=308.15 K

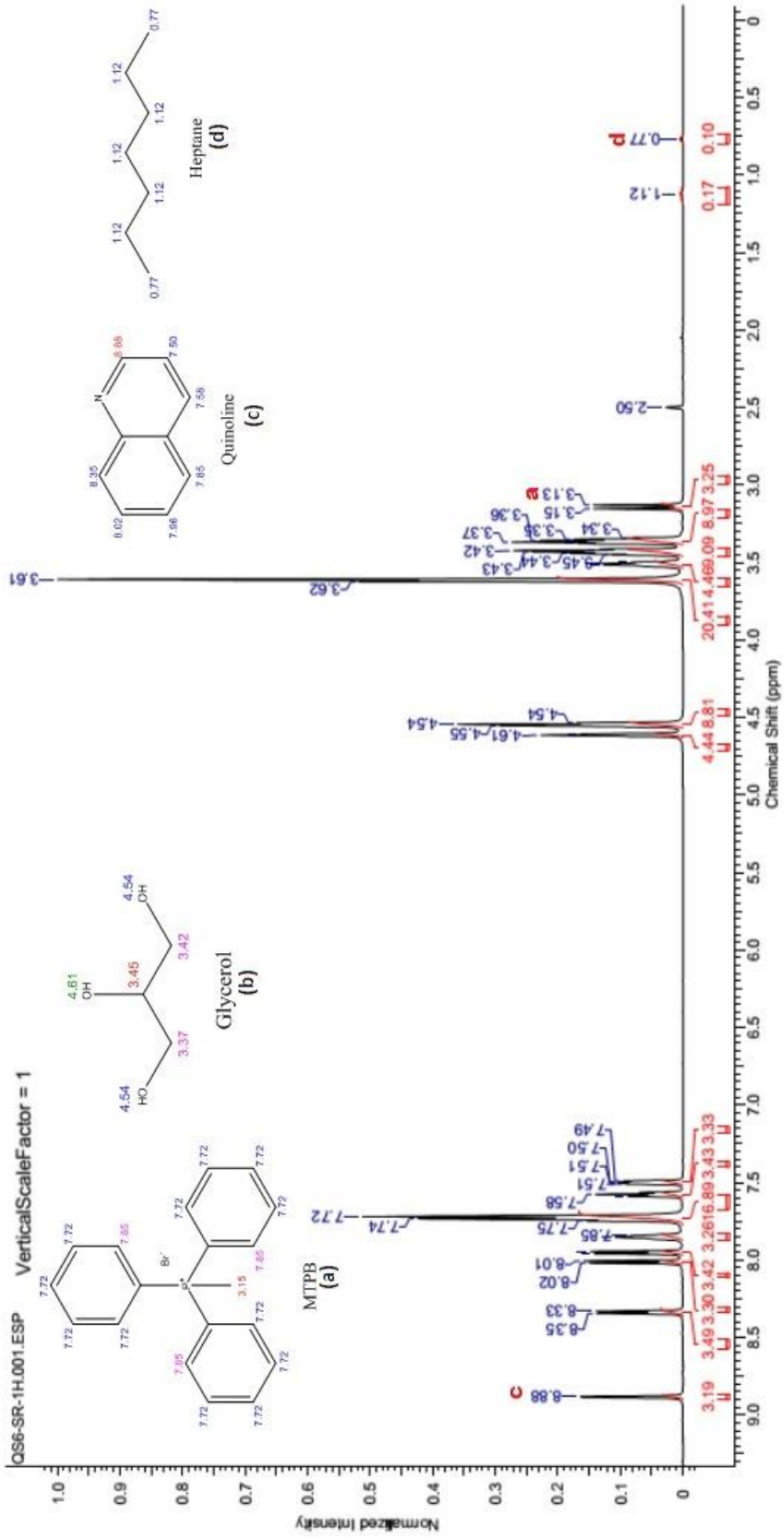

Figure 3.7: NMR spectra for the extract phase of system-4[DES2+ Quinoline + Heptane] at T=308.15

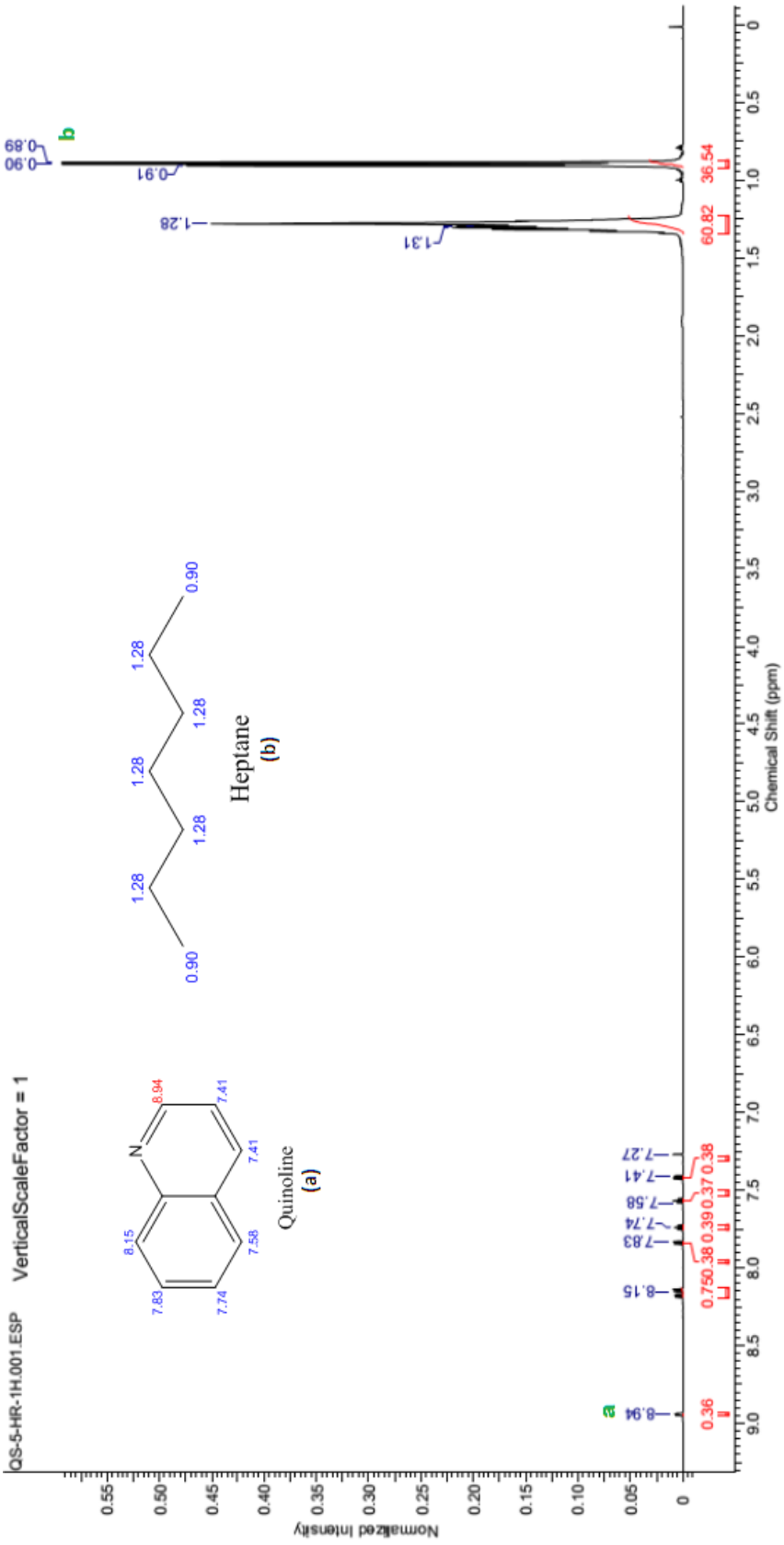

Figure 3.8: NMR spectra for the raffinate phase of system-4[DES2+ Quinoline + Heptane] at T=308.15 K

The spectra of the third system (DES1+ Quinoline+ Heptane) are shown in Figures 3.5 and Figure 3.6. Due to the overlap of peak with quinoline, we consider the $–CH_3–$ peak (~3 ppm) of MTPB for DES1. For quinoline, the peak at ~8.7 ppm due to the single H atom was considered for quantification. Like the previous system,$(–CH_3–)_2$ consisting of 6 hydrogen atoms was used for the quantification of heptane. In system-4, (DES2+ Quinoline+ Heptane), the methyl peak ($–CH_3–$) of MTPB at ~3.15 ppm consisting of 3 hydrogen atoms was used for the quantification of DES2. This was necessitated as the glycerol –OH peak is not a stable one for quantification. Similarly, for quinoline and heptane, we have taken the reference peak as before namely ~8.7 ppm and ~0.9 ppm respectively. The NMR spectra of the ternary systems are reported in Figure 3.7 and Figure 3.8. A sample calculation for calculation of the mole fraction from NMR spectra is also given in the Appendix-A (Figure A.1). In all cases, it is clear that the concentration of DES is zero in the raffinate phase, which indicates that DES acts as a solvent and it nearly eliminates the necessity of a solvent recovery step. The reproducibility of the NMR derived mole fractions were checked on known mixtures of toluene-DES1 and quinoline-DES1 and it was found that the mole fractions lie within the uncertainty range of ±0.01. However it is generally acknowledged that concentrations of about 1-2% mole fraction, may not be well detected by proton NMR as the peaks are lost or diminished in the baseline of the spectrum. Therefore, some small amounts of the solvent might be continuously lost in a real extraction unit in an industrial process if no attempts were made to recover the solvent from the raffinate stream.

3.3 Computational Details

3.3.1 NRTL and UNIQUAC Models

Even though DES is a mixture of two components, still it behaves as a single pseudo solvent for liquid-liquid extraction. This is consistent with the ratio of 1:4 (hydrogen bond donor: hydrogen bond acceptor) as validated from NMR spectra from Figures 3.1-3.8. We have also observed a similar ratio in both the DES and hydrocarbon rich phase of the studied systems. Hence in our formalism, we have adopted the two components as a single pseudo solvent namely DES in our regression studies. The NRTL and UNIQUAC model regression are usually solved using GA as they are highly non-linear. Even if we consider them as quaternary system, the compositions in Tables 3.2-3.5 will merely change the mole fractions of MTBP and ethylene glycol or glycerol in the ratio of 1:4.Further the number of binary interaction parameters will now be 12 in place of 6 for the ternary system. In order to remove this complexity, we have followed up with the assumption of a single solvent for DES. This assumption is also in line with many authors [19,26] who have studied DES for aromatic extraction where DES is considered as a single solvent in NRTL [27] and UNIQUAC [28] model.

The non-ideal mixture of liquids is quantified by the activity coefficient (γ) of the component. The results are then analyzed in terms of root mean square deviation (RMSD) value between experimental and model predictions. For the UNIQUAC model, the structural parameter r and q are predicted using the polarizable continuum model (PCM) via GEPOL algorithm [29]. The final output of the PCM calculation contains the cavity surface area (A^{pcm}) and cavity volume (V^{pcm}) of the DES.

$$r = \frac{(V^{pcm}\text{Å}^3)(10^{-8}cm)^3 N_{av}}{V_{ws}} \tag{3.2}$$

$$q = \frac{(A^{pcm}\text{Å}^3)(10^{-8}cm)^2 N_{av}}{A_{ws}} \tag{3.3}$$

Here 'N_{av}' is the Avogadro's number, V_{ws} the standard segment volume (15.17 cm^3/mol) and A_{ws} the standard segment area (2.5×10^9 cm^2/mol). The *r* and *q* value of DES1 and DES2 are calculated by equation 3.2 and 3.3 respectively. Finally, by adding values of each component (Salt and HBD) of DES, we obtain the *r* and *q* values of DES1 and DES2 respectively.

GA toolbox was then used for minimization of the objective function (*F*) which is merely minimizing the total error between experiment and model calculated mole fraction.

$$F_{\left(\begin{array}{c}\text{with respect to Aij}\\ \text{where } i,j=1,2,3\\ \text{and } \ j\neq i\end{array}\right)} = -\sum_{k=1}^{m}\sum_{l=I}^{II}\sum_{i=1}^{c}\left(x_{ik}^{l} - \hat{x}_{ik}^{l}\right)^2 \tag{3.4}$$

This is in fact a minimization even due to the presence of negative sign. This was necessitated due to the fact that the MATLAB GA toolbox tends to maximize a function. The details of the calculation can be found from our earlier work [30]. The binary interaction parameter A_{ij} is calculated for both the NRTL and UNIQUAC model. Here we have taken population size *npop*=100, and the number of generations *ngen*=200 for the genetic algorithm (GA) program [31]. In both the models, the possible fitness of the data are measured by root mean square deviation (RMSD) which is defined as:

$$RMSD(in\ \%) = \left(-\frac{F}{2mc}\right)^{1/2} = \left[\sum_{k=1}^{m}\sum_{l=I}^{II}\sum_{i=1}^{c}\frac{\left(x_{ik}^{l} - \hat{x}_{ik}^{l}\right)^2}{2mc}\right]^{1/2} \times 100 \tag{3.5}$$

Where m=number of tie lines and c=number of components. Here x_{ik}^{l} and $\hat{x}_{ik}^{l}$ are experimental and predicted values of the mole fraction composition.

3.4 Results and Discussion

The LLE experimental data for DES1(1)+Toluene(2)+Heptane(3), DES2(1)+Toluene(2)+Heptane(3), DES1(1)+quinoline(2)+Heptane(3), and DES2(1)+ quinoline(2)+Heptane(3) were performed at 308.15 K and atmospheric pressure. The ternary LLE data are available from Tables 3.2-3.5 respectively. Extraction capacity of a solvent is usually expressed by parameters such as distribution coefficient (β) and selectivity (S). These are in turn computed from experimental mole fractions. These are given as:

$$\beta = \frac{x_{aro}^{E}}{x_{aro}^{R}} \tag{3.6}$$

$$S = \frac{x_{aro}^{E} / x_{aro}^{R}}{x_{hep}^{E} / x_{hep}^{R}} \tag{3.7}$$

Where x^E and x^R are mole fraction of extract and raffinate phase. Figure 3.9 and Figure 3.10 show the comparison of β and S values with respect to the solute mole fraction in the aromatic feed composition. When compared with the selectivity values, we may need to tune the selection of solvent based on its concentration in the raffinate phase. For e.g. at a lower concentration of toluene, DES1 may be preferred, while DES2 emerges as the recommended solvent at high concentration. Due to an absence of LLE data for quinoline, a similar comparison could not be performed. For DES1(1)+Toluene(2)+Heptane(3)(Table 3.2 and Figure 3.11), the solubility of heptane in DES1 is negligible. The solute distribution

coefficient (β) values are less than unity and increase gradually. The DES concentration here is nearly zero in the upper raffinate layer or the hydrocarbon rich phase. The distribution coefficient and selectivity values were found to range from 0.23 to 0.29, and selectivity from 48.5-12.6 respectively. Thus with an increase in concentration of toluene in the feed, the deviation in β and S are contrary in nature. Similarly for DES2(1)+Toluene(2)+Heptane(3) (Table 3.3 and Figure 3.12), β value ranges from 0.14-0.22 and the selectivity tends to decrease with toluene concentration. It is interesting to observe that among the reported IL's and sulfolane, both the DES possess a lower distribution coefficient (Figure 3.9). This fact is vindicated in the conventional process where sulfolane (developed by Shell and UOP) is the most employed technology to extract aromatics at industrial scale. However, the recovery cost of the sulfolane process is quite high. This is inherently due to two reasons: a high boiling point of sulfolane (280 ^{0}C) and high solubility of sulfolane in the raffinate stream. Hence, DES may be recommended for the recovery of toluene albeit with a lower selectivity (Figure 3.10). This also follows a similar trend as observed from previous authors [31-33] where β and S were found to decrease with increase in aromatic feed concentration.

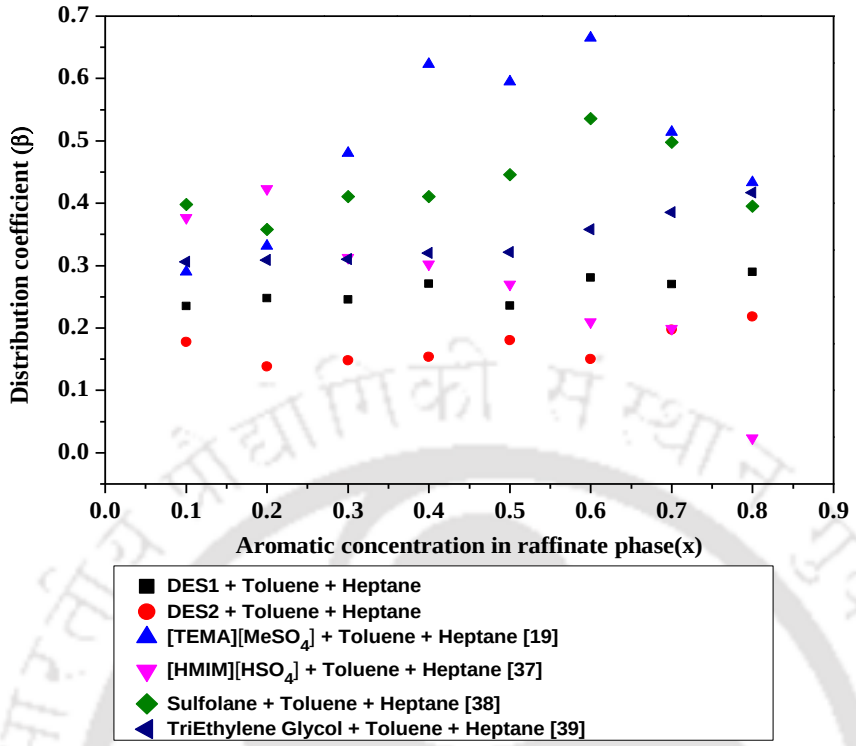

Figure 3.9: Distribution coefficient and comparison with existing solvents

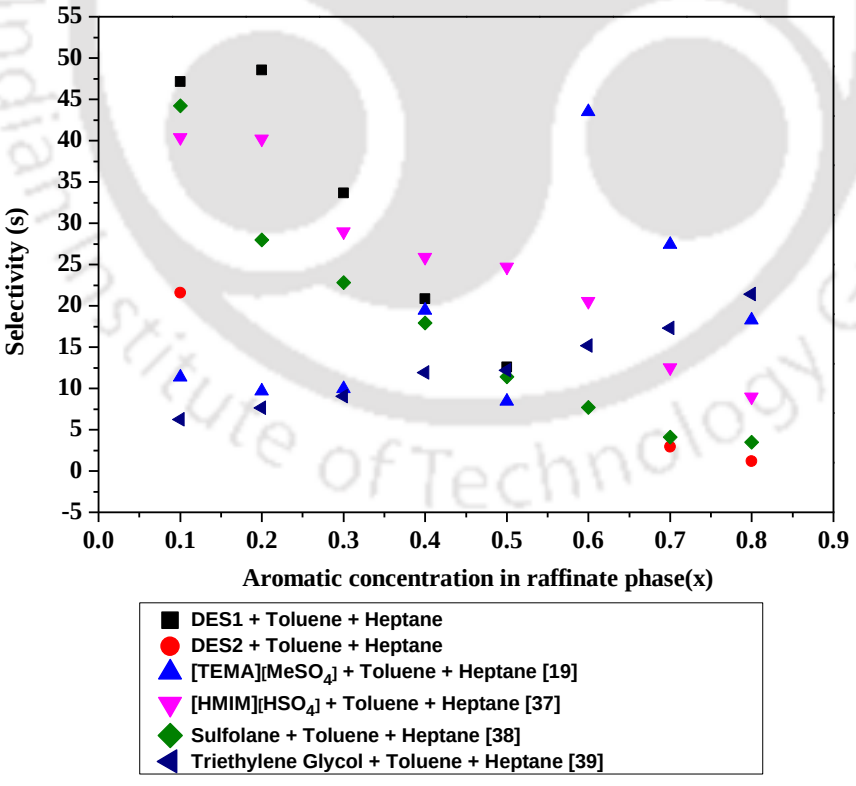

Figure 3.10: Selectivity and comparison with existing solvents

Table 3.2: Experimental tie line data with selectivity (*S*) and distribution ratio (β) for DES1(1)+ Toluene(2)+ Heptane(3) at *T*=308.15 K and atmospheric pressure[a]

Extract phase			Raffinate phase			β_{tol}	Selectivity
x_{DES}	x_{tol}	x_{hep}	x_{DES}	x_{tol}	x_{hep}		(*S*)
0.996	0.000	0.004	0.000	0.000	1.000	∞	∞
0.962	0.034	0.004	0.000	0.143	0.857	0.23	47.1
0.931	0.065	0.004	0.000	0.264	0.736	0.25	48.5
0.899	0.097	0.004	0.000	0.394	0.606	0.24	33.6
0.851	0.143	0.006	0.000	0.526	0.474	0.27	20.8
0.845	0.148	0.007	0.000	0.628	0.372	0.24	12.6
0.802	0.198	0.000	0.000	0.703	0.297	0.28	∞
0.786	0.214	0.000	0.000	0.792	0.208	0.27	∞
0.747	0.253	0.000	0.000	0.875	0.125	0.29	∞
0.654	0.346	0.000	0.000	1.000	0.000	∞	∞

[a] Standard uncertainties *u* are *u*(T)=0.01K, *u*(x)=0.001.

Table 3.3: Experimental tie line data with selectivity (*S*) and distribution ratio (β) for DES2(1)+ Toluene(2)+ Heptane(3) at *T*= 308.15 K and atmospheric pressure[a]

Extract phase			Raffinate phase			β_{tol}	Selectivity
x_{DES}	x_{tol}	x_{hep}	x_{DES}	x_{tol}	x_{hep}		(*S*)
0.998	0.000	0.002	0.000	0.000	1.000	∞	∞
0.968	0.025	0.007	0.000	0.142	0.858	0.18	21.6
0.960	0.040	0.000	0.000	0.293	0.708	0.14	∞
0.940	0.060	0.000	0.000	0.407	0.593	0.15	∞
0.919	0.081	0.000	0.000	0.530	0.470	0.15	∞
0.884	0.116	0.000	0.000	0.644	0.356	0.18	∞
0.890	0.110	0.000	0.000	0.729	0.271	0.15	∞
0.828	0.159	0.013	0.000	0.806	0.194	0.19	2.9
0.786	0.192	0.021	0.000	0.883	0.117	0.22	1.2
0.745	0.255	0.000	0.000	1.000	0.000	∞	∞

[a] Standard uncertainties *u* are *u*(T)=0.01K, *u*(x)=0.001.

Table 3.4: Experimental tie line data with selectivity (*S*) and distribution ratio (β) for DES1(1)+ Quinoline(2)+ Heptane(3) at *T*=308.15 K and atmospheric pressure[a]

Extract phase			Raffinate phase			β_{qui}	Selectivity
x_{DES}	x_{qui}	x_{hep}	x_{DES}	x_{qui}	x_{hep}		(*S*)
0.996	0.000	0.004	0.000	0.000	1.000	∞	∞
0.808	0.170	0.022	0.000	0.005	0.995	35.27	1592.3
0.698	0.295	0.007	0.000	0.013	0.987	23.13	3204.7
0.561	0.434	0.005	0.000	0.024	0.976	17.95	3344.2
0.446	0.542	0.012	0.000	0.035	0.965	15.63	1260.3
0.354	0.638	0.008	0.000	0.062	0.938	10.32	1298.2
0.290	0.699	0.011	0.000	0.097	0.903	7.22	583.2
0.184	0.797	0.019	0.000	0.123	0.877	6.46	293.5
0.115	0.850	0.036	0.000	0.144	0.856	5.92	142.4

[a] Standard uncertainties *u* are *u*(T)=0.01K, *u*(x)=0.001.

Table 3.5: Experimental tie line data with selectivity (*S*) and distribution ratio (β) for DES2(1)+ Quinoline(2)+ Heptane(3) at *T*=308.15 K and atmospheric pressure[a]

Extract phase			Raffinate phase			β_{qui}	Selectivity
x_{DES}	x_{qui}	x_{hep}	x_{DES}	x_{qui}	x_{hep}		(*S*)
0.998	0.000	0.002	0.000	0.000	1.000	∞	∞
0.868	0.132	0.000	0.000	0.008	0.992	16.66	∞
0.690	0.311	0.000	0.000	0.019	0.981	16.48	∞
0.547	0.453	0.000	0.000	0.038	0.962	11.83	∞
0.433	0.568	0.000	0.000	0.041	0.959	13.91	∞
0.331	0.664	0.005	0.000	0.056	0.944	11.89	2246.5
0.253	0.744	0.004	0.000	0.068	0.932	10.90	2539.2
0.166	0.827	0.007	0.000	0.090	0.910	9.23	1201.1
0.106	0.879	0.015	0.000	0.112	0.888	7.83	463.5

[a] Standard uncertainties *u* are *u*(T)=0.01K, *u*(x)=0.001.

It is interesting to note that both the systems (Figures 3.11-3.12) indicate a negative sloping of the tie lines which implies that toluene preferentially adheres to the raffinate phase or in other words, depicts a low toluene extraction capacity. This agrees with the earlier work of Manohar *et al*. [34] where they used an IL based on a phosphonium cation namely tributyl methyl phosphonium methyl sulphate for the extraction of toluene. In their work, the distribution coefficient (β) values were found to be less than unity. Figure 3.13 and 3.14 represents the liquid liquid extraction for the removal of quinoline, a potential carcinogenic compound from DES1 and DES2 respectively. The distribution ratios for DES1(1)+quinoline(2)+Heptane(3)(Table 3.4 and figure 3.13) ranges from 35.27-9.92 and decreases with an increase in quinoline concentration in raffinate phase. A pretty large selectivity of 3344.2 is observed for a 30% concentration of quinoline. The selectivity values are also high for low concentration of aromatic feed and decrease with increase in quinoline concentration. In a similar trend for DES2(1)+quinoline(2)+Heptane(3)(Table 3.5 and figure 3.14), β values decreases from 16.66-7.83. The selectivities values .were found to be much higher than those of toluene (Figure 3.11 and 3.12). It is also very evident that the sloping of the tie lines for toluene and quinoline are of opposite in nature. While toluene has a preferential solubility in the hydrocarbon phase, quinoline appears to diffuse to the extract (DES) phase rich. Hence, the selectivity of toluene + heptane system (Tables 3.2-3.3) are lower than quinoline+heptane system (Tables 3.4-3.5). From the phase equilibrium data, it is clear that the extraction of quinoline is much easy and effectively done as compared to toluene using phosphonium based DES. Further, the β values are less than unity in toluene implies a higher amount of DES.

It is interesting to note that the Figures 3.11-3.14 corresponds to a type two diagram [35]. For e.g. in Figure 3.13 the binary namely heptane-DES1 exhibit immiscibility while the binaries heptane-quinoline and quinoline-DES1 are completely miscible. The binary solubility of heptane-DES1 is further confirmed from the LLE plot as evident in Table 3.6. We did not observe any plait point and the tie lines near the edge of the graph are nearly parallel with the sides of the triangle.

Table 3.6: Binary solubility of heptane(x) in DES1 and heptane rich phase

Temperature (°C)	x_{DES1}	$x_{Hpetane}$
25	0.002	1.000
35	0.004	1.000
45	0.005	1.000
55	0.006	1.000

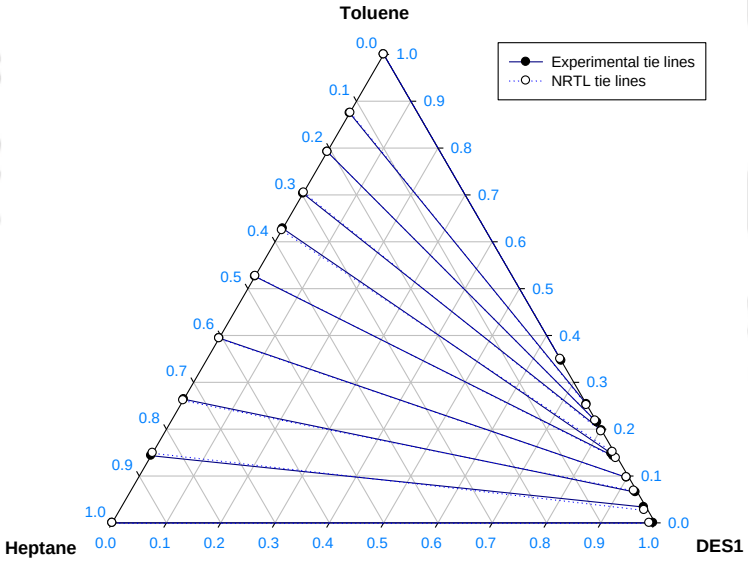

Figure 3.11: Experimental and NRTL tie lines for DES1(1)+ Toluene(2)+ Heptane(3) at T=308.15 K and p=1 bar

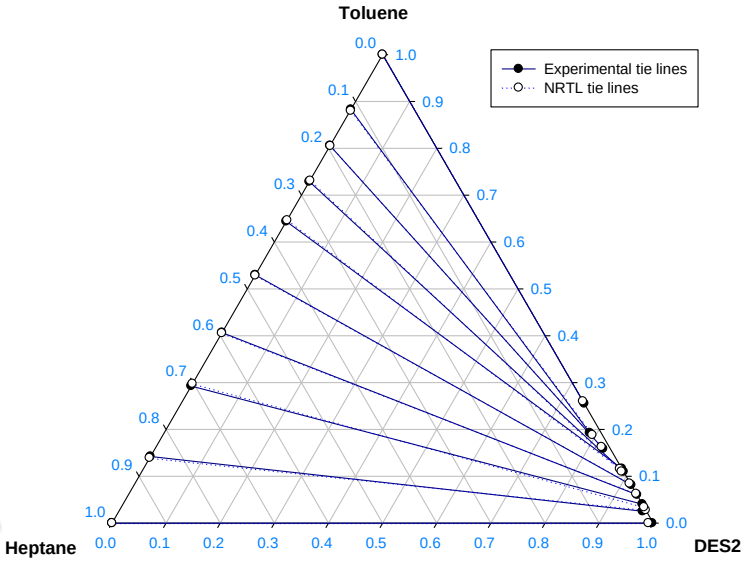

Figure 3.12: Experimental and NRTL tie lines for DES2(1)+ Toluene(2)+ Heptane(3) at *T*=308.15 K and *p*=1 bar

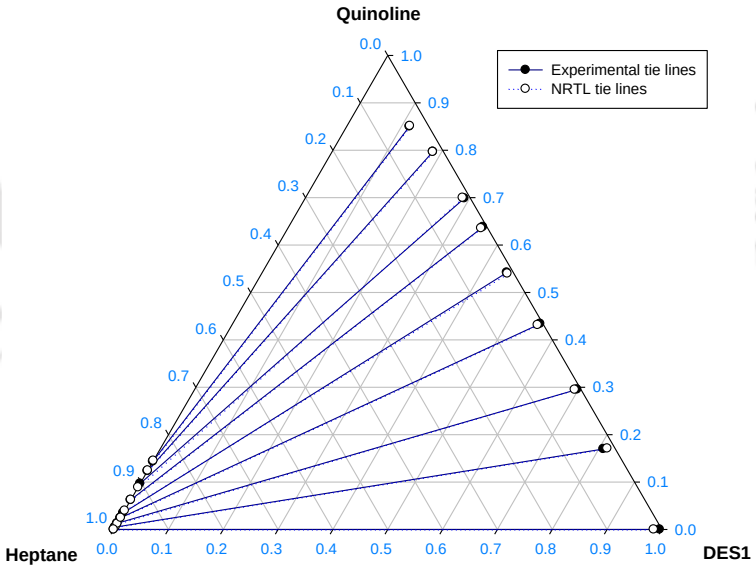

Figure 3.13: Experimental and NRTL tie lines for DES1(1)+ Quinoline(2)+ Heptane(3) at *T*= 308.15 K and *p*=1 bar

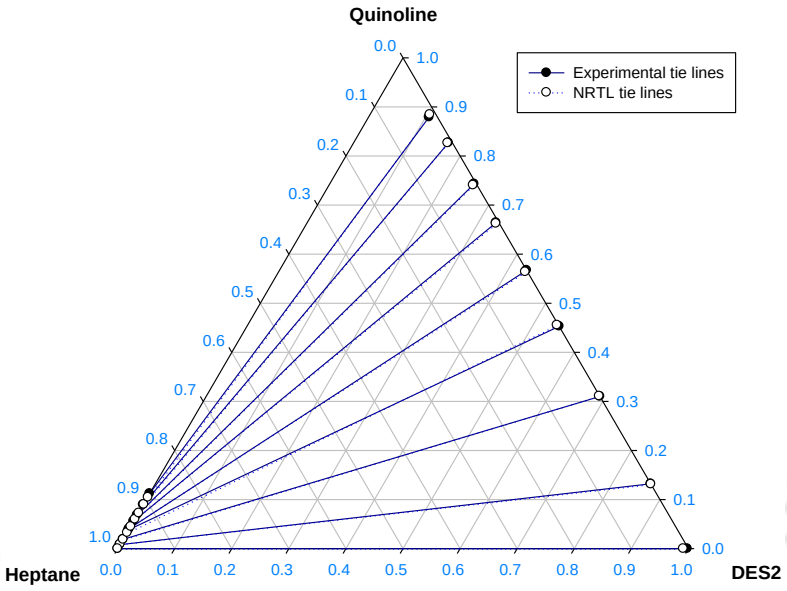

Figure 3.14: Experimental and NRTL tie lines for DES2(1)+ Quinoline(2)+ Heptane(3) at *T*= 308.15 K and *p*=1 bar

The variation of the hydrogen bond donor namely glycerol and ethylene glycol did not alter the selectivity by a large magnitude. However, from Tables 3.4-3.5, it is clear that the distribution coefficient and selectivity value are higher for DES1 as compared to DES2. Thus, it is evident that it is the inorganic salt that controls the extraction. In order to study the effect of the phosphonium salt, we have performed the LLE experiments using ethylene glycol as solvent for the extraction of both toluene and quinoline. The choice of ethylene glycol is due to the fact that DES1 (Table 3.4) has proved to be better solvent in terms of selectivity as compared to DES2 (Table 3.5). In order to compare the predictions with DES1, four aromatic feed points with compositions: 10%, 30%, 50% and 70% (% of toluene or quinolone) were prepared. Thereafter LLE data for the two systems namely: Heptane(1)+Toluene(2)+Ethylene glycol(3) and Heptane(1)+Quinoline(2)+Ethylene glycol(3) were measured and reported in the Tables 3.7 and 3.8 respectively. Both the

systems were found to have lower selectivity with ethylene glycol as compared to DES. The increase in selectivity is more pronounced for quinoline (Table 3.8). In both cases, it is seen that the distribution coefficient are lower than that of pure DES (Table 3.7). The ternary diagrams are also plotted in Figures 3.15 and 3.16 respectively. Overall, the presence of bromide salt in the mixture influences the extraction procedure due to its phenyl ring. Hence the direct utilization of the mixture of the solvent namely ethylene glycol with the bromide salt is justified and can provide pathways for several other solvent formulations. In such a scenario, the Quantum Chemical based COSMO-RS model or Molecular Dynamics simulations may provide further insights into this phenomena.

Table 3.7: Experimental tie lines with selectivity (S) and distribution ratio (β) for Ethylene glycol(1)+ Toluene(2)+ Heptane(3) at T=308.15 K and atmospheric pressure[a]

Extract phase			Raffinate phase			β_{tol}	Selectivity	Selectivity
x_{eg}	x_{tol}	x_{hep}	x_{eg}	x_{tol}	x_{hep}		(S_{eg})	(S_{DES})
0.995	0.000	0.005	0.000	0.000	1.000	-	-	-
0.982	0.015	0.003	0.000	0.176	0.824	0.080	23.4	47.1
0.979	0.019	0.002	0.000	0.447	0.553	0.043	11.8	33.6
0.977	0.022	0.001	0.000	0.648	0.352	0.034	11.9	12.6
0.962	0.037	0.001	0.000	0.855	0.145	0.043	6.3	∞
0.945	0.055	0.000	0.000	1.000	0.000	-	-	-

[a] Standard uncertainties u are u(T)=0.01K, u(x)=0.001.

Table 3.8: Experimental tie lines with selectivity (S) and distribution ratio (β) for Ethylene glycol(1)+ Quinoline(2)+ Heptane(3) at T=308.15 K and atmospheric pressure[a]

Extract phase			Raffinate phase			β_{tol}	Selectivity (S_{eg})	Selectivity (S_{DES})
x_{eg}	x_{qui}	x_{hep}	x_{eg}	x_{tol}	x_{hep}			
0.997	0.000	0.003	0.000	0.000	1.000	-	-	-
0.845	0.151	0.004	0.000	0.030	0.970	5.040	1100.5	1592.3
0.588	0.388	0.024	0.000	0.066	0.934	5.848	230.3	3344.2
0.355	0.578	0.067	0.000	0.112	0.888	5.171	68.39	1298.2
0.178	0.704	0.119	0.000	0.150	0.850	4.703	33.73	293.5

[a] Standard uncertainties u are u(T)=0.01K, u(x)=0.001.

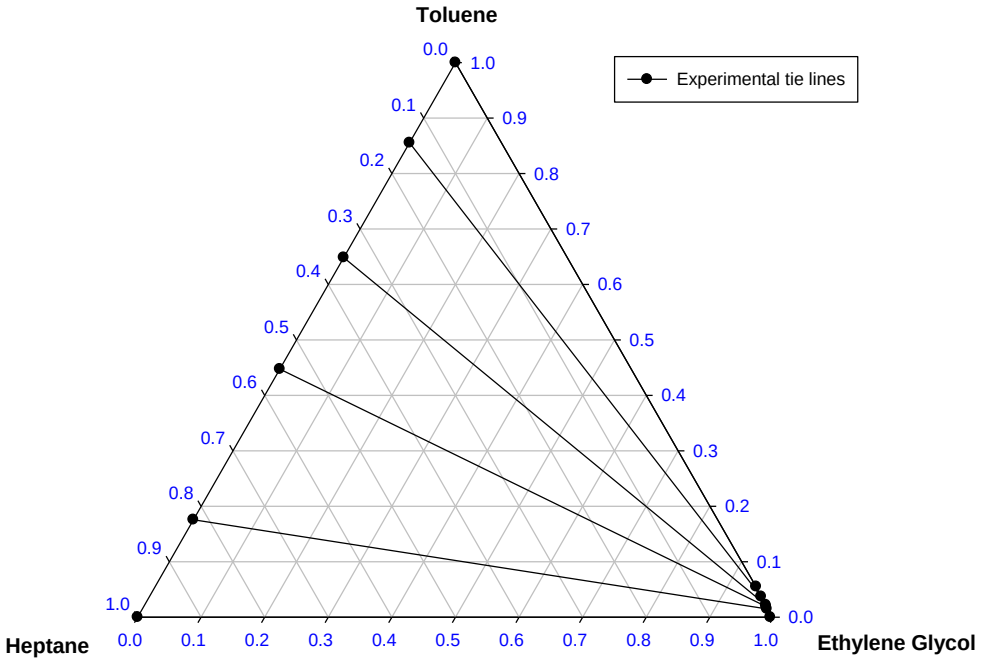

Figure 3.15: Experimental tie lines for Ethylene glycol(1)+ Toluene(2)+ Heptane(3) at T=308.15 K and p=1 bar

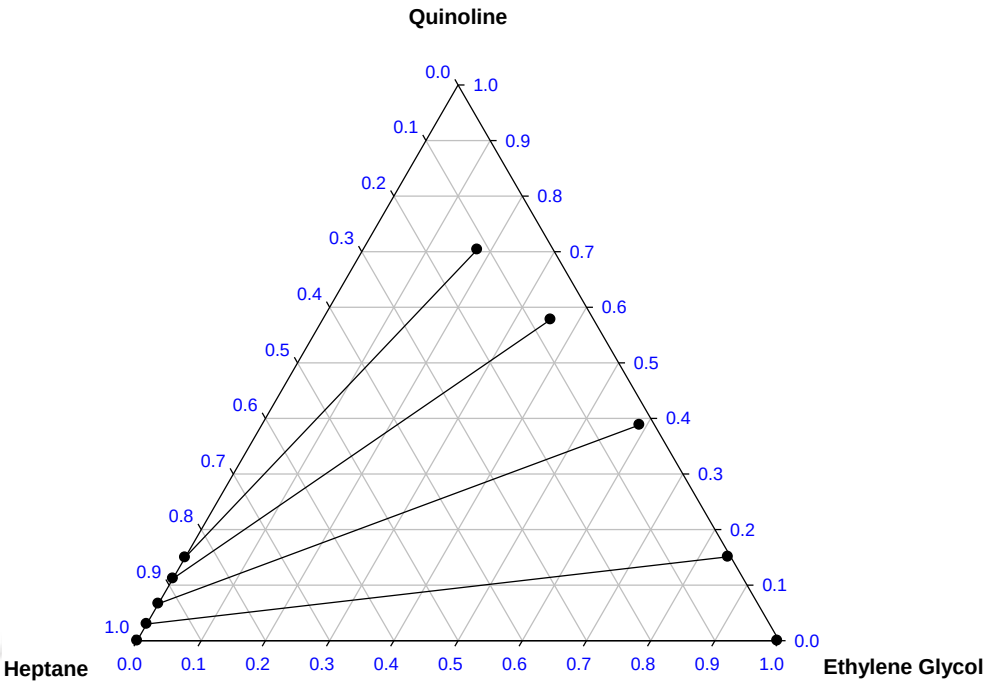

Figure 3.16: Experimental tie lines for Ethylene glycol(1)+ Quinoline(2)+ Heptane(3) at *T*=308.15 K and *p*=1 bar

Nevertheless, DES1 with lower number of –OH groups (ethylene glycol) reduces the intramolecular hydrogen bonding between the DES1 molecules as compared to glycerol. This is due to the fact that the hydrogen bond allows the incoming quinoline molecules for entrapment. This is possible as the interaction of DES with quinoline molecule is strong when compared to toluene. Due to this reason, the extraction with DES1 or DES2 is more preferential towards quinoline. An important observation lies in the fact that DES is totally immiscible with heptane rich layer unlike the traditional solvent sulfolane. Thus for the separation of aromatic and aliphatic hydrocarbon, DES is a recommended solvent. Thus in summary, we did not observe any solvent loss as we did not notice any prominent peak resembling DES solvent in the raffinate phase (Fig 3.1-3.8).

Table 3.9: UNIQUAC structural parameters for different component (*r* and *q*) in LLE system

Sl.no	Compound	Volume parameter [*r*]	Surface area parameter [*q*]
1	Heptane	5.174	4.396
2	Toluene	3.923	2.968
3	Quinoline	4.939	3.727
4	DES1[a]	14.113	10.993
5	DES2[a]	15.146	11.713

[a] Calculated as per procedure in [29]

Table 3.10: NRTL interaction parameter for studied LLE system

i-j	NRTL model parameters			
	τ_{ij}	τ_{ji}	*F**	*RMSD***
	DES1(1)+ Toluene(2)+ Heptane(3)			
1-2	19.52	19.811		
1-3	3.927	11.097	-3.76×10^{-4}	0.28
2-3	5.829	8.001		
	DES2(1)+ Toluene(2)+ Heptane(3)			
1-2	19.609	1.064		
1-3	17.678	15.926	-4.86×10^{-4}	0.31
2-3	6.309	5.531		
	DES1(1)+ Quinoline (2)+ Heptane(3)			
1-2	-1.590	1.811		
1-3	2.504	5.031	-4.51×10^{-4}	0.30
2-3	18.182	1.55		
	DES2(1)+ Quinoline (2)+ Heptane(3)			
1-2	5.024	3.971		
1-3	9.815	7.386	-4.3×10^{-4}	0.29
2-3	-2.594	0.678		

*Eq. 3.4; **Eq. 3.5

However, as stated earlier concentrations of about 1-2% mole fraction may not be well detected by proton NMR as the peaks are lost or diminished in the baseline of the spectrum. The NRTL and UNIQUAC models were further used to correlate the experimental tie lines data for ternary systems (Table 3.2-3.5). Here we have used α=0.2 as a non-randomness factor for NRTL model. The UNIQUAC structural parameters are listed in Table 3.9.

Table 3.11: UNIQUAC interaction parameter for studied LLE system

i-j	UNIQUAC model parameters			
	A_{ij}	A_{ji}	*F**	*RMSD***
	DES1(1)+ Toluene(2)+ Heptane(3)			
1-2	113.96	413.04		
1-3	391.99	-26.467	-1.02×10^{-3}	0.46
2-3	95.493	-229.66		
	DES2(1)+ Toluene(2)+ Heptane(3)			
1-2	200.51	-277.42		
1-3	238.68	243.43	-2.62×10^{-3}	0.73
2-3	-21.036	761.25		
	DES1(1)+ Quinoline(2)+ Heptane(3)			
1-2	-292.94	325.95		
1-3	341.37	-12.31	-1.27×10^{-3}	0.51
2-3	511.06	-52.266		
	DES2(1)+ Quinoline(2)+ Heptane(3)			
1-2	-225.48	279.73		
1-3	889.07	-72.157	-2.42×10^{-4}	0.22
2-3	323.25	2.6017		

*Eq. 3.4; **Eq. 3.5

The binary interaction parameters for the NRTL and UNIQUAC model are given in Tables 3.10-3.11. The deviation between experimental and model predictions as given in RMSD values (equation 5) ranging from 0.28- 0.31% and 0.22- 0.73% for NRTL and UNIQUAC model respectively. Values of RMSD within unity implies that the models accurately correlate the experimental data. After the ternary LLE measurements, we shall now provide its effect on the simultaneous removal namely of indoline and quinoline from heptane rich phase using the same set of DES. This shall be attempted in the next chapter.

3.5 Conclusion

Deep Eutectic Solvents with common salt (Methyltriphenylphosphoniun bromide) along with hydrogen bond donors namely glycerol and ethylene glycol were synthesized. Liquid-liquid Equilibria experiments were performed for the extraction of toluene and quinoline from heptane by employing DES as solvents at ambient conditions. The distribution coefficient and selectivity were found to be much higher for quinoline as compared to toluene. Both the values were found to be higher at low concentration of the aromatic feed. NMR analysis gave a near absence of DES concentration in the raffinate phase. This indicates that the DES does not contaminate the hydrocarbon phase, thereby enabling the ease of solvent recycling. Among the two deep eutectic solvents, DES2 shows a less value of solute distribution ratio, hence DES1 is the recommended solvent for quinoline extraction. Further, the sloping of the tie lines were found to be contrary for toluene and quinoline. Both NRTL and UNIQUAC model gave RMSD value less than unity thereby giving an excellent agreement with the experimental data.

References

[1] Y. Yongtan, Determination of nitrogen compounds in catalytic diesel oil using gas chromatography, Chin. J. Chromatogr. 26 (2008) 478-483.

[2] M. Macaud, M. Sévignon, A. Favre-Réguillon, M. Lemaire, E. Schulz, M. Vrinat, Novel methodology toward deep desulfurization of diesel feed based on the selective elimination of nitrogen compounds, Ind. Eng. Chem. Res. 43 (2004) 7843-7849.

[3] N.R. Varma, A. Ramalingam, T. Banerjee, Experiments, correlations and COSMO-RS predictions for the extraction of benzothiophene from n-hexane using imidazolium-based ionic liquids, Chemical engineering journal 166 (2011) 30-39.

[4] L. Kumar, T. Banerjee, K. Mohanty, Prediction of selective extraction of cresols from aqueous solutions by ionic liquids using theoretical approach, Separation Science and Technology 46 (2011) 2075-2087.

[5] S.R. Pilli, T. Banerjee, K. Mohanty, Ionic liquids as green solvents for the extraction of endosulfan from aqueous solution: a quantum chemical approach, Chemical Product and Process Modeling 8 (2013) 1-14.

[6] E.J. González, N. Calvar, I. Dominguez, Á. Domínguez, (Liquid+liquid) equilibrium data for the ternary systems (cycloalkane+ethylbenzene+1-ethyl-3-methylimidazolim ethylsulfate) at T=298.15K and atmospheric pressure, The Journal of Chemical Thermodynamics 43 (2011) 725-730.

[7] N. Calvar, I. Domínguez, E. Gómez, J. Palomar, Á. Domínguez, Evaluation of ionic liquids as solvent for aromatic extraction: Experimental, correlation and COSMO-RS predictions, The Journal of Chemical Thermodynamics 67 (2013) 5-12.

[8] A. Marciniak, M. Wlazło, Ternary (liquid+liquid) equilibria of {trifluorotris(perfluoroethyl)phosphate based ionic liquids+thiophene+heptane}: Part 2, The Journal of Chemical Thermodynamics 86 (2015) 196-201.

[9] Y. Hou, Y. Gu, S. Zhang, F. Yang, H. Ding, Y. Shan, Novel binary eutectic mixtures based on imidazole, J. Mol. Liq. 143 (2008) 154-159.

[10] K. Shahbaz, S. Baroutian, F. Mjalli, M. Hashim, I. AlNashef, Densities of ammonium and phosphonium based deep eutectic solvents: Prediction using

artificial intelligence and group contribution techniques, Thermochim. Acta 527 (2012) 59-66.

[11] Z. Helalat-Nezhad, K. Ghanemi, M. Fallah-Mehrjardi, Dissolution of biological samples in deep eutectic solvents: an approach for extraction of polycyclic aromatic hydrocarbons followed by liquid chromatography-fluorescence detection, J Chromatogr A 1394 (2015) 46-53.

[12] K. Shahbaz, F. Mjalli, M. Hashim, I. AlNashef, Prediction of the surface tension of deep eutectic solvents, Fluid Phase Equilib. 319 (2012) 48-54.

[13] K. Shahbaz, F.S. Mjalli, M.A. Hashim, I.M. AlNashef, Using Deep Eutectic Solvents Based on Methyl Triphenyl Phosphunium Bromide for the Removal of Glycerol from Palm-Oil-Based Biodiesel, Energy & Fuels 25 (2011) 2671-2678.

[14] H. Lu, P. Li, C. Deng, W. Ren, S. Wang, P. Liu, H. Zhang, Deep catalytic oxidative desulfurization (ODS) of dibenzothiophene (DBT) with oxalate-based deep eutectic solvents (DESs), Chem Commun (Camb) 51 (2015) 10703-10706.

[15] F. Pena-Pereira, J. Namiesnik, Ionic liquids and deep eutectic mixtures: sustainable solvents for extraction processes, ChemSusChem 7 (2014) 1784-1800.

[16] S. Chowdhury, R.S. Mohan, J.L. Scott, Reactivity of ionic liquids, Tetrahedron 63 (2007) 2363-2389.

[17] K.J. Fraser, D.R. MacFarlane, Phosphonium-based ionic liquids: an overview, Australian journal of chemistry 62 (2009) 309-321.

[18] M.A. Kareem, F.S. Mjalli, M.A. Hashim, M.K. Hadj-Kali, F.S.G. Bagh, I.M. Alnashef, Phase equilibria of toluene/heptane with tetrabutylphosphonium bromide based deep eutectic solvents for the potential use in the separation of aromatics from naphtha, Fluid Phase Equilib. 333 (2012) 47-54.

[19] M.A. Kareem, F.S. Mjalli, M.A. Hashim, I.M. AlNashef, Liquid–liquid equilibria for the ternary system (phosphonium based deep eutectic solvent–benzene–hexane) at different temperatures: A new solvent introduced, Fluid Phase Equilib. 314 (2012) 52-59.

[20] M.A. Kareem, F.S. Mjalli, M.A. Hashim, I.M. AlNashef, Phosphonium-based ionic liquids analogues and their physical properties, J. Chem. Eng. Data 55 (2010) 4632-4637.

[21] L. Alonso, A. Arce, M. Francisco, A. Soto, (Liquid+ liquid) equilibria of [C 8 mim][NTf 2] ionic liquid with a sulfur-component and hydrocarbons, J. Chem. Thermodyn. 40 (2008) 265-270.

[22] S. García, M. Larriba, J. García, J.S. Torrecilla, F. Rodríguez, Separation of toluene from n-heptane by liquid–liquid extraction using binary mixtures of [bpy][BF4] and [4bmpy][Tf2N] ionic liquids as solvent, J. Chem. Thermodyn. 53 (2012) 119-124.

[23] A. Ramalingam, S. Kanniayan, Phase Equilibria upon Denitrification of Liquid Fuels Using Imidazolium-Based Ionic Liquids: Experiment and Quantum Chemical Calculations, Ind. Eng. Chem. Res. 54 (2015) 12948-12959.

[24] S. Potdar, R. Anantharaj, T. Banerjee, Aromatic Extraction Using Mixed Ionic Liquids: Experiments and COSMO-RS Predictions, Journal of Chemical & Engineering Data 57 (2012) 1026-1035.

[25] R. Anantharaj, T. Banerjee, Liquid–liquid equilibria for quaternary systems of imidazolium based ionic liquid+ thiophene+ pyridine+ iso-octane at 298.15 K: experiments and quantum chemical predictions, Fluid Phase Equilib. 312 (2011) 20-30.

[26] M.A. Kareem, F.S. Mjalli, M.A. Hashim, M.K. Hadj-Kali, F.S.G. Bagh, I.M. Alnashef, Phase equilibria of toluene/heptane with deep eutectic solvents based on ethyltriphenylphosphonium iodide for the potential use in the separation of aromatics from naphtha, J. Chem. Thermodyn. 65 (2013) 138-149.

[27] H. Renon, J.M. Prausnitz, Local compositions in thermodynamic excess functions for liquid mixtures, AlChE J. 14 (1968) 135-144.

[28] D.S. Abrams, J.M. Prausnitz, Statistical thermodynamics of liquid mixtures: a new expression for the excess Gibbs energy of partly or completely miscible systems, AlChE J. 21 (1975) 116-128.

[29] T. Banerjee, M.K. Singh, R.K. Sahoo, A. Khanna, Volume, surface and UNIQUAC interaction parameters for imidazolium based ionic liquids via polarizable continuum model, Fluid Phase Equilib. 234 (2005) 64-76.

[30] M.K. Singh, T. Banerjee, A. Khanna, Genetic algorithm to estimate interaction parameters of multicomponent systems for liquid–liquid equilibria, Comput. Chem. Eng. 29 (2005) 1712-1719.

[31] V.A. Dukhande, T.S. Choksi, S.U. Sabnis, A.W. Patwardhan, A.V. Patwardhan, Separation of toluene from n-heptane using monocationic and dicationic ionic liquids, Fluid Phase Equilibria 342 (2013) 75-81.

[32] R.P. Tripathi, A.R. Ram, P.B. Rao, Liquid-liquid equilibriums in ternary system toluene-n-heptane-sulfolane, Journal of Chemical and Engineering Data 20 (1975) 261-264.

[33] M.A. Hughes, Y. Haoran, Liquid-liquid equilibria for separation of toluene from heptane by benzyl alcohol tri (ethylene glycol) mixtures, Journal of chemical and engineering data 35 (1990) 467-471.

[34] C. Manohar, D. Rabari, A.A.P. Kumar, T. Banerjee, K. Mohanty, Liquid–liquid equilibria studies on ammonium and phosphonium based ionic liquid–aromatic–aliphatic component at T= 298.15 K and p= 1bar: correlations and a-priori predictions, Fluid Phase Equilib. 360 (2013) 392-400.

[35] J.M. Sørensen, T. Magnussen, P. Rasmussen, A. Fredenslund, Liquid-liquid equilibrium data: Their retrieval, correlation and prediction Part I: Retrieval, Fluid Phase Equilib. 2 (1979) 297-309.

CHAPTER 4

Simultaneous Extraction of Quinoline and Indoline from Fuel

4.1 Introduction

Sulfur and nitrogen containing poly aromatic hydrocarbons (PAH) impurities are the most hazardous compounds found in the fuel oil. These are gaining importance for removal from fuel oil due to the strict limits set by government agencies. These are very difficult to remove completely [1]. Further, these PAHs are the major source of pollution as it releases SO_x and NO_x to the atmosphere. This emission causes harmful effect on the environment and contributes to air pollution, greenhouse effect and acid rain [2]. Thus, it becomes invariably necessary to extract the sulfur and nitrogen containing PAH species from fuel oil by using physical methods at ambient condition.

Among the physical methods, the solvent extraction process is an imminent operation for removal of PAHs at moderate conditions [3]. The conventional solvents like sulfolane and n-methyl pyrrolidone (NMP) having some limitations for the removal of sulphur and nitrogen contents [3-6]. The new generation green solvents such as Ionic Liquid (IL) and Deep Eutectic Solvents (DES) have been used for extraction of PAH and has hence gained enormous importance [7]. Due to the advantage of DES over ILs, we have used DES as extraction media for removal of PAH from fuel oil. The details on DES and its application are described in chapter 1 with ternary LLE measurements conducted and reported in chapter 3.We have already conducted the extraction of quinoline and toluene within the ternary system with the phosphonium based DES as selected in chapter 2. In this chapter, we shall focus our attention on the nitrogen containing PAH such as quinoline and indoline. An attempt shall be made to separate them simultaneously from the fuel oil. DES are also known as second generation ILs and are considered as replacement for the ILs [8]. The

first DES was prepared by Abbot et al. [9] for the mixture of choline chloride and urea in a 1:2 molar ratio.

Liquid-Liquid separation of aromatics with ILs are well known, [10-12] but the application of DESs for aromatic separation are limited [13,14]. Kareem et al. [13] reported that phosphonium based DES has the greater extraction capacity of aromatics from fuel oil as compared to conventional solvent and ILs. Mohammad et al. [15] also demonstrated the physicochemical character of DESs in achieving superior denitrogenation performance. Recently, Hizaddin et al. applied the Conductor-like Screening Model for Real Solvents (COSMO-RS) model for denitrification of fuel in DES based solvents [16].

From our previous chapter, the DES methyltriphenyl phosphonium bromide [MTPB]-ethylene glycol (1:4) was found to be an effective solvent for the removal of quinoline from heptane. The fuel oil in the hydrocarbon stream having both aromatic as well as PAH simultaneously along with other aliphatic. Therefore, it is necessary need to study the simultaneous extraction of both toluene and quinoline component within the hydrocarbon stream. This is required since both the component co-exist together in fuel and can affect the selectivity and distribution coefficients. To achieve such an objective, quaternary LLE data is required for the separation of quinoline and indoline from toluene – heptane mixture at 35 °C and atmospheric pressure. Gibb's free energy models such as Non- random two liquid (NRTL) and UNiversal QUAsi Chemical (UNIQUAC) ware then used to correlate the experimental data. Furthermore, the continuum solvation model is employed to predict the phase behavior of studied systems.

4.2 Materials and Methods

4.2.1 Materials

Ethylene glycol, heptane and toluene were purchased from Merck, India with purity of ≥ 99%. Quinoline (≥ 98%) and indoline (≥ 99%) were procured from Sigma-Aldrich, Germany. The salt methyltriphenyl phosphonium bromide [MTBP] (≥ 98%) and NMR solvent such as deuterated chloroform ($CDCl_3$, > 99.8%) were supplied by SRL, India Pvt. Ltd. The chemicals were further kept under vacuum at 50 °C for 48 hours to remove the moisture present in the substance. Purities of all chemicals were confirmed by ^{1}H NMR spectroscopy and used without further purification.

4.2.2 Experimental Procedure

The procedure for the preparation of DES is already reported in our previous chapter 2. Both MTPB and EG were weighed on a digital weighing balance (Denver Instrument, Model SI-234) having an accuracy of ±0.0001 g. The mixture [MTPB]-EG (1:4) was taken in a 100 mL of conical flask and placed on a magnetic hot plate (Tarson Spin, MC-02, India) with a stirring speed of 800 rpm at a temperature of 80 °C until the homogenous clear liquid solution was formed. The temperature of the system was consistently monitored with a digital thermometer probe inserted within it. After preparation of DES, ^{1}H and ^{13}C NMR spectra were taken to confirm the purity of prepared DES (Figure 2.8 and Figure 4.1).

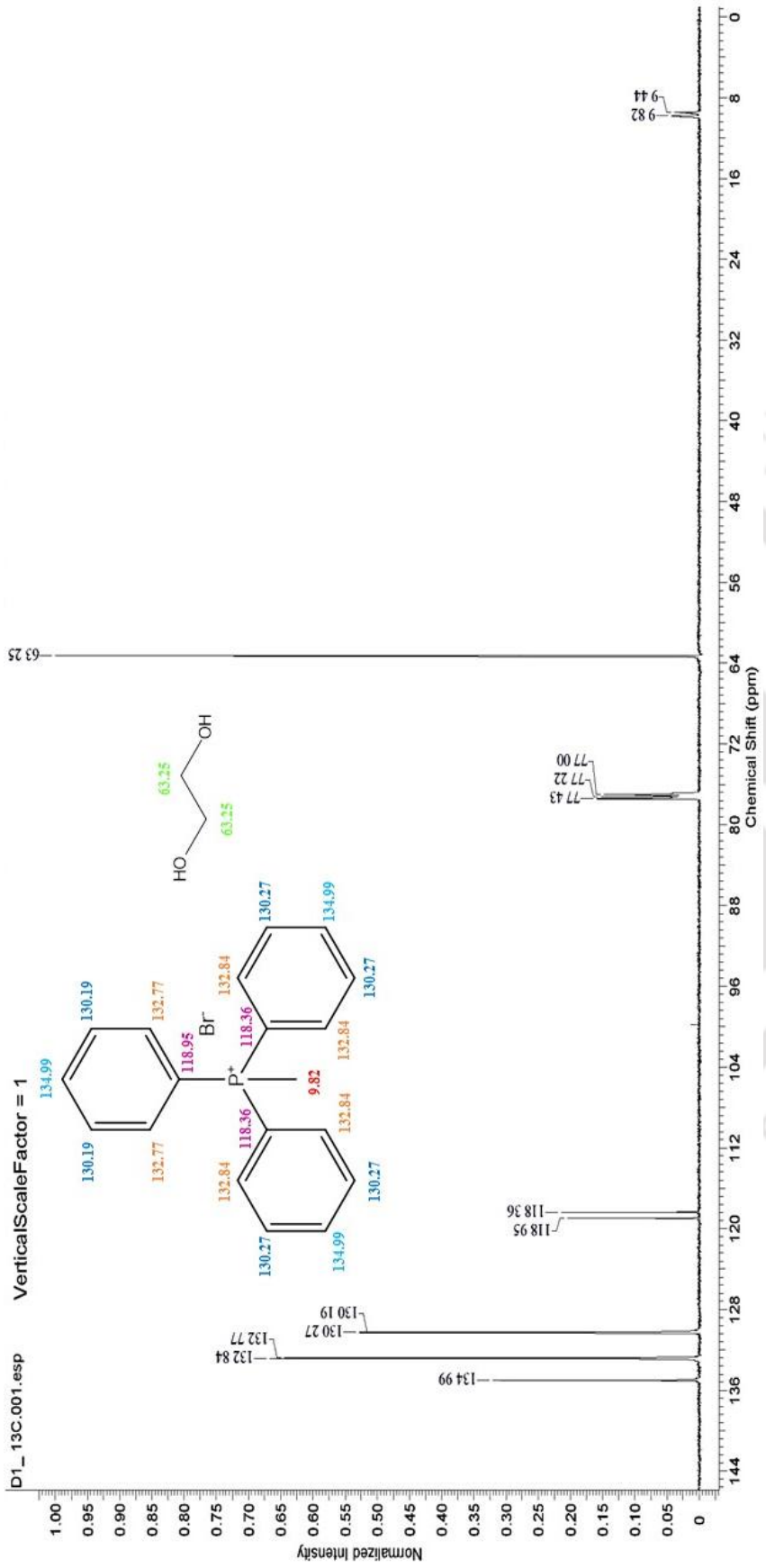

Figure 4.1: ^{13}C NMR spectra of DES [Methyltriphenyl phosphonium bromide+ Ethylene glycol (1:4)]

The LLE experiments were performed on mixtures such that they lie in the immiscible region. An equimolar concentration of DES and heptane was taken in a 15 mL stripped vial using 5 ml syringe. Quinoline and indoline were added to DES-heptane mixtures by varying the concentrations from 5% to 70% (5, 10, 20, 30, 40, 50, 60 and 70%) for eight different combinations, which gives eight tie line data points. The mixtures were compactly sealed with parafilm tape to prevent losses. The vials are kept inside a water shaker bath (Dailhan Lab, China) at 35 °C. The mixture was allowed to shake for 6 to 12 h. In order to evaluate whether the system has reached the equilibrium state, samples were drawn at different time intervals and then measured their concentrations. When two successive sample concentrations reveal no change in their concentrations, the measured concentration corresponds to the phase equilibrium of the particular component at desired temperature.

4.2.3 Phase Analysis

^{1}H NMR spectroscopy (600MHz NMR, Brucker, Germany) was performed to analyze both extract and raffinate phase compositions. The phase equilibrated samples from both phases were withdrawn with using 1 mL fine syringe. 0.1 mL of phase equilibrated sample was dissolved in 0.6 mL of $CDCl_3$ in a thrift grade NMR tube. After that, the ^{1}H NMR spectra were recorded for both raffinate and extract phases and the spectra's are presented in Figures 4.2-4.5. From the NMR spectra's, we integrate the respective peak areas for the number of hydrogen atoms present within each functional group of a component. The compositional analysis procedure for the determination of mole fraction is explained in the section 3.2.4 (chapter-3).

The contribution in the area of such hydrogen atom for all the components are then added and divided with the respective area to get the individual mole fraction. ACD/NMR software [17] was used for the processing of the raw NMR data. The equation for calculation of mole fraction is given as;

$$x_i = \frac{H_i}{\sum_{i=1}^{n} H_i} \qquad (4.1)$$

Where H_i is the peak area of the single 'H' atom and x_i is the mole fraction of the i^{th} component in the sample. 'n' is the total number of the component present in the sample. Hence, n=3 and n=4 represent the ternary and quaternary systems, respectively.

From the NMR spectra (Figures 4.2-4.5), the hydrogen atom (which was attached to nitrogen atom) of quinoline present at ~8.89 ppm was used to quantify its concentration. Similarly, for indoline concentration, the peak at ~6.5-6.8 ppm are considered and was corresponds to the hydrogen atom attached to the nitrogen heterocycle. The peak area of –CH_3– at 2.4 ppm was used to quantify the toluene. The reference peak of $CDCl_3$ was set to 7.27 ppm. Similarly, for DES, the peak for salt MTPB is assigned to the aromatic ring at ~7.7-7.6 ppm and –CH_3– peak at ~2.9 ppm. We have adopted the methyl peak as a reference for quantification of DES in all the samples. Heptane shows a peak at ~0.8 ppm due to the $(–CH_3–)_2$ and ~1.14 ppm due to $(–CH_2–)_3$. The identification peak marked for each compound were used for quantification of mole fraction in both phases using Eq. (4.1). The sample calculation of mole fraction from NMR spectra is described in the Appendix-A.

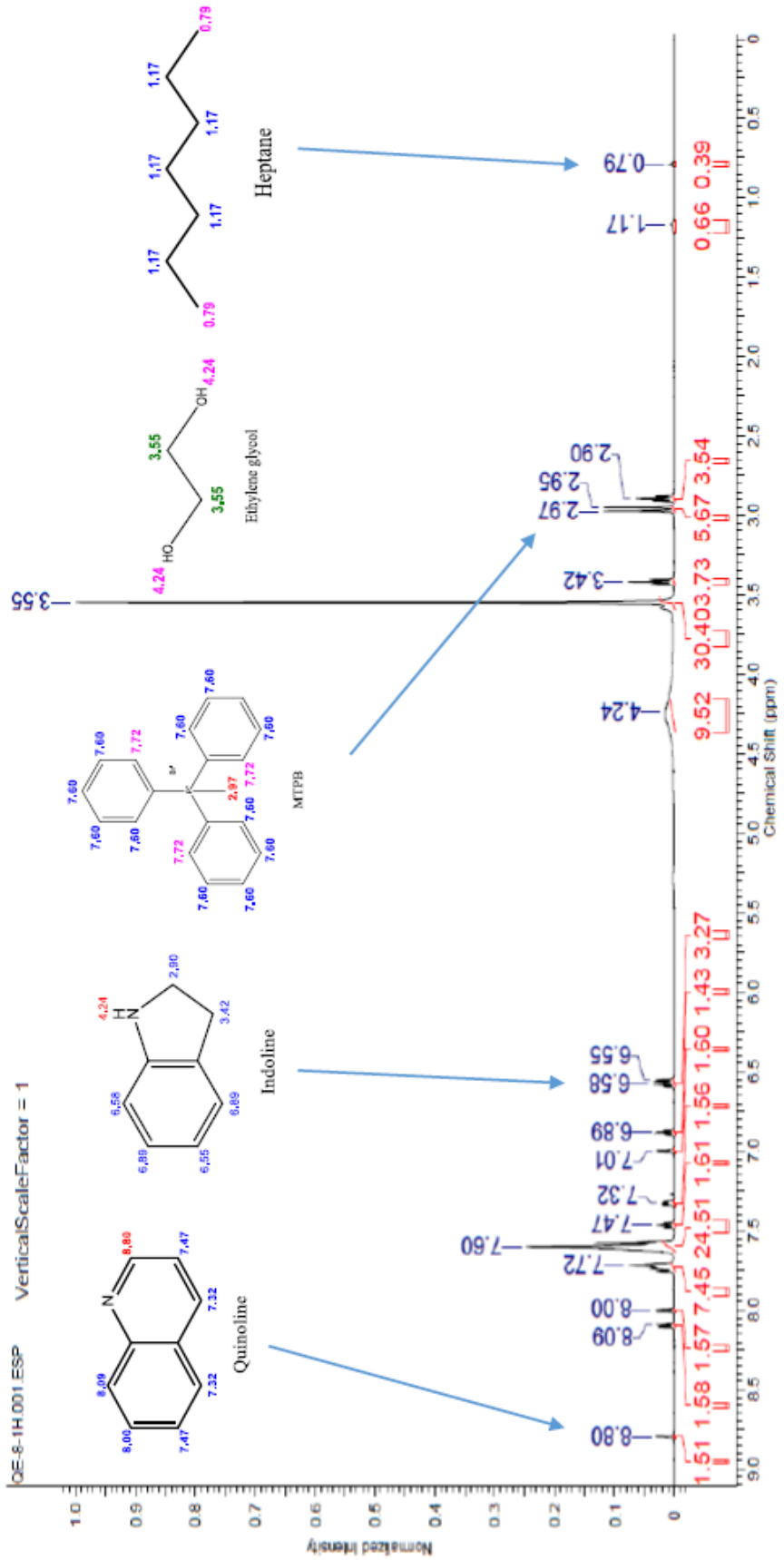

Figure 4.2: NMR spectra for the extract phase of system -1 [DES(1)+ Quinoline(2)+ Indoline(3)+ Heptane(4)] at *T*=308.15 K

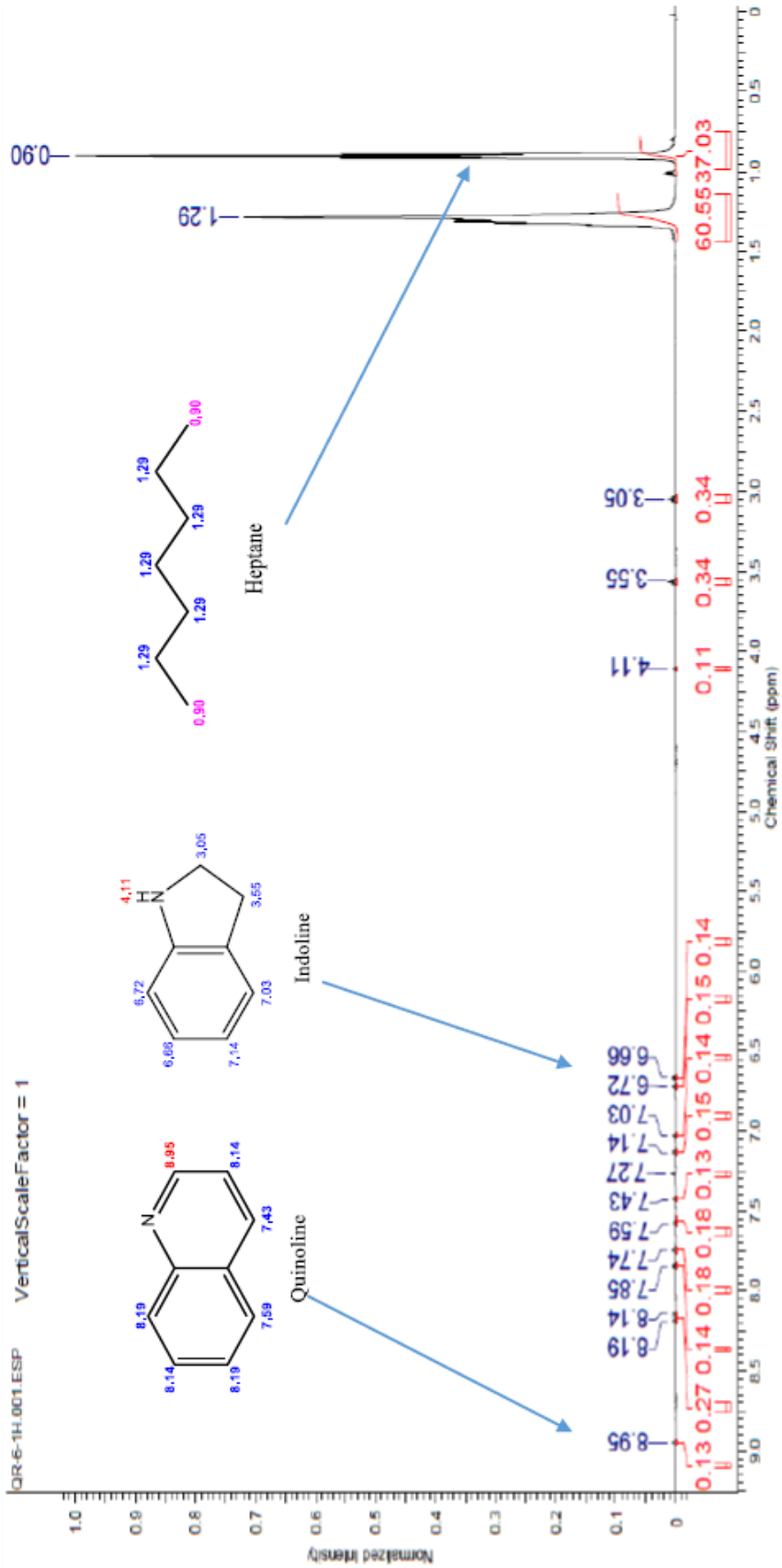

Figure 4.3: NMR spectra for the raffinate phase of system -1 [DES(1)+ Quinoline(2)+ Indoline(3)+ Heptane(4)] at T=308.15

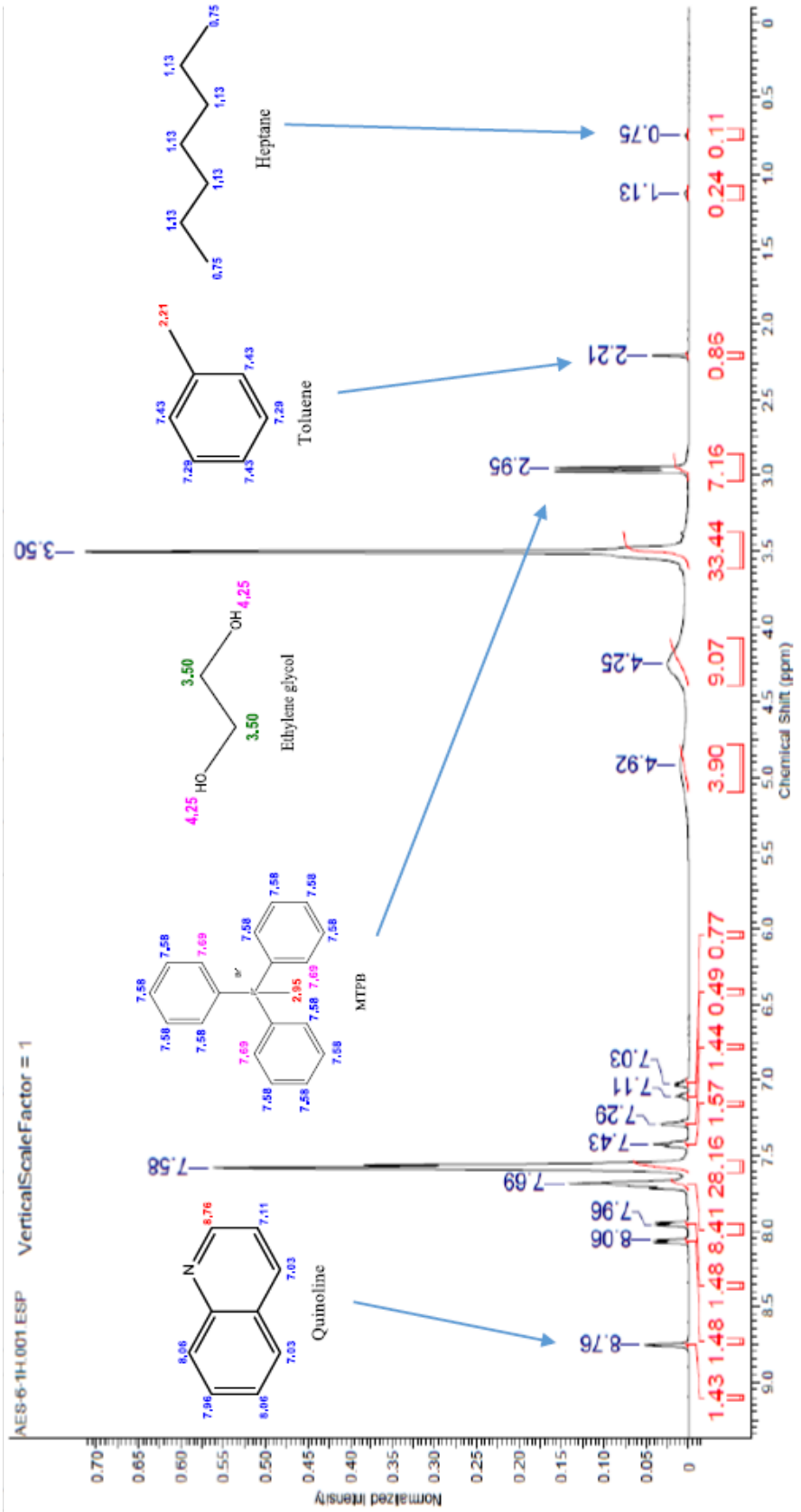

Figure 4.4: NMR spectra for the extract phase of system -2 [DES(1)+ Quinoline(2)+ Toluene(3)+ Heptane(4)] at T=308.15 K

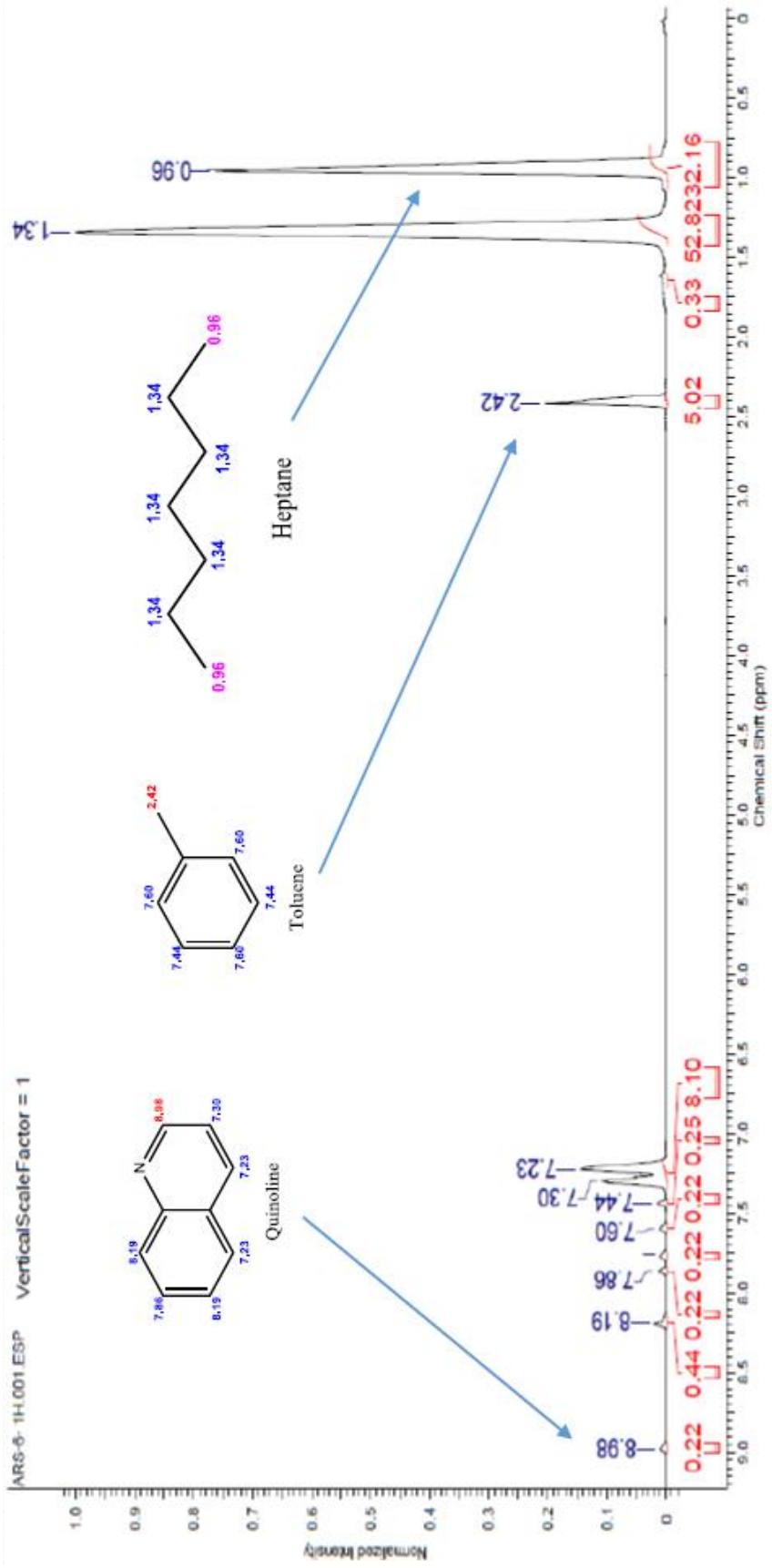

Figure 4.5: NMR spectra for the raffinate phase of system -2 [DES(1)+ Quinoline(2)+ Toluene(3)+ Heptane(4)] at T=308.15 K

4.3 Regression and Predictions using Thermodynamic Models

4.3.1 NRTL and UNIQUAC Models

The mole fractions of both phases are presented in Tables 4.1-4.3. To ascertain the validity of the tie lines, excess Gibb's free energy models such as NRTL [18] and UNIQUAC [19] models are applied to obtain the binary interaction parameters. These models are used to correlating the experimental LLE data of ternary and quaternary systems of the present study. The detailed description about these models can be found elsewhere [18,19]. The binary interaction parameter (τ_{ij}) is calculated from experimental data by minimizing the objective function (F) by using Genetic Algorithm (GA) program [20] which is given as:

$$F_{\left(\begin{array}{c}\text{with respect to } \tau_{ij} \\ \text{where } i,j=1,2,3 \\ \text{and } \ j\neq i\end{array}\right)} = -\sum_{k=1}^{m}\sum_{l=I}^{II}\sum_{i=1}^{c}\left(x_{ik}^{l}-\hat{x}_{ik}^{l}\right)^{2} \qquad (4.2)$$

The equation being non-linear in nature needs to be regressed by a suitable optimization routine. We have used GA tool to perform the same. The details of such as calculation are given elsewhere [21]. The population size, *npop* =100 and number of generations, *ngen* = 200 were used for the minimization of the total error in Eq. (4.2). The compositions of the extract and raffinate phases are calculated using the standard Modified Rashford-Rice algorithm [22]. The details equations used is given in Appendix-A (Table A.1).

4.3.2 COSMO-RS model

COSMO-RS model is used to predict the tie lines from the experimental feed concentration. First, the chemical structures of [MTBP], HBDs, and PAHs were drawn in

the Avogadro free software [23]. The molecular geometry optimization of investigated compounds were fully optimized at B3LYP level of theory using 6-31* basis set by using Gaussian 09 [24]. After geometry optimization step, COSMO file is generated at PBVP86 level of density functional theory [25] using the triple zeta valence potential (TZVP) basis set with the DGA1 density fitting [26]. The first step of the COSMO calculation is to generate the sigma profiles. The sigma profile contains a histogram of all the surface charges within the molecule. The screening charge (σ) for the molecules gives the sigma profile which in turn computes the individual segment activity coefficient [27,28]. The summation of the entire segment activity coefficient gives us the component activity coefficient in either phase. The details of the calculation and methodology are not discussed here as it is given in our earlier work [20,21].

For the sigma profile calculation of DES, a suitable feed ratio was inserted for both HBD and HBA molecule. The charge distribution for such a DES was the algebraic sum of all the sigma profiles calculated separately [29]. It takes the form:

$$p_{DES}(\sigma) = p_{HBA}(\sigma) + p_{HBD}(\sigma) = f_{HBA}p_{HBA}(\sigma) + f_{HBD}p_{HBD}(\sigma) \quad (4.3)$$

$$p_{HBA}(\sigma) = p_{MTBP}(\sigma) + p_{Br}(\sigma) \quad (4.4)$$

Here $p_{HBA}(\sigma)$ and $p_{HBD}(\sigma)$ are the sigma profiles of the constituent of DES. f_{HBA} and f_{HBD} are the mole ratio's that have been adopted in the experimental work (*i.e.,* 1:4). The sigma profiles of DES is normalized so that it would appear as the sigma profile of a single molecule. The pseudo-ternary tie lines are then predicted and then compared with experimental tie lines. The root mean square deviation (RMSD) is used to compare the agreement between the predicted model data and experimental data.

$$RMSD(\%) = \left[\sum_{k=1}^{m} \sum_{j=I}^{II} \sum_{i=1}^{c} \frac{\left(x_{ik}^{l} - \hat{x}_{ik}^{l} \right)^2}{2mc} \right]^{1/2} \times 100 \qquad (4.5)$$

Here x_{ik}^{l} and $\hat{x}_{ik}^{l}$ are the experimental and predicted mole fractions and the subscripts *i, j,* and *k* are component, phase and tie lines, respectively. The various equations used in COSMO-RS calculations are presented in Appendix-A (Table A.2).

4.4 Results and Discussions

The need for the experiments is due to the fact that a simultaneous recovery of both PAH (indoline or quinoline) and aromatic components (toluene) are desired from the fuel oil. Our earlier chapter reports the selection of DES ([MTPB] + Ethylene Glycol) for the extraction of quinolone (PAH) and toluene from fuel oil [30]. The LLE of the three quaternary systems namely, DES (1) + quinoline (2) + indoline (3) + heptane (4), DES (1) + quinoline (2) + toluene (3) + heptane (4) and DES (1) + indoline (2) + toluene (3) + heptane (4) were carried out at 35 °C. The respective mole fractions along with their distribution coefficient (β) and selectivity (S) for quaternary systems are given in Tables 4.1-4.3.

Table 4.4 summarizes the individual selection parameters (S and β) of the corresponding quaternary system. The corresponding pseudo-ternary plot for the quaternary system are represented in Figures 4.6-4.8. The present work also reported the recovery of indoline by performing LLE experiments for DES (1) + indoline (2) + heptane (3) systems (Table 4.5 and Figure 4.9).

Table 4.1: Experimental tie line data with corresponding distribution coefficient (β) and selectivity (*S*) for DES(1)+ Quinoline(2)+ Indoline(3)+ Heptane (4) at T = 308.15 K and atmospheric pressure (p = 1 Atm.)

Sl. No.	DES rich phase					Heptane rich phase					β	S
	x_1^I	x_2^I	x_3^I	x_4^I	x_{23}^I	x_1^{II}	x_2^{II}	x_3^{II}	x_4^{II}	x_{23}^{II}		
1	0.819	0.088	0.088	0.005	0.175	0.000	0.003	0.002	0.994	0.006	29.17	5798.33
2	0.748	0.119	0.125	0.008	0.244	0.000	0.006	0.005	0.989	0.011	22.18	2742.23
3	0.644	0.169	0.182	0.006	0.351	0.000	0.006	0.006	0.987	0.013	27.00	4441.50
4	0.578	0.201	0.214	0.007	0.415	0.000	0.008	0.009	0.983	0.017	24.41	3428.11
5	0.502	0.238	0.252	0.009	0.490	0.000	0.011	0.013	0.976	0.024	20.42	2214.07
6	0.428	0.272	0.288	0.012	0.560	0.000	0.020	0.022	0.957	0.043	13.02	1038.60
7	0.403	0.280	0.306	0.012	0.586	0.000	0.016	0.019	0.966	0.034	17.24	1387.44
8	0.371	0.296	0.321	0.013	0.617	0.000	0.019	0.022	0.959	0.041	15.05	1110.14

Table 4.2: Experimental tie line data with corresponding distribution coefficient (β) and selectivity (*S*) for DES(1)+ Quinoline(2)+ Toluene(3)+ Heptane (4) at *T*= 308.15 K and atmospheric pressure (*p* = 1 Atm.)

Sl.No.	DES rich phase					Heptane rich phase					β	S
	x_1^I	x_2^I	x_3^I	x_4^I	x_{23}^I	x_1^{II}	x_2^{II}	x_3^{II}	x_4^{II}	x_{23}^{II}		
1	0.927	0.062	0.006	0.005	0.068	0.000	0.005	0.028	0.967	0.033	2.06	398.52
2	0.858	0.120	0.015	0.007	0.135	0.000	0.003	0.047	0.950	0.050	2.70	366.43
3	0.755	0.207	0.030	0.008	0.237	0.000	0.006	0.087	0.907	0.093	2.55	288.92
4	0.720	0.242	0.034	0.004	0.277	0.000	0.014	0.129	0.857	0.143	1.94	415.02
5	0.647	0.297	0.052	0.004	0.349	0.000	0.016	0.169	0.815	0.185	1.89	384.37
6	0.579	0.347	0.070	0.004	0.416	0.000	0.030	0.231	0.739	0.261	1.59	294.47
7	0.611	0.333	0.052	0.004	0.385	0.000	0.028	0.197	0.775	0.225	1.71	331.53
8	0.549	0.379	0.067	0.005	0.446	0.000	0.040	0.249	0.711	0.289	1.54	219.45

Table 4.3: Experimental tie line data with corresponding distribution coefficient (β) and selectivity (*S*) for DES(1)+ Indoline(2)+ Toluene(3)+ Heptane(4) at *T*= 308.15 K and atmospheric pressure (*p* = 1 Atm.)

Sl.No.	DES rich phase					Heptane rich phase					β	S
	x_1^I	x_2^I	x_3^I	x_4^I	x_{23}^I	x_1^{II}	x_2^{II}	x_3^{II}	x_4^{II}	x_{23}^{II}		
1	0.904	0.078	0.012	0.007	0.090	0.000	0.003	0.026	0.971	0.029	3.10	430.49
2	0.844	0.127	0.021	0.007	0.148	0.000	0.007	0.045	0.948	0.052	2.85	385.45
3	0.747	0.210	0.037	0.006	0.247	0.000	0.011	0.090	0.899	0.101	2.45	366.42
4	0.671	0.269	0.053	0.007	0.322	0.000	0.015	0.136	0.849	0.151	2.13	258.64
5	0.623	0.309	0.061	0.007	0.370	0.000	0.024	0.162	0.815	0.185	2.00	232.86
6	0.592	0.330	0.071	0.006	0.401	0.000	0.028	0.186	0.786	0.214	1.87	245.47
7	0.558	0.356	0.081	0.005	0.437	0.000	0.036	0.218	0.746	0.254	1.72	256.69
8	0.519	0.381	0.094	0.006	0.475	0.000	0.035	0.255	0.710	0.290	1.64	193.82

Table 4.4: Individual Selection parameters for all three quaternary LLE systems

System-1*				System-2**				System-3***			
β_{qui}	β_{ind}	S_{qui}	S_{ind}	β_{qui}	β_{tol}	S_{qui}	S_{tol}	β_{ind}	β_{tol}	S_{ind}	S_{tol}
29.33	44.00	5831.47	8747.20	12.40	0.21	2398.16	41.44	26.00	0.46	3606.57	64.02
19.83	25.00	2451.90	3090.63	40.00	0.32	5428.57	43.31	18.14	0.47	2457.06	63.20
28.17	30.33	4633.42	4989.83	34.50	0.34	3911.44	39.09	19.09	0.41	2860.45	61.60
25.13	23.78	3528.27	3339.08	17.29	0.26	3703.46	56.47	17.93	0.39	2175.06	47.27
21.64	19.38	2346.34	2102.15	18.56	0.31	3782.11	62.69	12.88	0.38	1499.02	43.84
13.60	13.09	1084.60	1044.00	11.57	0.30	2136.94	55.98	11.79	0.38	1543.93	50.01
17.50	16.11	1408.75	1296.47	11.89	0.26	2304.24	51.14	9.89	0.37	1475.42	55.44
15.58	14.59	1149.25	1076.36	9.48	0.27	1347.35	38.26	10.89	0.37	1288.14	43.62

* DES (1) + Quinoline (2) + Indoline (3) + Heptane (4); ** DES (1) + Quinoline (2) + Toluene (3) + Heptane (4); *** DES (1) + Indoline (2) +Toluene (3) + Heptane (4)

Table 4.5: Experimental tie line data with corresponding distribution coefficient (β) and selectivity (*S*) for DES(1)+ Indoline(2)+ Heptane(3) at T = 308.15 K and atmospheric pressure (p = 1 Atm.)[a]

Sl. No.	DES rich phase			Heptane rich phase			β	S
	x_1^I	x_2^I	x_3^I	x_1^{II}	x_2^{II}	x_3^{II}		
1	0.860	0.134	0.006	0.000	0.009	0.991	14.89	2459.15
2	0.698	0.296	0.006	0.000	0.016	0.984	18.50	3034.00
3	0.594	0.398	0.008	0.000	0.017	0.983	23.41	2876.72
4	0.476	0.514	0.010	0.000	0.024	0.976	21.42	2090.27
5	0.352	0.635	0.013	0.000	0.045	0.955	14.11	1036.62
6	0.270	0.712	0.018	0.000	0.067	0.933	10.63	550.83
7	0.197	0.777	0.026	0.000	0.096	0.904	8.09	281.41
8	0.128	0.829	0.043	0.000	0.143	0.857	5.80	115.54

[a] Standard uncertainties are u(T) = 0.01 K, u(x) = 0.001

Figure 4.6-4.8 presents the correlation between experimental tie lines data and local thermodynamic models (NRTL and UNIQUAC). For all the investigated systems, the concentration of n-heptane in the extract phase is almost negligible. It is also noteworthy to observe that the concentration of DES in the raffinate phase is zero. Therefore, it results in a favorable environment for the simultaneous extraction of PAHs since the interaction between DES and heptane are negligible. Hence, this phenomenon will make easier solvent recovery without additional heat. It was also confirmed from the NMR spectroscopy where no trace amount of DES (absence of peaks) was present in the raffinate phase (Figures 4.2-4.5).

The pseudo-ternary diagram indicates that the system exhibited type-2 phase behavior, implying that the DES is able to extract PAH very effectively from heptane. The terms distribution coefficient (β) and selectively (S) were used to measure the effectiveness of solute removal and the recovery of the solvent. The values of β and S were given in Table 4.4 for individual selection parameters for all three studied quaternary LLE systems.

$$\beta = \frac{x_{PAH}^{E}}{x_{PAH}^{R}} \tag{4.6}$$

$$S = \frac{\beta_{PAH}}{\beta_{hep}} = \frac{x_{PAH}^{E} / x_{PAH}^{R}}{x_{hep}^{E} / x_{hep}^{R}} \tag{4.7}$$

Here, x_{PAH}^{E} and x_{PAH}^{R} are the mole fractions of PAH component(s) in the extract and raffinate phase, respectively. x_{hep}^{E} and x_{hep}^{R} are mole fractions of heptane in both phases. The values of β and S are greater than unity for all LLE systems. The value of β decreases with an increase in the mole fraction of PAH in the raffinate phase. From Table 4.1, it is clearly showing the distribution coefficient of quinoline and indoline was seen to be decreased with increase in the solute concentration. It was also noticed that the pseudo component (PAH + toluene) has higher selectivity (Table 4.2-4.3) when compared to individual (Table 4.5). Similarly, the selectivity of the pure PAH (quinoline or indoline) was higher than that of a mixture of toluene and PAH. Therefore, the presence of toluene in mixture leads to decrease the PAH extraction efficiency. On the other hand, the selectivity was much higher at a lower concentration of the PAH feed composition which was beneficial as the amount of PAH in fuel oil is usually lower.

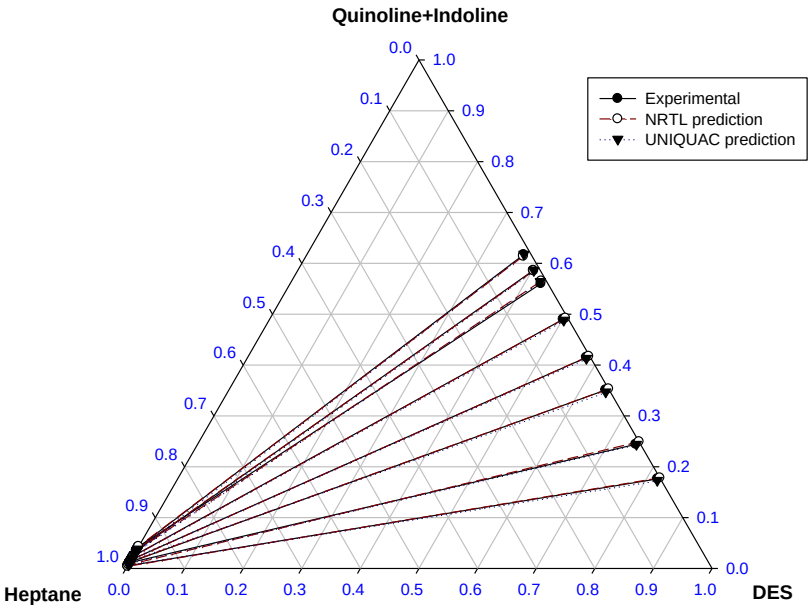

Figure 4.6: Pseudo ternary LLE tie lines with NRTL and UNIQUAC model predictions for DES(1)+ Quinoline(2)+ Indoline(3)+ Heptane(4) at T = 308.15 K

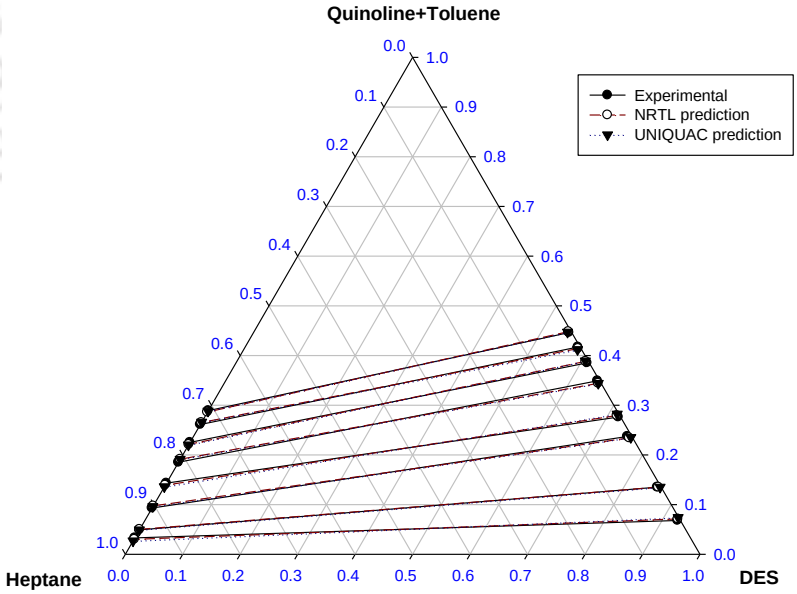

Figure 4.7: Pseudo ternary LLE tie lines with NRTL and UNIQUAC model predictions for DES(1)+ Quinoline(2)+ Toluene(3) + Heptane(4) at T = 308.15 K

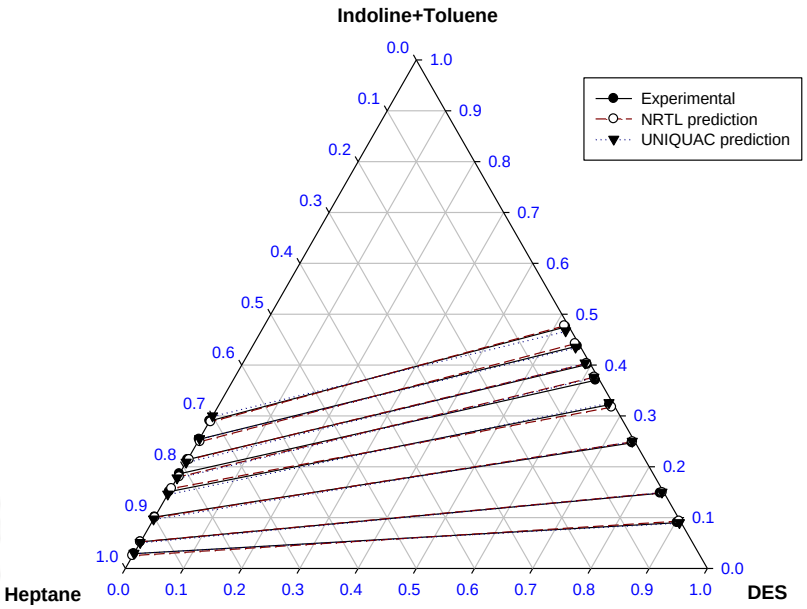

Figure 4.8: Pseudo ternary LLE tie lines with NRTL and UNIQUAC model predictions for DES(1)+ Indoline(2)+ Toluene(3)+ Heptane(4) at T = 308.15 K

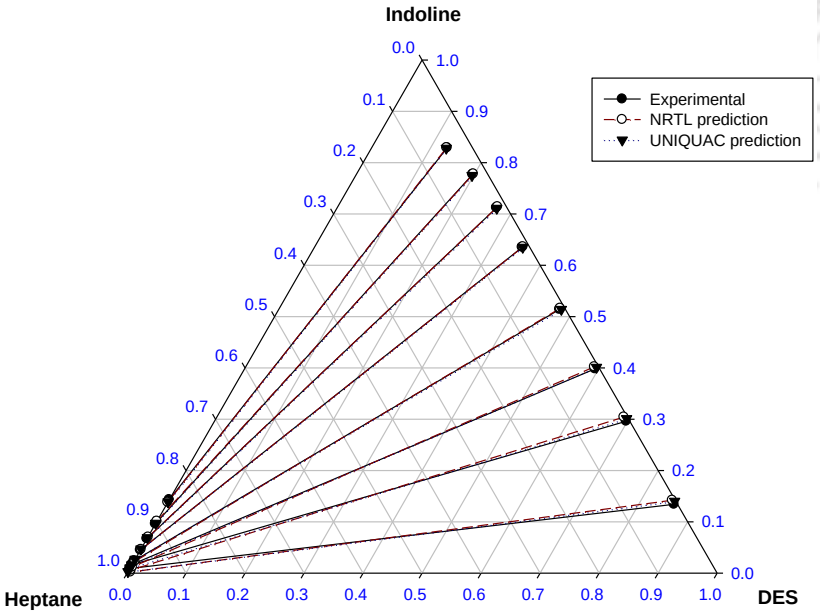

Figure 4.9: Ternary LLE tie lines between with NRTL and UNIQUAC model predictions for DES(1)+ Indoline(2)+ Heptane(3) at T= 308.15 K

From the previous chapter 3, sloping of tie lines were opposite in nature for quinoline and toluene in case of ternary systems. But in this work, all the tie lines are positively sloped towards DES which implying that the mixture of PAHs are efficiently and selectively extracted when compared to heptane or toluene. Higher values of β (>1), lower amount of DES was required (Tables 4.1-4.3). The PAH molecules were known to interact preferentially with DES molecules by π-π interaction [31]. From Tables 4.1-4.4, it was noticed that an increase in PAH concentration leads to decrease in the distribution coefficient and selectively. This is due to the fact that the cation has phenyl groups which are able to accommodate less number of PAH molecules due to steric hindrance [32]. Further, the PAH molecule consists of an extra lone pair of electron on nitrogen which make the quinoline or indoline more electronegative and exert greater affinity towards DES cation.

Thus results in higher hydrogen bonding interaction with the methyl group of the HBA and incoming PAH molecule. This is contrary to toluene, where due to the unavailability of the lone pair, the interaction decreases. Hence the selection of the cationic species or HBA is critical in such an extraction. The ternary diagram shows a longer tie line length in the immiscible region. This suggests that the DES have a higher affinity for PAHs than n-heptane or toluene.

The quaternary system of DES (1) + quinoline (2) + indoline (3) + heptane (4) (Table 4.1 and Figure 4.6) exhibited the highest value of distribution coefficient and selectivity among all the systems. The distribution coefficient was found in the range between 29.17 to 13.02 and selectivity from 5798.33 to 1038.6, respectively. Both values were found to decrease with increase in PAH concentration. For the system DES (1)+ quinoline (2) +

toluene (3)+ heptane (4) (Table 4.2 and Figure 4.7), distribution coefficient and selectivity was significantly lower than other systems. Here *S* values ranging from 415.02 to 219.45 and β values from 2.7 to 1.54. Similarly, the distribution coefficient for DES (1)+ indoline (2)+ toluene (3) + heptane (4) (Table 4.3 and Figure 4.8) ranging from 3.1 to 1.64 which was decreasing gradually with PAH concentration. Finally, the ternary system DES (1)+ indoline (2)+ heptane (3) also gave large values of the distribution coefficient (23.41 to 5.8) and selectivity (3034.0 to 115.54) (Table 4.5 and Figure 4.9). These obtained values were very close to our previous work on DES (1) + quinoline (2) + heptane (3) system [30].

For comparing the efficiency of the DES, the selectivity (Figure 4.10) and distribution coefficients (Figure 4.11) of all the LLE systems were compared at 30 % aromatic concentration as this is the limit where we obtain the highest selectivity. It was observed that the selectivity of quinoline and indoline in simultaneous mode is much higher than that of toluene or heptane. Individually, both quinoline and indoline gave higher selectivity than toluene. However, it may be noticed that irrespective of simultaneous or individual mode the selectivity remains the same for both quinoline and indoline. With respect to distribution coefficient which is an indicator for solvent requirement, we observe a lower ratio for a simultaneous recovery.

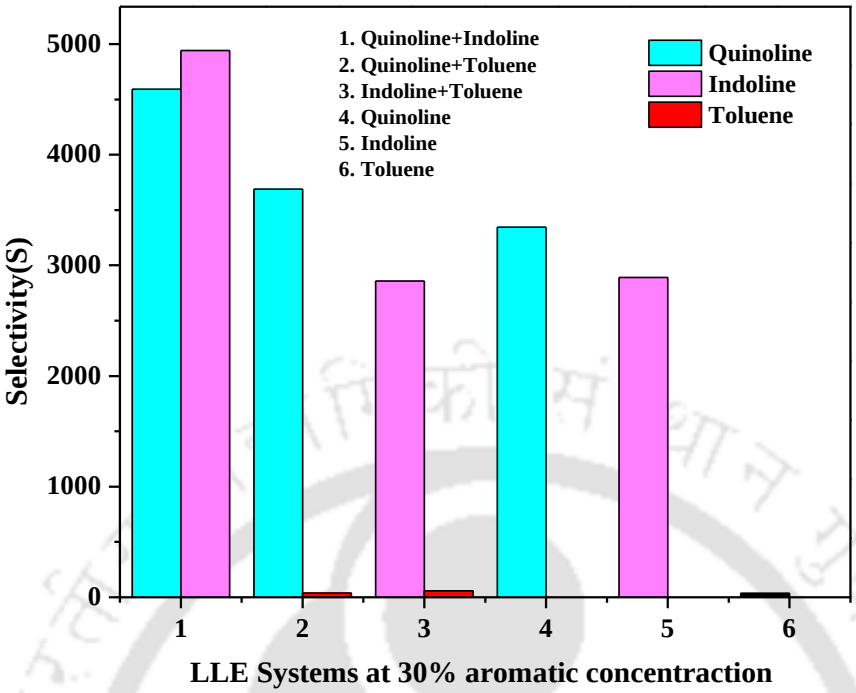

Figure 4.10: Selectivity (S) of all LLE system at 30 % aromatic concentration

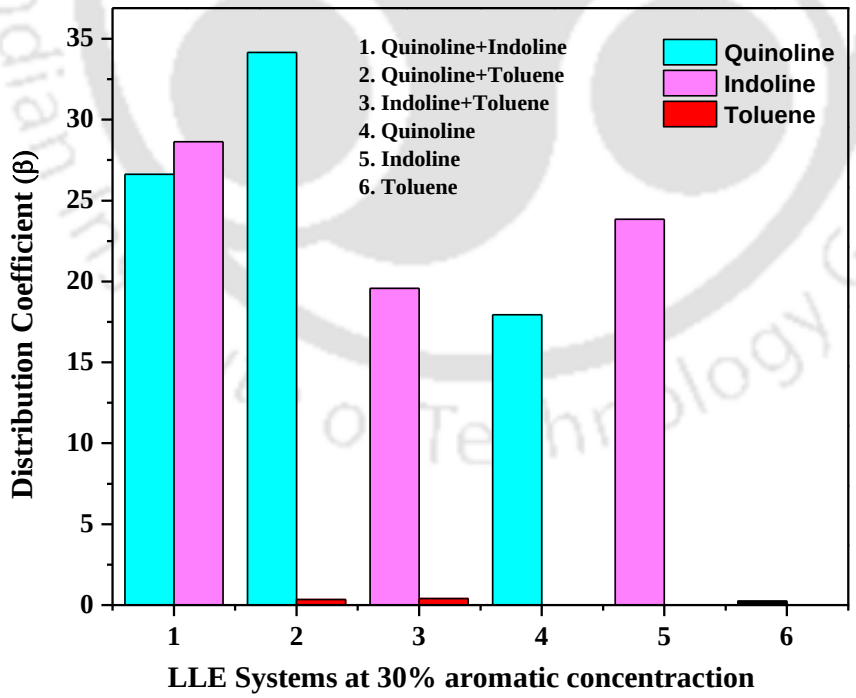

Figure 4.11: Distribution coefficient (β) of all LLE system at 30 % aromatic concentration

4.4.1 Correlation with Thermodynamic Models

4.4.1.1 NRTL and UNIQUAC

The correlation between the experimental data with NRTL and UNIQUAC model tie-line data were measured with root mean square deviation (RMSD) (Eq. (7)). The predicted tie line data along with experimental data for all systems were presented in Figures 4.6-4.8 based on Tables 4.1-4.3. For the UNIQUAC model, the structural parameters (*r* and *q*) were reported in Table 4.6. The calculated binary interaction parameters for these models are given in Tables 4.7-4.10 along with their RMSD values. The RMSD value of all quaternary systems varies from 0.27 to 0.31% for NRTL and 0.19 to 0.35% for UNIQUAC model.

Table 4.6: UNIQUAC structural parameters for different component (*r* and *q*) in LLE system

Sl. No	Compound	*r*	*q*
1	Heptane	5.174	4.396
2	Toluene	3.923	2.968
3	Quinoline	4.939	3.727
4	Indoline	4.724	3.638
5	DES	14.113	10.993

The ternary system DES (1) + indoline (2) + heptane (3) gave a RMSD value of 0.37% and 0.28% for both models (Table-S5). The RMSD value, which is less than 1%, indicate that the thermodynamic models gave an excellent agreement between them. This can be visualized from Figures 4.6-4.8 where the tie lines are seen to overlap with each other. We have set the lower and upper bounds for estimation of interaction parameters for

all the systems in such a way that all parameters are lies within the same range. The lower and upper bound for NRTL and UNIQUAC model were used as -100 to +100 and -1000 to +1000, respectively. The objective functions are calculated according to the eq. (4) (Tables 4.7-4.10).

4.4.1.2 COSMO-RS

The first step of the COSMO calculation is to generate the sigma profiles of investigated compounds and are presented in Figure 4.12. The hydrogen bonding contribution [27] is non-zero only if one segment has a negative charge density less than the cutoff value -0.0084 e/Å^2 and the other side has a positive charge density greater than 0.0084 e/Å^2. In this way, hydrogen bonding is limited to segment pairs of opposite charge and larger magnitudes.

From Figure 4.12, it is clear that the σ-profile of the DES possess a large fraction of peak towards the positive region indicating the possibility of hydrogen bonding with MTPB cation. Quinoline and indoline both displays a symmetrical profile and has a higher fraction of charge both in the hydrogen bonding acceptor and donor region. This enables them to initiate hydrogen bonding with DES molecules. Further, the complementary profiles [27,28] of DES and PAH does indeed refer excellent miscibility which is magnified in the experimental tie line data (Tables 4.1-4.3). It is interesting to note that toluene has a lower fraction of charge in the hydrogen bonding acceptor or donor region. Thus, toluene was less extracted as compared to PAH. Heptane being non-polar in nature is resistant to hydrogen bonding due to its non-availability of acceptor or donor groups.

Table 4.7: NRTL and UNIQUAC binary interaction parameters for DES(1)+ Quinoline(2)+ Indoline(3)+ Heptane (4) at *T*= 308.15 K and atmospheric pressure

i-j	NRTL parameters				UNIQUAC parameters			
	τ_{ij}	τ_{ji}	F[a]	% RMSD[b]	A_{ij}	A_{ji}	F[a]	% RMSD[b]
1-2	64.45	-78.66	-4.8×10^{-4}	0.27	-65.68	997.86	-2.3×10^{-4}	0.19
1-3	-9.29	8.86			-134.33	992.28		
1-4	0.58	36.69			384.97	144.91		
2-3	97.34	-72.09			666.53	-6.407		
2-4	-7.84	3.55			70.99	131.98		
3-4	54.55	-3.88			936.37	285.08		

[a] equation (4.2), [b] equation (4.5)

Table 4.8: NRTL and UNIQUAC binary interaction parameters for DES(1)+ Quinoline (2)+ Toluene(3)+ Heptane (4) at *T*= 308.15 K and atmospheric pressure

i-j	NRTL parameters				UNIQUAC parameters			
	τ_{ij}	τ_{ji}	F[a]	%RMSD[b]	A_{ij}	A_{ji}	F[a]	%RMSD[b]
1-2	-35.81	16.31	-4.66×10^{-4}	0.27	-961.09	-211.45	-6.79×10^{-4}	0.32
1-3	-34.56	-34.13			-112.19	-772.89		
1-4	28.91	38.29			437.3	843.97		
2-3	11.37	7.01			-164.86	102.1		
2-4	-66.93	-4.79			-489.6	-754.59		
3-4	3.39	99.38			-62.33	-889.26		

[a] equation (4.2), [b] equation (4.5)

Table 4.9: NRTL and UNIQUAC binary interaction parameters for DES(1)+ Indoline(2)+ Toluene(3) + Heptane (4) at *T*= 308.15 K and atmospheric pressure

i-j	NRTL parameters				UNIQUAC parameters			
	τ_{ij}	τ_{ji}	F[a]	%RMSD[b]	A_{ij}	A_{ji}	F[a]	%RMSD[b]
1-2	-63.73	-60.68	-6.35×10^{-4}	0.31	-10.91	500.02	-7.96×10^{-4}	0.35
1-3	-51.89	-99.19			423.32	250.87		
1-4	25.26	83.96			421.74	765.38		
2-3	-71.81	-39.42			915.99	34.71		
2-4	-89.16	-75.04			-17.92	579.91		
3-4	3.65	-33.45			44.38	195.22		

[a] equation (4.2), [b] equation (4.5)

Table 4.10: NRTL and UNIQUAC binary interaction parameters for DES(1)+ Indoline(2)+ Heptane(3) at *T*= 308.15 K and atmospheric pressure

i-j	NRTL parameters				UNIQUAC parameters			
	τ_{ij}	τ_{ji}	F[a]	%RMSD[b]	A_{ij}	A_{ji}	F[a]	%RMSD[b]
1-2	-2.85	2.03	-6.66×10^{-4}	0.37	75.74	29.89	-3.7×10^{-4}	0.28
1-3	3.69	3.40			503.16	8.75		
2-3	15.71	1.38			-150.63	154.33		

[a] equation (4.2), [b] equation (4.5)

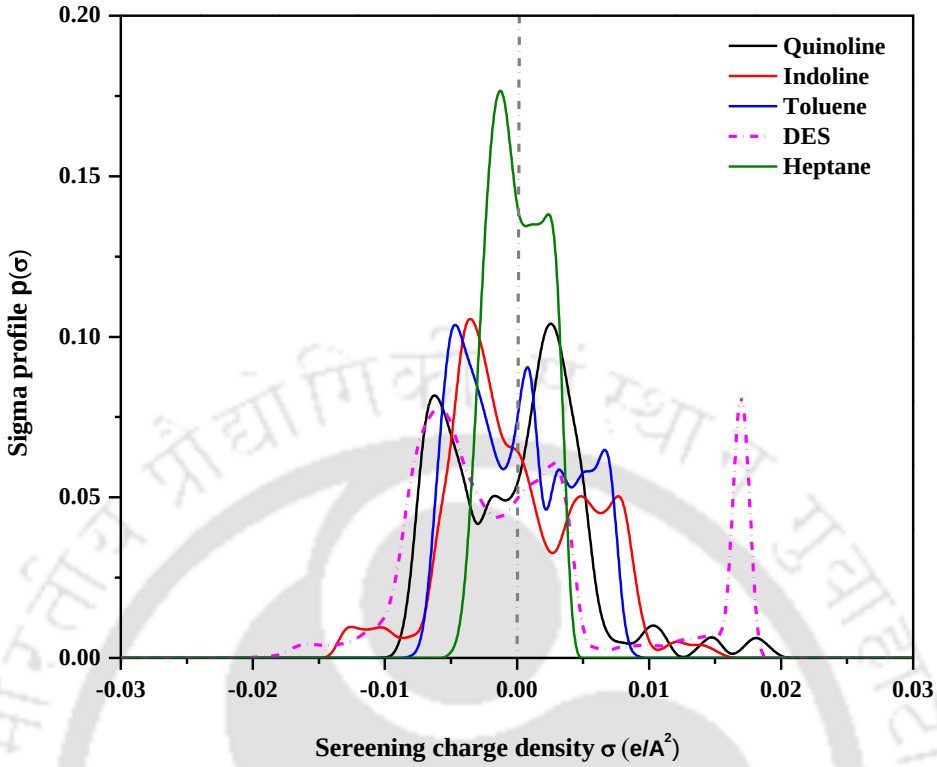

Figure 4.12: Normalized sigma profile comparison for all studied compounds

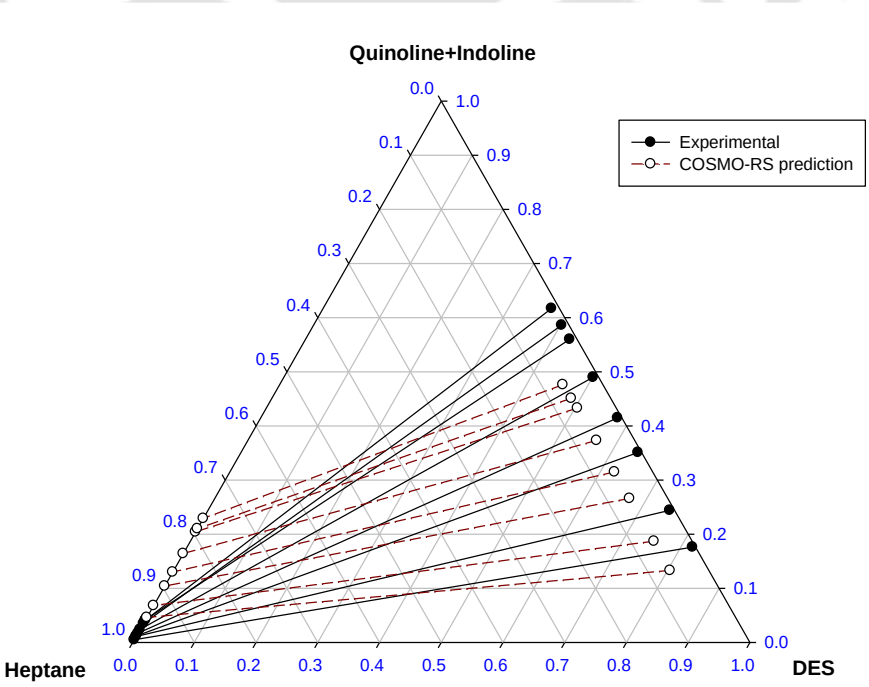

Figure 4.13: Pseudo ternary LLE tie lines and COSMO-RS prediction for DES(1)+ Quinoline(2)+ Indoline(3)+ Heptane(4) at T = 308.15 K

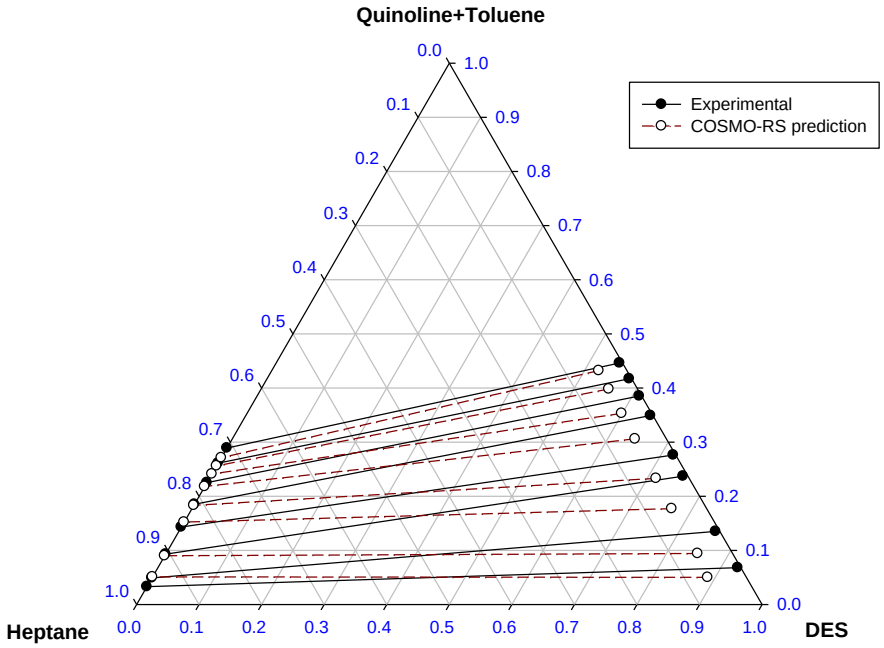

Figure 4.14: Pseudo ternary LLE tie lines and COSMO-RS prediction for DES(1)+ Quinoline(2)+ Toluene(3)+ Heptane(4) at T = 308.15 K

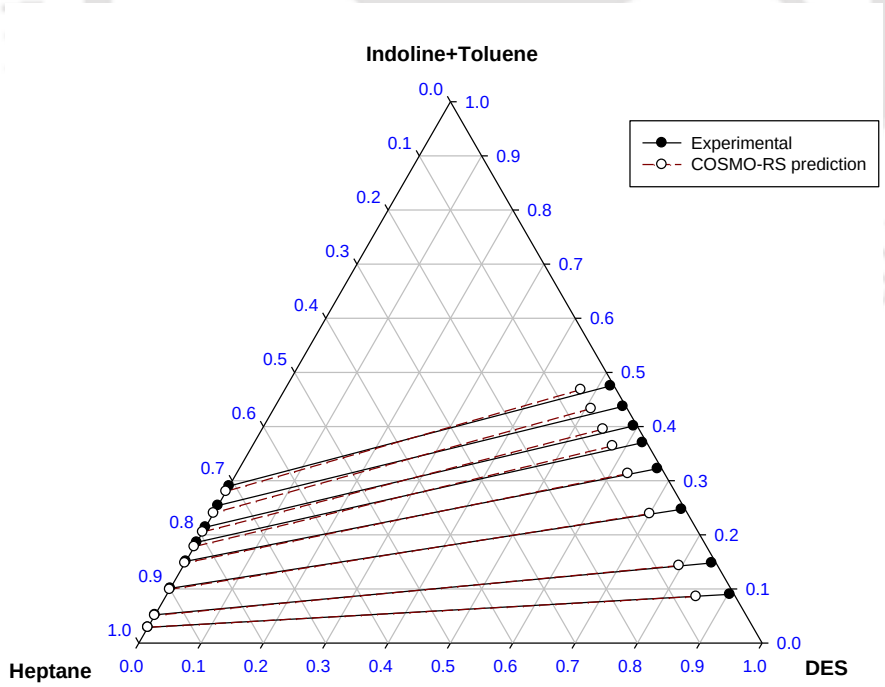

Figure 4.15: Pseudo ternary LLE tie lines and COSMO-RS prediction for DES(1)+ Indoline(2)+ Toluene(3)+ Heptane (4) at T= 308.15 K

Figure 4.13-4.15 shows the pseudo-ternary diagram of the three quaternary systems validated with the COSMO-RS prediction along experimental tie lines along with their RMSD values. In the quinoline + indoline PAH mixture (Figure 4.13), the deviation between the COSMO-RS tie lines and experimental tie lines were shown to be higher. For other systems, the deviation was lower and had better agreement with experimental data. As evident from experimental data, the COSMO-RS model also predicts a negligible DES fraction in the raffinate phase. These values of RMSD indicate that COSMO-RS model is indeed consistent and can be used for the prediction of phase equilibria predictions.

4.5 Conclusion

The current study reported the extraction of PAH and toluene from n-heptane using a novel DES [MTBP]-Ethylene glycol at 35 °C. The ternary system DES (1) + indoline (2)+ heptane (3) shows higher extraction efficiency of indoline from n-heptane than quaternary systems. The DES [MTBP]-EG was able to extract both toluene and PAH significantly in the case of ternary system. The presence of toluene in the quaternary system reduced the efficiency of DES when compared to PAH. The distribution coefficient and selectively of all systems were further determined, where it was found that an increase in the solute concentration of PAH leads to decrease in selectivity. It was also observe that the concentration of DES in raffinate phase was zero. This will necessitate a lesser number of operations were required for solvent recovery. The experimental tie line data were correlated with the three thermodynamic models such as NRTL, UNIQUAC and COSMO-RS model. All the thermodynamic models gave very good agreement with experimental data. The study reveals that the phosphonium based DES can be used as a potential solvent for the selective removal of PAH from fuel oil.

References

[1] A. Jayaraman, F.H. Yang, R.T. Yang, Effects of nitrogen compounds and polyaromatic hydrocarbons on desulfurization of liquid fuels by adsorption via π-complexation with Cu (I) Y zeolite, Energy & Fuels 20 (2006) 909-914.

[2] Y. Yongtan, Determination of nitrogen compounds in catalytic diesel oil using gas chromatography, Chin. J. Chromatogr. 26 (2008) 478-483.

[3] S. Zhang, Q. Zhang, Z.C. Zhang, Extractive desulfurization and denitrogenation of fuels using ionic liquids, Ind. Eng. Chem. Res. 43 (2004) 614-622.

[4] S.H. Ali, H.M. Lababidi, S.Q. Merchant, M.A. Fahim, Extraction of aromatics from naphtha reformate using propylene carbonate, Fluid Phase Equilib. 214 (2003) 25-38.

[5] E.J. González, N. Calvar, B. González, Á. Domínguez, (Liquid+ liquid) equilibria for ternary mixtures of (alkane+ benzene+ [EMpy][ESO 4]) at several temperatures and atmospheric pressure, J. Chem. Thermodyn. 41 (2009) 1215-1221.

[6] J. Zhang, C. Huang, B. Chen, P. Ren, Z. Lei, Extraction of aromatic hydrocarbons from aromatic/aliphatic mixtures using chloroaluminate room-temperature ionic liquids as extractants, Energy & Fuels 21 (2007) 1724-1730.

[7] Y. Hou, Y. Gu, S. Zhang, F. Yang, H. Ding, Y. Shan, Novel binary eutectic mixtures based on imidazole, J. Mol. Liq. 143 (2008) 154-159.

[8] A.P. Abbott, D. Boothby, G. Capper, D.L. Davies, R.K. Rasheed, Deep eutectic solvents formed between choline chloride and carboxylic acids: versatile alternatives to ionic liquids, J. Am. Chem. Soc. 126 (2004) 9142-9147.

[9] A.P. Abbott, G. Capper, D.L. Davies, R.K. Rasheed, V. Tambyrajah, Novel solvent properties of choline chloride/urea mixtures, Chem. Comm. DOI (2003) 70-71.

[10] C.C. Cassol, A.P. Umpierre, G. Ebeling, B. Ferrera, S.S. Chiaro, J. Dupont, On the extraction of aromatic compounds from hydrocarbons by imidazolium ionic liquids, Int. J. Mol. Sci. 8 (2007) 593-605.

[11] U.K. Ravilla, T. Banerjee, Liquid liquid equilibria of imidazolium based ionic liquid+ pyridine+ hydrocarbon at 298.15 K: Experiments and correlations, Fluid Phase Equilib. 324 (2012) 17-27.

[12] M.R. Shah, R. Anantharaj, T. Banerjee, G.D. Yadav, Quaternary (liquid+ liquid) equilibria for systems of imidazolium based ionic liquid+ thiophene+ pyridine+ cyclohexane at 298.15 K: Experiments and quantum chemical predictions, J. Chem. Thermodyn. 62 (2013) 142-150.

[13] M.A. Kareem, F.S. Mjalli, M.A. Hashim, M.K. Hadj-Kali, F.S.G. Bagh, I.M. Alnashef, Phase equilibria of toluene/heptane with deep eutectic solvents based on ethyltriphenylphosphonium iodide for the potential use in the separation of aromatics from naphtha, J. Chem. Thermodyn. 65 (2013) 138-149.

[14] F.S. Oliveira, A.B. Pereiro, L.P. Rebelo, I.M. Marrucho, Deep eutectic solvents as extraction media for azeotropic mixtures, Green Chem. 15 (2013) 1326-1330.

[15] M.C. Ali, Q. Yang, A.A. Fine, W. Jin, Z. Zhang, H. Xing, Q. Ren, Efficient removal of both basic and non-basic nitrogen compounds from fuels by deep eutectic solvents, Green Chem. 18 (2016) 157-164.

[16] H.F. Hizaddin, A. Ramalingam, M.A. Hashim, M.K. Hadj-Kali, Evaluating the performance of deep eutectic solvents for use in extractive denitrification of liquid fuels by the conductor-like screening model for real solvents, J. Chem. Eng. Data 59 (2014) 3470-3487.

[17] ACD/Structure Elucidator, Advanced Chemistry Development, Inc., Toronto, ON, Canada, 2010, https://www.acdlabs.com.

[18] H. Renon, J.M. Prausnitz, Local compositions in thermodynamic excess functions for liquid mixtures, AlChE J. 14 (1968) 135-144.

[19] D.S. Abrams, J.M. Prausnitz, Statistical thermodynamics of liquid mixtures: a new expression for the excess Gibbs energy of partly or completely miscible systems, AlChE J. 21 (1975) 116-128.

[20] T. Banerjee, M.K. Singh, R.K. Sahoo, A. Khanna, Volume, surface and UNIQUAC interaction parameters for imidazolium based ionic liquids via polarizable continuum model, Fluid Phase Equilib. 234 (2005) 64-76.

[21] M.K. Singh, T. Banerjee, A. Khanna, Genetic algorithm to estimate interaction parameters of multicomponent systems for liquid–liquid equilibria, Comput. Chem. Eng. 29 (2005) 1712-1719.

[22] J.D. Seader, E.J. Henley, Membrane separations. In Separation Process Principles,

John Wiley & Sons, New York, 2006.

[23] Avogadro: an open-source molecular builder and visualization tool. Version 1.0. 3 http://avogadro.cc/.

[24] M. Frisch, G. Trucks, H. Schlegel, G. Scuseria, M. Robb, J. Cheeseman, G. Scalmani, V. Barone, B. Mennucci, G. Petersson, Gaussian 09 Program; Gaussian, Inc, Wallingford, CT DOI (2009).

[25] J.P. Perdew, Density-functional approximation for the correlation energy of the inhomogeneous electron gas, Phys. Rev. B. 33 (1986) 8822.

[26] A. Schäfer, C. Huber, R. Ahlrichs, Fully optimized contracted Gaussian basis sets of triple zeta valence quality for atoms Li to Kr, J. Chem. Phys. 100 (1994) 5829-5835.

[27] A. Klamt, G. Schüürmann, COSMO: a new approach to dielectric screening in solvents with explicit expressions for the screening energy and its gradient, J. Chem. Soc. Perkin Transactions 2 DOI (1993) 799-805.

[28] A. Klamt, Conductor-like screening model for real solvents: a new approach to the quantitative calculation of solvation phenomena, Journal of Physical chemistry 99 (1995) 2224-2235.

[29] T. Banerjee, K.K. Verma, A. Khanna, Liquid–liquid equilibrium for ionic liquid systems using COSMO-RS: Effect of cation and anion dissociation, AlChE J. 54 (2008) 1874-1885.

[30] P.K. Naik, P. Dehury, S. Paul, T. Banerjee, Evaluation of Deep Eutectic Solvent for the selective extraction of toluene and quinoline at T= 308.15 K and p= 1 bar, Fluid Phase Equilib. 423 (2016) 146-155.

[31] M. Sarwono, M. Hadj-Kali, I. Alnashef, Application of deep eutectic solvents for the separation of aliphatics and aromatics, Technology, Informatics, Management, Engineering, and Environment (TIME-E), 2013 International Conference on, IEEE, 2013, pp. 48-53.

[32] A.R. Hansmeier, M. Jongmans, G.W. Meindersma, A.B. de Haan, LLE data for the ionic liquid 3-methyl-N-butyl pyridinium dicyanamide with several aromatic and aliphatic hydrocarbons, J. Chem. Thermodyn. 42 (2010) 484-490.

CHAPTER 5

Molecular Dynamics Validation of LLE in Ternary System

5.1 Introduction

As discussed earlier, extraction processes are reliable, cost-effective, and biocompatible as compared to that of hydrodenitrification process [1-3]. However, this depends on the efficiency of the solvent, its cost, recyclability, and environmentally friendliness [4-8]. In our previous chapters namely 2- 4, we have reported that DES consisting of methyltriphenylphosphonium bromide [MTPB] salt and ethylene glycol can effectively remove quinoline from heptane. We have also observed that the use of DES, MTPB-ethylene glycol mixture in the extraction of PAH has shown higher values of selectivity and distribution coefficients as compared to the other conventional solvents.

Very few research work have been devoted to the investigation of the mechanism by which the extraction process takes place by using computer simulation methods such as molecular dynamic (MD) simulations. Classical MD simulation provides a fundamental molecular level understanding. Further, classical MD simulations are also useful in carrying out the processes under extreme conditions that cannot be attained with conventional experimental techniques. Moreover, different computational methods also help us in exploring new solvent systems and screen optimum ones among many alternatives in the most economical way [9,10]. Though theoretical studies are important, they are not anticipated to replace experiments, rather accompany them and enhance their application. For example, Stephenson et al. [11] carried out MD simulations for the extraction of ethanol from long chain alcohols using MD simulations. Further, Taha and Lee [12] reported the phase separation of organic solvents from water using the biological buffer as an external solvent by MD simulations. In a recent study, Dehury et al. [13] have

investigated the phase behavior of butanol in between ionic liquid and water by both LLE experimental and MD simulation studies. Perkins et al. [14] also performed the experimental and computational study to get insights into choline chloride based DES.

Real experiments are performed for a duration of the order of hours/minutes or seconds. In such an order, the atomic scale simulation is not feasible due to computational restrictions. To make the system affordable, atomic scale phenomena are generally recorded at nano second (ns) scale or in other words the velocities are computed after every 1 femto second. Chemical phenomena such as disengagement at atomic level occur at fraction of seconds which even digital instruments are even unable to detect. Therefore, theoretical calculations and simulations aim to capture this phenomenon through a statistical mechanical framework or ensemble theory. In such a scenario, the Liquid-Liquid Equilibrium simulation results defined in this chapter is one such result or trajectory. This inherently connects properties generated by chemical engineers namely the activity coefficient implicit for the computation of mole fractions using first principles. Hence, the role of molecular simulations in the LLE based experiments is very important to understand the behavior of different molecules and the mechanism involved in different ternary systems. Therefore, the present study aims at the extraction of quinoline from heptane using DES by classical MD simulations at 308.15 K and 1 atm pressure condition. In the chapter, we have compared MD simulation results with our previous experimental results as measured in chapter 3 and 4.

5.2 Molecular Dynamics Simulation Details

Initially, the structures of isolated ions of DES, quinoline, and heptane were drawn in GaussView05 software with their geometries optimized by Gaussian09 [15] at B3LYP/6-31G* theory. The partial charges for different atomic sites of the isolated molecules were obtained by using the same level of theory *i.e.*, B3LYP/6-31G* [16]. The chemical structures of these species are shown in Figure 5.1 along with their atom notations. The partial charges for different species (as obtained from the quantum calculations) were then fitted with Restricted Electrostatic Potential (RESP) [17] module of AMBER12 [18]. The final partial charges for different atomic sites of these molecules are shown in Table 5.1.

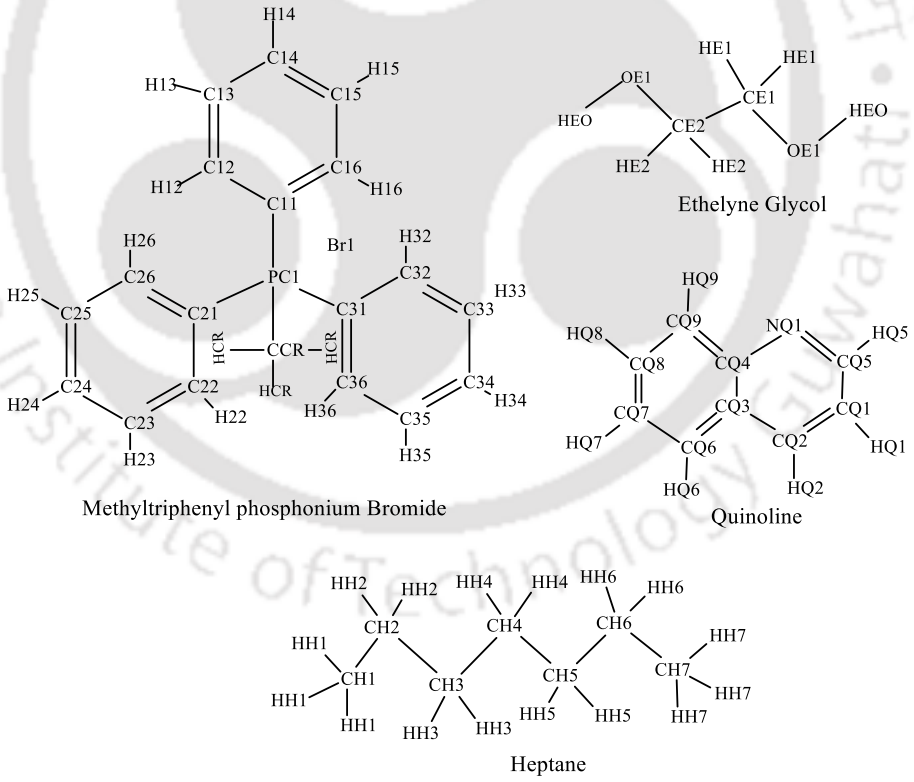

Figure 5.1: Structures with atom notations of different molecular species

Table 5.1: Partial charges of different atoms in the molecules species

MTPB		Ethylene Glycol		Quinoline		Heptane	
Atom Type	Partial Charge	Atom Type	Partial Charge	Atom Type	Partial Charge	Atom Type	Partial Charge
PC1	0.526019	CE1	0.28673	CQ1	-0.47650	CH1	-0.32290
C11	-0.03824	HE1	0.00555	CQ5	0.41660	HH1	0.07130
C12	-0.12645	HE1	0.00555	HQ5	0.06248	HH1	0.07130
C13	-0.14442	OE1	-0.72930	NQ1	-0.73080	HH1	0.07130
C14	-0.06429	HEO	0.43152	HQ1	0.19525	CH2	0.19185
C15	-0.14442	CE2	0.28673	CQ2	0.04030	HH2	-0.03270
C16	-0.12645	HE2	0.00555	HQ2	0.13483	HH2	-0.03270
H16	0.145970	HE2	0.00555	CQ3	-0.15630	CH3	0.05983
H15	0.166293	OE1	-0.72930	CQ6	-0.18200	HH3	-0.01760
H14	0.159398	HEO	0.43152	HQ6	0.15698	HH3	-0.01760
H13	0.166293	--	--	CQ4	0.72289	CH4	-0.07840
H12	0.145970	--	--	CQ9	-0.42290	HH4	-0.00300
C21	-0.03824	--	--	HQ9	0.19914	HH4	-0.00300
C22	-0.12645	--	--	CQ8	-0.06020	CH5	0.05983
C23	-0.14442	--	--	HQ8	0.14352	HH5	-0.01760
C24	-0.06429	--	--	CQ7	-0.20030	HH5	-0.01760
C25	-0.14442	--	--	HQ7	0.15695	CH6	0.19185
C26	-0.12645	--	--	--	--	HH6	-0.03270
H26	0.145970	--	--	--	--	HH6	-0.03270
H25	0.166293	--	--	--	--	CH7	-0.32290
H24	0.159398	--	--	--	--	HH7	0.07130
H23	0.166293	--	--	--	--	HH7	0.07130
H22	0.145970	--	--	--	--	HH7	0.07130
CCR	-0.57439	--	--	--	--	--	--
HCR	0.209798	--	--	--	--	--	--
HCR	0.209798	--	--	--	--	--	--
HCR	0.209798	--	--	--	--	--	--
C31	-0.03824	--	--	--	--	--	--
C32	-0.12645	--	--	--	--	--	--
C33	-0.14442	--	--	--	--	--	--
H33	0.166293	--	--	--	--	--	--
H32	0.145970	--	--	--	--	--	--
C36	-0.12645	--	--	--	--	--	--
H36	0.145970	--	--	--	--	--	--
C35	-0.14442	--	--	--	--	--	--
H35	0.166293	--	--	--	--	--	--
C34	-0.06429	--	--	--	--	--	--
H34	0.159398	--	--	--	--	--	--
Br1	-1.00000	--	--	--	--	--	--

All the force field parameters (that are required for performing MD simulation) were generated according to the Generalized Amber Force Field (GAFF) [19] functional form using the ANTECHAMBER [20] module of AMBER12 [18]. The details description on AMBER force fields is given in Appendix-A. The generated force field parameters were further validated by comparing the simulated density of DES (1.261 gm/cm^3) at 308.15 K temperature and ambient pressure condition with that of experimental density value (1.277 gm/cm^3) at the same temperature and pressure condition. Classical MD simulations were then performed for two experimental LLE tie-line data points in order to understand their behavior and phase separations. These ternary systems consisted of DES + quinoline + heptane system. These experimental tie line data points were taken from Chapter 3, Table 3.4. Due to the limitation and constraint, MD simulations were carried out for only two tie-line data points, tie-line-2 (System 1) and tie-line-5 (System 2), at their corresponding feed compositions. The number of molecules considered for different systems are presented in Table 5.2. The representation and molecular analysis of System-1 were carried out since it has a maximum value of distribution coefficient and selectivity. As can be seen from Table 5.2, we have reported 400 (S1: System 1) and 250 (S2: System 2) molecules of DES which are considered for MD simulations. It should be noted that DES here is representing a solvent with the mixture of two components at a 1:4 molar ratio. Therefore for MD simulations involves DES (1:4 molar ratio) i.e 400 molecules of MTPB mixed with 1600 molecules of ethylene glycol for the S1 system. Similarly, 250 molecules of salt MTPB were mixed with 1000 molecules of ethylene glycol for the S2 system. Nanoscale Molecular Dynamics (NAMD) was used for simulation. The NAMD configuration file is given in Appendix-A.

Table 5.2: Experimental composition and considered number of molecules in MD simulations for different tie-line data points

System	Tie-line no.	Mole fraction				Number of molecules			
		DES	Quinoline	Heptane	Total	DES	Quinoline	Heptane	Total
S1	2	0.40	0.20	0.40	1	400	200	400	1000
S2	5	0.25	0.50	0.25	1	250	500	250	1000

Table 5.3: Experimental and MD simulated liquid-liquid equilibrium data for DES (1)-Quinoline (2)-Heptane (3) ternary system at T= 308.15 K and 1 Atm. pressure[a]

System	Tie-line No	Type of data	DES rich phase			Heptane rich phase			Distribution coefficient (β)	Selectivity (S)
			x_{DES}	x_{qui}	x_{hep}	x_{DES}	x_{qui}	x_{hep}		
S1	2	Exp.	0.698	0.295	0.007	0.000	0.013	0.987	22.69	3204.70
		Comp.	0.676	0.321	0.003	0.005	0.027	0.968	11.88	3419.18
S2	5	Exp.	0.354	0.638	0.008	0.000	0.062	0.938	10.29	1298.20
		Comp.	0.340	0.655	0.005	0.004	0.075	0.921	8.73	1476.00

[a] Tie-line values are taken from chapter -3, RMSD = 0.01%

The initial configuration of different systems consisting of DES, quinoline and heptane molecules were generated using PACKMOL [21]. At first, DES molecules were put in a cubical box (75 Å × 75 Å × 75 Å) and heptane molecules were packed in a different cubic box (75 Å × 75 Å × 75 Å). Then the joining of these two boxes created a two-phase system, one is DES rich and the second one is heptane rich. Thereafter, the quinoline molecules were randomly distributed in these two phases. Therefore, the considered geometry was similar to the experimental condition. The experimental procedure was provided in chapter 3 section 3.2. All the MD simulations were run in NAMD 2.9 package [22] using Langevin thermostat and Nose-Hoover Langevin barostat [23,24]. A time integration step of 1 fs was used for all simulations. Initially, the systems were energy minimized for 1 ns and thereafter each of the systems were gradually heated from 0 K to 308.15 K in 0.5 ns. After that, the systems were equilibrated for 8 ns in isothermal-isobaric (NPT) ensemble at 308.15 K temperature and 1 atm pressure. For maintaining the desired temperature Langevin dynamics method [25] with a collision frequency of 1 ps^{-1} was used. Nose-Hoover Langevin barostat was used for controlling the pressure with an oscillation period of 100 fs and damping factor of 50 fs [26]. Thereafter, the production runs lasted for 200 ns for each of the systems with NVT ensemble. At every 5 ps, the trajectory data was saved for structural and transport analysis. For analysis of the trajectories, Visual Molecular Dynamics (VMD) package was used [27]. SHAKE algorithm was used to restrain the bonds involving hydrogen atoms [28]. The particle mesh Ewald (PME) method was used to calculate the long-range intermolecular electrostatic interactions [29] and for treating short-ranged intermolecular interactions, a cut-off distance of 12 Å was used. To remove edge effect, periodic boundary conditions were applied in all three directions.

5.3 Results and Discussion

5.3.1 Comparison of Experimental and MD Simulated Results

We first compare the LLE experimental and MD simulated tie-line data for the system DES (1)-quinoline (2)-heptane (3) as shown in Table 5.3. Figure 5.2 depicts a tie line which is commonly used in chemical engineering community for indicating the distribution of a component or solute in two phases namely extract and raffinate phase. Here the two ends of the tie lines represent the composition in the extract and raffinate phase. The tie line will invariably pass through the initial feed mixture (Figure 5.2). To get a complete phase diagram we have to vary the solute concentration (i.e., quinoline) while keeping the other two components at the same volume ratio. In this way, the entire heterogeneity of the system is captured. Here, the LLE data shows a type 2 behavior [30].

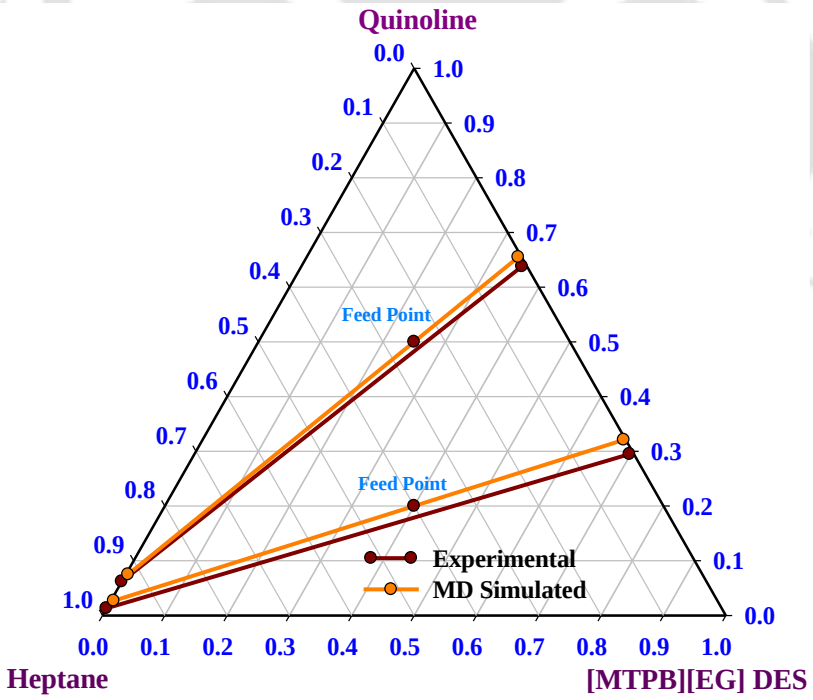

Figure 5.2: Experimental and MD simulation correlated tie-lines data points for the ternary system: DES(1)+ Quinoline(2)+ Heptane(3) at T = 308.15 K and p = 1 Atm.

A type-II system exhibits a phase envelope that spans the composition space and connects two binary miscibility gaps. As shown in Figure 5.2 the binary system namely DES-quinoline shows miscibility while the other binaries, DES-heptane and heptane-quinoline are completely immiscible. From Figure 5.2, it can be noticed that the raffinate phase data occupies the extreme corner point of the ternary diagram. Thus, the quinoline molecules have actually transferred to the extract DES rich phase. Moreover, in Figure 5.2 we have also compared the experimental ternary phase diagram of DES-quinoline-heptane system with that of simulated one. It is clear that it gave good agreement between the experimental and simulated values. For the calculation of distribution coefficient (β) and selectivity (S), the following equations were used (Eq. 5.1 and 5.2) [31].

$$\beta = \frac{x^{E}_{Quinoline}}{x^{R}_{Quinoline}} \tag{5.1}$$

$$S = \frac{\beta_{Quinoline}}{\beta_{Heptane}} = \frac{x^{E}_{Quinoline} / x^{R}_{Quinoline}}{x^{E}_{Heptane} / x^{R}_{Heptane}} \tag{5.2}$$

Here, $x^{E}_{Quinoline}$ and $x^{R}_{Quinoline}$ refer to the mole fractions of quinoline in extract and raffinate phases, respectively. $x^{E}_{Heptane}$ and $x^{R}_{Heptane}$ are the mole fractions of heptane in extract and raffinate phases. As can be seen from Table 5.3, the values of β and S are greater than unity for both tie-lines. The higher values of S indicates the better ability of DES for the extraction of quinoline from heptane. The distribution coefficient indicates that the distribution of quinoline molecules from heptane rich phase to DES rich phase. Higher the β value better will be the distribution of quinoline from heptane to DES rich phase. This observation suggests a significant extraction of quinoline (from heptane solvent) by DES.

From the observation of Table 5.3, the MD predicted mole fraction of quinoline in both raffinate and extract phases is quite higher than that of experimental value. However, on the contrary, it gives a lower distribution coefficient for quinoline when compared to experimental value.

A closer look into the β values for the first tie-line data reveals a reasonably lower value when compared to its experimental value. In specific for this tie-line, the experimental value of β is twice that of its simulated value. This difference in the β values may occur due to the failure in exactly locating the number of molecules at the predetermined interface because a small uncertainty can lead to a marked change in the distribution values. The reported mole fraction values are the average of three different random structural molecular simulation results. Similar deviations in the β values were also observed by Dehury et al. [13] during the extraction of butanol from water using IL as a solvent. The MD results show better selectivity values for both the tie-line data when compared to the experimental values (Table 5.3).

In Figure 5.3, we present the snapshots of system-1 at different simulation times, which reveal a gradual distribution of quinoline molecules from heptane rich phase to DES rich phase and hence supports the observations discussed above. The system with interfacial geometry, therefore, mimics the phase equilibria where the considered geometry was similar to the experimental procedure in a manner that quinoline molecules were randomly dispersed in DES and heptane rich phases. The distribution of quinoline molecules from heptane to DES phase starts from the beginning of the production run and the maximum distribution is seen to complete at around 200 ns. At 200 ns, the system was observed to be DES in the middle and heptane on two sides (Figure 5.3d).

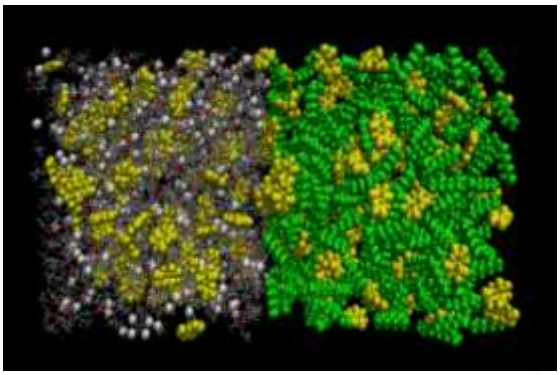

(a) DES-QUI-HEP (0 ns)

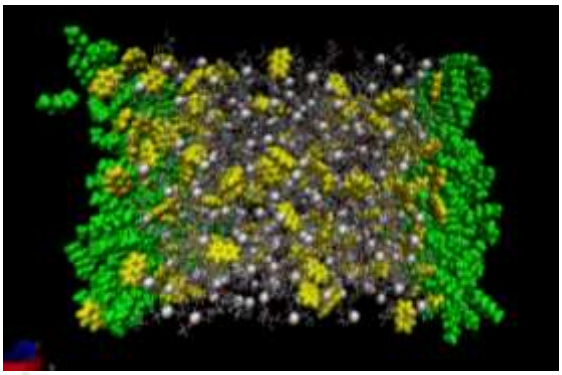

(c) DES-QUI-HEP (100 ns)

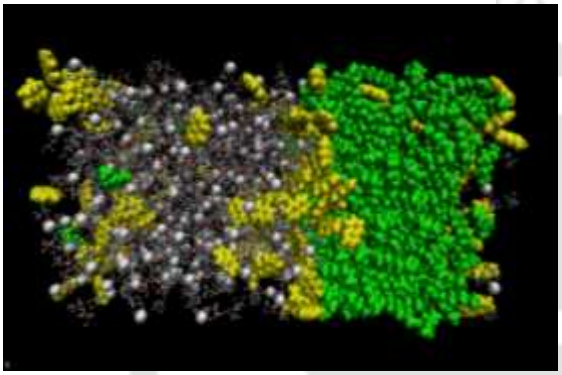

(b) DES-QUI-HEP (50 ns)

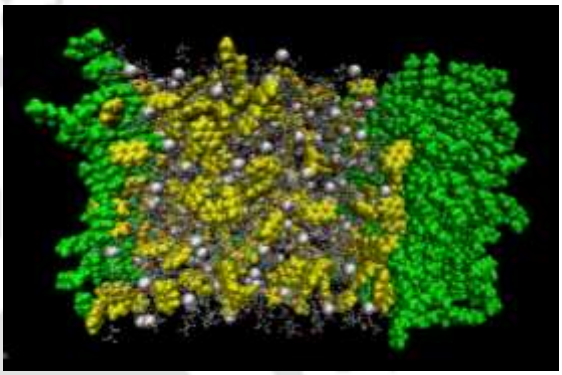

(d) DES-QUI-HEP (200 ns)

Figure 5.3: Distribution snapshots of quinoline in solvent throughout the system at different time (a) 0 ns, (b) 50 ns, (c) 100 ns and (d) 200 ns respectively (Yellow: Quinoline molecules; Green: Heptane molecules; Grey: DES molecules) for system-1 (S1)

A similar slab geometry was also reported by Taha and Lee (2013) [12] in their study on the separation of water and organic solvents using the biological buffer as an external solvent. We also observed that an increase in the simulation runtime did not cause a significant change in the distribution of quinoline molecules. It should be noted that the selectivity of DES is much higher as compared to that of the ionic liquids (ILs) used in previous work [32-34]. Thus, the solvent DES is capable of extracting more of quinoline from the hydrocarbon solvent than that of ILs, which is an alternative green solvent. The MD simulation is computationally expensive as it relates to the prediction of dynamic properties as compared to solvent-accessible molecular surfaces model like COSMO-RS.

Where, the computational cost is lower compared to that of MD simulation. However, only solute properties such as solvation energy, rather than equilibrium properties could be modeled. Here the MD simulation is used to study the inhomogeneous systems behavior.

5.3.2 Non-Bonded Interaction Energy

In order to quantify the interactions between different system species, we decomposed the total non-bonded interaction energies into electrostatic and van der Waals (vdW) components. These are shown in Table 5.4. For this, we consider the tie-line data point of system-1. It can be noticed that the non-bonded interaction between DES-quinoline is more favorable than that for both DES-heptane and heptane-quinoline. A close inspection into the total interaction energies between these species suggests that the interaction between DES-heptane is the least favorable. This observation acts as corroborative evidence of what we discussed in our previous section 5.3.1.

Table 5.4: MD simulated interaction energies (kJ/mole) between different ionic pairs of DES-quinoline-heptane ternary system calculated at 308.15 K and 1 Atm. pressure

Ionic Pair	Electrostatic Interactions (E_{elec})	van der Waals Interactions (E_{vdW})	Total Non-Bonded Interactions (E_{total}[a])
MTP-Quinoline	-7.02	-17.85	-24.87
MTP-Heptane	-0.12	-4.23	-4.35
Br-Quinoline	-2.04	-1.16	-3.21
Br-Heptane	0.08	-0.22	-0.14
EG-Quinoline	-4.25	-12.75	-17.01
EG- Heptane	-0.01	-4.32	-4.33
Quinoline-Heptane	-0.03	-7.73	-7.76
DES-Quinoline	-13.31	-31.76	-45.09
DES-Heptane	-0.05	-8.77	-8.82

[a] $E_{total} = E_{elec} + E_{vdW}$

A further investigation into the different components of total non-bonded interaction energies implies that it is the vdW, which contributes significantly higher energy than that of electrostatic energy component to total non-bonded interaction energies. For example, in the total non-bonded interaction energy between DES and quinoline within DES-heptane-quinoline ternary system, the electrostatic energy component contributes only -13.31 kJ/mol, whereas -31.76 kJ/mol energy comes from the vdW interactions. A further decomposition of total DES-quinoline interactions into MTP-quinoline, EG-quinoline and bromide ion-quinoline interaction indicates that it is the DES-quinoline interaction, which is most favorable and this is then followed by EG-quinoline interaction. The least favorable interaction among these three is the bromide ion-quinoline interaction. In a similar manner, the decomposition of DES-heptane total non-bonded interaction suggests that, MTP-heptane and EG-heptane interactions contribute almost equally. Furthermore, it should be noted that lower the interaction energy between the molecules, lower the solubility and higher the phase separations. The degree of interaction energy is found to be in the following order: DES-quinoline > DES-heptane > Quinoline-heptane.

5.3.3 Radial and Combined Distribution Functions

In order to explore in detail structural properties of DES-quinoline-heptane ternary system, we first concentrate on the selected site-site radial distribution functions (RDFs). The RDFs provide information about the overall structure and interactions between different species of the system considered here, albeit qualitatively. These RDFs are shown in Figure 5.4. The atomic sites that are considered for calculating these pair correlation functions are PC1 atom of MTP, bromide ion (*i. e.*, Br1), OE1 and HEO atoms of EG, NQ1 atomic site of quinoline, and HH1 atom of heptane (Figure 5.1). Considering the distribution functions

involving different atomic sites of solvent DES and quinoline (Figure 5.4 (a)-(c)), we found a strong and well-defined first solvation peak for all of them. This suggests strong interactions between DES and quinoline.

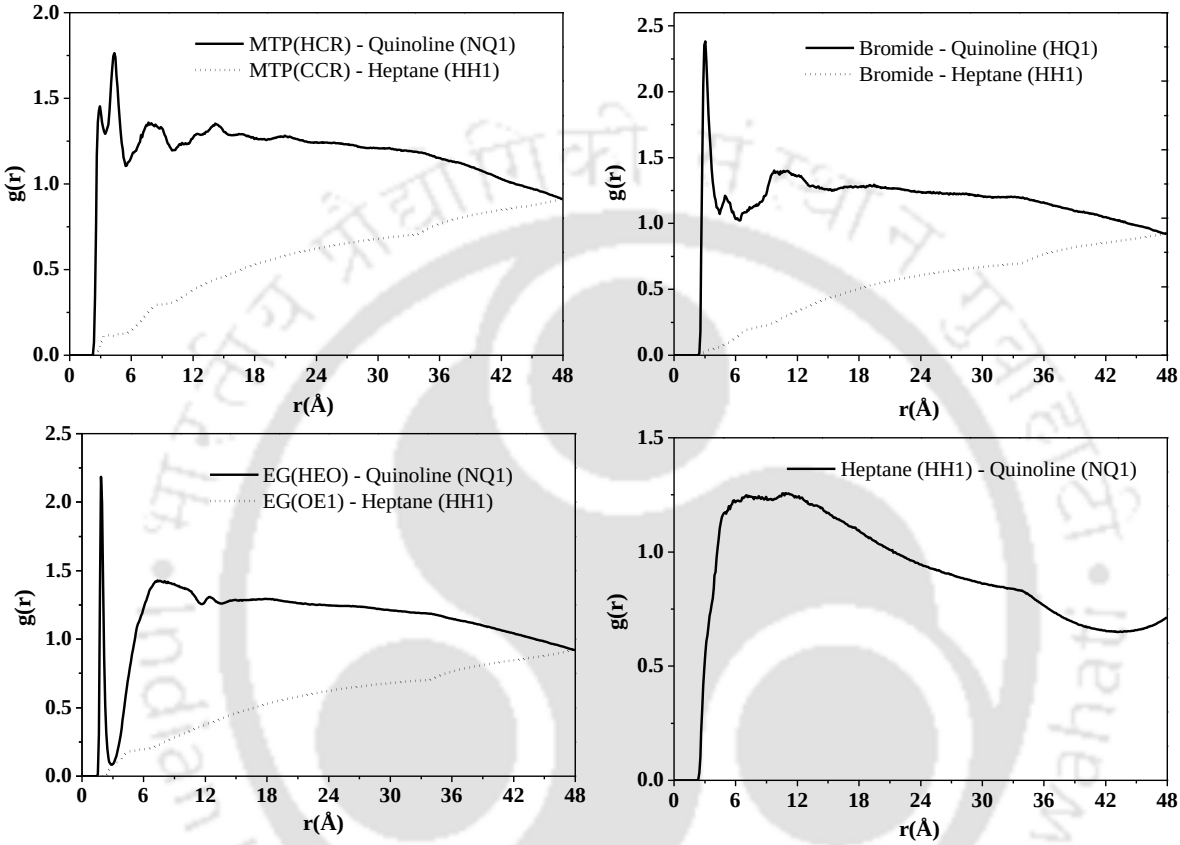

Figure 5.4: Atom-atom radial distribution function (RDF) plots between the different molecules present in the ternary system (a) MTP-Quinoline and MTP-Heptane (b) Br-Quinoline and Br-Heptane (c) EG-Quinoline and EG-Heptane (d) Quinoline-Heptane obtained at 200 ns

From the observation of Figure 5.4 ((a)-(c)), the quinoline molecule reaches within bromide moiety at 3 Å indicating that the formation of weak bond, whereas in the case of MTP and EG, quinoline reaches within 3 Å and 1.5 Å, respectively. In contrast, the bromide ion exhibits a large g(r) peak when compared to other DES species. This signifies that the density distribution of quinoline molecule is higher for bromide ion. This phenomenon is

further elucidated by the spatial distribution functions (discussed in the next section 5.3.4). On the other hand, the inter-molecular distances of DES species with quinoline and heptane is now calculated and reported in Table 5.5. As can be seen from Table S2, the inter-molecular distances (which includes first and second solvation peaks) of bromide-quinoline is obtained at larger distances (7.64 Å) as compared to MTP-quinoline (4.97 Å) and EG-quinoline (7.03 Å).

Table 5.5: Inter-molecular distances between the DES-quinoline, DES-heptane, and quinoline-heptane

Atom pairs	Distance (Å)
Br1-NQ1	7.64
HCR-NQ1	4.97
HEO-NQ1	7.03
OE1-HH1	45.84
CCR-HH1	49.86
OE1-HH1	37.01
NQ1-HH1	37.91

In a similar manner, Figure 5.4 also presents the pair correlation functions involving different sites of DES and heptane. The unfavorable interactions between these molecules are quite apparent, as we do not find any sharp peak of these RDFs and the maximum peak heights are well below than that of bulk density. The RDF involving the atomic sites of heptane and quinoline (Figure 5.4 (d)) shows a broad peak with a maximum g(r) = 1.2, which is much lower than the maximum values of g(r) obtained for DES-quinoline RDFs. Further, quinoline gave larger g(r) peak with bromide as compared with heptane which reveals that bromide ion also has pronounced prominence role in the extraction process. On the other hand, the inter-molecular distances between DES and heptane were obtained

at 37-50 Å. Therefore, these findings suggest that the interactions between DES-quinoline are much more favorable than that of heptane and quinoline.

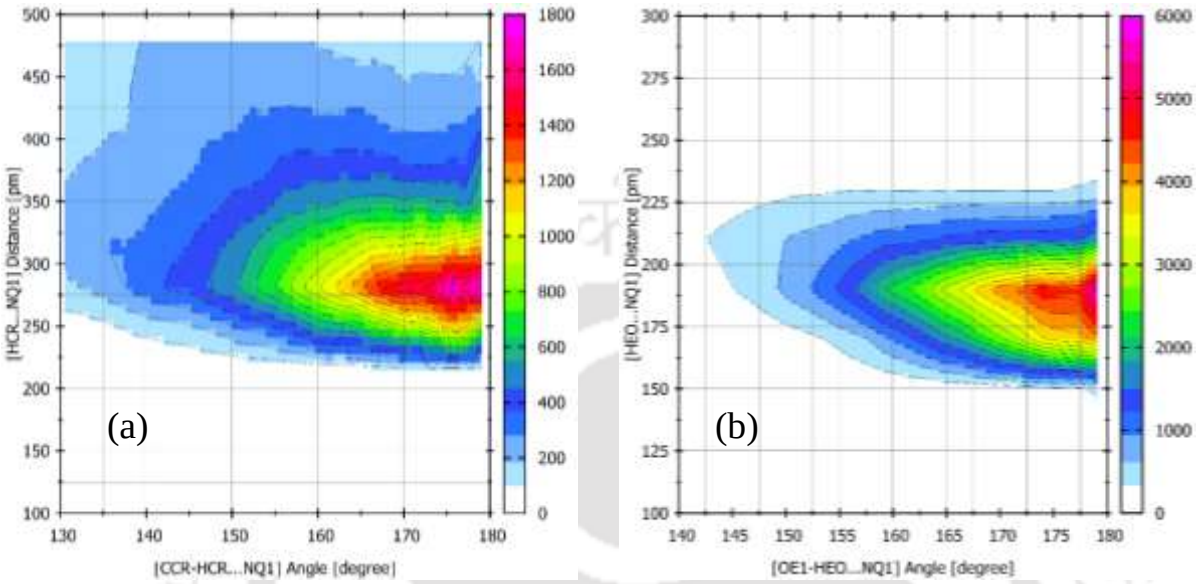

Figure 5.5: Combined distribution functions (CDF) used to confirm the hydrogen bonds formed between the DES-quinoline by plotting the hydrogen bond distance (RDF) vs hydrogen bond angle (ADF) for the ternary system (a) CCR–HCR…NQ1 angle against corresponding HCR…NQ1 distance (MTP-quinoline) and (b) OE1–HEO…NQ1 angle against corresponding HEO…NQ1 distance (EG-quinoline)

Furthermore, combined (angular and radial) distribution functions (CDFs) were also evaluated to confirm the presence of hydrogen bonding formation as a function of donor-acceptor distance and donor-hydrogen-acceptor angle and the same is shown in Figure 5.5. For this, the CDF was plotted between the MTP (HCR)-quinoline (NQ1) and EG (HE1 and HEO)-quinoline (NQ1). The CDF was obtained by using the TRAVIS package and the procedure for calculating this function were reported elsewhere [35]. From this analysis, we observed that the C–H…N bond was formed for both MTP-quinoline and EG-quinoline (Figure 5.5(a) and Figure 5.6), while the O–H…N bond was formed for the EG-quinoline

system (Figure 5.5(b)). These H-bonds were formed at ~3.0 Å and 1.95 Å for C–H…N and O–H…N with an angle of 140° to 180°, respectively. Therefore, this confirms our observations with RDF peaks which were obtained at 3.0 Å and 1.95 Å for both molecular systems.

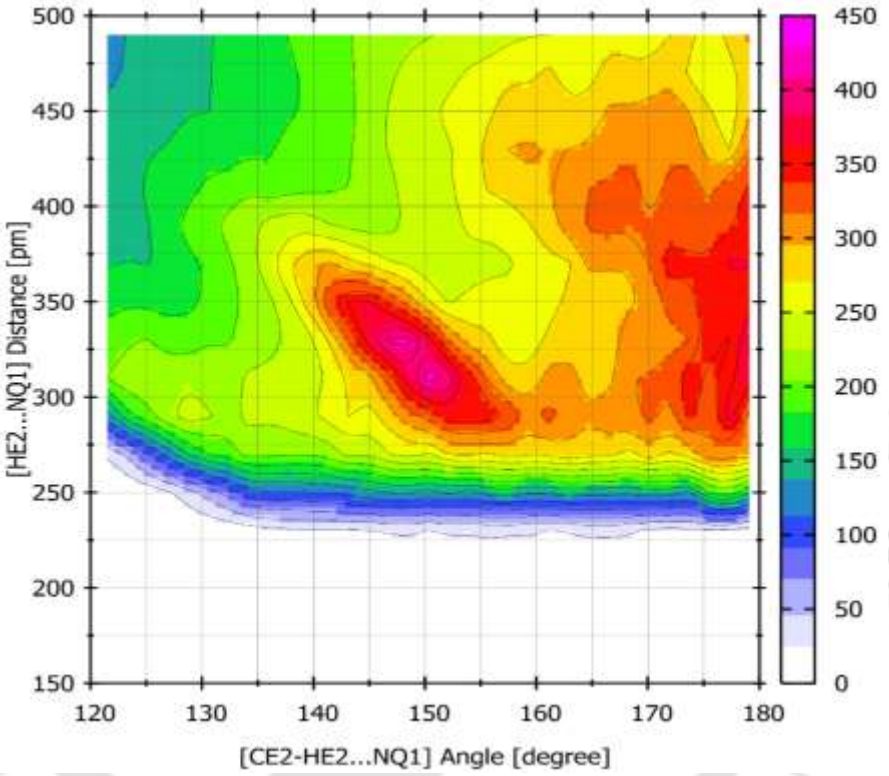

Figure 5.6: Combined distribution functions (CDF) used to confirm the hydrogen bonds formed between the EG-quinoline by plotting the hydrogen bond distance (RDF) *vs* hydrogen bond angle (ADF) for the ternary system. CE1–HE1…NQ1 angle against the corresponding HE1…NQ1 distance

5.3.4 Spatial Distribution Functions

Spatial distribution functions (SDFs) provides the average density distribution of different species around a reference quinoline and heptane molecules in DES solution and are shown in Figure 5.7. These SDFs are obtained by using TRAVIS package [35]. The isovalues

employed for the SDF corresponding to the DES-quinoline is 1.5 particle Å while the same for the DES-heptane is 0.05 particle Å. As can be seen that the more active ('N atom') site of quinoline molecule is surrounded by MTP molecule whereas the less active sites of quinoline surround the bromide ion and heptane. From the observation of Figure 5.7(a) and 5.7(b), the bromide ion is highly distributed around the quinoline molecule as compared with other species. This fact is further confirmed by their RDF plots that the bromide ion exhibits large g(r) peak with quinoline than others. Therefore, the interaction energy between bromide and quinoline is lower than MTP-quinoline and EG-quinoline.

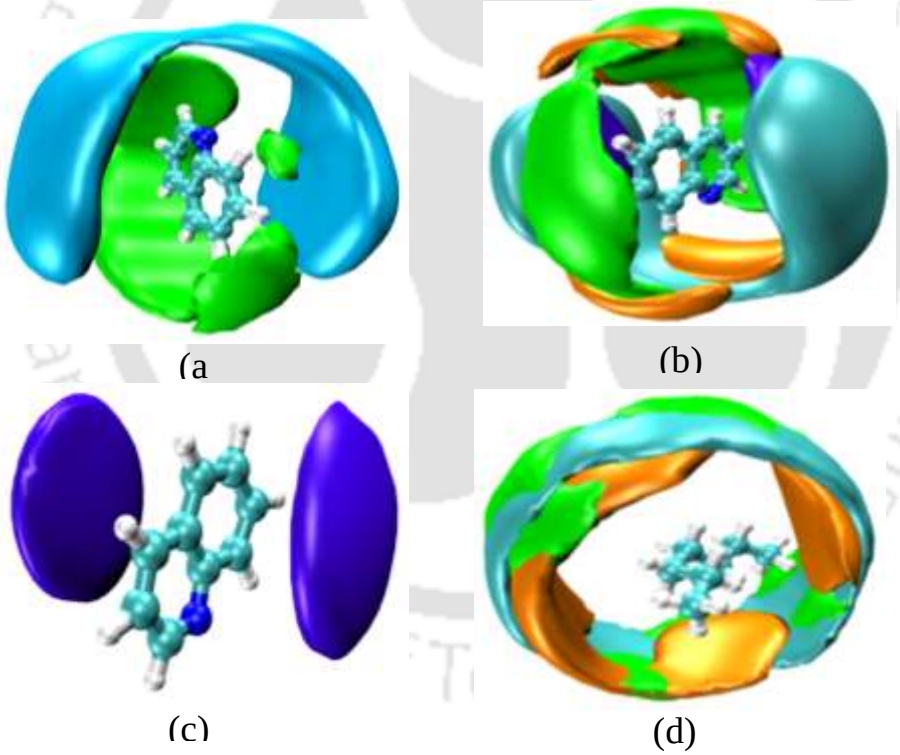

Figure 5.7: Spatial Distribution functions (SDFs) of DES-quinoline-heptane system. (a) MTP and Br around quinoline, (b) EG, Br, MTP and heptane around quinoline, (c) heptane around quinoline and (d) DES around heptane molecule. Orange, green, cyan and violet surfaces refer to EG, Br, MTP of DES, and heptane, respectively

Moreover, the appearance of the distribution of EG molecule around the active side of quinoline is closer than that of MTP. In specific, the positions of the first peaks of these RDFs appeared at 1.95 Å and 2.85 Å, respectively. Furthermore, the densities of bromide ion and heptane molecules are distributed around the inactive side of quinoline (Figure 5.7(a)-(c)). It is also quite apparent that DES molecules are distributed at a distance that is very far from heptane molecule (Figure 5.7(d)) which hinders the interactions between DES and heptane. Therefore, the surfaces of DES are very closely distributed around the active sides of quinoline. Thus the quinoline molecules are susceptible in getting attracted towards the DES molecule in the solution.

5.3.5 Hydrogen Bond Properties

Figure 5.8 presents the average number of DES-quinoline hydrogen bonds per quinoline molecule as a function of simulation time. We have used geometric criteria of hydrogen bond calculation as used in some previous studies [36-38]. The last 50 ns of the production time was considered for criteria. The geometric criteria of hydrogen bond relate to the distance between the acceptor and donor atoms which should fall within a cut-off distance and simultaneously, the donor-hydrogen-acceptor angle should be greater than or equal to a cut-off angle. It should be noted that MTP forms C–H…N bond with quinoline at an average distance of ~3.0 Å (Figure 5.5(a)). In the case of ethylene glycol, two different types of H-bonds are involved, namely C–H…N (~3.0 Å; Figure 5.6) and O–H…N (1.95 Å; Figure 5.5(b). Therefore, from the evidence of RDF (Figure 5.4) and CDF plots (Figure 5.5), the conditions for the acceptor-donor distance is fixed to 3.5 Å while the cutoff angle is taken from 140°-180° for both the systems (MTP-quinoline and EG-quinoline).

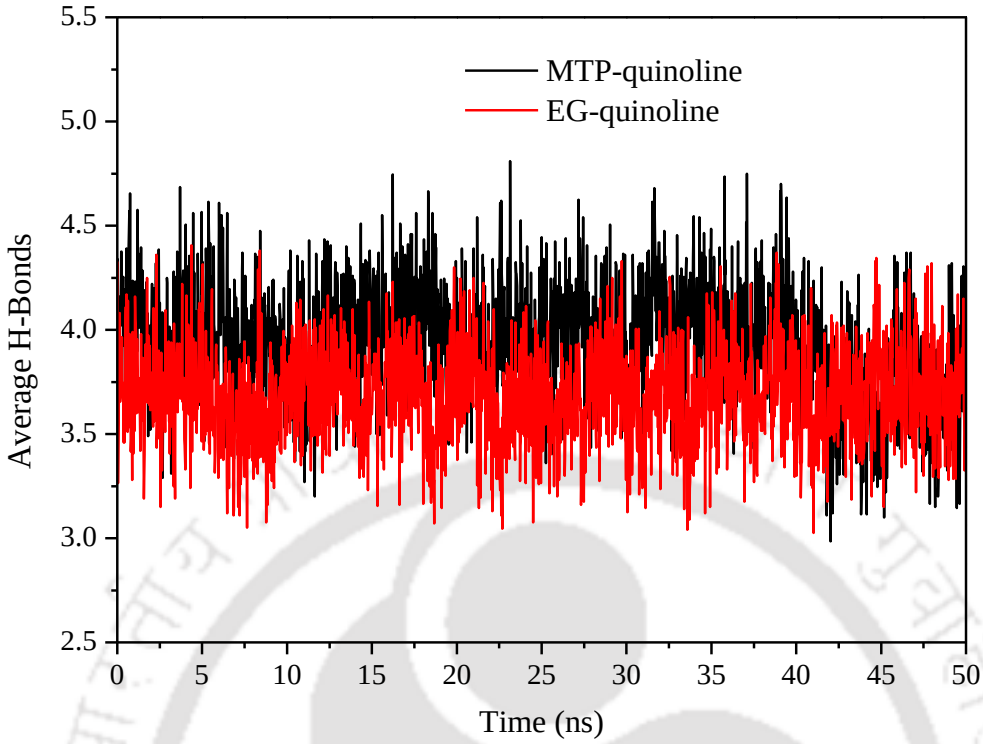

Figure 5.8: Average number of MTP-quinoline and EG-quinoline hydrogen bonds per quinoline molecule as a function of simulation time

From Figure 5.8, it was observed that HBD of DES (*i.e.*, EG) engages in forming a slightly lesser number of H-bonds with quinoline molecules than its salt partner (HBA, MTP). Again, between MTP-quinoline and bromide-quinoline molecules, MTP established a higher number of H-bonds with quinoline than bromide. The average H-bond numbers of bromide-quinoline are not significant (not shown). Here, it is worth to mention that, as expected, we do not notice any hydrogen bonding interactions between DES-heptane and quinoline-heptane molecules.

5.3.6 Mean Square Displacement

The overall mobility of the different species in the phase equilibrium can be obtained by estimating the self-diffusion coefficient (D). The self-diffusion coefficients of different species were calculated by using the Einstein equation (eq. 5.3) [39-42].

$$D = \frac{1}{6}\lim_{t\to\infty}\frac{d}{dt}\left\langle \sum_{i=1}^{N}\left|r_i(t) - r_i(0)\right|^2 \right\rangle \qquad (5.3)$$

Where $r_i(t)$ and $r_i(0)$ are the positions of the i^{th} atom at time t and 0, respectively. Here, the expression within bracket indicates the mean square displacement (MSD) of the molecule. The presence of factor 1/6 is attributed to the three-dimensionality of the system. The self-diffusion coefficients of respective species are calculated from the longtime slope of the MSD curve (Figure 5.9). From Figure 5.9, all the MSD plots were linearity exists. Here, it is worth to mention that the diffusion coefficient values for different species are calculated on averaging over different time origins and reported in Table 5.6, which are listed against different time intervals with a time window of 10 ns.

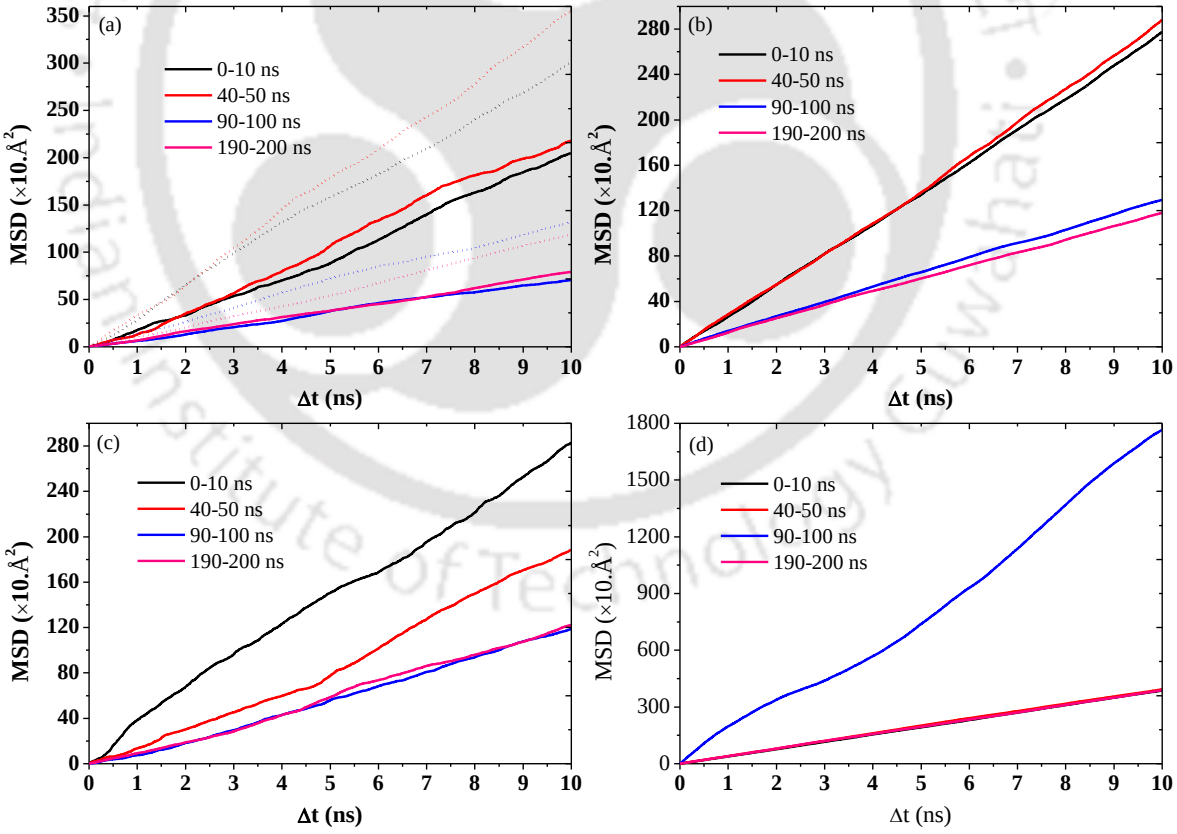

Figure 5.9: MSD plot of (a) MTPB (solid lines corresponds to MTP and dashed lines corresponds to Br), (b) Ethylene glycol (EG), (c) Quinoline, and (d) Heptane

Table 5.6: Self-diffusivity of different molecular species in ternary systems at 308.15 K[a]

Molecule species	Diffusion coefficient × 10^{-9} m^2 s^{-1}			
	0-10 ns	40-50ns	90-100 ns	190-200 ns
Bromide ion	0.4921	0.5910	0.2196	0.2010
MTP cation	0.3503	0.3898	0.1231	0.1300
Ethylene glycol	0.4587	0.4776	0.2145	0.1940
Quinoline	0.4454	0.3264	0.2067	0.2110
Heptane	0.6466	0.6569	0.7006	0.6430

[a] Diffusion coefficient values are reported at a time window of 10 ns

This can shed some light on the overall transfer process of quinoline molecules from heptane rich phase to DES phase. From Table 5.6, we make few interesting observations: (i) at the beginning of the production run (0-10 ns), the self-diffusion coefficient values of all components were found to be relatively close and, (ii) further increase in simulation runtime tends to lower the diffusion coefficient of both quinoline and DES. These species possess similar self-diffusivities which makes the transfer of quinoline molecules towards DES phase possible. On the other hand, it was observed that the closer the self-diffusion coefficient value of two components, higher the interaction between the molecules and vice versa. The self-diffusion coefficient value of heptane remains practically unchanged throughout the simulation time.

From these observations we propose: (i) The transfer of quinoline from heptane phase to DES phase takes place at about 50 ns; (ii) The strong favorable electrostatic interactions between quinoline-MTP cation, quinoline-bromide ion and quinoline-EG (Table 5.4) causes a sharp drop in the diffusion coefficient value of quinoline (*i.e.*, quinoline moving along with the DES). This in turn, decreases the translational motion of MTP, bromide ion

and EG molecules; and (iii) since the electrostatic interactions between quinoline-heptane are very weak, the removal of quinoline molecules from the heptane phase does not influence the self-diffusion coefficient of heptane.

5.4 Conclusion

The classical MD simulation study was carried out to understand the experimental phase equilibria of DES-quinoline-heptane by means of their interaction energy and structural properties. The deviation between experimental and simulated data was found to give fairly good agreement between them. Further, the interaction energies between the investigated molecules were calculated for the ternary system using MD simulations. Overall, the van der Waals interactions were found to be higher than the electrostatic interactions, signifying that the van der Waals interactions are the controlling parameter for DES-quinoline-heptane interactions. In DES-quinoline system, MTP gave higher interaction energy with quinoline which is then followed by ethylene glycol and bromide. This was further confirmed by their H-bonds and RDF plots. The SDF results suggest that the surfaces of DES were very closely distributed around the more active side of quinoline. From MSD, it is found that closer the values of the self-diffusion coefficient within the species, higher the miscibility and more interaction between the molecules. This makes quinoline to be more susceptible towards the DES molecule. In summary, the cation (MTP) of hydrogen bond acceptor (HBA) plays a predominating role in the quinoline extraction process. Therefore, from the MD results, it was suggested that this study provides new insights for computational analysis of LLE equilibria in the absence of experimental data. Further, the low-cost DES could be used as a potential solvent for the extraction of PAH compounds from fuel oil.

References

[1] C.C. Cassol, A.P. Umpierre, G. Ebeling, B. Ferrera, S.S. Chiaro, J. Dupont, On the extraction of aromatic compounds from hydrocarbons by imidazolium ionic liquids, Int. J. Mol. Sci. 8 (2007) 593-605.

[2] U.K. Ravilla, T. Banerjee, Liquid liquid equilibria of imidazolium based ionic liquid+ pyridine+ hydrocarbon at 298.15 K: Experiments and correlations, Fluid Phase Equilib. 324 (2012) 17-27.

[3] R. Anantharaj, T. Banerjee, Liquid–liquid equilibria for quaternary systems of imidazolium based ionic liquid+ thiophene+ pyridine+ iso-octane at 298.15 K: experiments and quantum chemical predictions, Fluid Phase Equilib. 312 (2011) 20-30.

[4] E.J. González, N. Calvar, B. González, Á. Domínguez, (Liquid+ liquid) equilibria for ternary mixtures of (alkane+ benzene+ [EMpy][ESO 4]) at several temperatures and atmospheric pressure, J. Chem. Thermodyn. 41 (2009) 1215-1221.

[5] M.K. Hadj-Kali, S. Mulyono, H.F. Hizaddin, I. Wazeer, L. El-Blidi, E. Ali, M.A. Hashim, I.M. AlNashef, Removal of Thiophene from Mixtures with n-Heptane by Selective Extraction Using Deep Eutectic Solvents, Ind. Eng. Chem. Res. 55 (2016) 8415-8423.

[6] M.A. Kareem, F.S. Mjalli, M.A. Hashim, I.M. AlNashef, Liquid–liquid equilibria for the ternary system (phosphonium based deep eutectic solvent–benzene–hexane) at different temperatures: A new solvent introduced, Fluid Phase Equilib. 314 (2012) 52-59.

[7] Y. Hou, Z. Li, S. Ren, W. Wu, Separation of toluene from toluene/alkane mixtures with phosphonium salt based deep eutectic solvents, Fuel Process. Technol. 135 (2015) 99-104.

[8] M.C. Ali, Q. Yang, A.A. Fine, W. Jin, Z. Zhang, H. Xing, Q. Ren, Efficient removal of both basic and non-basic nitrogen compounds from fuels by deep eutectic solvents, Green Chem. 18 (2016) 157-164.

[9] S. Jayaraman, Computing thermodynamic and transport properties of room temperature ionic liquids and molten salts from atomistic simulations, University of Notre Dame2010.

[10] M. Mohan, P.K. Naik, T. Banerjee, V.V. Goud, S. Paul, Solubility of glucose in tetrabutylammonium bromide based deep eutectic solvents: Experimental and molecular dynamic simulations, Fluid Phase Equilib. 448 (2017) 168-177.

[11] S. Stephenson, R. Offeman, G. Robertson, W. Orts, Ethanol and water capacities of alcohols: a molecular dynamics study, Chem. Eng. Sci. 61 (2006) 5834-5840.

[12] M. Taha, M.-J. Lee, TES buffer-induced phase separation of aqueous solutions of several water-miscible organic solvents at 298.15 K: Phase diagrams and molecular dynamic simulations, J. Chem. Phys. 138 (2013) 244501.

[13] P. Dehury, U. Mahanta, T. Banerjee, Partitioning of butanol between a hydrophobic ionic liquid and aqueous phase: Insights from Liquid Liquid Equilibria measurements and Molecular Dynamics simulations, Fluid Phase Equilib. 425 (2016) 421-431.

[14] S.L. Perkins, P. Painter, C.M. Colina, Experimental and computational studies of choline chloride-based deep eutectic solvents, J. Chem. Eng. Data 59 (2014) 3652-3662.

[15] M. Frisch, G.W. Trucks, H.B. Schlegel, G.E. Scuseria, M.A. Robb, J.R. Cheeseman, G. Scalmani, V. Barone, B. Mennucci, G.A. Petersson, H. Nakatsuji, M. Caricato, Li X, H.P. Hratchian, A.F. Izmaylov, J. Bloino, G. Zheng, J.L. Sonnenberg, M. Hada, M. Ehara, K. Toyota, R. Fukuda, Hasegawa, J, , M. Ishida, T. Nakajima, Y. Honda, O. Kitao, H. Nakai, Vreven, , M. T, Jr J A,, J.E. Peralta, F. Ogliaro, M. Bearpark, J.J. Heyd, E. Brothers, K.N. Kudin, V.N. Staroverov, T. Keith, R. Kobayashi, J. Normand, K. Raghavachari, A. Rendell, J.C. Burant, S.S. Iyengar, J. Tomasi, M. Cossi, N. Rega, J.M. Millam, M. Klene, J.E. Knox, J.B. Cross, V. Bakken, C. Adamo, J. Jaramillo, R. Gomperts, R.E. Stratmann, O. Yazyev, A.J. Austin, R. Cammi, C. Pomelli, J.W. Ochterski, R.L. Martin, K. Morokuma, V.G. Zakrzewski, G.A. Voth, P. Salvador, J.J. Dannenberg, S. Dapprich, A.D. Daniels, O. Farkas, J.B. Foresman, J.V. Ortiz, J. Cioslowski, D.J. Fox, Gaussian 09 Revision B. 01, Gaussian, Inc, Wallingford, CT, DOI (2010).

[16] W. Kohn, A.D. Becke, R.G. Parr, Density functional theory of electronic structure, J. Phys. Chem. 100 (1996) 12974-12980.

[17] C.I. Bayly, P. Cieplak, W. Cornell, P.A. Kollman, A well-behaved electrostatic potential based method using charge restraints for deriving atomic charges: the RESP model, J. Phys. Chem. 97 (1993) 10269-10280.

[18] D. Case, T. Darden, T. Cheatham, C. Simmerling, J. Wang, R. Duke, R. Luo, R. Walker, W. Zhang, K. Merz, Amber 12 reference manual, University of California, San Francisco DOI (2012).

[19] J. Wang, R.M. Wolf, J.W. Caldwell, P.A. Kollman, D.A. Case, Development and testing of a general amber force field, J. Comput. Chem. 25 (2004) 1157-1174.

[20] J. Wang, W. Wang, P.A. Kollman, D.A. Case, Automatic atom type and bond type perception in molecular mechanical calculations, J. Mol. Graph. Model. 25 (2006) 247-260.

[21] L. Martínez, R. Andrade, E.G. Birgin, J.M. Martínez, PACKMOL: a package for building initial configurations for molecular dynamics simulations, J. Comput. Chem. 30 (2009) 2157-2164.

[22] J.C. Phillips, R. Braun, W. Wang, J. Gumbart, E. Tajkhorshid, E. Villa, C. Chipot, R.D. Skeel, L. Kale, K. Schulten, Scalable molecular dynamics with NAMD, J. Comput. Chem. 26 (2005) 1781-1802.

[23] S. Nosé, A unified formulation of the constant temperature molecular dynamics methods, J. Chem. Phys. 81 (1984) 511-519.

[24] W.G. Hoover, Canonical dynamics: equilibrium phase-space distributions, Phys. Rev. A. 31 (1985) 1695.

[25] P.H. Hünenberger, Thermostat algorithms for molecular dynamics simulations, Adv. Comput. Simul. DOI (2005) 130-130.

[26] S.E. Feller, Y. Zhang, R.W. Pastor, B.R. Brooks, Constant pressure molecular dynamics simulation: the Langevin piston method, J. Chem. Phys. 103 (1995) 4613-4621.

[27] W. Humphrey, A. Dalke, K. Schulten, VMD: visual molecular dynamics, J. Mol. Graph. 14 (1996) 33-38.

[28] H.C. Andersen, Rattle: A "velocity" version of the shake algorithm for molecular dynamics calculations, J. Comput. Phys. 52 (1983) 24-34.

[29] U. Essmann, L. Perera, M.L. Berkowitz, T. Darden, H. Lee, L.G. Pedersen, A smooth particle mesh Ewald method, J. Chem. Phys. 103 (1995) 8577-8593.

[30] J.M. Sørensen, T. Magnussen, P. Rasmussen, A. Fredenslund, Liquid-liquid equilibrium data: Their retrieval, correlation and prediction Part I: Retrieval, Fluid Phase Equilib. 2 (1979) 297-309.

[31] F.S. Oliveira, A.B. Pereiro, L.P. Rebelo, I.M. Marrucho, Deep eutectic solvents as extraction media for azeotropic mixtures, Green Chem. 15 (2013) 1326-1330.

[32] C. Manohar, D. Rabari, A.A.P. Kumar, T. Banerjee, K. Mohanty, Liquid–liquid equilibria studies on ammonium and phosphonium based ionic liquid–aromatic–aliphatic component at T= 298.15 K and p= 1bar: correlations and a-priori predictions, Fluid Phase Equilib. 360 (2013) 392-400.

[33] L. Alonso, A. Arce, M. Francisco, A. Soto, (Liquid+ liquid) equilibria of [C 8 mim][NTf 2] ionic liquid with a sulfur-component and hydrocarbons, J. Chem. Thermodyn. 40 (2008) 265-270.

[34] M.R. Shah, R. Anantharaj, T. Banerjee, G.D. Yadav, Quaternary (liquid+ liquid) equilibria for systems of imidazolium based ionic liquid+ thiophene+ pyridine+ cyclohexane at 298.15 K: Experiments and quantum chemical predictions, J. Chem. Thermodyn. 62 (2013) 142-150.

[35] M. Brehm, B. Kirchner, TRAVIS-a free analyzer and visualizer for Monte Carlo and molecular dynamics trajectories, J. Chem. Inf. Model. 51 (2011) 2007–2023.

[36] B. Sharma, S. Paul, Understanding the Role of Temperature Change and the Presence of NaCl Salts on Caffeine Aggregation in Aqueous Solution: From Structural and Thermodynamics Point of View, J. Phys. Chem. B 119 (2015) 6421-6432.

[37] S. Paul, S. Paul, The influence of trehalose on hydrophobic interactions of small nonpolar solute: A molecular dynamics simulation study, J. Chem. Phys. 139 (2013) 044508.

[38] G. Borgohain, S. Paul, Temperature-mediated switching of protectant-denaturant behavior of trimethylamine-N-oxide and consequences on protein stability from a

replica exchange molecular dynamics simulation study, Mol. Simul. 43 (2017) 52-64.

[39] M.P. Allen, D.J. Tildesley, Computer simulation of liquids, Oxford university press1989.

[40] S.S. Sarangi, W. Zhao, F. Müller-Plathe, S. Balasubramanian, Correlation between Dynamic Heterogeneity and Local Structure in a Room-Temperature Ionic Liquid: A Molecular Dynamics Study of [bmim][PF6], ChemPhysChem 11 (2010) 2001-2010.

[41] R. Biswas, V. Pasumarthi, T. Banerjee, P. Ghosh, S.M. Ali, J.M. Joshi, Interfacial insights on the dibenzo-based crown ether assisted cesium extraction in [BMIM][Tf2N]–water binary system, J. Radioanal. Nucl. Chem. 311 (2017) 427-438.

[42] G. Sarkar, D. Kundu, T. Banerjee, Effects of functionality on the transport properties of thiol-ene/acrylate systems: A molecular dynamics study, J. Mol. Liq. 224 (2016) 859-871.

CHAPTER 6

Hydrogenation and Degradation of Quinoline using Reactive Force Field Simulations

6.1 Introduction

The previous chapters have discussed the extraction of PAH by methods such as extraction. An alternative method corresponds to its degradation to finer products and radicals. We shall adopt and discuss the same in this chapter where we will report the breaking and formation of bonds within the quinoline moiety using Reactive Force Field Simulations. The hydrogenation of nitrogenous Poly Aromatic Hydrocarbon (PAH) compounds are of great importance especially in the context of hydrodenitrogenation (HDN) in which nitrogen is removed from fuels. After the extraction of PAHs, these need to be utilized or converted to some useful products. A commonly accepted HDN mechanism implicates the hydrogenation of C=N and C=C bonds as key steps prior to nitrogen removal [1,2]. The extent of hydrogenation of quinoline and related PAH molecules are reported with Pt/Ni based catalyst [3-6]. Complete degradation of quinoline to small aliphatic compounds however is scarce [7]. The nitrogen-containing compounds like quinoline are also very harmful because of their poisoning and deactivating effect on hydroprocessing catalysts [7]. They are known to form NO_x upon combustion. Recent works reported the experiments for quinoline hydrogenation using commercial transition-metal sulfides like Pt/SiO_2, and $NiMo/Al_2O_3$ catalysts [8-11].

The choice of quinoline as a model compound lies from the fact that it is a representative of heterocyclic nitrogen compounds found in substantial concentrations in the middle distillate fraction of fuels derived from oil shale, coal and low-grade petroleum [12]. This is first separated from the fuel oil by liquid-liquid extraction with solvents such as sulfolane or glycols or newer solvents such as deep eutectic solvents. The details can be found in previous chapters 3 and 4 [13-15]. Once the quinoline is separated, a need is felt

to convert it into smaller compounds. This compound is known to be the most difficult to convert to hydrocarbons and ammonia by hydrodenitrogenation (HDN). Hence knowledge of the hydrogenation reaction of quinoline is considered and also assumes as a representative feedstock [16,17]. Catalytic hydrogenation is a key reaction for the degradation of most of the compounds. In this work, we have considered quinoline such that it can be reduced to a simple structure with hydrogenation at high temperature.. The molecule structure of quinoline being bulky possesses conformers with one hetero nitrogen atom. The aromatic ring of quinoline, which is chemically most stable, requires large energy for breaking it so as to initiate degradation.

The previous experimental studies on the degradation of PAH did not completely provide the degradation pathways.[7-10] The mechanism of the degradation indeed depends on both structural composition and the severe working condition (>400 °C). Hence, the relevant information for hydrogenation is not fully accessible. As a result, it is very difficult to perform an in-situ analysis of these reaction systems. The reactive force field (ReaxFF) method is capable of describing the bond breaking, bond formation and chemical reactivity [18]. Thus, it has been developed as an effective method for studying complex chemical reactions and other complicated phenomena under extreme conditions. So, to simulate such kind of reactions, Molecular Dynamics (MD) simulations involving bond breaking and bond formation is desired. This is typically implemented in the ReaxFF suite of programs, which provide suitable mechanism using a computationally affordable time scale [18-21].

Reaction mechanisms, reaction and activation energies along with rate constants have been obtained from ReaxFF simulations with respect to combustion and pyrolysis

techniques [22-26]. Although ReaxFF shows significant deviations for some reaction properties [18], the simulation results were found to be in good agreement with available experimental data in most cases [27-30]. Ding et al. studied pyrolysis of n-heptane at high temperature by a series of ReaxFF simulations, which came reasonably consistent with the experimental results [28]. Cheng et al. applied ReaxFF to investigate the mechanisms and kinetics of oxidation of toluene at high temperature [29]. Chen et al. investigated the hydrogenation reaction of several common coal related model compounds using ReaxFF MD [21]. Zhang et al. studied the decomposition characteristics of C_3F_7CN (heptafluoroisobutyronitrile) based and found various smaller intermediate and stable products after decomposition [31]. These successful applications demonstrate that ReaxFF is an accurate and computationally feasible approach for studies involving catalysis or pyrolysis study.

In the present work, MD simulations for quinoline are carried out by employing the ReaxFF as implemented in ADF software [32]. A series of simulations were performed to investigate the reaction mechanism, the intermediate product distributions, along with the correlated kinetic behavior of quinoline hydrogenation. Here, the extended focus is the intermediate reaction mechanisms followed by degradation of quinoline to form smaller stable products. The outcome is anticipated to provide a comprehensive portrayal of the quinoline hydrogenation at atomistic level and afford a reference for viable application. For e.g., the reaction rate constant (k) and activation energy (E_a) of quinoline hydrogenation are determined from simulation results quantitatively using the simple first order kinetics and Arrhenius expression.

6.2 ReaxFF

ReaxFF is a molecular dynamics software for simulating large-scale chemical systems. Antagonistic to conventional force fields and QM methods, it is able to demonstrate chemical reactions. ReaxFF replaces unequivocal bonds by bond orders, which permits persistent bond forming/breaking. It is built-up to be as common as conceivable and has been parameterized and applicable for hydrocarbon reactions. ReaxFF allows MD simulations with computational costs nearly as low as for general non-reactive force fields. It is known to reproduce the accuracy of quantum mechanics for reaction systems, including reactants, transition states and products for the thermal decomposition and oxidation. Thus, it shall help us in elucidating the mechanism and the primary reaction pathways for the initiation reaction leading to the hydrogenation of quinoline and for describing the formation of intermediates (IMs) and products.

In the current work, we have performed a range of ReaxFF MD simulations at different temperatures with constant N (number), V (volume) and T (temperature), designating these conditions as NVT. It should be noted that the essential charge redistribution, i.e. charges on atoms alter due to nature of chemical bonds and it is this dynamic bonding which signifies ReaxFF and its difference from classical MD [33]. The strength of the bond between a pair of atoms *i* and *j* is described by the bond order through the number of chemical bonds. This can be expressed as (Eq. 6.1):

$$BO_{ij}^{\alpha'}(r_{ij}) = \exp\left[a_{\alpha} \left(\frac{r_{ij}}{r_{0_{\alpha}}} \right)^{b_{\alpha}} \right] \qquad (6.1)$$

Here, the bond order depends on the types of atoms *i* and *j* and the distance between them. α corresponds to $\sigma - \sigma$, $\sigma - \pi$, or $\pi - \pi$ bonds. *a* and *b* are parameters belonging to the bond type. r_{0_α} is the length which is optimal for the bond type. Since the actual bond type is unknown during simulation, the total bond order equals the following sum as follows (Eq. 6.2):

$$BO'_{ij} = BO_{ij}^{\alpha'} + BO_{ij}^{\pi'} + BO_{ij}^{\pi\pi'} \tag{6.2}$$

Again, taking into account the total coordination number of each atom and 1–3 bond corrections in valence angles, correction accounting the same is given below (Eq. 6.3):

$$BO_{ij} = BO'_{ij} * f_1(\Delta'_i, \Delta'_j) * f_4(\Delta'_i, BO'_{ij}) * f_5(\Delta'_j, BO'_{ij}) \tag{6.3}$$

Here, Δ'_i stands for the deviation of atom *i* from its optimal coordination number, $f_1(\Delta'_i, \Delta'_j)$ for the over coordination correction; and $f_4(\Delta'_i, BO'_{ij})$ and $f_5(\Delta'_j, BO'_{ij})$ for 1–3 bond order corrections. After bond orders are computed, the charge assignment is then incorporated. Thereafter, ReaxFF simulation continues much like a classical MD simulation. The dynamic bonding properties of ReaxFF atoms lie behind different charges during the entire simulation. For redistribution of charges periodically, it is most accurate to employ ab-initio methods. To make the ReaxFF method scalable, the charge equilibration can be approximated by assignment of charges to atoms that minimize the electrostatic energy of the system with constant net charge [34].

$$\begin{aligned} E(q_1 \ldots q_N) = & \sum_i Atomic\ Energy\ of\ \ i\ \ due\ to\ \ q_i \\ & + \sum_{i<j} Coulomb\ Energy\ between\ \ i\ and\ \ j \end{aligned} \tag{6.4}$$

Where *i* and *j* represent atom indices and q_i is referred to as the partial charge on atom *i*. The final minimized corrected equation is given as (Eq. 6.5):

$$Minimize\, E(q_1 \ldots q_N) = \sum_i \left(E_{i0} + \lambda_i^0 q_i + \frac{1}{2} H_{ii}^0 q_i^2 \right) + \sum_{i<j} H_{ij} q_i q_j$$
$$subject\, to\ q_{net} = \sum_{i=1}^{N} q_i \qquad (6.5)$$

Here, E_{i0} denotes the energy of an isolated neutral atom. λ_i^0 is the electronegativity. H_{ii}^0 stands for the idem potential or self-Coulomb of *i*, while H_{ij} corresponds to the Coulomb interaction between atoms *i* and *j*.

The total energy expression of ReaxFF is presented as follows:

$$E_{System} = E_{bond} + E_{over} + E_{under} + E_{val} + E_{pen} + E_{tors} + E_{conj} + E_{vdWaals} + E_{Coulomb} \qquad (6.6)$$

Where E_{bond} corresponds to bond energy; E_{over} and E_{under} denote the over and under coordinated atoms, respectively, in the energy contribution; E_{val}, E_{pen}, E_{tors}, E_{conj}, $E_{vdWaals}$, and $E_{Coulomb}$ represent the valence angle term, penalty energy, torsion energy, conjugation effects to energy, nonbonded van der Waals interaction, and Coulomb interaction, respectively. The details of ReaxFF with its equations and methodology can be found elsewhere [18-20].

In this chapter, the hydrogenation reaction of quinoline and its probable pathways of the hydrogenated products are studied in detail. All the simulations are performed in the temperature range from 2500 – 4500 K.

6.3 Computational Details

All simulations were performed with fixed number of atoms (N), fixed volume (V) and a fixed temperature (T), known as NVT-MD simulation. To simulate the hydrogenation reaction, we placed 10 quinoline molecules and 100 hydrogen molecules in a 30 Å × 30 Å × 30 Å periodic box. The simulation procedure began with the minimization of each reaction system with NVT-MD for 5000 steps at 10 K followed by the reaction simulation for 700 ps production run. Several test runs were performed which showed the absence of reactions at temperatures below 2500 K. Thus, the systems were simulated at the higher temperatures from 3000 - 4500 K. ReaxFF MD simulations in this work were processed using a velocity Verlet approach, with a time step of 0.25 fs. A Berendsen thermostat with a damping constant of 100 fs was used for temperature control [35]. The parameters used in the present work were the set of (CHONSFPtClNi.ff) ReaxFF force field parameters [36].

To determine all the possible reactions available in the ReaxFF MD simulations, we adopted three simulations for each reaction system and then analyzed the trajectories for every 0.25 fs. Fragment number and molecular species were then taken directly to obtain the most favorable reaction steps. The molecular species formed during the simulations were analysed using a 0.3 bond order cut-off [27]. The time step used in the current work is 0.1 fs, which is appropriate for hydrocarbon systems [18,19]. The simulations were run on an eight core based Intel Xeon E5-1607 processor. The simulation conditions used in this work are not equivalent to that of actual reaction conditions. The time scale of the simulation (700 ps) is orders of magnitude shorter than that of the experiment. The experiments are performed for real systems which are in the order of hours/minutes or

seconds. In such range, the molecular simulation reaction is not feasible due to computational limitations. To form the framework reasonable, molecular scale simulations are generally performed at nanoscale or picosecond level. Thus, in the ReaxFF simulations, we increase the temperature from 500–1200 K (as used in experiments) to 3000–4500 K to allow chemical reactions to be observed on the computational affordable time scale. This difference in time and temperature scales between simulation and experiment may certainly affect product distributions. However, the high temperature used in the simulation is known to only influence the reaction rates but not reaction mechanisms. Such artificially increased temperatures in ReaxFF MD simulation are available in some of the previously reported literatures and possess good agreement with experiments [21,28,31,37]. We hereby expect to find a qualitative agreement between the experimental and simulation results as well as various insights related to reaction mechanisms such as initiation step and the formation of major products through ReaxFF MD simulations.

6.4 Results and Discussion

To analyse the thermal decomposition and direct hydrogenation of quinoline and the effect of temperature on the product distribution, a series of ReaxFF simulation are carried out at different temperature ranging from 2500–4500 K. The reactive force field simulation is applied to the degradation of quinoline to study the intermediate compounds formations and then a comparison with the reported literature is done [4,7,11,38]. The total reaction progresses through two parts, namely, the hydrogenation of quinoline to intermediate (IMs) and then its degradation at high temperature to form unstable smaller IMs compounds (Figure 6.1). Later, these IMs form stable smaller aliphatic compounds, which are considered as the residual products of the reaction (Figure 6.2).

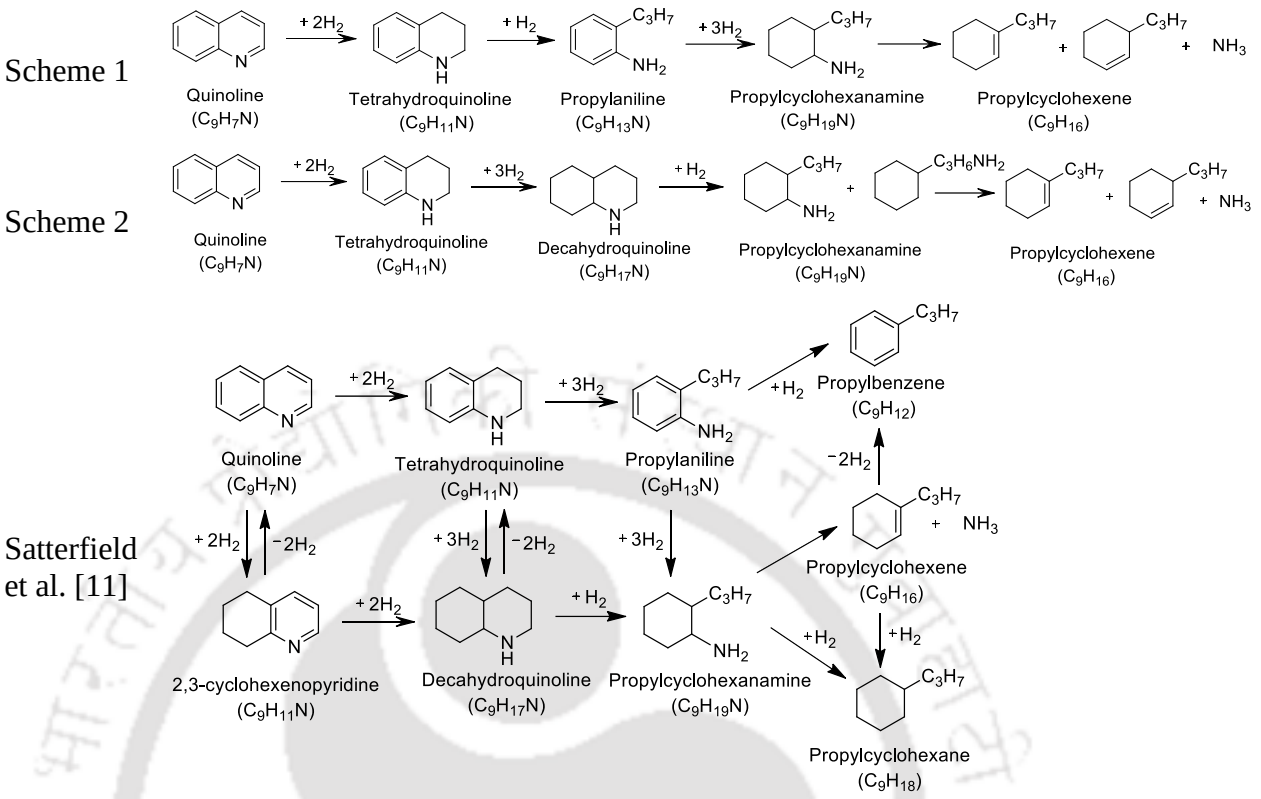

Figure 6.1: Initial and experimental reaction pathway for hydrogenation of quinoline

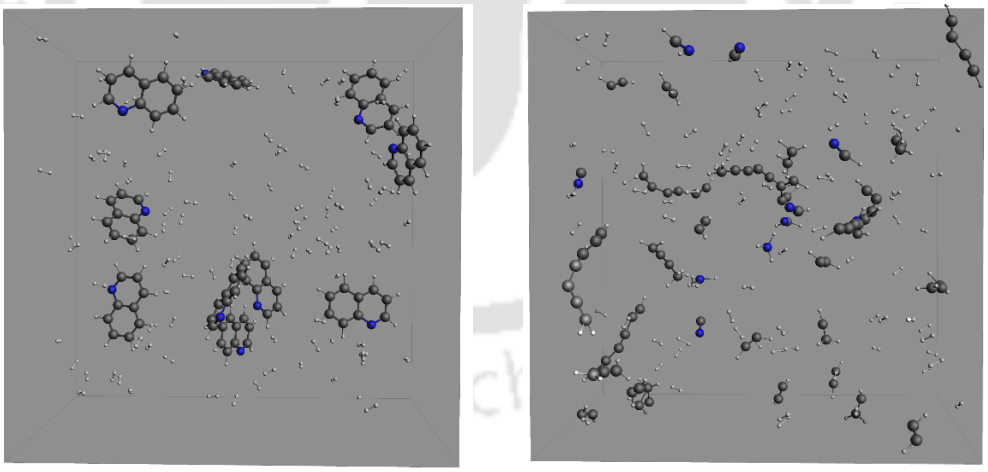

(a) (b)

Figure 6.2: Snapshot of the reaction box (a) before and (b) after 700 ps ReaxFF simulation at 3000K.

Hence, quinoline is degraded to IMs and smaller stable products. No reactions are seen to occur at temperature below 2500 K. It suggests an initial temperature is required where quinoline starts to decompose. Above 3000 K, the hydrogenation of quinoline starts with NVT simulation.

Two pathways are seen in the initial stage of reaction, depending on the temperature regime:

i. At temperatures 3000 K to 3500K, the reaction rate of quinoline is lower with time.
ii. At temperatures 4000 K to 4500K, the reaction rate of quinoline generally increases with time.

Up to 10 ps, no product or intermediate species are formed. This is due to the initial delay period for an effective collision to take place and sample the entire reaction states within the system. Starting from 10 ps, the number of quinoline molecules start to decrease whereby intermediate molecules start to generate. At the same time, the hydrogen molecules also start to decrease or consumed (Figure 6.3). The intermediates begin to decompose at 100 ps, thereby producing C_2H_2 or acetylene (Figure 6.4).

6.4.1 Initial Hydrogenation

Finding out the initiation reaction channel of quinoline is important for understanding the quinoline hydrogenation/degradation mechanism. Time dependent distributions of the reactions related to the quinoline are investigated. It is found that reactions related to the fission of C−C and C−H bonds and hydrogenation are the dominant mode in the initiation stage. Most of the quinoline molecules react through the intermolecular reactions with hydrogen followed by some intramolecular reactions.

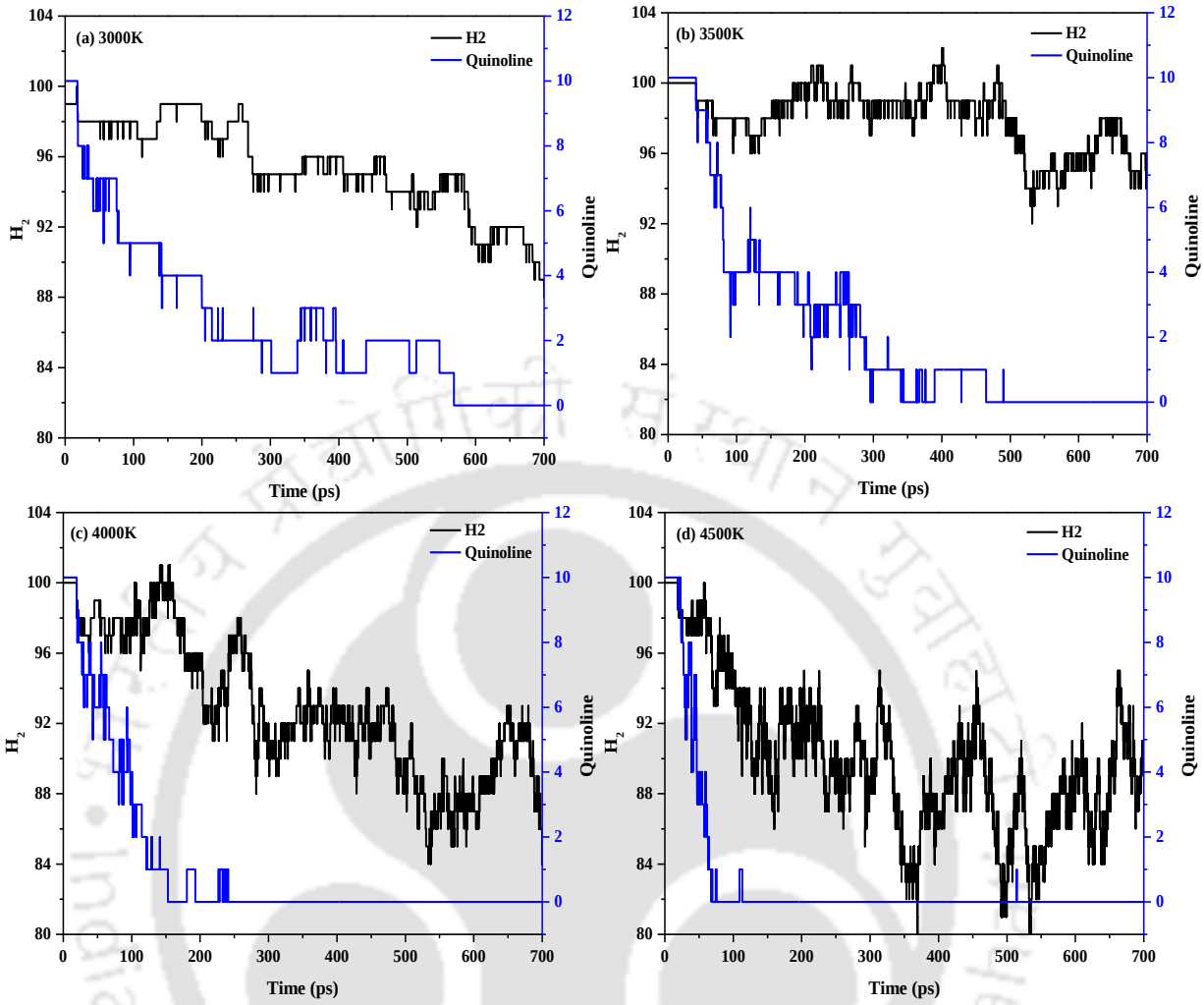

Figure 6.3: Changes of the number of total hydrogen and quinoline molecules with time during 700 ps ReaxFF simulation at different temperatures

Many researchers have indicated that the hydrogenation initiation reaction of aromatic hydrocarbons mainly occurs at the substitution sites [39-41]. In other words, the hydrogen atom attacks the aromatic carbon atoms at the substitution site to form the corresponding hydrogenated free radicals. The final hydrogenated products are obtained from these free radicals via hydrogenation/hydrocracking reactions [42]. The hydrogen accepting capacity of these carbon atoms is stronger than those of the other carbon atoms present [43].

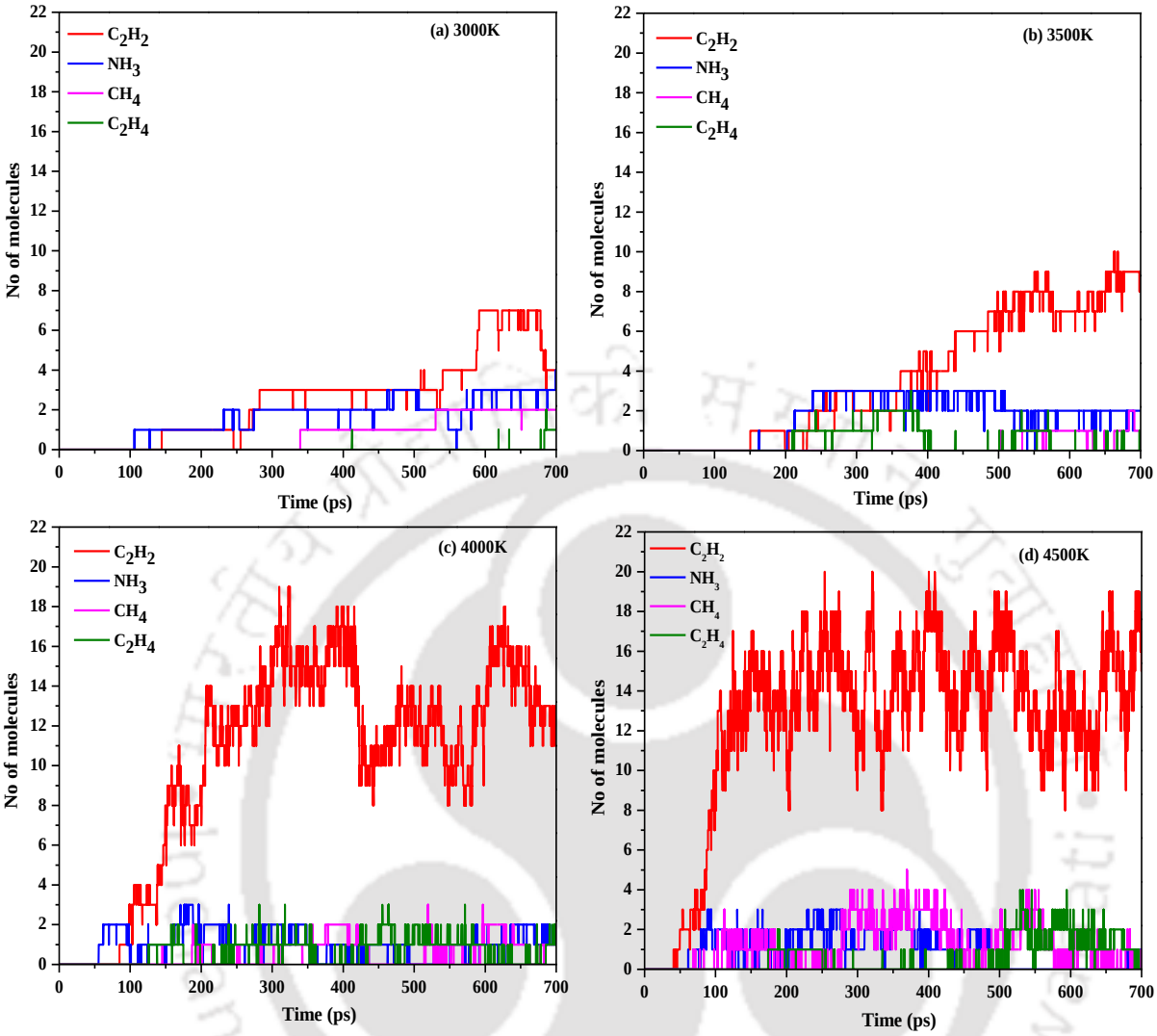

Figure 6.4: Changes of the number of different product molecules trends with time during 700 ps ReaxFF simulation at different temperatures

Further schemes proposed for primary hydrogenation include intermediate product. To further analyse the influence of temperature on the decomposition process of quinoline, the molecular dynamic simulation of the quinoline system is performed at five temperature zones namely 2500 K, 3000 K, 3500 K, 4000 K and 4500 K for a total simulation time of 700 ps. The earliest hydrogenation reaction pathways are shown in Figure 6.1.

The predicted and experimental reaction mechanism (Figure 6.1, Scheme I-III) for quinoline was previously studied by Satterfield et al. [7,11] under catalytic environments. Tetrahydroquinoline (THQ) and 2,3-cyclohexenopyridine (CHP) and decahydroquinoline (DHQ) are the major intermediates formed. The hydrogenation of quinoline to yield THQ is a very fast reaction. It proceeds almost quantitatively up to the equilibrium concentration. The aromatic nitrogen-containing six-membered ring in quinoline is obviously much more reactive than the corresponding ring. At high temperature (>450°C) after elimination of ammonia finally, propylcyclohexane (PCHE) and propylbenzene (PB) were produced [11].

The reaction pathway observed in this investigation proceeds through scheme-1 i.e. tetrahydroquinoline (THQ) and propylaniline (PA). The scheme-2 proceeds through decahydroquinoline (DHQ). The reaction pathway through scheme-1 is the primary pathway since substantial amounts of THQ are present compared to only small quantities of DHQ. Substantially, a higher rate of hydrogenation and denitrogenation of quinoline is achieved with propylaniline (PA) reaction system as compared to decahydroquinoline (DHQ). On further hydrogenation forms propylcyclohexanamine (PCHA). The next step removes the amine nitrogen and hydrogenates the alkyl aromatic to propylcyclohexene (PCHE). The primary denitrogenation products produced is propylcyclohexene (PCHE) with the equivalent release of ammonia for both cases. This denitrification occurs at approximately 60 ps within the reaction time. The ammonia (NH_3) released at this stage does not react with others and hence exist as a stable product until the end of the reaction. In this manner, the nitrogen (N) transformation, occurs by absorbing 76.83 kcal/mol of energy. The propylcyclohexene (PCHE) is here the stable intermediate product, which is formed after successfully nitrogen release from the quinoline molecule.

As the amine group is removed, in all the cases, the saturation of the aromatic ring occurs. Here a substantial difference in the activity and selectivity is observed. To simulate the quinoline reaction system, after the near completion of hydrogenation, we further extended the reaction time (up to 700ps) to see the degradation of propylcyclohexene (PCHE). Here PCHE is again hydrogenated to form propylcyclohexane (PCH) (Figure 6.1). Further degradation of PCH leads to smaller fragments. The results associated with the previous literature where the above intermediate formed have been reported [7]. Here almost similar intermediates were formed. This indicates that it would be reliable to investigate the quinoline hydrogenation by using the ReaxFF-MD simulation.

6.4.2 Degradation

In order to make the reaction more adequate so as to obtain a higher abundant product information and to comprehensively understand the reaction system, the reaction time is prolonged to 700 ps. Figure 6.2 shows the snapshots of the reaction box before and after 700 ps ReaxFF MD simulation at 3000 K. Several key species of stable products (e.g., C_2H_2, C_2H_4, and CH_4), including the intermediates, are observed throughout the experiments. Although the simulated temperature in the present calculation is higher than the experimental values, the hydrogenated intermediate species observed in the reaction at different temperatures could be fully covered by our ReaxFF MD simulations. Figure 6.5 shows the time evolution of the potential energy at different temperatures considered. The growth rate of the potential energy is evidently accelerated with the increase of temperature, indicating that the increase of temperature will lead to the acceleration in the reaction rate till it remains constant. In all the cases, it was observed that the energy growth rate in the time range of 10 ps to 150 ps is significantly higher than that of 150–700 ps.

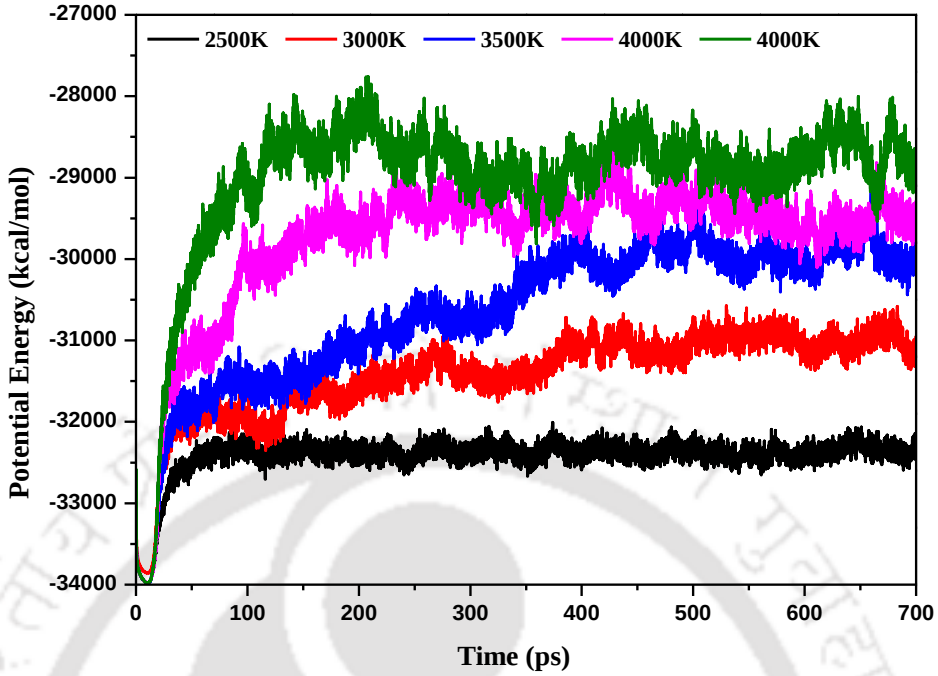

Figure 6.5: Changes of the potential energy of the system with time during 700 ps ReaxFF simulation at different temperatures

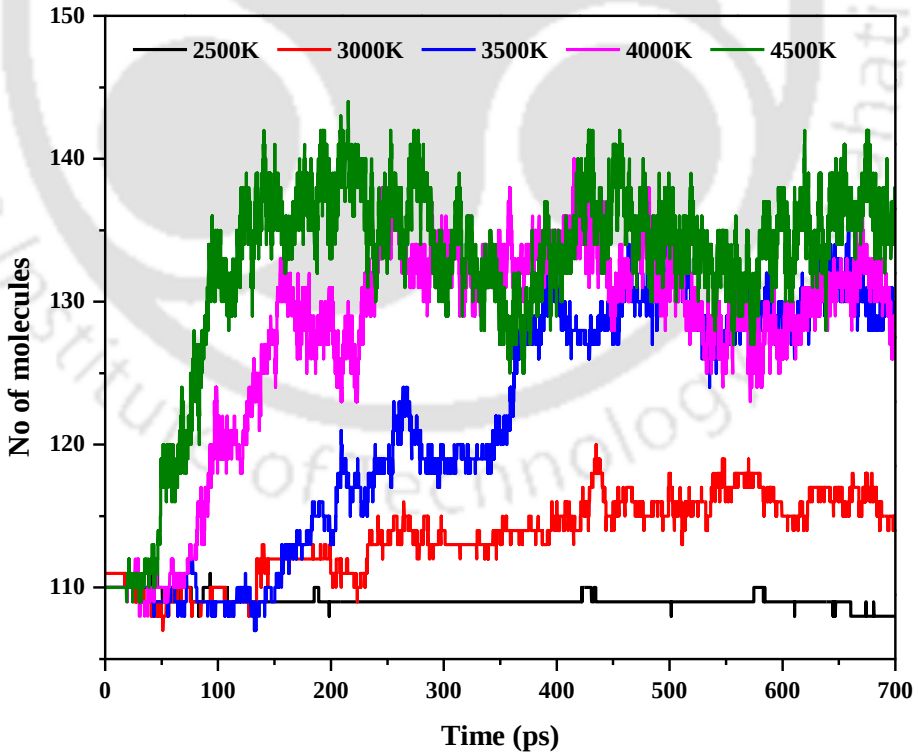

Figure 6.6: Changes of the number of total molecules with time during 700 ps ReaxFF simulation at different temperatures

This result indicates that the reactions in the system before 150 ps are primarily endothermic in nature. Moreover, exothermic reactions may occur in the system after 150 ps, thereby leading to the considerably gradual growth of the overall potential energy. Figure 6.6 shows the numbers of molecular species generated in the complete reaction. The decomposition rate and the quantity of quinoline molecules are evidently accelerated with the increase of temperature. There are no new molecules formed at 3000 K whereas at 4500 K almost 140 products/IMs or compounds are formed at the end of the simulation. Many species, including the saturated and unsaturated or the short-lived and long-lived compounds, are observed during the process. Generally, acetylene is the most abundant product whose amount quickly increases with time and reaches a constant value at the end of the simulation. The ten most possible secondary degradation reactions with time are shown in Table 6.1. A large number of unstable radical intermediates are produced during the simulation (Table 6.2). The amount of these intermediates reaches maximum at the middle of the simulations and then becomes constant. The whole reaction process mainly occurs during 10−150 ps.

The hydrogenated products of quinoline observed in the ReaxFF MD simulations are listed in Table 6.2. Figure 6.3 shows the consumption rate of hydrogen and quinoline molecules in the reaction at different temperatures. As shown in Figure 6.3, all quinoline compounds are hydrogenated within 100 ps after which the degradation reaction starts. For example at t=580 ps this decomposes all the quinoline molecules at 3000 K, whereas at 4500 K all quinoline molecules are decomposed by 110 ps.

Table 6.1: Probable reactions in the hydrogenation process

No	Reaction
1	$C_9H_{16} + H_2 \longrightarrow C_9H_{18}$
2	$C_9H_{18} \longrightarrow C_4H_8 + C_5H_{10}$
3	$C_9H_{16} \longrightarrow C_5H_{10} + C_4H_6$
4	$C_9H_{18} \longrightarrow C_3H_6 + C_6H_{12}$
5	$C_6H_{12} \longrightarrow C_2H_2 + C_4H_{10}$
6	$C_5H_{10} \longrightarrow C_4H_6 + CH_4$
7	$C_9H_{16} \longrightarrow C_3H_8 + C_6H_8$
8	$C_6H_8 \longrightarrow C_2H_6 + C_4H_2$
9	$C_4H_6 \longrightarrow C_2H_2 + C_2H_4$
10	$C_3H_6 \longrightarrow C_2H_2 + CH_4$

The intermediates produced by the hydrogenation of quinoline continuously degrade to generate small products. The major fragment distributions and temperature profile of the simulations as a function of time are given in Figure 6.4, which shows the amount of the product at each temperature. The number of acetylene molecules formed is the highest among all the products, while the contents of C_2H_4, CH_4, and NH_3 are lower. In the present calculations, we marked each atom of the model system and traced these atoms to find out all the possible reactions during the reaction process. According to the simulation results, it could be found that the initiation of quinoline hydrogenation is mainly through intramolecular reaction channels. The intermolecular reactions are very important in the later degradation stage. This can be explained by the Rice-Kossiakoff theory [44,45]. The denitrogenation occurs in the first 20 ps of the reaction with the formation of NH_3. In the last stage of the process, the reactions including acetylene, become the main component. Moreover, the other aliphatic stable products are formed in a low amount.

Table 6.2: Product species during 700 ps ReaxFF MD simulation at different temperatures

Temperature (K)	Product species	
	Intermediate states	Stable compounds
3000	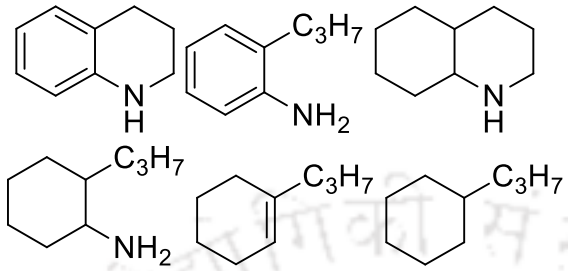 CH_3, C_8H_7, C_3H_3, C_4H_4, C_4H_3, C_7H_3, C_5H_3, C_9H_4	C_2H_2, NH_3, CH_4, C_2H_4, C_2H_6
3500	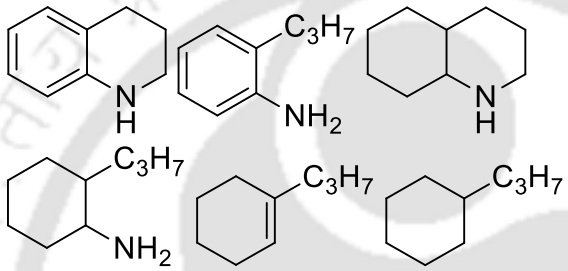 C_5H_3, C_6H_6, C_3H_3, C_4H_4, C_6H_4, C_8H_6, C_5H_2, C_3H_2, C_4H_2, C_7H_3, C_6H_2	C_2H_2, NH_3, CH_4, C_2H_4, C_2H_6
4000	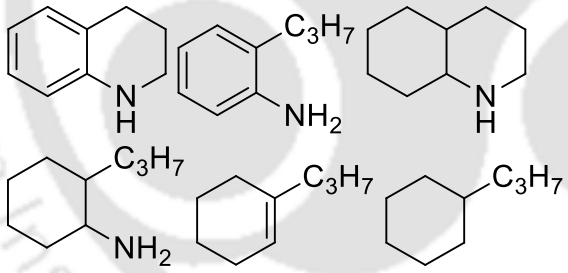 CH_3, C_3H_5, C_6H_2, C_6H_3, C_4H_4, C_5H_2, C_3H_2, C_4H_2	C_2H_2, NH_3, CH_4, C_2H_4, C_2H_6
4500	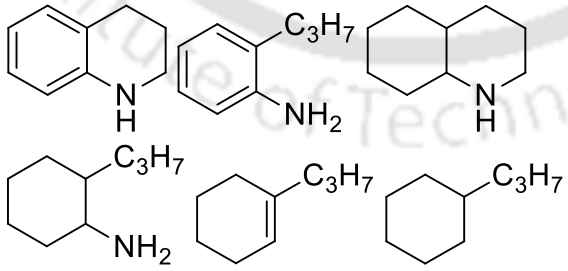 C_4H_2, CH_3, C_3H_4, C_4H_3, C_5H_2, C_5H_3, C_7H_3, C_5H_4	C_2H_2, NH_3, CH_4, C_2H_4, C_2H_6

After the complete decomposition of quinoline, the reaction systems become constant and with no further new molecules formed (Figure 6.6). The number of unsaturated hydrocarbons such as acetylene increases after the complete decomposition of quinoline molecule. Among the reactions, the top 10 most frequent reactions are listed in Table 6.1. The proportion of the intermolecular reaction increases as the temperature increases.

In general, the degradation of quinoline is a very complex multibody chemical process in which the majority of the intermediate reactions proceeds through an intramolecular cracking reaction. During the MD simulation at 4500 K, a total of 140 main species including the stable products and the unstable intermediates are observed. Part of the produced fragments would further take part in the reaction during the quinoline reaction. The main produced small fragments have a higher number at the end of the simulation. The stable products are one type of the important products of the quinoline degradation, which could be easily detected. Acetylene is the most important stable product of quinoline hydrogenation with the highest yield. Figure 6.7 displays the time-dependent distribution of acetylene during the process at different temperatures.

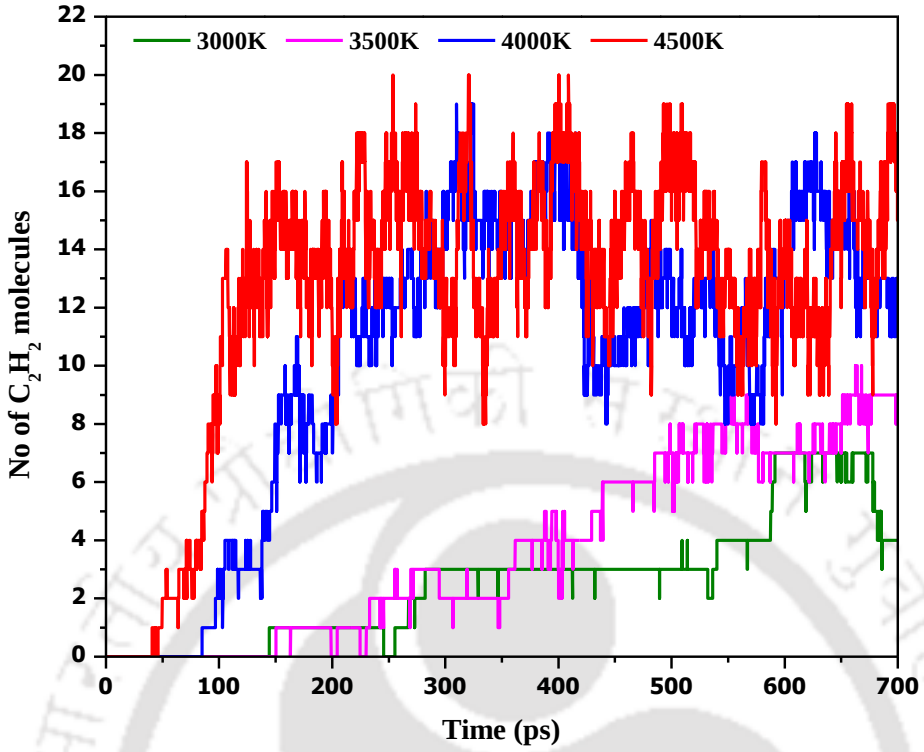

Figure 6.7: Changes of the number of C_2H_2 molecules with time during 700 ps ReaxFF simulation at different temperatures

6.4.3 Kinetic Analysis

Figure 6.3 represents the change of number of total quinoline molecules or average quinoline concentration as a function of simulation time obtained from ReaxFF NVT-MD simulations at different temperatures ranging from 3000 K to 4500 K. For each temperature, the number of decayed molecules averaged at for every time instant from 5 independent simulations are obtained as a function of time. The consumption rate of the quinoline molecules is hence found to be a function of temperature. ReaxFF-MD simulations indicate that for the initial stages of the simulations, the quinoline concentration decreases more quickly with increasing temperature. The consumption rate of quinoline was also used to study the first-order kinetics of the reactants. Here, the

reactant concentration was replaced by the number of reactant molecules. The decomposition trends of quinoline molecules indicate their activation energies. Thus, using this information, the rate constant (k) of the reaction was determined at each temperature. We used the integrated first order rate law equation for calculation of rate constant (Eq. 6.7).

$$\ln(N_0) - \ln(N_t) = kt \tag{6.7}$$

Where N_0 is the number of molecules initially present in the system and N_t is the number of molecules present at time t. For each temperature, the quantity $\ln(N_0) - \ln(N_t)$ is calculated at each time step. First, we plotted this against time and the linear fit gave the rate constant at that temperature. Next, we used these rate constants from different temperatures to generate the Arrhenius plot. The slope of the line gives the activation energy (E_a). The Arrhenius equation is described as (Eq. 6.8):

$$k = k_0 e^{\frac{-E_a}{RT}} \tag{6.8}$$

Where R is the universal gas constant. The Arrhenius plot of the quinoline decomposition is shown in Figure 6.8. The overall activation energy of reaction obtained from ReaxFF-MD simulations was 36.7 kcal/mol. Bearing in mind the difference of the conditions for the experiments and ReaxFF MD simulation, this is well agreed with experimental results by Ahmed et al. [46].

In addition, we have computed the different energy difference (relative energy) for the intermediate formed during the reaction. Figure 6.9 and 6.10 shows the various relative energy dissipated for the most favorable immediate formation step of hydrogenation of quinoline observed in the ReaxFF simulation at 3000K (Figure 6.2) for both scheme-I and

scheme-II, respectively. Here, the first step, namely THQ formation was same as 38.48 kcal/mol for both cases i.e scheme I and II. This forms a reasonable agreement with the Arrhenius activation energy value (36.7 kcal/mol) as obtained earlier. Figure 6.9 (scheme-I) indicates the energy for conversion of PA (79.11 kcal/mol), PCHA (99.2 kcal/mol) and PCHE (142.5 kcal/mol). Figure 6.10 (scheme-II) indicates the energy of formation of DHQ (87.03 kcal/mol), PCHA (98.54 kcal/mol) and PCHE (142.39 kcal/mol). The energy for final stable products formation for both cases were nearly same (210 kcal/mol). From the above relative energy values, it was confirmed that the intermediates formed were short lived and the reaction process ware fast. However, the final decomposition product were stable and no further reaction occurs. Therefore, the quinoline degradation study using ReaxFF method was very positive and revealed the hydrogenation mechanism clearly.

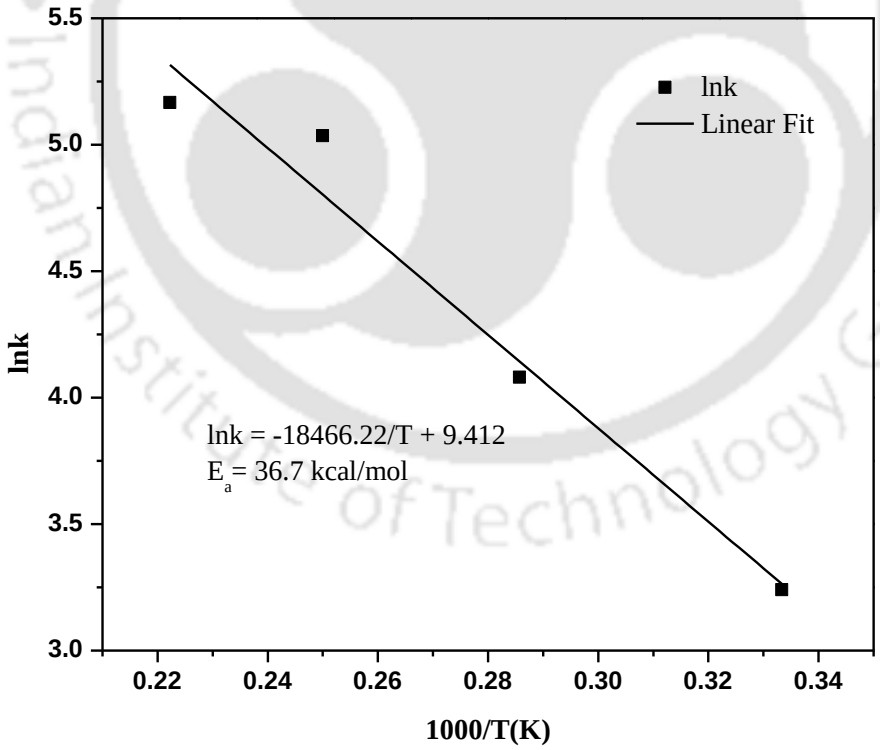

Figure 6.8: Arrhenius plot for the overall reaction and determination of activation energy hydrogenation of quinoline

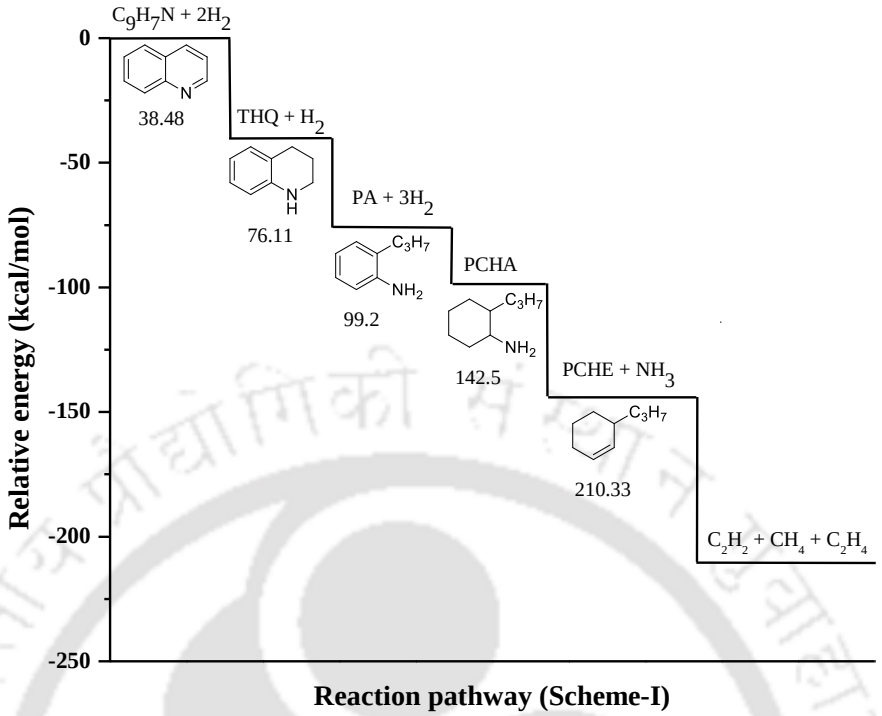

Figure 6.9: Relative energy of rate determining step for hydrogenation of quinoline observed in the ReaxFF simulation at 3000K (Scheme-I)

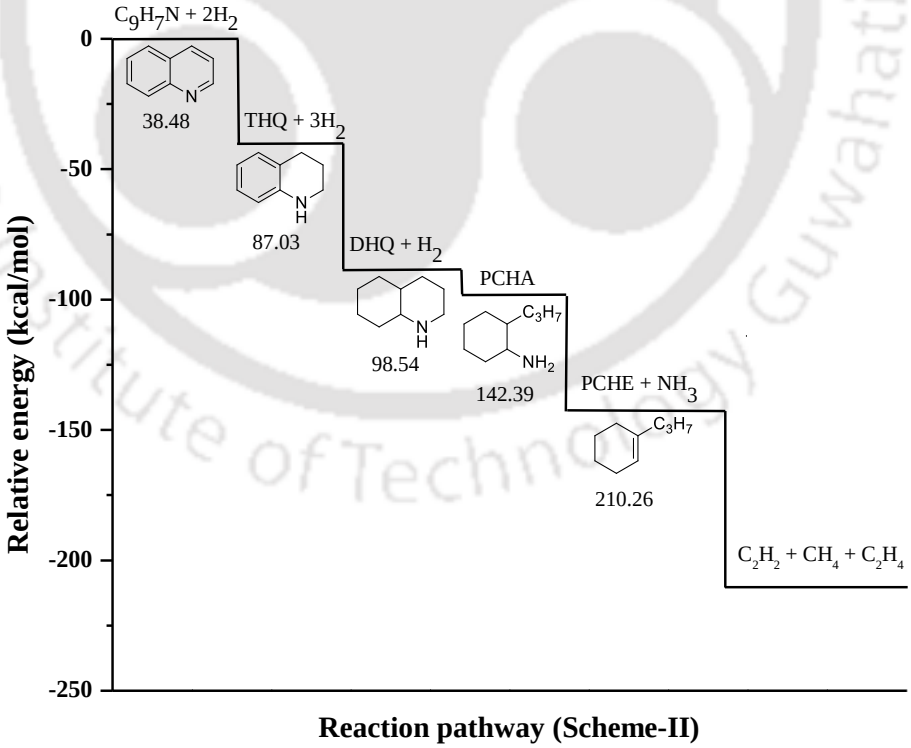

Figure 6.10: Relative energy of rate determining step for hydrogenation of quinoline observed in the ReaxFF simulation at 3000K (Scheme-II)

6.5 Conclusion

In this work, hydrogenation with degradation of quinoline at high temperature is intensively analyzed by a series of MD simulations based on ReaxFF. The intermediate mechanism, the overall product/ intermediate distributions, and the corresponding reaction behavior for the quinoline hydrogenation are investigated. The main decomposition pathways and the composition of the main decomposition products of quinoline at different temperatures are revealed. The results indicate that the active site of hydrogenation initiation reaction is the aromatic ortho-position of the quinolone. Further degradation of quinoline gives smaller stable products along with many intermediates. Most of the intermediate reactions proceed through intramolecular and intermolecular reaction as observed at high temperature. For the initiation stage, hydrogenation of quinoline is mainly through the C−C bond fission pathways for denitrification. In the process, the main products include ammonia, ethylene, methane, ethane, and acetylene. The THQ and DHQ are the most important intermediates that are confirmed by comparing the simulation results of this work. For the stable product, the number of the species would reach its maximum after the complete decomposition of quinoline molecule. Acetylene is the major compound formed. The decomposition rate of quinoline and generation rate of the products increases with the increase of temperature. In conclusion, the ReaxFF MD simulation method provides an effective approach towards the study of hydrogenation/degradation reactions of quinoline at the molecular level.

References

[1] R.A. Sánchez-Delgado, Organometallic modeling of the hydrodesulfurization and hydrodenitrogenation reactions, Springer Science & Business Media2002.

[2] J.G.d. Vries, The handbook of homogeneous hydrogenation, Wiley-Vch2007.

[3] M. Campanati, A. Vaccari, O. Piccolo, Mild hydrogenation of quinoline: 1. Role of reaction parameters, J. Mol. Catal. A: Chem. 179 (2002) 287-292.

[4] Y.-P. Sun, H.-Y. Fu, D.-l. Zhang, R.-X. Li, H. Chen, X.-J. Li, Complete hydrogenation of quinoline over hydroxyapatite supported ruthenium catalyst, Catal. Commun. 12 (2010) 188-192.

[5] D. Ren, L. He, L. Yu, R.-S. Ding, Y.-M. Liu, Y. Cao, H.-Y. He, K.-N. Fan, An unusual chemoselective hydrogenation of quinoline compounds using supported gold catalysts, J. Am. Chem. Soc. 134 (2012) 17592-17598.

[6] R.A. Sánchez-Delgado, N. Machalaba, Hydrogenation of quinoline by ruthenium nanoparticles immobilized on poly (4-vinylpyridine), Catal. Commun. 8 (2007) 2115-2118.

[7] C.W. Curtis, D.R. Cahela, Hydrodenitrogenation of quinoline and coal using precipitated transition-metal sulfides, Energy & fuels 3 (1989) 168-174.

[8] C.N. Satterfield, S.H. Yang, Catalytic hydrodenitrogenation of quinoline in a trickle-bed reactor. Comparison with vapor phase reaction, Ind. Eng. Chem. Process Des. Dev. 23 (1984) 11-19.

[9] C.N. Satterfield, M. Modell, R.A. Hites, C.J. Declerck, Intermediate reactions in the catalytic hydrodenitrogenation of quinoline, Ind. Eng. Chem. Process Des. Dev. 17 (1978) 141-148.

[10] C.N. Satterfield, J.F. Cocchetto, Reaction network and kinetics of the vapor-phase catalytic hydrodenitrogenation of quinoline, Ind. Eng. Chem. Process Des. Dev. 20 (1981) 53-62.

[11] J.F. Cocchetto, C.N. Satterfield, Chemical equilibriums among quinoline and its reaction products in hydrodenitrogenation, Ind. Eng. Chem. Process Des. Dev. 20 (1981) 49-53.

[12] G. Perot, The reactions involved in hydrodenitrogenation, Catal. Today 10 (1991) 447-472.

[13] P.K. Naik, P. Dehury, S. Paul, T. Banerjee, Evaluation of Deep Eutectic Solvent for the selective extraction of toluene and quinoline at T= 308.15 K and p= 1 bar, Fluid Phase Equilib. 423 (2016) 146-155.

[14] P.K. Naik, S. Paul, T. Banerjee, Liquid Liquid Equilibria measurements for the extraction of poly aromatic nitrogen hydrocarbons with a low cost Deep Eutectic Solvent: Experimental and theoretical insights, J. Mol. Liq. 243 (2017) 542-552.

[15] P.K. Naik, M. Mohan, T. Banerjee, S. Paul, V.V. Goud, Molecular Dynamic Simulations for the Extraction of Quinoline from Heptane in the Presence of a Low-Cost Phosphonium-Based Deep Eutectic Solvent, J. Phys. Chem. B 122 (2018) 4006-4015.

[16] J. Shaw, P. Stapp, Regiospecific hydrogenation of quinolines and indoles in the heterocyclic ring, J. Heterocycl. Chem. 24 (1987) 1477-1483.

[17] M. Freifelder, Hydrogenation of Pyridines and Quinolines, Adv. Catal. 14 (1963) 203.

[18] A.C. Van Duin, S. Dasgupta, F. Lorant, W.A. Goddard, ReaxFF: a reactive force field for hydrocarbons, J. Phys. Chem. A 105 (2001) 9396-9409.

[19] K. Chenoweth, A.C. Van Duin, W.A. Goddard, ReaxFF reactive force field for molecular dynamics simulations of hydrocarbon oxidation, J. Phys. Chem. A 112 (2008) 1040-1053.

[20] A.M. Kamat, A.C. van Duin, A. Yakovlev, Molecular dynamics simulations of laser-induced incandescence of soot using an extended ReaxFF reactive force field, J. Phys. Chem. A 114 (2010) 12561-12572.

[21] B. Chen, Z.-J. Diao, Y.-L. Zhao, X.-X. Ma, A ReaxFF molecular dynamics (MD) simulation for the hydrogenation reaction with coal related model compounds, Fuel 154 (2015) 114-122.

[22] N. Lümmen, ReaxFF-molecular dynamics simulations of non-oxidative and non-catalyzed thermal decomposition of methane at high temperatures, Physical Chemistry Chemical Physics 12 (2010) 7883-7893.

[23] Z. He, X.-B. Li, L.-M. Liu, W. Zhu, The intrinsic mechanism of methane oxidation under explosion condition: A combined ReaxFF and DFT study, Fuel 124 (2014) 85-90.

[24] M. Döntgen, M.-D. Przybylski-Freund, L.C. Kröger, W.A. Kopp, A.E. Ismail, K. Leonhard, Automated discovery of reaction pathways, rate constants, and transition states using reactive molecular dynamics simulations, Journal of chemical theory and computation 11 (2015) 2517-2524.

[25] C. Ashraf, S. Shabnam, A. Jain, Y. Xuan, A.C. van Duin, Pyrolysis of binary fuel mixtures at supercritical conditions: A ReaxFF molecular dynamics study, Fuel 235 (2019) 194-207.

[26] Q. Zhong, Q. Mao, J. Xiao, A. van Duin, J.P. Mathews, Sulfur removal from petroleum coke during high-temperature pyrolysis. Analysis from TG-MS data and ReaxFF simulations, Journal of Analytical and Applied Pyrolysis 132 (2018) 134-142.

[27] K. Chenoweth, A.C. Van Duin, S. Dasgupta, W.A. Goddard Iii, Initiation mechanisms and kinetics of pyrolysis and combustion of JP-10 hydrocarbon jet fuel, J. Phys. Chem. A 113 (2009) 1740-1746.

[28] J. Ding, L. Zhang, Y. Zhang, K.-L. Han, A reactive molecular dynamics study of n-heptane pyrolysis at high temperature, J. Phys. Chem. A 117 (2013) 3266-3278.

[29] X.-M. Cheng, Q.-D. Wang, J.-Q. Li, J.-B. Wang, X.-Y. Li, ReaxFF molecular dynamics simulations of oxidation of toluene at high temperatures, J. Phys. Chem. A 116 (2012) 9811-9818.

[30] T. Qi, C.W. Bauschlicher Jr, J.W. Lawson, T.G. Desai, E.J. Reed, Comparison of ReaxFF, DFTB, and DFT for phenolic pyrolysis. 1. Molecular dynamics simulations, J. Phys. Chem. A 117 (2013) 11115-11125.

[31] X. Zhang, Y. Li, D. Chen, S. Xiao, S. Tian, J. Tang, R. Zhuo, Reactive molecular dynamics study of the decomposition mechanism of the environmentally friendly insulating medium C 3 F 7 CN, RSC Adv. 7 (2017) 50663-50671.

[32] A.C. Van Duin, W.A. Goddard, H. van Schoot, A.L. Yakovlev, ReaxFF, SCM, Theoretical Chemistry, Vrije Universiteit, Amsterdam, The Netherlands, http://www.scm.com, 2016.

[33] H.M. Aktulga, S.A. Pandit, A.C. van Duin, A.Y. Grama, Reactive molecular dynamics: Numerical methods and algorithmic techniques, SIAM J. Sci. Comp. 34 (2012) C1-C23.

[34] A.K. Rappe, W.A. Goddard III, Charge equilibration for molecular dynamics simulations, J. Phys. Chem. 95 (1991) 3358-3363.

[35] H.J. Berendsen, J.v. Postma, W.F. van Gunsteren, A. DiNola, J. Haak, Molecular dynamics with coupling to an external bath, J. Chem. Phys. 81 (1984) 3684-3690.

[36] D. Fantauzzi, J.E. Mueller, L. Sabo, A.C. Van Duin, T. Jacob, Surface buckling and subsurface oxygen: Atomistic insights into the surface oxidation of Pt (111), ChemPhysChem 16 (2015) 2797-2802.

[37] S. Bhoi, T. Banerjee, K. Mohanty, Insights on the combustion and pyrolysis behavior of three different ranks of coals using reactive molecular dynamics simulation, RSC Adv. 6 (2016) 2559-2570.

[38] H. Schulz, M. Schon, N.M. Rahman, Hydrogenative denitrogenation of model compounds as related to the refining of liquid fuels, Studies in Surface Science and Catalysis, Elsevier1986, pp. 201-255.

[39] X.-Y. Wei, E. Ogata, E. Niki, FeS2-catalyzed hydrocracking of α, ω-diarylalkanes, Bull. Chem. Soc. Jpn. 65 (1992) 1114-1119.

[40] X.-Y. Wei, E. Ogata, S. Futamura, Y. Kamiya, Thermal decomposition and hydrocracking of hydrogenated di (1-naphthyl) methanes, Fuel Process. Technol. 26 (1990) 135-148.

[41] T. Autrey, J.C. Linehan, D.M. Camaioni, L.E. Kaune, H.M. Watrob, J.A. Franz, Mechanistic investigations of iron/sulfur-catalyzed bond scission in aromatic hydrocarbons. A catalytic hydrogen atom transfer step involving a late transition state, Catal. Today 31 (1996) 105-111.

[42] K. Ouchi, M. Makabe, Hydrogen transfer in the hydrogenation of model compounds, Fuel 67 (1988) 1536-1541.

[43] S. Futamura, S. Koyanagi, Y. Kamiya, The hydrogenolysis of diarylmethane: mechanism for hydrogen transfer from solvents and additive effects of hydrogen shuttlers and organic radical sources, Fuel 67 (1988) 1436-1440.

[44] F. Rice, The thermal decomposition of organic compounds from the standpoint of free radicals. I. Saturated hydrocarbons, J. Am. Chem. Soc. 53 (1931) 1959-1972.

[45] A. Kossiakoff, F.O. Rice, Thermal decomposition of hydrocarbons, resonance stabilization and isomerization of free radicals1, J. Am. Chem. Soc. 65 (1943) 590-595.

[46] A.K. Aboul-Gheit, The Kinetics of Quinoline Hydrodenitrogenation through Reaction Intermediate Products, Canadian Journal of Chemistry 53 (1975) 2575-2579.

CHAPTER 7

Conclusion and Future Scope

7.1 Conclusions

Fuel oil consisting of impurities such as aromatic and polyaromatic compounds are the main cause for air pollution. Thus, there is a need for removal of the PAH impurities from fuel oil. The thesis aims to comprehensively study these effects such as extraction of PAH like quinoline with the help of green solvent named deep eutectic solvents (DES). According to literature survey data, we have chosen four phosphonium and ammonium based DESs, which are prominent for known for their aromatic extraction i.e benzene and toluene. In the present study methyltriphenyl phosphonium bromide [MTPB] and tetra butyl ammonium bromide [TBAB] salt hydrogen bond acceptor were mixed with ethylene glycol or glycerol as hydrogen bond donor at a molar ratio of 1:4 to form the DESs. The thermophysical properties and the molecular stability of the DESs were analysed with the classical molecular dynamics and physicochemical characterization. It was found that the DESs are more thermally and chemically stable than other ionic liquids and organic solvents.

Liquid-liquid equilibria data were then generated for both single and multi-component system. The quinoline or indoline was more effective in extracting heptane as compared to toluene. Larger values of selectivity (142-3344) indicate the easier separation of quinoline from heptane. The larger values of distribution coefficient indicated a lesser solvent requirement for PAH separation. Higher quinoline and indoline selectivity indicated the better separation of both PAH from the feed in quaternary systems. The presence of toluene slightly decreases the extraction capacity in case of simultaneous removal but however, extraction is easy than toluene alone. The raffinate phase was found to comprise mainly heptane hydrocarbon rich with mole composition as high as 99% for

all systems. Further, liquid-liquid equilibria data for all systems were correlated with the NRTL, UNIQUAC, and COSMO-RS models. RMSD results are extremely encouraging, with deviations in phase compositions less than unity for all systems indicating a better fit. In terms of distribution co-efficient, selectivity and solvent loss, DES1 (MTPB + ethylene glycol (1:4)), was found to be the best solvent for the extraction of PAH from heptane.

The thesis further focuses on the correlation of experimental LLE data with the molecular dynamics simulated data for the DES1 (MTPB+ ethylene glycol (1:4))+ quinoline + heptane ternary system in order to understand the detailed mechanism for extraction in the molecular level. The experimental tie line data depicted an excellent agreement with simulated results. From MD simulations, it was found that the van der Waals interactions are the controlling parameter for DES-quinoline-heptane interactions. The phosphonium cation gave higher interaction energy with quinoline, which is then followed by ethylene glycol and bromide anion. DES was very closely distributed around the more active side of quinoline. Hence quinoline was efficiently extracted by DES. In addition, this study provides new insights for the computational analysis of LLE equilibria in the absence of experimental data. Finally, the DES1 (MTPB + ethylene glycol (1:4)) is strongly recommended for the extraction of PAH.

The final chapter includes the reactive molecular dynamics (ReaxFF MD) simulations, which gave insights in understanding the reaction mechanism and product distribution for the hydrogenation and degradation of quinoline at high temperature. Initially, hydrogenation of quinoline is mainly through the C−C bond fission pathways for denitrification. The tetrahydroquinoline (THQ) and decahydroquinoline (DHQ) are the most important intermediates formed. Main products include ammonia, ethylene, methane, ethane, and acetylene among which acetylene is the major product.

7.2 Future Work

Overall DESs are excellent candidates for the extraction of aromatic as well as polyaromatic compound from fuel oil. Using this DES, the entire process can be optimized in Aspen Plus and based on that, further studies can be carried out for the development at the industrial level process using a combination of multistage extractor and distillation column. Further molecular dynamics approach can be implemented for quaternary systems which include both indoline and quinoline. This will help in identifying the competing forces for individual extraction. This may also be complemented by Quantum chemical calculations within the supramolecular approach. In the penultimate step, the DES recovery study can be carried out for the system by analyzing the recycling extraction efficiency of DES.

APPENDIX A

A.1 Deep Aspect of DES

A DES is generally composed of two or three cheap and safe components, which are capable of associating with each other, through hydrogen bond interactions, to form a eutectic mixture. Melting point lower than that of each individual component characterizes the resulting DES. Generally, DESs are characterized by a very large depression of freezing point and are liquid at temperatures lower than 150 °C. Note that most of them are liquid between room temperature and 70 °C. In most cases, a DES is obtained by mixing a quaternary ammonium salt with metal salts or a hydrogen bond donor (HBD) that has the ability to form a complex with the halide anion of the quaternary ammonium salt.

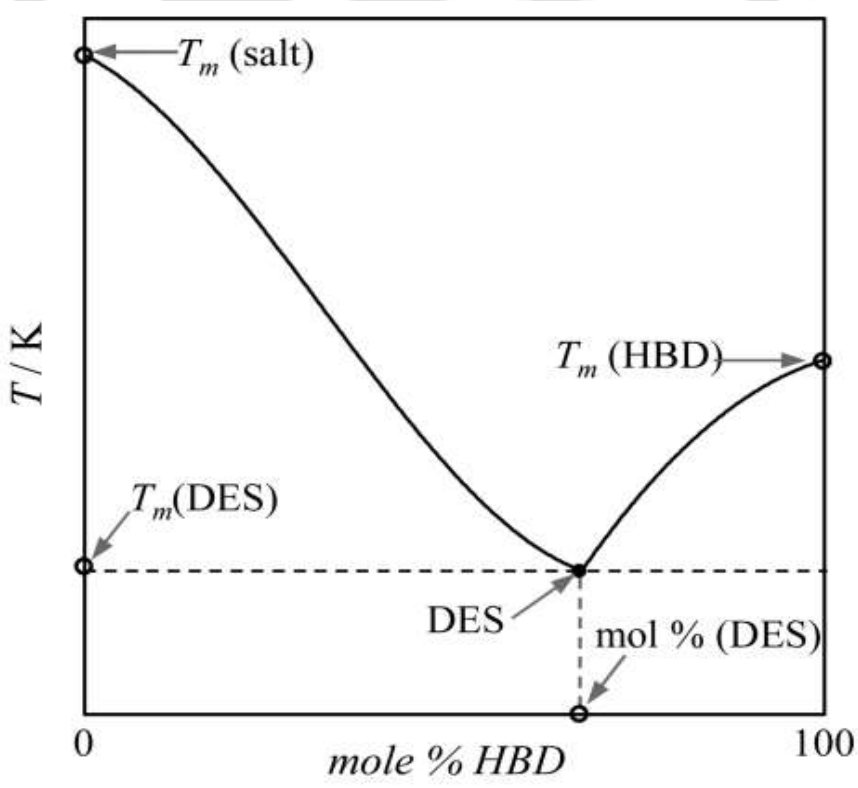

Figure A.1: Schematic solid−liquid phase diagram for a binary mixture between a salt and an HBD

In figure A.1, the appearance of "deep" depression of the individual component melting temperature of the DES at the mixture composition and temperature is shown. T_m stands for the melting point. The solid line shows the melting point temperature as a function of mixture composition, and the dashed lines show the temperature and composition of the eutectic mixture. It should be noted that the eutectic composition is a single value that corresponds to the minimum melting temperature in the phase diagram. The very low melting points of DESs in comparison with those for the salts (HBAs) and HBDs forming them is one of their most relevant and distinct known properties. This signifies the clear definition of the word "deep" in the DES, which shows the DES deviates from its ideal behavior.

Ionic liquids have been described as "green solvents" largely because of their low vapor pressure. However, the toxicity have been investigated which has proven that they are not inherently "green". DESs may offer a "greener" alternative to many traditional ILs, but they are also not by definition "green". Some DESs will be inherently nontoxic being composed of benign constituents. In some eutectics which contain metal salts have toxicity. On the other hand, the phosphonium and ammonium halide salt along with polyols such as glycerol, ethylene glycol, have low inherent toxicity. In our case, both components of the DESs are non-harmful to the environment, and both are readily biodegradable, with the resultant DES. The ethylene glycol based liquid was not harmful for the environment as compared to most ILs. In addition, DESs do have lower vapor pressures than most molecular solvents which decrease their emission to the atmosphere; however, they are partly miscible with water and could inevitably end up in the aqueous environment. For DESs to be truly "green" a method for recycling needs to be ascertained.

Although components of a DES can be nontoxic and of low environmental impact, it does not necessarily follow that mixtures of these components will be nontoxic and inherently "green". This is underpinned by the fact the DESs have special properties that neither of the individual components have. Methyltriphenylphosphonium bromide and Tetrabutylammonium bromide having slightly acute toxicity for oral, skin and inhalation. Overall, DES are the most promising discoveries of recent years in the area of Green Chemistry. DESs not only allows the design of safer processes but also provides a straightforward access to new chemicals and materials over the existing solvent.

A.2 COSMO-SAC Model and Solubility Thermodynamics of DES

The COSMO-SAC model was designed by Lin and Sandler [1]. Its purpose is to predict different phase equilibria thermodynamic properties using quantum and statistical mechanics. The model is based on the original work of Andreas Klamt [2] who developed Conductor-like Screening Model" (COSMO) for its ability to determine the screening charges around a solute in a conductor by using density functional theory (DFT) for real solvents (COSMO-RS). The COSMO-SAC allows the thermodynamic properties of molecules to be predicted from the activity coefficients of tiny segments (SAC = "Segment Activity Coefficient"). The COSMO-SAC model uses quantum chemical methods for the representation of the charge distribution of the molecules (σ-profiles), and statistical thermodynamics to get the molecular interactions for predicting the chemical potential of a molecule from its structure. To determine the activity coefficient, only the σ-profiles and the van der Waals surface and volume are needed, which makes COSMO-SAC a fully predictive model.

The model gives an expression of the solvation free energy ΔG^{*solv}, which defines, at constant temperature and pressure, the energy difference between an ideal solution and the solute in the real solvent. The molecules are regarded as a collection of surface segments and the chemical potential of each segment is determined. The difference in the segment activity coefficient between a mixture and a pure liquid gives the segment activity coefficients, and the activity coefficient of a molecule is obtained from the summation over the segment activity coefficients. The activity coefficient $\gamma_{i/s}$ of solute *i* in the solution *s* is derived from the following equation 1.

$$\ln \gamma_{i/s} = \frac{\Delta G_{i/s}^{*res} - \Delta G_{i/s}^{*res}}{RT} + \ln \gamma_{i/s}^{SG} \quad (1)$$

Here ΔG^{*res} is the restoring solvation free energy, superscript *SG* denotes the Staverman-Guggenheim combinatorial term (Table A.2). Finally, the activity coefficient is calculated and given as equation 2.

$$\ln\gamma_{i/s} = n_i \sum_{\sigma} P_i(\sigma_m)\left[\ln\Gamma_s(\sigma_m) - \Gamma_i(\sigma_m)\right] + \ln\gamma_{i/s}^{SG} \quad (2)$$

Here $\Gamma_s(\sigma_m)$ and $\Gamma_i(\sigma_m)$ are the activity coefficient of the segment in the mixture and in the component *i*, respectively. σ_m is the surface charge density of segment mixture. The three-dimensional screening charge density distribution $p_i(\sigma_m)$ is quantified using the σ-profile, which is the probability of finding a surface segment with screening charge density σ, i.e., $p(\sigma) = \{A_i(\sigma)\}/A_i$, where $A_i(\sigma)$ is the surface area with a charge density of value σ and A_i is total surface area of species *i*. The term, $n_i = A_i/a_{eff}$, here, a_{eff} is the effective area of the standard surface segment. The interactions, both electrostatic and hydrogen bonding are taken into account through a ΔW term (equation 3).

$$\Delta W(\sigma_m, \sigma_n) = \left(\frac{\alpha'}{2}\right)(\sigma_m + \sigma_n)^2 + c_{hb} \max[0, \sigma_{acc} - \sigma_{hb}] \min[0, \sigma_{don} + \sigma_{hb}] \quad (3)$$

Where σ_m and σ_n are charge densities of the paired segments m and n in mixture. $\alpha'/2$ is a constant for the misfit energy, c_{hb} the hydrogen bonding parameter, and σ_{hb} a cutoff value for the hydrogen bonding interactions. Hydrogen bonds can occur between two segments. To express them, the segments are divided into two categories: acceptor and donor. In fact, segments can be either neutral segments, acceptor segments (σ_{acc}), or donor segments (σ_{don}). The global adjustable parameters for generating the activity coefficient via a statistical mechanical framework were the effective area of the standard surface segment (a_{eff} = 6.32 Å^2), the misfit energy interaction constant [α' = 8419 kcal Å^4/(mol e^2)], the cutoff for hydrogen-bonding interaction (σ_{hb} = 0.0084 e/Å^2), and the hydrogen-bonding interaction constant [c_{hb} = 75,006 kcal Å^4/(mol e^2)].

The DES have interaction between the hydrogen bond donor and acceptor. This renders a new chemical entity with a melting point lower than those of the initial compounds that result a eutectic point. Thus, the lowest temperature that needs to be computed in such a manner that a liquid phase of DES coexist. This can be initiated through quantum chemical calculations followed by statistical-based approach. Hence, the COSMO-SAC model is adopted. COSMO-SAC applies the concept of mutual solubility as a function of temperature and hence predicts the eutectic composition and temperature employing solid−liquid equilibrium (SLE) theory [3]. The procedure starts with the geometry optimization followed by COSMO-SAC predictions. The geometry optimization on all the structures was carried out using the density functional theory (DFT). Thereafter the COSMO file was generated. Thereafter, the mole fraction was predicted for both HBD

and HBA by the activity coefficient in either phase at different temperatures (T) with the following equation 4.

$$\ln\left(\gamma_{solute} x_{solute}\right) = \frac{-\Delta H_f}{RT_m}\left(\frac{1}{T} - \frac{1}{T_m}\right) \tag{4}$$

Where γ_{solute}, x_{solute}, ΔH_f, and T_m are the activity coefficient, the mole fraction, the enthalpy of fusion, and the melting point, respectively. For the ideal situation, the activity coefficient of the solute in the liquid phase is unity. i.e., γ_{solute} =1. Then the ideal solubility equation is (equation 5).

$$\ln x_{solute} = \frac{-\Delta H_f}{RT_m}\left(\frac{1}{T} - \frac{1}{T_m}\right) \tag{5}$$

For the prediction of experimental mole fraction, mole fraction at ideal solvation from equation (5) is predicted. This value is then used to obtain the activity coefficient of the component in the mixture using COSMO-SAC model in equation (2). Thereafter the desired mole ratio for HBA:HDB can be found for the eutectic formation.

References

[1] S.-T. Lin, S.I. Sandler, A priori phase equilibrium prediction from a segment contribution solvation model, Ind. Eng. Chem. Res. 41 (2002) 899-913.

[2] A. Klamt, Conductor-like screening model for real solvents: a new approach to the quantitative calculation of solvation phenomena, J. Phys. Chem. 99 (1995) 2224-2235.

[3] I.I. Alkhatib, D. Bahamon, F. Llovell, M.R. Abu-Zahra, L.F. Vega, Perspectives and guidelines on thermodynamic modelling of deep eutectic solvents, J. Mol. Liq. DOI (2019) 112183.

A.3 Sigma Profile and Sigma Potential of the Starting Material of DES

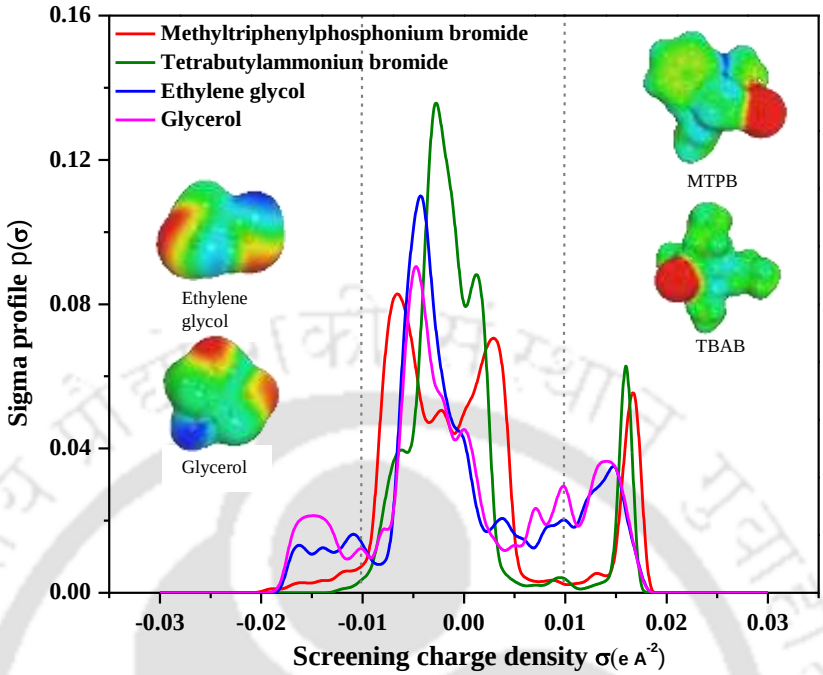

Figure A.2: σ-Profiles of starting material of the DESs used. The dashed vertical lines represent the threshold value for the hydrogen bond interaction, σ_{hb} = ± 0.0084 e.Å^{-2}

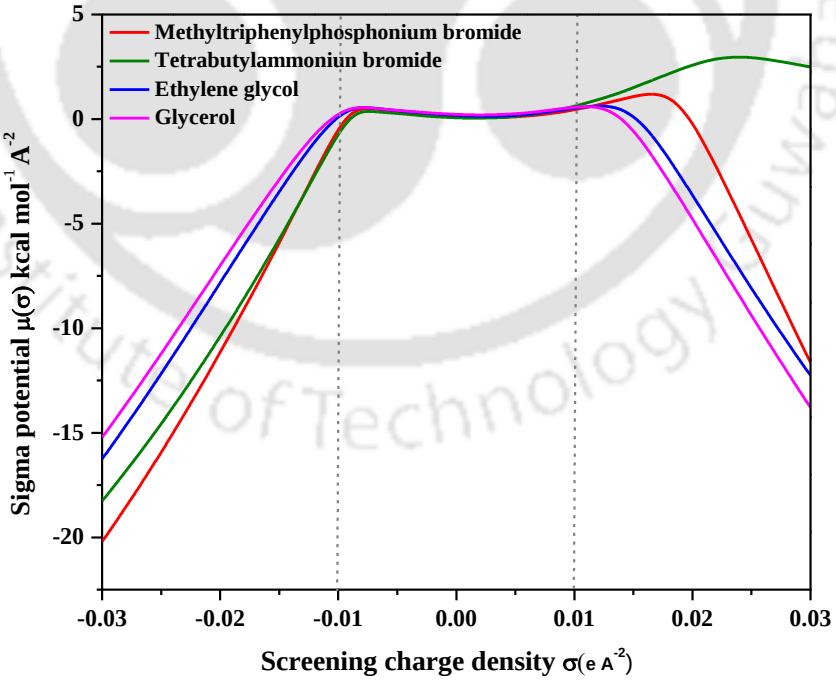

Figure A.3: σ-Potential of starting material of DESs used. The dashed vertical lines represent the threshold value for the hydrogen bond interaction, σ_{hb} = ± 0.0084 e.Å^{-2}

A.4 ^{1}H NMR of Starting Material and 2D–NOSEY Spectra of DES

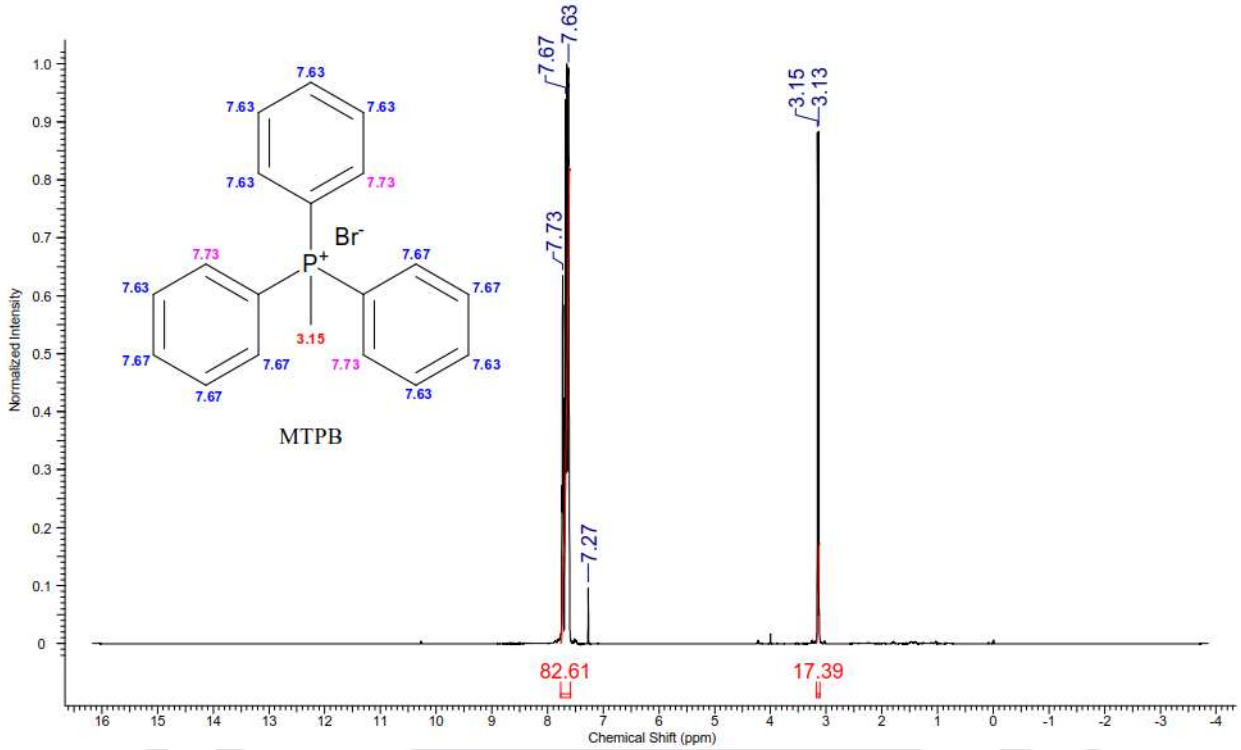

Figure A.4: ^{1}H NMR spectra of methyltriphenylphosphonium bromide

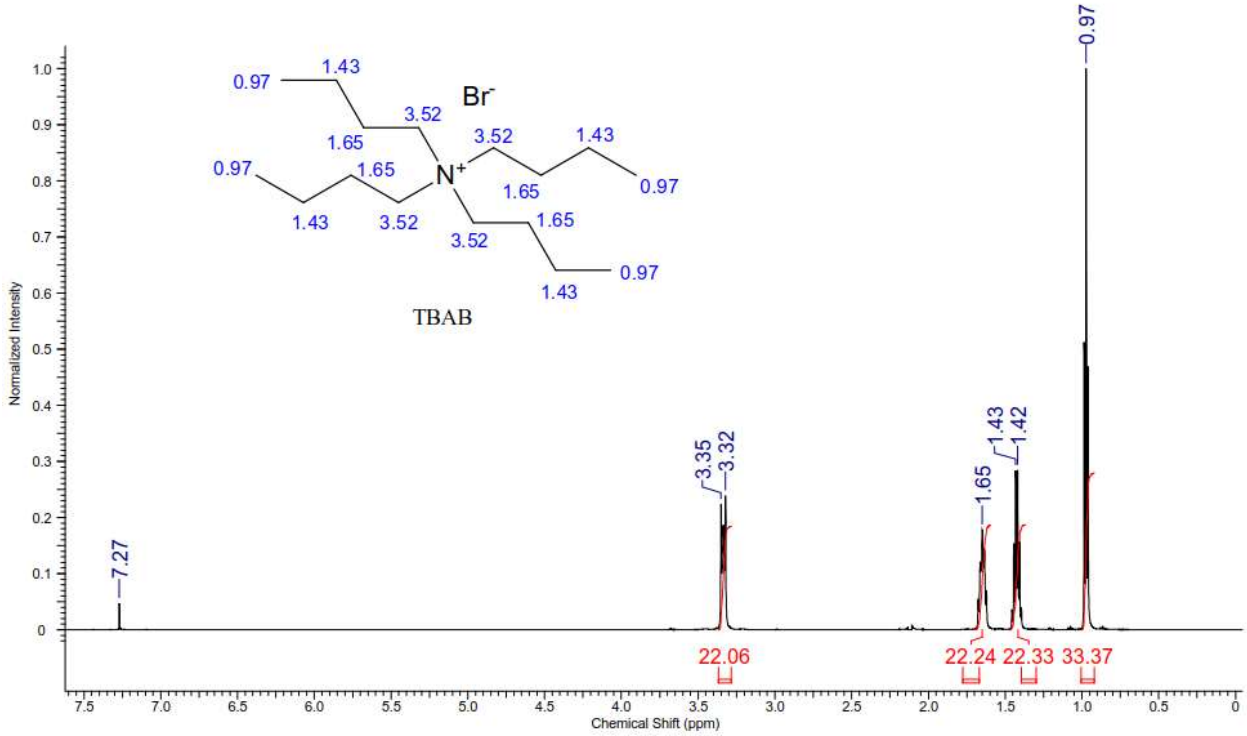

Figure A.5: ^{1}H NMR spectra of tetrabutylammonium bromide

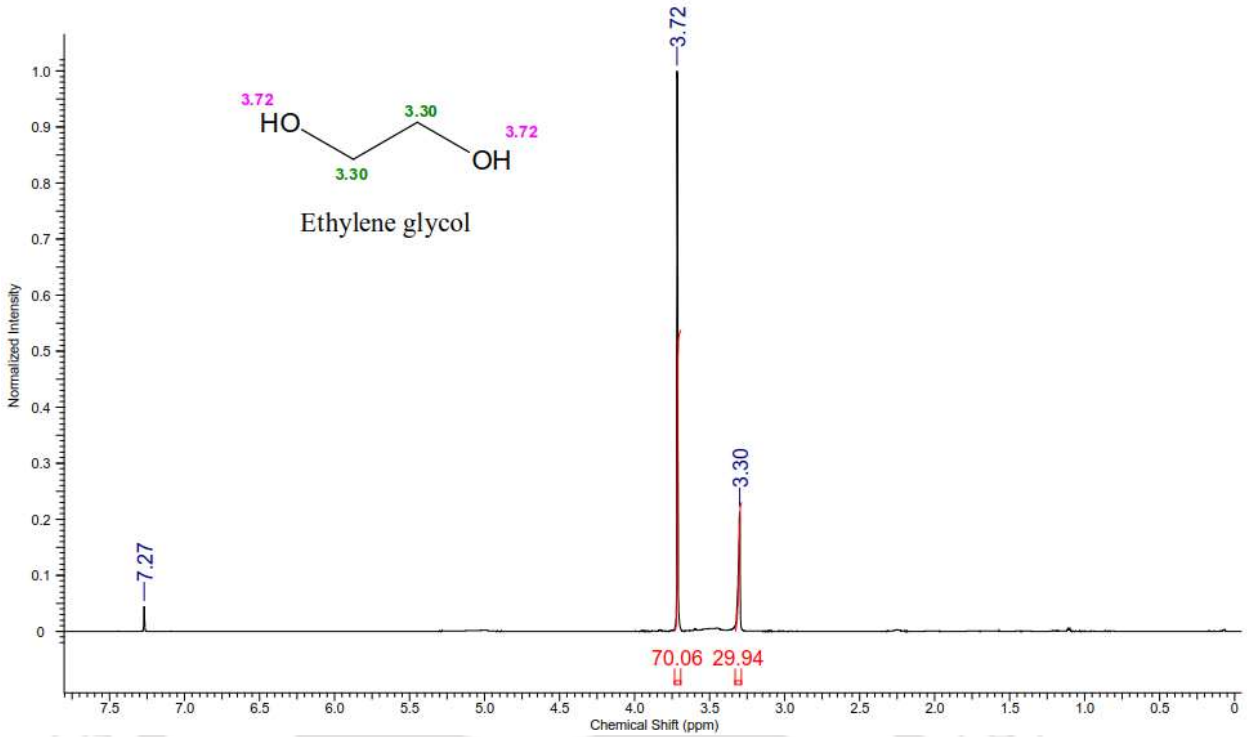

Figure A.6: ^{1}H NMR spectra of ethylene glycol

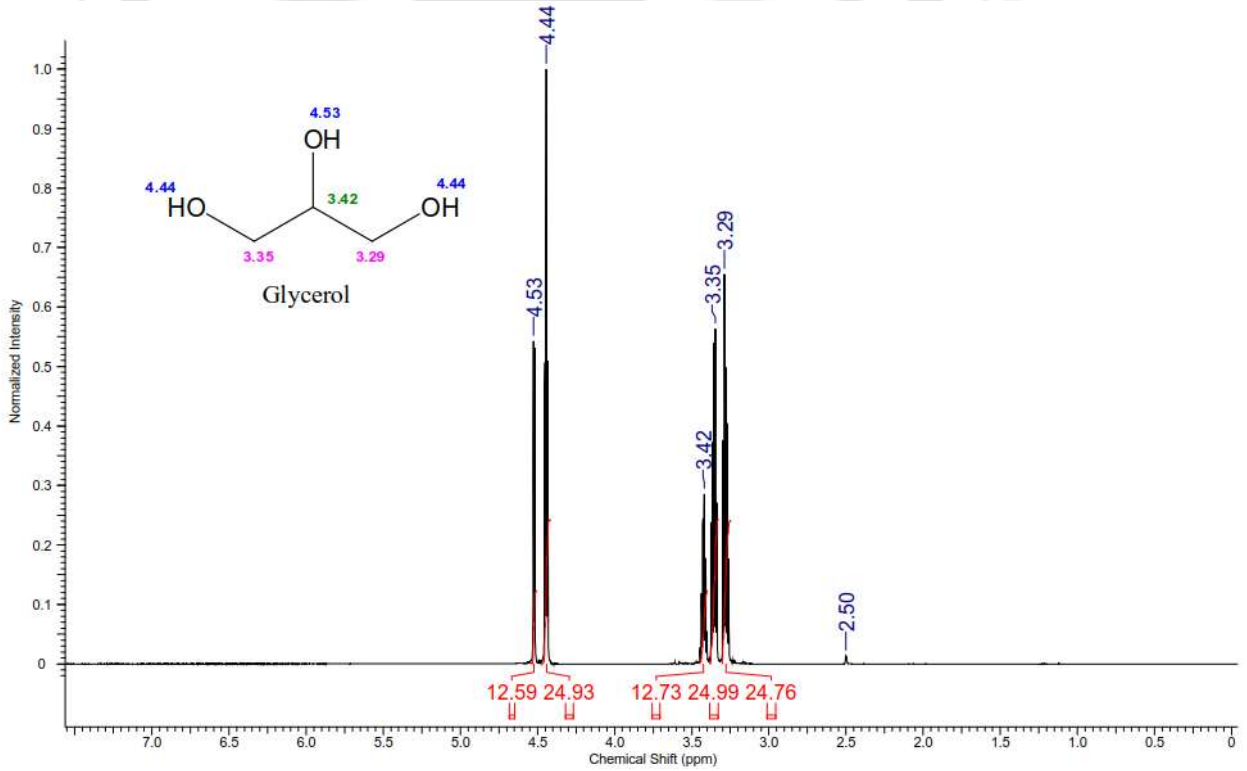

Figure A.7: ^{1}H NMR spectra of glycerol

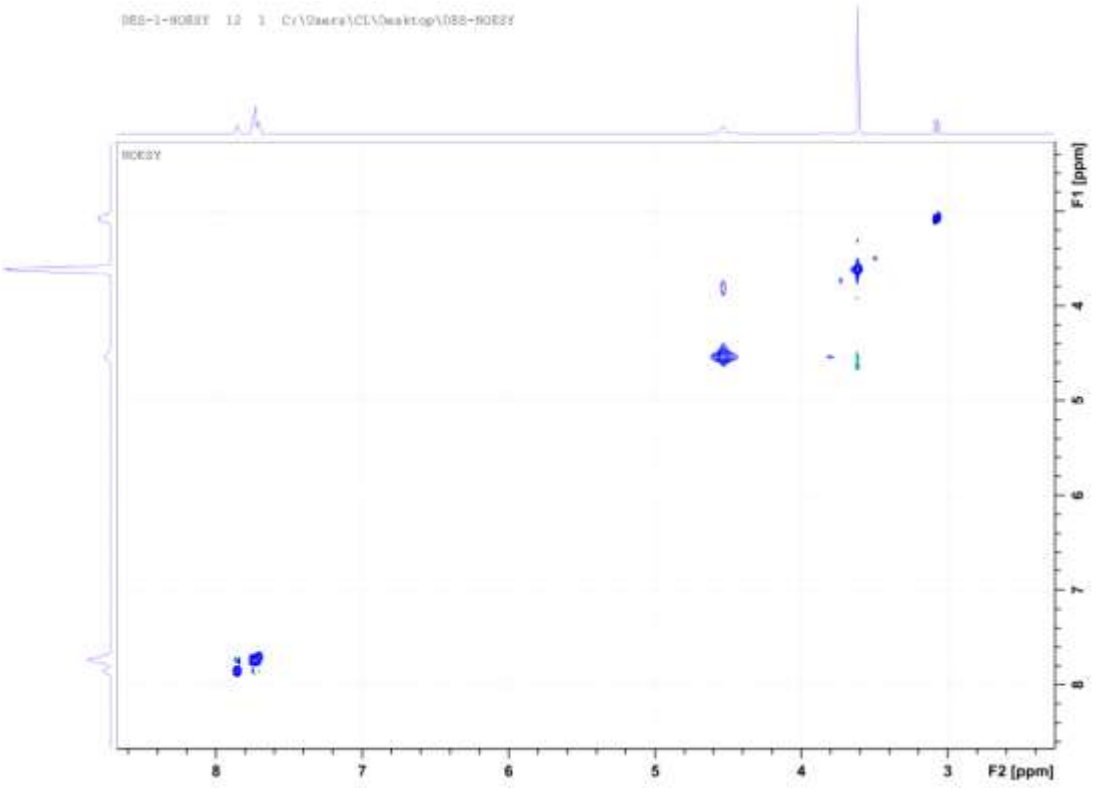

Figure A.8: NOSEY-2D NMR spectra of DES1

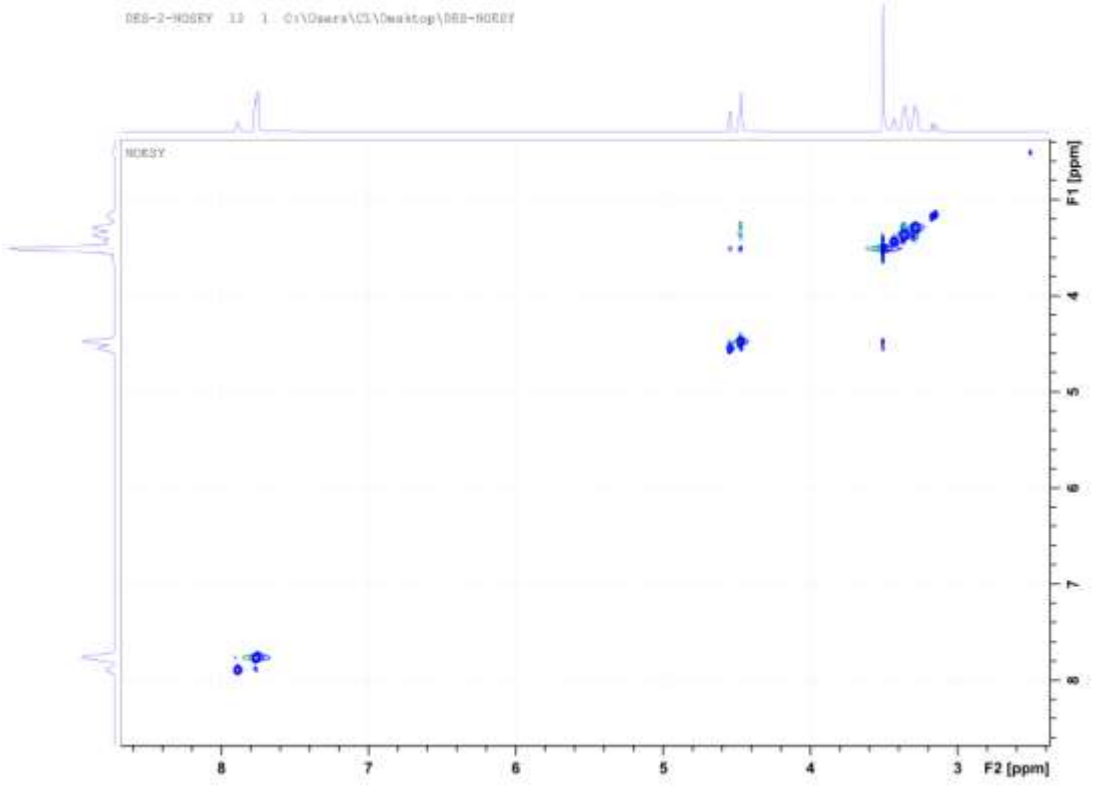

Figure A.9: NOSEY-2D NMR spectra of DES2

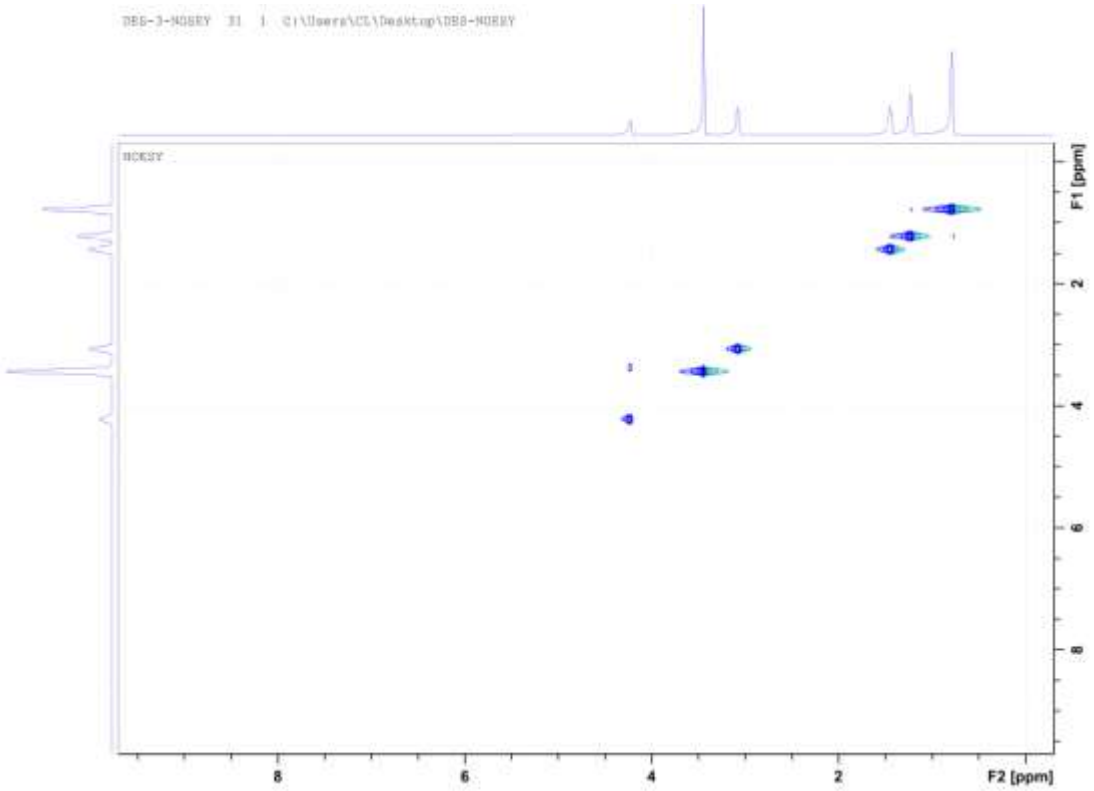

Figure A.10: NOSEY-2D NMR spectra of DES3

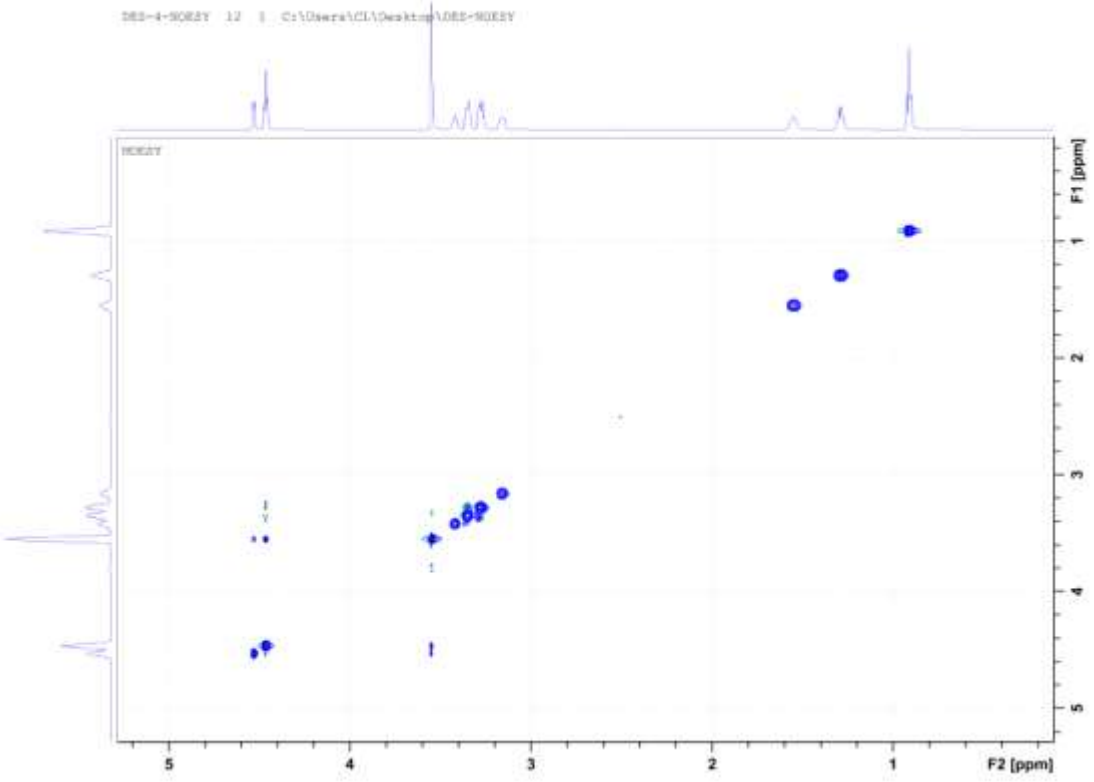

Figure A.11: NOSEY-2D NMR spectra of DES4

A.5 Spatial Distribution Function between HBD and HBA of the DES

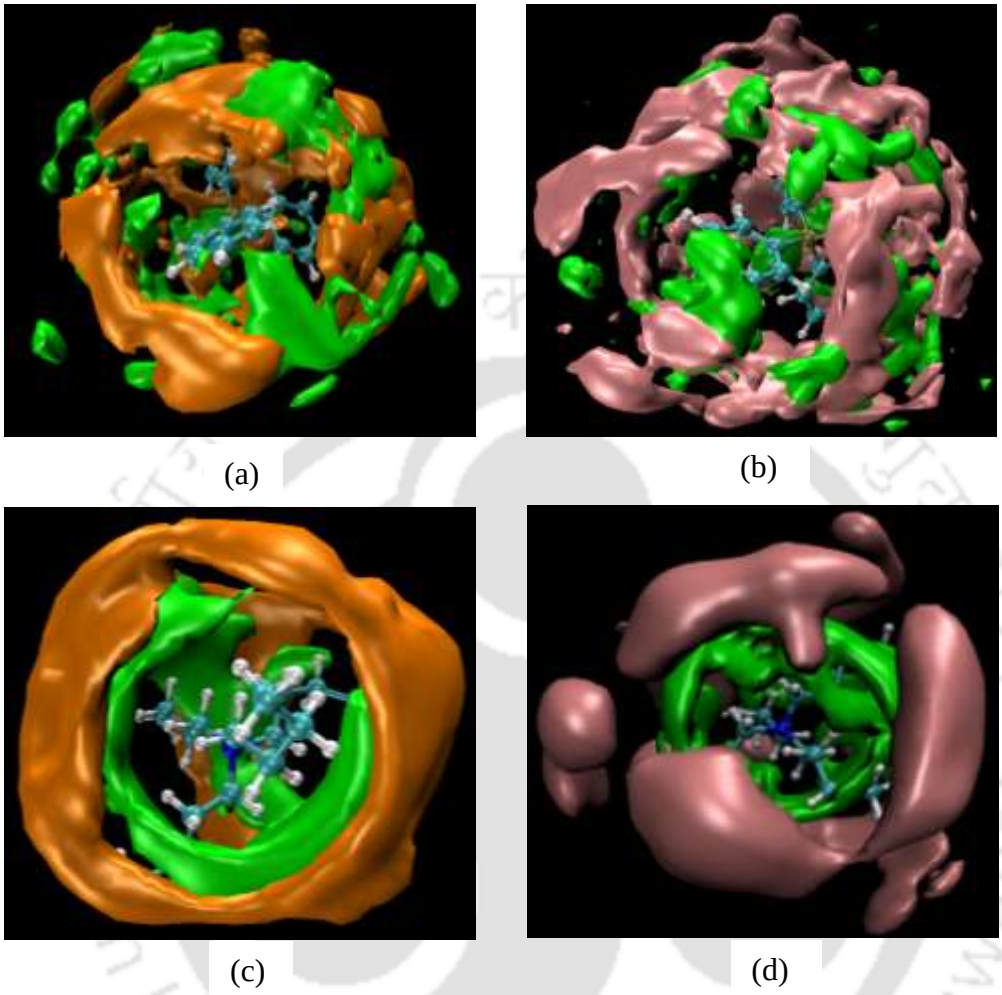

Figure A.12: Spatial distribution functions (SDF) of all four deep eutectic solvents (DES) studied in chapter 2. (a) DES1, EG and Br around MTP cation, (b) DES2, glycerol and Br, around MTP cation, (c) DES3, EG and Br around TBA cation and (d) DES4, glycerol and Br, around TBA cation. Orange, green, and pink surfaces refer to EG, Br, and glycerol of the respective DES

A.6 Sample Calculation for Mole Fraction from NMR Spectra

The following sample calculation has been used for the quantification of the known composition of DES1, quinoline and heptane in the mixture. The peak position and its components are located in Figure A1 below.

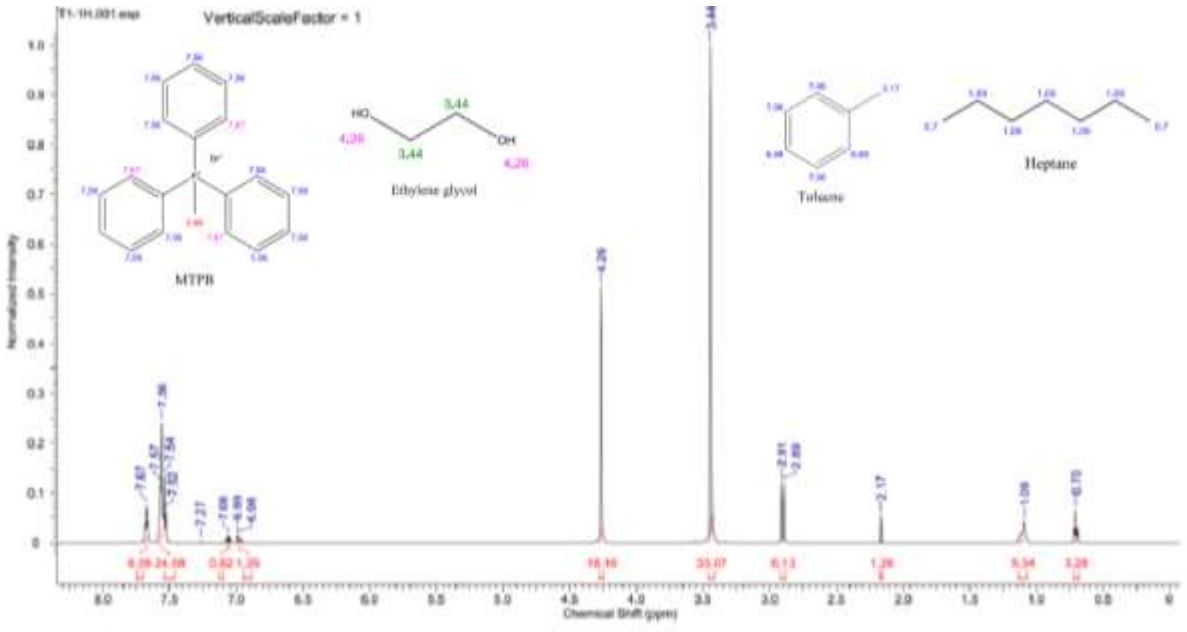

Figure A.13: NMR spectra of extract phase of ternary system DES+ Heptane+ Toluene

Peak area equivalent to 1 Hydrogen of DES(Peaks of MTBP) = (6.09+24.58)/15 = 2.04

= 6.13/3 = 2.04

It is interesting to observe that the peak area of $–CH_2$ in Ethylene glycol contributes an area of 33.07 or 33.07/4=8.267. This is exactly four times the contribution on hydrogen atom of MTBP i.e. 2.04. This proves the fact that the mixture MTBP and Ethylene Glycol are in the ratio of 1:4 and is a solution or solvent as a whole. Further continuing the calculation, we have:

Peak area equivalent to 1 Hydrogen of Toluene= (0.82+1.25)/5 = 0.41

Peak area equivalent to 1 Hydrogen of Heptane= 3.28/6 = 0.54

Now $\sum_{i=1}^{3} H_i$ = (2.04+0.41+0.54) = 2.99

Mole fraction of DES= 02.04/2.99 = 0.68

Mole fraction of Toluene = 0.41/2.99 = 0.14

Mole fraction of Heptane = 0.54/2.99 = 0.18

The reproducibility of the NMR derived mole fractions were checked on known mixtures of toluene-DES1 and quinoline-DES1 and it was found that the mole fractions lie within the uncertainty range of ±0.01. This was necessitated as all mixtures of DES-Toluene/Quinoline-Heptane were found to lie in the heterogeneous region.

Table A.1: Equations used in the NRTL and UNIQUAC model

NRTL Model

$$\ln \gamma_i = \frac{\sum_{j=1}^{c} \tau_{ji} G_{ji} x_j}{\sum_{k=1}^{c} G_{ki} x_k} + \sum_{j=1}^{c} \left[\frac{G_{ij} x_j}{\sum_{k=1}^{c} G_{kj} x_k} \left(\tau_{ij} - \frac{\sum_{i=1}^{c} \tau_{ij} G_{ij} x_i}{\sum_{k=1}^{c} G_{kj} x_k} \right) \right]$$

$$G_{ij} = \exp\left(-\alpha_{ji}\tau_{ji}\right),\ \tau_{ji} = \left[\left(g_{ji} - g_{ii}\right)/RT\right] \text{ and } \alpha_{ji} = \alpha_{ij} = \alpha$$

UNIQUAC Model

$$\ln \gamma_i = \ln\left(\frac{\Phi_i}{x_i}\right) + \frac{z}{2} q_i \ln\left(\frac{\theta_i}{\Phi_i}\right) + l_i - \frac{\Phi_i}{x_i}\sum_{j=1}^{c} x_j l_j + q_i \left(1 - \ln\sum_{j=1}^{c} \theta_j \tau_{ji} - \sum_{j=1}^{c} \frac{\theta_j \tau_{ij}}{\sum_{k=1}^{c} \theta_k \tau_{kj}}\right)$$

$$\tau_{ji} = \frac{g_{ji} - g_{ii}}{RT} = \frac{A_{ji}}{T};\ \theta_i = \frac{q_i x_i}{q_T};\ q_T = \sum_k q_k x_k\ ;\ \Phi_i = \frac{r_i x_i}{r_T}$$

$$r_T = \sum_k r_k x_k\ ;\ l_i = \frac{z}{2}(r_k - q_k) + 1 - r_k$$

Table A.2: Equations used in the COSMO-RS calculations

Sigma profile of component and mixture	$P_s(\sigma) = \sum_{i \in S} x_i p^{x_i}(\sigma)$	
Sigma profile averaging	$\sigma_m = \dfrac{\sum_n \sigma_n^* \dfrac{r_n^2 r_{eff}^2}{r_n^2 + r_{eff}^2} \exp\left(-\dfrac{d_{mn}^2}{r_n^2 + r_{eff}^2}\right)}{\sum_n \dfrac{r_n^2 r_{eff}^2}{r_n^2 + r_{eff}^2} \exp\left(-\dfrac{d_{mn}^2}{r_n^2 + r_{eff}^2}\right)}$, $r_{eff} = \sqrt{a_{eff}/\pi}$, $r_n = \sqrt{a_n/\pi}$	
Sigma potential (Chemical potential of segment)	$\mu_s(\sigma) = -kT \ln\left\{\sum_{\sigma'} \exp\left[\dfrac{-E_{pair}(\sigma,\sigma') + \mu_s(\sigma')}{kT}\right]\right\} + kT \ln p_s(\sigma)$	(a)
	$p_s(\sigma)\Gamma_s(\sigma) = \exp\left(\dfrac{\mu_s(\sigma)}{kT}\right)$	(b)
Activity coefficient of Segment	$\ln \Gamma_s(\sigma) = -\ln\left\{\sum_{\sigma'} p_s(\sigma)\Gamma_s(\sigma) \exp\left[\dfrac{-E(\sigma,\sigma')}{kT}\right]\right\}$	
Solubility equation	$\ln(\gamma^L_{solute} x^L_{solute}) = \dfrac{-\Delta h_f}{R}\left(\dfrac{1}{T} - \dfrac{1}{T_m}\right) - \dfrac{\Delta c_p}{R}\left(\dfrac{T_m - T}{T}\right) + \dfrac{\Delta c_p}{R} \ln\left(\dfrac{T_m}{T}\right)$	
Activity coefficient in mixture	$\ln\gamma_{i/s} = n_i \sum_{\sigma} P_i(\sigma)\left[\ln\Gamma_s(\sigma) - \Gamma_i(\sigma)\right] + \ln\gamma^{SG}_{i/s}$	(a)
	$\ln \gamma^{SG}_{i/s} = \ln \dfrac{\phi_i}{x_i} + \dfrac{z}{2} q_i \ln \dfrac{\theta_i}{\phi_i} + li - \dfrac{\phi_i}{x_i} \sum_j x_j l_j$	(b)
Staverman-Guggenheim term	Where $\theta_i = \dfrac{x_i q_i}{\sum_j x_j q_j}$, $\phi_i = \dfrac{x_i r_i}{\sum_j x_j r_j}$, $l_i = \dfrac{z}{2}\left((r_i - q_i) - (r_i - 1)\right)$	(c)

A.7 Description of AMBER Force Field

$$E_{Total} = E_{Bonded} + E_{Nonbonded}$$

$$E_{Total} = \left(E_{Bond} + E_{Angle} + E_{Dihedral} \right) + \left(E_{vdW} + E_{Electrostatic} \right)$$

$$E_{Total} = \sum_{Bonds} K_b (r - r_0)^2 + \sum_{Angles} K_\theta (\theta - \theta_0)^2 + \sum_{Dihedrals} \frac{V_n}{2} [1 + \cos(n\phi - \gamma)] + \sum_{i=j}^{N-1} \sum_{i<j}^{N} \left\{ 4\varepsilon_{ij} \left[\left(\frac{\sigma_{ij}}{r_{ij}} \right)^{12} - \left(\frac{\sigma_{ij}}{r_{ij}} \right)^{6} \right] + \frac{q_i q_j}{4\pi\varepsilon_0 r_{ij}} \right\}$$

The total energy of the system includes both bonded and nonbonded terms. The first there bonded interactions are for bonds, angles and torsions terms. The nonbonded interactions are described in the last term, which includes van der Waals (vdW) and electrostatic interactions of atom-centered point charges. Electrostatic and vdW interactions are calculated between only the atoms in different molecules or for the atoms in the same molecule separated by at least three bonds. Where, Bond parameters K_b is the bond force constant (kcal·mol^{-1} Å^{-2}) and r_o is the equilibrium bond length in Å; Angle parameters K_θ is the angle force constant (kcal·mol^{-1} radian^{-2}) and θ_o is the equilibrium angle (degree); Dihedral parameters V_n is the dihedral force constant in kcal mol^{-1} and γ in degree; Non bonded parameters ε in kcal·mol^{-1} and σ_{ij} in Å. The vdW energy is calculated with a standard 12-6 Lennard-Jones potential and the electrostatic energy with a Columbic potential. In the Lennard-Jones potential above, the σ_{ij} is the distance between atoms i and j, at which the energy of the two atoms reaches zero.

A.8 NAMD Configuration File

```
#############################################################
## JOB DESCRIPTION                                         ##
#############################################################

# Minimization of 400 DES, 400 heptane and 200 molecules of quinoline


#############################################################
## ADJUSTABLE PARAMETERS                                   ##
#############################################################

ambercoor               ../common/ER4.inpcrd

set temperature         0
set outputname          ER4_min
set restart             0

# Continuing a job from the restart files
if {$restart} {
set inputname             $outputname
Coordinates               ../$inputname.restart.coor
Velocities                ../$inputname.restart.vel
extendedSystem            ../$inputname.xsc
}

firsttimestep     0


#############################################################
## SIMULATION PARAMETERS                                   ##
#############################################################

# Input
amber                   on
parmfile                ../common/ER4.prmtop
if {$restart-1} {
temperature             $temperature
}
```

```
# Force-Field Parameters
dielectric          1.0          ;# Value of the dielectric constant
exclude             scaled1-4
nonbondedScaling    1.0
1-4scaling          1.0
cutoff              12.0         ;#Angstorm
switching           on
switchdist          10.0         ;#Angstorm
pairlistdist        14.0         ;#Angstorm

# Integrator Parameters
timestep            1.0          ;# 1fs/step
rigidBonds          all
rigidTolerance      0.00001
rigidIterations     100          ;# Maximum number of SHAKE iterations
nonbondedFreq       1
vdwGeometricSigma   yes
fullElectFrequency  2
stepspercycle       20
pairlistsperCycle   2

# Periodic Boundary Conditions
if {$restart-1} {
set X     150.00
set Y     75.00
set Z     75.00
set C     0.00
set C1    0.00
cellBasisVector1   $X     0.0     0.0     ;#Angstorm
cellBasisVector2   0.0    $Y      0.0     ;#Angstorm
cellBasisVector3   0.0    0.0     $Z      ;#Angstorm
cellOrigin         $C     $C1     $C1     ;#Angstorm

# PME (for full-system periodic electrostatics)
PME                 yes
PMEGridSpacing      1.0
PMETolerance        0.000001
```

```
#manual grid definition
#PMEGridSizeX          150
#PMEGridSizeY          75
#PMEGridSizeZ          75
}
wrapAll                on

# Constant Temperature Control
if {0} {
langevin               on              ;# do langevin dynamics
langevinDamping        1               ;# damping coefficient (gamma) of 1/ps
langevinTemp           $temperature
langevinHydrogen       off             ;# don't couple langevin bath to hydrogens
}

# Constant Pressure Control (variable volume)
if {0} {
useGroupPressure       yes              ;# needed for rigidBonds
useFlexibleCell        no
useConstantArea        no

langevinPiston         on
langevinPistonTarget   1.01325          ;#  in bar -> 1 atm
langevinPistonPeriod   100.0
langevinPistonDecay    50.0
langevinPistonTemp     $temperature
}

# Fixed Atoms Constraint (set PDB beta-column to 1)
if {0} {
fixedAtoms             on
fixedAtomsForces       on
fixedAtomsFile         myfixedatoms.pdb
fixedAtomsCol          B
}

# IMD Settings (can view sim in VMD)
if {0} {
IMDon                  on
IMDport                3000            ;# port number (enter it in VMD)
```

```
IMDfreq          1          ;# send every 1 frame
IMDwait          no         ;# wait for VMD to connect before running?
}

# Output
outputName       $outputname
XSTfile          $outputname.xst

restartfreq      500        ;# 500steps = every 1ps
dcdfreq          2000
outputEnergies   100
outputPressure   100

binaryoutput     no
binaryrestart    no

#############################################################
## EXTRA PARAMETERS                                        ##
#############################################################


#############################################################
## EXECUTION SCRIPT                                        ##
#############################################################

# Minimization
minimization     on
seed             1536       ;# Random number
minimize         500000     ;# Number of integration steps
```

APPENDIX B

List of Publications and Conferences

List of Publications & Conference Presentations

B.1 Journals Publications

1. **Papu Kumar Naik**, Pyarimohan Dehury, Sandip Paul and Tamal Banerjee, "Evaluation of Deep Eutectic Solvent for the Selective Extraction of Toluene and Quinoline at T=308.15 K and p=1 bar" *Fluid Phase Equilibria*, 423 (2016): 146-155.
2. Mood Mohan, **Papu Kumar Naik**, Tamal Banerjee, Vaibhav V. Goud, and Sandip Paul. "Solubility of Glucose in Tetrabutylammonium Bromide based Deep Eutectic Solvents: Experimental and Molecular Dynamic Simulations" *Fluid Phase Equilibria*, 448 (2017): 168-177.
3. **Papu Kumar Naik**, Sandip Paul, and Tamal Banerjee, "Liquid-Liquid Equilibria Measurements for the Extraction of Poly Aromatic Nitrogen Hydrocarbons with a Low Cost Deep Eutectic Solvent: Experimental and Theoretical Insights" *Journal of Molecular Liquids*, 243 (2017): 542-552
4. **Papu Kumar Naik**, Mood Mohan, Tamal Banerjee, Sandip Paul and Vaibhav V Goud, "Molecular Dynamic Simulations for the Extraction of Quinoline from Heptane in the Presence of Low Cost Phosphonium Based Deep Eutectic Solvent" *J. Phys. Chem. B* 122 (14), (2018): 4006-4015.
5. **Papu Kumar Naik**, Sandip Paul, and Tamal Banerjee, "Physiochemical Properties and Molecular Dynamics Simulations of Phosphonium and Ammonium Based Deep Eutectic Solvents" *Journal of Solution Chemistry*, 48 (2019):1046–1065.
6. **Papu Kumar Naik**, Sandip Paul, and Tamal Banerjee, "Thermal Hydrogenation and Degradation of Quinoline from Reactive Force Field Simulations" *ChemistrySelect*, 4 (44), (2019):12996-13005.

B.2 International Conferences

1. Mood Mohan, **Papu Kumar Naik**, Tamal Banerjee and Vaibhav V. Goud, "Experimental and Quantum Chemical Calculation for the Dissolution of Cellulose/Hemicellulose in Ionic Liquids." *Introduction to Gaussian16: Theory and Practice*, 16-20 January 2017, SCUBE Scientific Software Solutions (P) Ltd, New Delhi, India.
2. **Papu Kumar Naik**, Sandip Paul and Tamal Banerjee, "Characterization of deep eutectic solvents by NMR and FTIR spectroscopy" *International Conference on Sophisticated Instruments in Modern Research* (ICSIMR-2017), 30th June - 1st July 2017, IIT Guwahati.
3. Tamal Banerjee, Sandip Paul, **Papu Kumar Naik**, Vaibhav V. Goud and Mood Mohan, "Solid Liquid Equilibria and Molecular Modeling Predictions of Glucose in Tetra Butyl Ammonium Bromide based Deep Eutectic Solvents." *Liquids 2017 (10th Liquid Matter Conference)*, 17-21 July 2017, Ljubljana, Slovenia.
4. **Papu Kumar Naik**, Sandip Paul and Tamal Banerjee, "Molecular Dynamic Simulations of the Ternary system: Quinoline, Heptane and Phosphonium Based Deep Eutectic Solvent (DES)" *Fourth International Symposium on Advances in Sustainable Polymers (ASP-17)*, 8 - 11 January 2018, IIT Guwahati.
5. **Papu Kumar Naik**, Sandip Paul and Tamal Banerjee, "Molecular Dynamic Simulations and Properties of Novel Deep Eutectic Solvents" *International Conference on Emerging Trends in Chemical Sciences (ICETCS-2018)*, 26-28 February 2018, Dibrugarh University, Dibrugarh.
6. **Papu Kumar Naik**, Sandip Paul and Tamal Banerjee, "Synthesis, Molecular Dynamic Simulations and Liquid Liquid Equilibria Measurements of Deep Eutectic Solvents" *International Symposium on Solubility Phenomena and Related Thermodynamic Properties (ISSP-18)*, 15-20 July 2018, Tours, France.
7. **Papu Kumar Naik**, Sandip Paul and Tamal Banerjee, "Synthesis and Molecular Dynamics Simulations of Novel Deep Eutectic Solvents (DES)" *International Conference on Synthetic Potent Molecule and Its Application* (ICSPMIA-2018), 30-31 October 2018, Sikkim Manipal Institute of Technology, Rangpo, Sikkim

8. **Papu Kumar Naik**, Sandip Paul and Tamal Banerjee," Hydrogenation of Quinoline at High Temperature: ReaxFF Simulation" International conference: *Frontier in Chemical science* (FICS-2018), 6-8 December 2018, IIT Guwahati.

B.3 National Conferences

1. **Papu Kumar Naik**, Sandip Paul and Tamal Banerjee, "Separation of Aromatic Hydrocarbon from Diesel oil using Deep Eutectic Solvent." *National Conference on Recent Advancement in Environmental Research* (RAER-2016), 4-5 June 2016, IIT Guwahati.
2. **Papu Kumar Naik**, Sandip Paul and Tamal Banerjee, "Molecular Dynamics Simulations of Phosphonium based Deep Eutectic Solvents." *Research Conclave-2017*, 19-21 May 2017, IIT Guwahati.
3. **Papu Kumar Naik**, Sandip Paul and Tamal Banerjee, "Sustainable Solvents for Green Extraction Processes." *Research Conclave-2018*, 8-11 March 2018, IIT Guwahati.
4. **Papu Kumar Naik**, Sandip Paul and Tamal Banerjee," Degradation kinetics of quinoline: A ReaxFF simulation" *The first DAE computational chemistry symposium* (DAE-CCS), 7-9 November 2019, BARC Mumbai.

B.4 Workshops

1. Attended the *Gaussian16: Theory and Practice* Workshop to be organized by SCUBE Scientific Software Solutions (P) Ltd, held at Radisson Blu, 16-20 January 2017, Delhi.
2. Attended the Molecular Simulations Workshop to be organized by Indian Institute of Chemical Engineers - Guwahati Regional Centre (IIChE-GRC), held at Department of Chemical Engineering, IIT Guwahati on 27th September 2017.
3. Attended the Workshop on Recent Advances on Bio-inspired Nanomaterials for Environment Applications to be organized by Centre for Environment, IIT Guwahati on 18th December 2018.

4. Attended the Workshop on theory and demonstration on thermal analysis (DSC and TG) of materials to be organized by Indian Institute of Chemical Engineers - Guwahati Regional Centre (IIChE-GRC), held at Department of Chemical Engineering in association with the Central Instrument Facility, IIT Guwahati on 24th May 2019.
5. Attended the workshop on "Augmenting Writing Skill for Articulating Research (AWSAR)" held at Guwahati University in association with Vigyan Prasar, Ministry of Science and Technology, Government of India on 9th July 2019.

APPENDIX C

Biography

Biography

Papu Kumar Naik was born and brought up in Jharsuguda, Odisha, India. He completed Higher Secondary Education (10th Std.) in 2001 from Bimbadhar High School, Bandhakani and Intermediate education (12th Std.) in 2003 from Kuchinda college, Kuchinda. He completed his graduation (B.Sc.), Bachelor's degree in Physics honors, in 2007, from Gangadhar Meher College (Auto), affiliated to Sambalpur University and was the 1st rank holder (Topper of College) along with distinction. He obtained his post-graduation (M.Sc.), Master's degree in Environmental Science, in 2013, from Sambalpur University with a specialization in Pollution Control and Environmental Biotechnology. He was the 1st rank holder and awarded with the Gold medal of the Sambalpur University in the Environmental Science discipline in 2013. He was also obtained his Master of Technology (M.Tech.) degree in Environmental Science and Engineering with a specialization in Hydrology and Waste Water Engineering from Sambalpur University in 2015. From 2008 to 2011, he was working as a process associate in the Vedanta Aluminum Ltd, Jharsuguda, Odisha.

He has received the prestigious INSPIRE Fellowship from the Department of Science and Technology, Government of India and joined as an INSPIRE Fellow research scholar at Centre for the Environment, IIT Guwahati in March 2015 for his doctoral studies under the joint supervision of Prof. Tamal Banerjee and Prof. Sandip Paul. His Ph.D. work focuses on the extraction study of polyaromatic hydrocarbon from fuel oil using deep eutectic solvent. His thesis work also emphasizes on molecular modeling, thermodynamic study, and synthesis of green solvent like deep eutectic solvent along with its application on liquid liquid extraction process. He has published six papers at the time of compilation of this thesis and communicated another two collaborative manuscripts. He qualified ICAR-NET in 2013 and UGC-NET in 2018.